
Electronic Thesis and Dissertation Repository

5-25-2015 12:00 AM

Exploring the Chemistry of Phosphorus for Photopolymer Applications

Ryan Guterman
The University of Western Ontario

Supervisor
Paul J. Ragogna
The University of Western Ontario Joint Supervisor
Elizabeth R. Gillies
The University of Western Ontario

Graduate Program in Chemistry
A thesis submitted in partial fulfillment of the requirements for the degree in Doctor of Philosophy
© Ryan Guterman 2015

Follow this and additional works at: <https://ir.lib.uwo.ca/etd>

 Part of the [Inorganic Chemistry Commons](#), [Materials Chemistry Commons](#), [Polymer and Organic Materials Commons](#), and the [Polymer Chemistry Commons](#)

Recommended Citation

Guterman, Ryan, "Exploring the Chemistry of Phosphorus for Photopolymer Applications" (2015).
Electronic Thesis and Dissertation Repository. 2859.
<https://ir.lib.uwo.ca/etd/2859>

This Dissertation/Thesis is brought to you for free and open access by Scholarship@Western. It has been accepted for inclusion in Electronic Thesis and Dissertation Repository by an authorized administrator of Scholarship@Western. For more information, please contact wlsadmin@uwo.ca.

Exploring the chemistry of phosphorus for photopolymer applications

(Thesis format: Integrated Article)

by

Ryan Guterman

Graduate Program in Chemistry

A thesis submitted in partial fulfillment
of the requirements for the degree of
Doctor of Philosophy

The School of Graduate and Postdoctoral Studies
The University of Western Ontario
London, Ontario, Canada

Ryan Guterman 2015

Abstract

Prior to this thesis, phosphorus-containing polymers and photopolymerization represented two distinct, non-overlapping fields of study. This thesis examined the prospect of combining these two approaches to create a system possessing the benefits of both techniques. By exploiting the chemistry of phosphorus, and using photopolymerization as a fabrication method, new materials were developed and assessed for their use in various applications.

Among the many phosphorus compounds that may be used in polymer science, phosphonium salts and primary phosphines were of specific focus. First, highly fluorinated phosphonium monomers were developed to create photopolymerized hydrophobic surfaces. A structure-activity relationship was established, as both the length and type of fluorinated chains used had a dramatic effect on the degree of hydrophobicity. After developing these hydrophobic salts, hydrophilic varieties possessing short alkyl chains were examined and incorporated into polymer networks. These molecules imparted hydrophilic behaviour to the resulting material and were used as a substrate to immobilize anionic gold nanoparticle. The low melting temperature of these salts allowed for the production of highly charged polyelectrolyte networks in seconds, without the need for solvent. Self-crosslinking phosphonium salts were also synthesized and unlike in the previous example, provided an opportunity to increase the stiffness and ion-content within the material simultaneously. The high charge, and low swelling nature of this system allowed it to serve as an excellent substrate for contact-printing applications. While these three approaches involve the photopolymerization of low molecular weight phosphonium salts, a new approach was developed that incorporated phosphonium polyelectrolyte into a photopolymer resin. Immobilization of the charged species within the resin provided a convenient means for the gel-phase synthesis of gold nanoparticles. Finally, using air-stable primary phosphines, phosphane-ene chemistry was used to generate a new class of polymer networks. This approach is analogous to thiol-ene chemistry but possesses the distinct advantages resulting from the ability to harness chemistry of phosphorus within the network.

Keywords

Phosphorus, phosphonium. polymer, networks, UV-curing, photopolymerization, ionic liquids, polyelectrolyte, coatings, phosphane-ene, phosphine

Co-Authorship Statement

The work described in chapter two was coauthored by Guterman, R.; Berven, B.B.; Corkery, T.C.; Nie, H.-Y.; Gillies, E.R.; Idacavage, M.J.; and Ragona, P.J. *J. Polym. Sci. A Polym. Chem.* **2013**, *51*, 2782 (Inside cover). Ryan Guterman was the primary experimentalist with Brad Berven and Chris Corkery contributing as well for the synthesis of **2.4[Cl]/[NTf₂]** and TOF-SIMS experiments. Ryan Guterman wrote the manuscript, but all authors contributed to the editing process.

The work described in chapter three was coauthored by Guterman, R.; Hesari, M.; Workentin M.S.; Ragona, P.J.* *Langmuir* **2013**, *29*, 6460. (Front Cover). Ryan Guterman and Mahdi Hesari were the primary experimentalists. Mahdi's contribution includes the synthesis of the gold nanoclusters, XPS, and photoluminescence experiments. Both Ryan and Mahdi wrote the manuscript and all authors contributed to the editing process.

The work described in chapter four was coauthored by Guterman, R.; Gillies, E.R.; Ragona, P.J.* *Langmuir* **2015**, *18*, 5181.

The work described in chapter five was coauthored by Guterman, R.; Gillies, E.R.; Ragona, P.J.*. Accepted to *Can. J. Chem* **2015**.

The work described in chapter six was coauthored by Guterman, R.; Kenaree, A.R.; Gilroy, J.B.; Gillies, E.R.; Ragona, P.J. Polymer network formation using the phosphane-ene reaction: a thiol-ene analogue with diverse post-polymerization chemistry *Chem. Mater.* **2015**, *27*, 1412. Amir and Joe were responsible for the synthesis of **6.5** and electrochemistry experiments.

Acknowledgments

I would first like to thank my supervisors Paul Ragona and Elizabeth Gillies for their excellent supervision and giving me the opportunity work with them over the past four years. I owe much of how I think and conduct science to both of these individuals, and I greatly value their input and guidance within the lab and beyond. I am especially grateful for the travelling opportunities they have given me during my time at Western to not only learn science, but also experience the world.

I would also like to thank my colleagues in the Ragona and Gillies groups for always being positive and creating an atmosphere of success. I would also like to thank Dr. Jonathon Dube, Dr. Chris Corkery, Dr. Brad Berven, Dr. Mahdi Hesari, and Dr. Yuqing Liu for their excellent discussions and helping me to become a better scientist.

Without the excellent staff members in the Chemistry department, none of this would be possible. I would like to specifically thank John Vanstone and Jon Aukema, two individuals who I cannot thank enough not only for repairing our instruments on short notice but for their conversation and putting up with me when I barge into the shop. Dr. Mathew Willans has also been crucial in helping me with my NMR spectroscopy related questions and concerns. I also thank Darlene McDonald for keeping the trains on time, and the ChemBio store staff.

A special thanks to my committee members Dr. Lars Konermann, Dr. Brian Pagenkopf, Dr. John de Bruyn, and Dr. Kevin Noonan for reading my thesis and for their feedback.

I would like to also thank my friends and family who have helped me along the way outside the lab, especially my parents Noah and Liora Guterman and brother Daniel for their boundless support and inspiration, and my amazing friends Ben Laufer and Kathryn Watson for helping me through this endeavor.

Table of Contents

Abstract	ii
Acknowledgments	v
List of Tables	x
List of Figures	xi
List of Appendices	xvi
Abbreviations	xvii
List of Compounds Reported	xxi
Chapter 1	1
1 From Molecules to Materials	1
1.1 Polymer Science – History	1
1.2 Polymer Science and Inorganic Chemistry	2
1.2.1 The Transition from Organic to Inorganic Polymer Science.....	4
1.2.2 Phosphorus-Containing Polymers.....	5
1.2.3 Polymerizing phosphorus – Side chain.....	6
1.2.4 Polymerizing phosphorus – Main chain.....	8
1.3 Photopolymerization	11
1.3.1 Background.....	11
1.3.2 Photopolymerization Chemistry.....	13
1.3.3 Photoinitiation.....	14
1.3.4 Propagation, Termination, and Inhibition.....	16
1.4 Scope of the Thesis	18

Chapter 2	23
2 Fluorinated polymerizable phosphonium salts from PH₃: Surface properties of photopolymerized films	23
2.1 Introduction	23
2.1.1 Synthesis	25
2.1.2 HFPPS Physical and Chemical Properties	28
2.1.3 Hydrophobic Surface Modification using HFPPS	31
2.2 Conclusions	37
2.3 Experimental	38
2.3.1 Solubility/Miscibility Tests	40
2.3.2 Film Preparation	40
2.3.3 Synthetic Details	40
Chapter 3	49
3 Anion exchange reactions on a robust phosphonium photopolymer for the controlled deposition of ionic gold nanoclusters	49
3.1 Introduction	49
3.2 Results and Discussion	52
3.3 Conclusions	62
3.4 Experimental	63
3.5 References	65
Chapter 4	68
4 Kinetically controlled patterning of highly charged phosphonium photopolymers using simple anion exchange	68
4.1 Introduction	68
4.2 Results and Discussion	70
4.2.1 Polymer Synthesis and Characterization	70
4.2.2 Ion-exchange properties and 2D patterning	75

4.3	Conclusions	80
4.4	Experimental	81
4.5	References	86
Chapter 5		90
5	The formation of gold nanoparticles in photopolymerized networks	90
5.1	Introduction	90
5.2	Results and Discussion	92
5.2.1	Synthesis and Characterization	92
5.2.2	In-situ Gold Nanoparticle Synthesis and Characterization	96
5.3	Conclusions	101
5.4	Experimental	102
Chapter 6		105
6	Polymer networks formation using the phosphane-ene reaction: a thiol-ene analogue with diverse post-polymerization chemistry	105
6.1	Introduction	105
6.2	Results and Discussion	108
6.2.1	Phosphane-ene Network Synthesis and Properties	108
6.2.2	Solid-supported Chemistry	111
6.2.3	Thermoresponsive Oxygen Scavenging	112
6.2.4	Formulation Stability	114
6.2.5	Metal-containing Phosphane-ene Networks	115
6.3	Conclusions	117
6.4	Experimental	117
Chapter 7		127
7	Conclusions and Future Work	127
7.1	Conclusions	127

7.2 Future Research 127

List of Tables

Table 2-1: Physical properties of all HFPPS used in this study.	29
Table 2-2: WCA for all HFPPS as a function of wt% in HDDA.....	33
Table 5-1: Composition of three formulations possessing different crosslink densities.	94
Table 5-2: Comparison of the properties of polymer networks with and without 5 wt% 5.3. The swelling and glass transition data follow predictable trends with small changes observed upon incorporation of the polyelectrolyte.....	94
Table 5-3: Formulations used for thin films studies and for the formation of AuNPs. All formulations possess 5 wt% phosphonium homopolymer.....	97
Table 6-1: Effect of changing olefin composition and PH ₂ /olefin ratios on network properties. The %mass increase upon oxidation, Ox was measured and compared to the calculated value, $Ox_{calc} = 100((n_{phos}M_{Oxy}+W_0)/W_0)-1$, where n_{phos} is the moles of phosphorus in the sample, M_{Oxy} is the atomic mass of oxygen, and W_0 is the weight of the sample.....	109

List of Figures

Figure 1-1: Structure comparison between linear polymers and crosslinked polymer networks.....	3
Figure 1-2: Various phosphorus functional groups and their structures.....	5
Figure 1-3: A selection of phosphorus-containing monomers polymerized by free-radical polymerization.....	7
Figure 1-4: A selection of phosphorus-containing monomers used in flame-retardant PET, polyamide, and polyurethane production.....	9
Figure 1-5: Examples using phosphorus for the polymerization reaction, including a) Phosphazenes b) Phosphaalkenes c) Phosphines.....	10
Figure 1-6: Three-dimensional photopolymerization methods, including a) Stereolithography b) Two-photon polymerization and c) Lattice photopolymerization.....	13
Figure 1-7: Schematic representation of polymer network synthesis by direct polymerization of multifunctional monomers (right) or crosslinking of linear chains (left).....	14
Figure 1-8: Common photoinitiators (PIs) and their trademark abbreviations used for free-radical polymerization.....	15
Figure 1-9: a) Photoinitiator is first dissolved in monomer. b) Upon irradiation, photoinitiators cleave to create micron-sized polymer networks. c) Upon gelation, a large polymer network system is formed with some leftover monomer.....	17
Figure 2-1: All HFPS synthesized in this study for applications in photopolymerizable systems.....	24
Figure 2-2: Solubilities of all HFPPS in various polar and non-polar solvents. Green = Soluble, Red = Insoluble, Yellow = Emulsion.....	28
Figure 2-3: Decomposition pathway of 2.4[CI] under inert atmosphere.....	30

Figure 2-4: a) AFM image of a photopolymerized film containing 0.1 wt% 2.4[NTf₂] in HDDA. b) Roughness profile isolated from the image in (a).	32
Figure 2-5: WCAs of droplets on a) HDDA b) 1.5 wt% of 2.1[NTf₂] c) 1.5 wt% of 2.2[NTf₂] d) 1 wt% of 2.3[NTf₂] and e) 0.5 wt% of 2.4[NTf₂] .	34
Figure 2-6: Negative ion mass spectrum in m/z ranges of 10-100 (a) and 100-300 (b) obtained on the surface of a photopolymerized film containing 1 wt% of 2.1[NTf₂] in HDDA.	36
Figure 2-7: Depth profiles of negative ion fragments of O ⁻ , CF ⁻ , C ₂ H ⁻ , and C ₂ F ₆ S ₂ O ₄ ⁻ (which is the anion [NTf ₂] ⁻) obtained using a 2 keV Cs ⁺ beam to sputter the surface and a 25 keV Bi ³⁺ ion beam to analyze the surface.	36
Figure 3-1: Representation of the overall process of applying the pre-polymer formulation containing phosphonium monomer 3.2 (A), drawing an even surface (B), irradiation (C) giving the cured ion exchange coating (D), followed by immersion of the substrate in [TOA][Au ₂₅ L ₁₈] solution (E) to give the final coating (F).	52
Figure 3-2: Photographs of a polyelectrolyte film containing 47.5 wt% polymerizable phosphonium salt. a, before and b after immersion in a 0.5 wt% (5.7 mM) solution of [TOA][Au ₂₅ L ₁₈] in acetonitrile.	55
Figure 3-3: UV-vis spectrum of a 0.025 mM solution of [TOA][Au ₂₅ L ₁₈] in acetonitrile (top); UV-vis spectra of the Au ₂₅ -PPF after 10 sec, 1 min, 3 min, 5 min and 10 min (a-e) dipping in a 1.9 mM solution of [TOA][Au ₂₅ L ₁₈] in acetonitrile (bottom). Figure inset; dipping time vs. absorbance. Plot shows the dipping time after 10 sec, 1 min, 3 min, 5 min and 10 min versus absorbance of [Au ₂₅ L ₁₈] ⁻ at 400 nm.	56
Figure 3-4: Electron Dispersion X-ray (EDX) spectra. Recorded spectrum of PPF before dipping (Top; a); After 10 minutes immersion in a 1.9 mM solution of [TOA][Au ₂₅ L ₁₈] in acetonitrile (Bottom; b); Energy peaks at 2.1205 keV and 2.3075 keV representing Au (M _α) and S (L _α) atoms on the Au ₂₅ -PPF.	57

Figure 3-5: Water contact images of (left) pristine PPF (WCA = $17^\circ \pm 3$) and (right) Au ₂₅ -PPF after dipping for 10 minutes in a 1.9 mM solution of [TOA][Au ₂₅ L ₁₈] in acetonitrile (WCA = $87^\circ \pm 1$).	59
Figure 3-6: a) Representation of the reversible exchange process and b) UV-vis data demonstrating zero loss of polymer activity through eight on/off cycles, monitored at 400 and 683 nm.	60
Figure 3-7: Red line, spectrum of [TOA][Au ₂₅ L ₁₈] collected in solution (acetonitrile, C = 0.3 mM). Black line, immobilized Au ₂₅ -PPF after 10 minutes immersion in the [TOA][Au ₂₅ L ₁₈] stock solution.	61
Figure 4-1: Representation of a photochemically synthesized polyelectrolyte from a crosslinking phosphonium salt (4.2) and poly(ethylene glycol)dimethacrylate.	69
Figure 4-2: WCA and charge density (a) percent swelling in H ₂ O (b) and DSC data of polymers containing differing amounts of 4.2 . WCA and charge density measurements were conducted on 25 microns films while the swelling and DSC data (c) were acquired from bulk polymer samples. (d) A polymer sample with 5 wt% 4.2 in PEG-DMA. This polymer is distinctly firmer, yet still flexible when compared to 100% PEG-DMA.	72
Figure 4-3: WCA, charge density (a) and percent swelling in H ₂ O (b) of polymer coatings containing differing amounts of phosphonium monomer possessing one acrylate group (2.1) combined with EB130 crosslinker.	74
Figure 4-4: Uptake of fluorescein into a 60 wt% 4.2 film as a function of time ($\lambda_{\max} = 501$ nm).	77
Figure 4-5: Uptake of fluorescein into a 60 wt% 4.2 film functionalized with either NTf ₂ or DBS as a function of time ($\lambda_{\max} = 501$ nm).	78
Figure 4-6: A PDMS stamp functionalized with sodium DBS is brought into contact with the phosphonium polymer coating. DBS ion exchanges on to the cationic polymer creating a hydrophobic surface. The untouched regions are then functionalized with a different anion (fluorescein).	79

Figure 5-1: Schematic illustration of the *in situ* synthesis of AuNPs within a photopolymer. First, phosphonium polymer is embedded in a photopolymerized film. The film is then treated with HAuCl_4 , resulting in functionalization of the immobilized phosphonium polymer with AuCl_4^- . Finally, the film is treated with NaBH_4 to create AuNPs. 92

Figure 5-2: Monomers used to create the photopolymer matrix. 93

Figure 5-3: Uptake of fluorescein (left) and HAuCl_4 (right) into different bulk polymer samples. Polymer 1 resulted in the greatest uptake of fluorescein due to its ability to swell, while 2 and 3 to lesser degrees. Control samples without dissolved polyelectrolyte displayed very little to no fluorescein uptake. Samples immersed in HAuCl_4 displayed a similar trend, however control samples were found to be unstable resulting in premature AuNP formation. 96

Figure 5-4: a) UV-vis spectra of 25- μm thick films after immersion in fluorescein dye. The inset shows films from formulation A (left) to formulation D (right). b) UV-vis spectra for formulations A-D after AuNP synthesis. The inset shows formulations A (left) to D (right) after AuNP synthesis..... 97

Figure 5-5: a) Schematic representation of the cyclic functionalization of the polymer film C with AuNPs. (b) Polymer film after 8 cycles. (c) Visual spectra of each cycle. The inset shows a plot of the intensity at 533 nm as a function of AuNP deposition cycles. (d) Patterned photopolymers can also be used to spatially orient the AuNPs..... 99

Figure 5-6: (a) SEM and EDX images of a polymer film functionalized 8 times with AuNPs. Gold appears to be present across the entire film with selected regions of increased density. (b) Magnification shows good coverage of AuNPs on the surface. (c and d) The large structures appear to be aggregates of smaller gold particles..... 100

Figure 5-7: TEM images of formulation C after 8 reduction cycles. Darker regions correspond to the presence of gold. Images a show the existence of microstructured gold throughout the polymer matrix. Magnification of the darker regions shows fine nanostructure localized in the larger regions (b and c)..... 101

Figure 6-1: a) Mechanism for hydrophosphination/phosphane-ene reaction and for hydrothiolation/thiol-ene reaction. b) Schematic representation of polymer network formation using 6.4 and photoinitiator Irgacure 819, where soft materials are created when using TEGDAE, while firm networks are made using TTT and can hold 1 kg of weight.	107
Figure 6-2: ^{31}P SS-NMR spectroscopy of SPN-1 showing the presence of only three phosphorus functional groups within the polymer network.	110
Figure 6-3: a) A schematic representation of the solid-supported reactions illustrates three separate functionalization steps and their effect on glass transition. b) $^{31}\text{P}\{^1\text{H}\}$ NMR spectra comparing identical chemistry (shown in a) performed on the small molecule 6.3 (blue spectra) in solution and SPN-1 (red spectra) in the solid-state.....	112
Figure 6-4: a) TGA thermographs for SPN-1 → SPN-3 (green lines and axis) and FPN-1 → FPN-3 (red lines and axis). All polymers were first held at 25 °C for 30 minutes to ascertain their stability at room temperature, followed by heating to either 100 °C for soft networks or 120 °C for firm networks. b) $^{31}\text{P}\{^1\text{H}\}$ NMR spectra of SPN-2 before and after oxidation in air.	114
Figure 6-5: $^{31}\text{P}\{^1\text{H}\}$ NMR spectra of formulation SPN-2 with 2 wt% diphenylamine in air, which imparts increased stability in air.	115
Figure 6-6: a) Synthesis of a ferrocene-containing polymer network (FcPN). b) Shaped ceramics can be formed from the pyrolysis of FcPN . A thin strip of polymer film was manually formed into a ring, dried in an oven, and retained its shape upon pyrolysis, c) Cyclic-voltammetry of a thin film of FcPN can undergo <i>pseudo</i> -reversible one-electron oxidation, demonstrating the redox activity of these materials.	116
Figure 7-1: Oxygen scavenging film composed of phosphine polymer.....	128

List of Appendices

Appendix A: Copyright Permissions.....	127
Appendix B: Supplementary Figures.....	129

Abbreviations

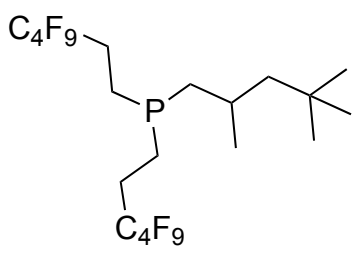
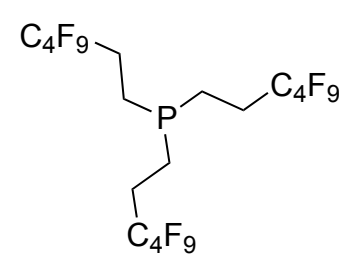
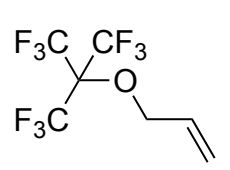
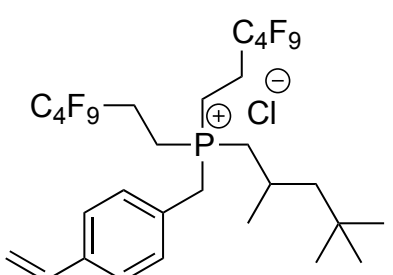
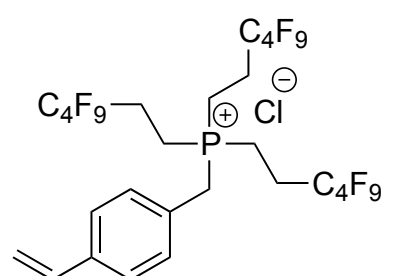
°	degrees
2D	two dimensional
3D	three dimensional
AFM	atomic force microscopy
AIBN	azobisisobutyronitrile
AuNC	gold nanocluster
AuNP	gold nanoparticle
BAPO	bisacyl phosphine oxide
BHT	butylated hydroxy toluene
Bu	butyl
cm	centimeter
DBS	dodecylbenzene sulfonate
DCM	dichloromethane
°C	degrees Celsius
δ_F	fluorine chemical shift (ppm)
δ_H	hydrogen chemical shift (ppm)
δ_P	phosphorus chemical shift (ppm)
DMA	dimethacrylate
DMAP	dimethylaminopyridine
DMF	dimethylformamide
DNA	deoxyribose nucleic acid
DSC	differential scanning calorimetry
EB130	Ebecryl 130
EB140	Ebecryl 140
EDX	energy dispersive X-ray spectroscopy
ESI	electrospray ionization
Et	ethyl
Et ₂ O	diethylether
Et ₃ N	triethylamine
<i>fcc</i>	face centered cubic

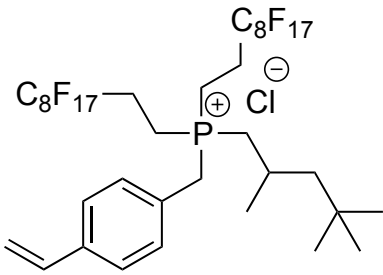
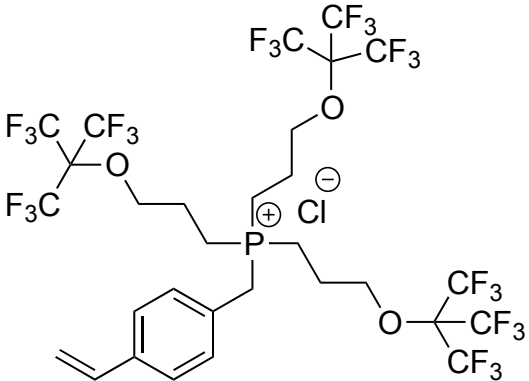
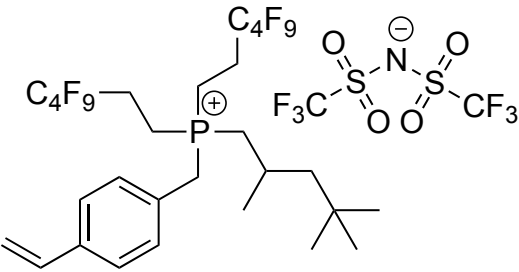
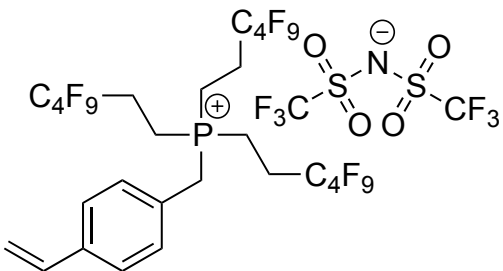
FTIR-ATR	fourier transform infrared attenuated total reflectance
g	gram
HDDA	hexanediol diacrylate
HDMAP	2-Hydroxy-2-methyl-1-phenyl- propanone
HEMA	hydroxyethyl methacrylate
HFPPS	highly fluorinated polymerizable phosphonium salt
IL	ionic liquid
<i>in situ</i>	on site
<i>in vacuo</i>	in a vacuum
IR	infrared
keV	kiloelectron volt
kHz	kilohertz
λ	wavelength
LbL	layer-by-layer
m	meter
M	molarity
m.p.	melting point
<i>m/z</i>	mass-charge ratio
Me	methyl
mg	milligram
MHz	megahertz
min	minute
mJ	milliJoule
mL	milliliter
mm	millimeter
mM	millimolar
MMA	methymethacrylate
mN	milliNewton
nm	nanometer
NMR	nuclear magnetic resonance
Oct	octyl
p-block	elements in group 13-18

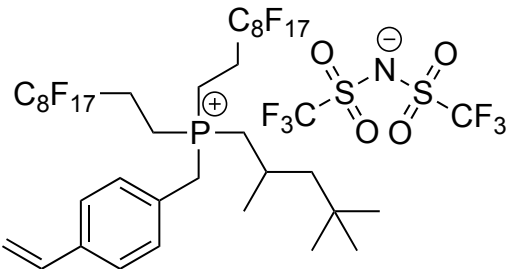
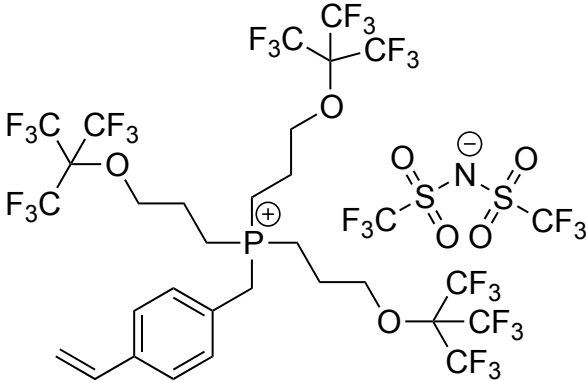
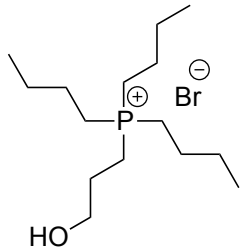
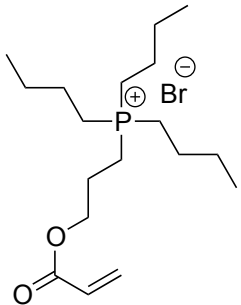
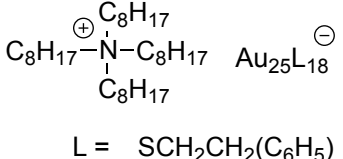
PDMS	polydimethylsiloxane
PE	polyelectrolyte
PEG	polyethyleneglycol
PET	polyester
pH	power of hydrogen
PI	photoinitiator
pnictogen	group 13 element
PPF	pristine phosphonium film
ppm	parts per million
PS	polystyrene
PXRD	powder X-ray diffraction
Q	swelling ratio
RAFT	reverse addition fragmentation chain transfer
Rfx	Perfluorinated carbon chain, x = # of carbons
RNA	Ribose nucleic acid
ROP	ring opening polymerization
rt	room temperature
s	second
SEM	scanning electron microscopy
SS-NMR	solid state nuclear magnetic resonance
T _{dec}	decomposition temperature
TEGDA	tetraethyleneglycol diacrylate
TEGDAE	tetraethyleneglycol diallyl ether
TEM	transmission electron microscopy
T _g	glass transition
TGA	thermal gravimetric analysis
THF	tetrahydrofuran
T _m	melting temperature
TOA	tetraoctyl ammonium
TOF-SIMS	time of flight secondary ion mass spectrometry
TTT	1,3,5-triallyl-1,3,5-triazine-2,4,6(1 <i>H</i> ,3 <i>H</i> ,5 <i>H</i>)-trione
μm	micrometer

UV	ultraviolet
V	volume
v/v	volume ratio
wavenumber	wavenumber
WCA	water contact angle
wt%	weight percent
XPS	X-ray photoelectron spectroscopy

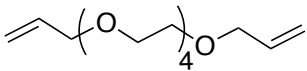
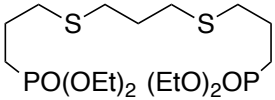
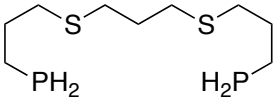
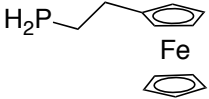
List of Compounds Reported

Structure	Compound Number
	2.0a
	2.0b
	2.0c
	2.1[Cl]
	2.2[Cl]

	2.3[Cl]
	2.4[Cl]
	2.1[NTf₂]
	2.2[NTf₂]

	2.3[NTf₂]
	2.4[NTf₂]
	3.1
	3.2
 <p style="text-align: center;">L = SCH₂CH₂(C₆H₅)</p>	3.3

	<p style="text-align: center;">4.1</p>
	<p style="text-align: center;">4.2</p>
	<p style="text-align: center;">5.1</p>
	<p style="text-align: center;">5.2</p>
	<p style="text-align: center;">5.3</p>

	<p>6.1</p>
<p>Br-CH₂-CH₂-CH₂-CH₂-PO(OEt)₂</p>	<p>6.2</p>
	<p>6.3</p>
	<p>6.4</p>
	<p>6.5</p>

Chapter 1

1 From Molecules to Materials

Polymer science is a discipline of chemistry that has grown considerably since its establishment, and continues to expand fueled by the requirements of industry and scientific interest. During the industrial revolution, modern scientists began to understand and later create these materials.¹ Hermann Staudinger proposed that the observed properties of polymers were a result of long chains composed of atoms bound by covalent bonds, and in 1953 he received the Nobel Prize for his “discoveries in the field of macromolecular chemistry”. It was during the post-WWII era that marked the beginning of modern polymer science.

1.1 Polymer Science – Historical Background

In the world we live in today, it is unfathomable to imagine life without polymers. Their discovery and exploitation have influenced virtually every aspect of human endeavor, from automobile manufacturing, space exploration, and electronics to medicine, and much more. The first type of polymer exploited in the Industrial Era was rubber, commercialized in the 19th century and used in tires and waterproof clothing.² All rubber during this time was derived from natural sources, and it was not until the early 20th century that synthetic rubber was developed. Later this laid the basis for the synthetic rubber industry during WWI rubber shortages.³ The war left an impact on the world as geographically locked rubber was found to be a national security issue, thus the synthetic polymer industry gained momentum. For the chemist, this was an era of exploration with profit in mind, discovering which chemical reactions and molecules were best suited for polymerizations and how to process these materials to create useful products. By the 1930s, synthetic rubbers such as Neoprene were in production, and by the end of WWII, the synthetic polymer industry was booming.⁴ While today we explore polymers for scientific merit, it's rarely the sole justification for its research. The importance of any given polymer is measured by its potential to generate wealth and create useful materials,

not only by its difficulty of preparation/isolation, or what it teaches the scientific community.

1.2 Polymer Science and Inorganic Chemistry

The sheer vastness of polymer science has traditionally been a testament to the chemistry of carbon, an element that modern chemistry continues to explore. This rich chemistry translates to polymers, allowing for the fabrication of a wide variety of materials with different densities, solubilities, flexibility, moduli, insulating properties, chemical resistance, refractive indices, and moldability into numerous shapes.⁵ While each of these properties is a result of specific processes that could be discussed in great length, they are generally governed by two factors, one on the molecular scale (monomer composition and structure) and the other on the nano/micro scale. Every useful property that polymeric materials possess are derived in some form from their large size, on the order of several hundred nanometers in length. Long polymer chains interact through intermolecular forces and even tangle together which manifests unique bulk properties not present in the smaller molecules from which they are derived (such as elasticity, viscosity, hardness, specific heat capacity, and melting temperature to name a few). While small molecules typically form brittle, crystalline, and mechanically useless materials, long-range interactions in polymers can distribute applied forces over large areas producing elastomers/rubbers, plastics, fibers, and thermosets. Manipulations on the nano or micro scale may be so pronounced that they dominate the behaviour of the material. For example, the viscosity of polymer solutions and the self-assembly behaviour of block copolymers is correlated directly to polymer molecular weight and the relative volume fractions of each block.^{5,6} In what can be considered the most extreme case, the introduction of only a few crosslinks between polymers prevents chains from slipping past each other or separating, rendering a material that was once freely soluble and moldable, into a completely insoluble substance incapable of melting/molding (Figure 1-1).

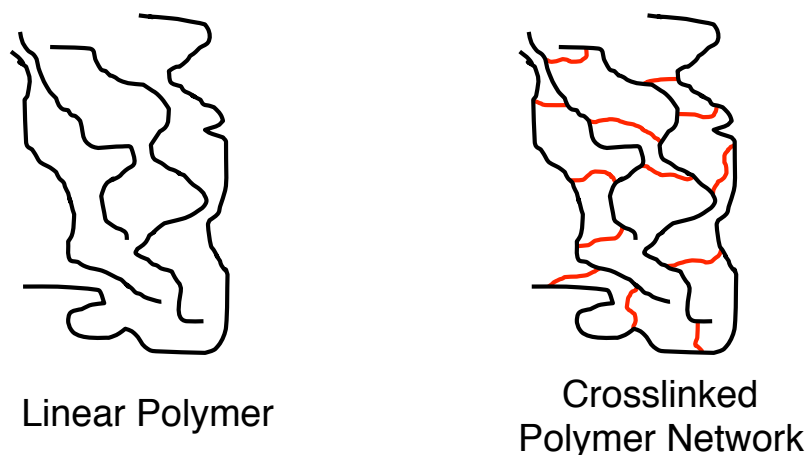


Figure 1-1: Structure comparison between linear polymers and crosslinked polymer networks.

Understanding these macro-scale phenomena required new theories and perspectives, prompting the creation of macromolecular science as a distinct and separate discipline from small molecule sciences. This discipline lends perspectives developed by physicists, chemists, and engineers to create suitable models to describe these materials in their entirety. The complexity and richness of polymer science is further expanded when one considers the molecular (or monomer) composition of polymers and its relationship to the larger polymeric architecture and material properties. Important intermolecular interactions such as hydrogen bonding, metal coordination, ionic bonding, hydrophilic/hydrophobic interactions, and π -stacking are often amplified in polymeric systems producing new phenomena not observed in small molecules. This fact can be appreciated with polymers such as Nylon (polyamides), which are highly crystalline because of hydrogen bonding interactions and the repeating monomeric structure.⁷ These polymers can undergo fiber and textile formation, a processing technique impossible using small molecules. Polymers possessing repeating ionic functionalities (polyelectrolytes; PEs) do not adopt the random coil conformation in solution typical of neutral polymers, but instead form rigid rods that dramatically affect their deposition behaviour and viscosity in solution.⁸ Finally, using water soluble triblock copolyelectrolytes, high modulus hydrogels have been formed through ionic crosslinking reactions, a process unique to polyelectrolytes.⁹

In all these examples, the intermolecular interactions that provide polymers with many of their unique features are dependent on both monomer structure and composition, representing two parameters that may be adjusted to affect the bulk properties of the material. By increasing the number and types of elements used to make polymers, the number of attainable properties should also increase. Variations on the molecular scale such as atomic radii, weight, electronegativity, bond angles, and bonding environment can have major effects on the macro scale properties and chemical behaviour.¹⁰ Some of the earliest and most established examples include polyphosphazenes, polymeric fluorocarbons, and silicones. All these materials possess distinct chemical and physical properties not attainable using organic elements exclusively.¹⁰ More recently, transition metals and heavier p-block elements have also been exploited giving rise to some exotic materials.^{11,12}

1.2.1 The Transition from Organic to Inorganic Polymer Science

Historically the role of inorganic polymers was geared towards overcoming deficiencies found in organic systems. For example, organic polymers ignite releasing toxic smoke when heated,¹³ degrade when exposed to oxygen and UV light over long periods of time,¹⁴ and may possess little resistance to solvents, oils, and other fluids during their use. Polymers containing inorganic elements such as silicone however may be used at high/low temperatures, are resistant to burning,¹⁵ non-toxic,¹⁶ and readily degrade in the presence of natural clays.¹⁷ Relative to C-C, C-O, or C-N bonds, inorganic element bonds may be stronger, more flexible, stable, and change the torsional mobility.¹⁰ For example, Si-O bonds are longer and less rigid than C-O bonds (1.64 vs 1.41 Å), while the Si-O-Si bond angle is much larger than the analogous C-O-C bond angle (142.5° vs 111.0°), leading to greater rotational freedom and flexibility.¹⁸ In fact, these differences are the source of all the defining properties silicone polymers possess and why they are so useful. More simple approaches such as blending or mixing inorganic components with organic polymers can also be sufficient for altering the mechanical and chemical properties of the material. For example, the addition of silica or clay to all-organic polymers has been shown to improve toughness,¹⁹ increase thermal stability,²⁰ and reduce the transport of gasses through the material.^{21,22} These constructs are referred to as

composite materials and are a separate field of study, but nonetheless it demonstrates the potential advantages and multifaceted nature of combining inorganic elements with polymer science. Currently, inorganic polymers are being explored for uses in biomaterials,²³ self-assembly,²⁴ and electronic displays,¹² thus illustrating the maturation of inorganic polymer science into an independent discipline in recent years. One inorganic element that has continuously been explored for some these applications is phosphorus.

1.2.2 Phosphorus-Containing Polymers

Phosphorus has an electron configuration of $[\text{Ne}]3s^23p^3$ and is a pnictogen found under nitrogen on the periodic table. While synthetic phosphorus-containing polymers have been around for approximately a century, natural polymers like DNA and RNA have been using phosphorus for billions of years. Phosphorus can form a large variety of hypervalent compounds and possesses a large number of oxidation states ($-3 \rightarrow +5$) (Figure 1-2).

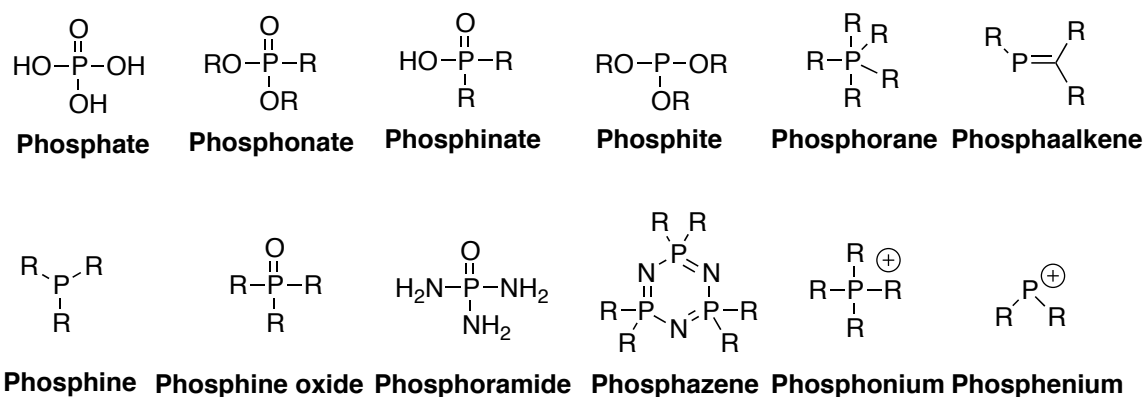


Figure 1-2: Various phosphorus functional groups and their structures.

This diversity is further exemplified by its capabilities to form stable bonds with a variety of elements such as hydrogen, carbon, oxygen, nitrogen, fluorine, sulphur, and most transition metals. While the chemistry of phosphorus has been explored extensively in small molecule science, it has yet to be equally explored for polymer applications. The simplest approach for classifying phosphorus-containing polymers is by the method via

which the polymer is synthesized, and the functionality surrounding the phosphorus atom, both of which contribute to the overall properties of the polymer.

1.2.3 Polymerizing phosphorus – Side chain

The term “side chain” refers to a scenario where the moiety in question is not present in the backbone of the polymer, in contrast to “main chain” polymers. One of the most widely used methods to incorporate phosphorus into the side chain of polymers is by free-radical polymerization of phosphorus-containing monomers bearing olefin functionality. This polymerization method is fast, tolerant to a wide variety of functional groups, and is easily scalable for commercial application. In the presence of a radical initiator, polymer is produced by sequential addition of monomer to the growing chain in a head-to-tail fashion. The most common functional groups used for this polymerization method are (meth)acrylates, (meth)acrylamides, vinyls, allyls, and styrenes.²⁵

Figure 1-3 shows a collection of phosphorus-containing monomers. The commonality between these monomers is the use of P(V) compounds, such as phosphates, phosphonates, phosphinates, or phosphonium salts. The stabilities of these functional groups makes their polymerization convenient as they can be treated and handled like any typical organic monomer.

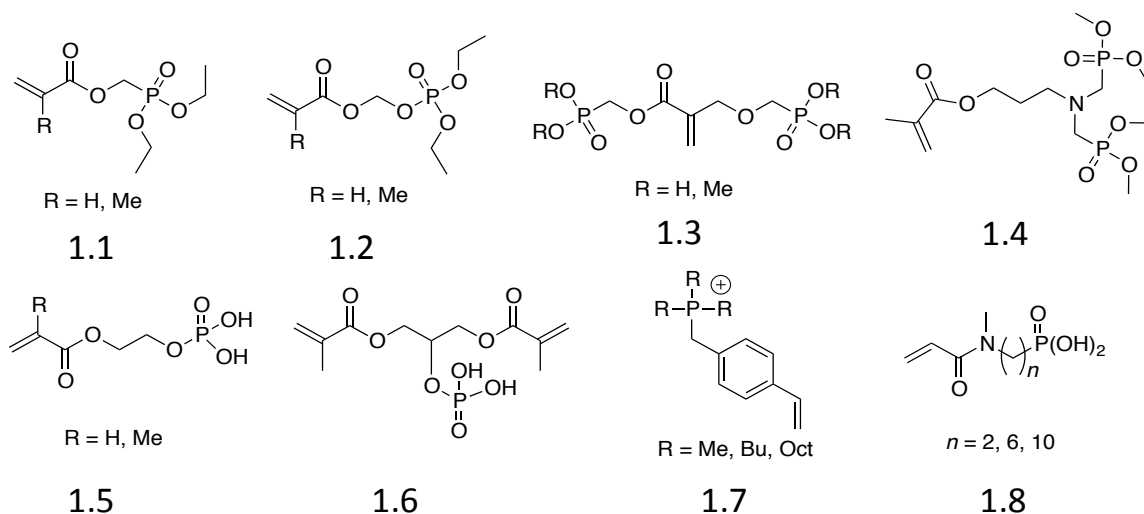


Figure 1-3: A selection of phosphorus-containing monomers polymerized by free-radical polymerization.

The flame retardant properties of phosphorus-containing polymers have long been known and are used in conjunction with or as alternatives to halogen-based systems.^{26,27} The mechanism resulting in flame retardancy is complex and is often material specific, however the presence of phosphorus promotes char formation and prevents the release of flammable gasses from the material. Often phosphorus-containing monomers are copolymerized with other organic molecules to design materials with the necessary mechanical and chemical properties. For example, a copolymer containing methyl methacrylate (MMA) and 10 mol% of **1.1** displayed flame retardant properties while retaining good mechanical strength.²⁸ Further investigations showed that the chemical structure surrounding the phosphorus atom plays a key role in material performance. Polystyrene (PS) copolymers containing phosphonate groups (**1.1**) displayed greater flame retardancy and retention of their physical and mechanical properties when compared to PS polymers containing phosphate groups (**1.2**).^{29,30} These approaches also apply to photopolymerized coatings containing bisphosphonates and bisphosphonic acids (**1.3** and **1.4**), which also impart good flame retardancy to the material, and even promotes adhesion and prevents corrosion on metal substrates.

Phosphorus-containing networks have also been examined for use in photopolymerized dental materials.²⁵ Upon polymerization, photopolymers undergo volumetric shrinkage resulting in cracks and delamination between the enamel and polymer, allowing liquids and bacteria to permeate through causing further complications. Phosphoric acid esters (**1.5**) are capable of decalcifying hydroxyapatite to create Ca^{2+} complexes, resulting in the formation of a microporous structure within the surface of the tooth. This porous structure allows the dental resin to mechanically bind to the tooth, preventing delamination. Phosphoric acid esters can also chemisorb, promoting adhesion through an additional mechanism. Another approach to prevent bacterial contamination within the dental cavity is by incorporating antimicrobial agents that counteract bacterial proliferation on the implant. Quaternary ammonium and phosphonium salts have long been known to kill bacteria by binding to and disrupting their cell membranes.³¹ A copolymer containing MMA, hydroxyethyl methacrylate (HEMA), and <3 mol% **1.6** has been shown to inhibit bacterial growth relative to control and ammonium-containing samples. The structure of the phosphonium salt also influences its antibacterial activity, with longer alkyl chains (Oct) showing greater efficacy when compared to shorter chains (Me, Bu).³¹ Phosphorus-containing acrylamides (**1.8**) have also been photopolymerized and were found to possess significantly increased resistance to hydrolysis under acidic conditions relative to their ester congeners.

1.2.4 Polymerizing phosphorus – Main chain

There are two methods by which main chain phosphorus polymers can be fabricated. Either phosphorus itself forms bonds to create the polymer, or external functional groups participate in the polymerization reaction. These methods may be performed in both step-growth or chain-growth fashion depending on the chemistry employed. Use of an external functionality to facilitate polymerization is often more convenient, as this approach exploits well-understood and scalable chemistry. Phosphorus-containing flame-retardant polyesters may be fabricated by adding phosphinic acids (**1.9** and **1.10**) to the synthesis process, and are marketed under the trade name Trevira CS™ used in fabrics (Figure 1-4).³²⁻³⁴ Polyamides and urethanes

containing bis(4-carboxyphenyl)phenylphosphine oxide (**1.11**) or phosphorus-containing diols (**1.12** and **1.13**) have also demonstrated flame retardancy while still retaining crystallinity.^{35,36} It was shown that phosphorus in the main chain improved flame retardancy relative to their side chain analogues, demonstrating how small changes in monomer architecture can influence performance.³⁷

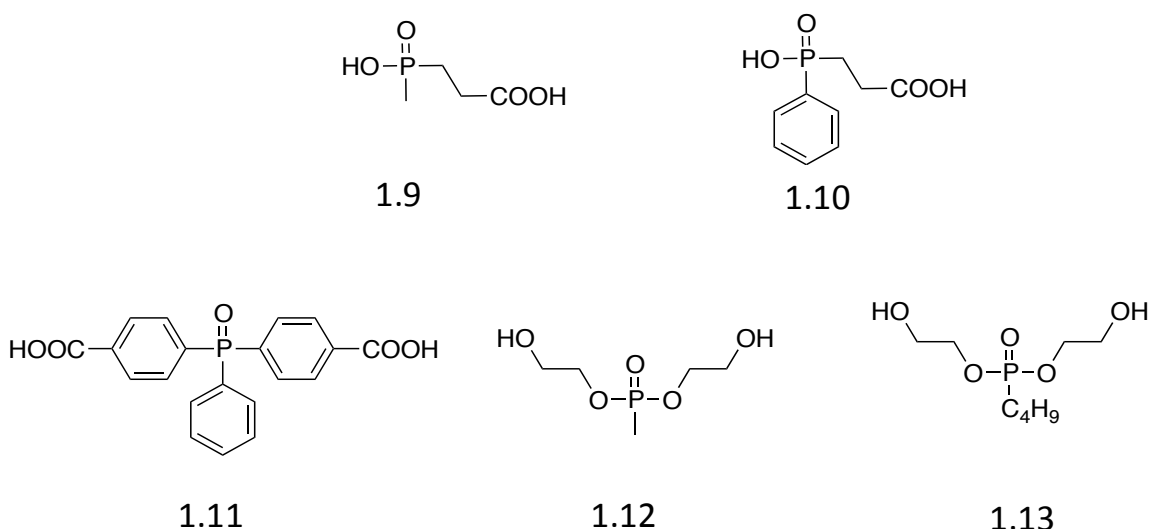


Figure 1-4: A selection of phosphorus-containing monomers used in flame-retardent PET, polyamide, and polyurethane production.

The utilization of phosphorus itself for the polymerization reaction is generally more difficult and less commonly performed. One well known class of main chain phosphorus-containing polymers are polyphosphazenes, which are among the most diverse inorganic polymers date with hundreds of varieties designed for applications in gas/liquid separations, ionic conductors, biotechnology, and other areas.¹⁰ The polymer was first prepared in 1897 by Stokes, however it was not until the 1960s that the synthetic protocols were developed to produce useful materials.³⁸ Typically hexachlorocyclotriphosphazene is subjected to ring-opening polymerization (ROP) with heat to create a linear polymer by an addition polymerization mechanism (Figure 1-5a). The key feature of polyphosphazenes is the exploitation of P-Cl functionality post polymerization using amines, alcohols, or alkoxides which often proceeds quantitatively to create a near limitless variety of polymeric systems.¹⁰ This approach harnesses

phosphorus chemistry to provide access to new materials that would otherwise be impossible using carbon based systems, highlighting the benefit of combining inorganic and polymer chemistry. More recently Gates *et al.* demonstrated that phosphalkenes (P=C) may undergo polymerization by anionic or free-radical polymerization (Figure 1-5b).^{39,40} This approach is analogous to the polymerization of C=C bonds typically performed using styrenes or (meth)acrylates and utilizes the chemistry of phosphorus to fabricate a new class of polymer. A combination of diphosphines and dibromides results in the formation of a polyelectrolyte (PE) containing phosphonium salts by a step-growth process (Figure 1-5c). These are referred to as phosphonium ionenes and have greater chemical and thermal stability than their side chain counterparts.⁴¹

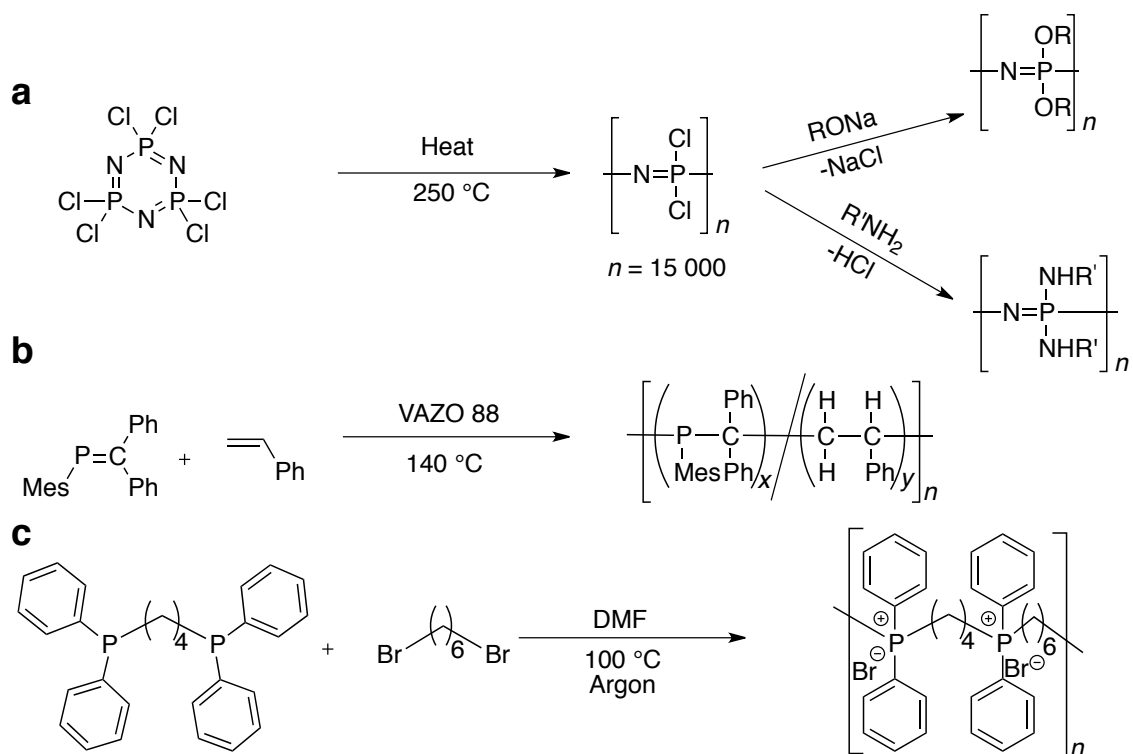


Figure 1-5: Examples using phosphorus for the polymerization reaction, including a) Phosphazenes b) Phosphaalkenes c) Phosphines.

1.3 Photopolymerization

Photopolymerization is a process in which polymer is formed upon exposure to light. From a practical standpoint, this material fabrication process is attractive as it simply involves the exposure of liquid monomer and photoinitiator to light, and polymer is made. This feature opens new possibilities for polymeric materials not possible using heat.

1.3.1 Background

The earliest recorded instance of photopolymerization (also called UV-curing) dates back to the ancient Egyptians who used sunlight to prepare linens for mummification.⁴² Today however, modern science has combined photochemistry and polymers to produce materials that have fundamentally altered human society. For example, the Information Age would not be possible without the integrated circuit found in all electronic devices, whose manufacture relies on photolithography, a process where polymers are patterned using light. Other products that utilize photopolymerization include optical fibers,⁴³ lenses,^{44,45} microfluidic devices,^{46,47} coatings,^{48,49} and dental resins.⁵⁰

Photopolymer science is distinct from traditional polymer science both in approach and application. Photopolymer science focuses on crosslinked polymer networks (referred to as thermosets, or simply “networks”) almost exclusively, which do not dissolve or melt, while traditional approaches utilize linear polymers (referred to as thermoplastics) that dissolve and can be manipulated/handled after fabrication. While these differences may appear superficial, in practice they are very different, starting from the monomers used to the final application. Unlike homopolymers, crosslinked polymers cannot undergo post processing (such as solvent casting, molding, or extrusion), limiting some of their applications while expanding into others (coatings, photoresists, and 3D printing to name a few). Networks may be created with heat (referred to as thermal curing), although using light has some specific advantages. Light is cheaper, uses less energy, requires less space, can be performed at room temperature, is faster, and can be controlled both in time and space.⁵¹ To fabricate a photopolymer network, a substrate or

mold is coated/filled with liquid monomer (also known as “resin”, usually containing no solvent), followed by irradiation with UV-light to induce hardening. The convenience of this technique has prompted its widespread use in coatings fabrication, often replacing thermal methods in recent years. Photopolymer coatings can be applied to metal, wood, glass, and even heat sensitive substrates like plastic and paper. Depending on the formulation, they can prevent weathering, provide impact or chemical resistance, and even prevent corrosion.^{52,53}

More elaborate techniques have been developed thanks to the use of lasers and optics, further expanding the influence of the photopolymerization method. Stereolithography is a 3D printing technique comprised of a pool of monomer on a moveable stage and a scanning laser (Figure 1-6a).⁵⁴ First, a cross section of the product (~0.05 mm) is polymerized on the stage using the laser, and then the stage is lowered by a distance equal to the layer thickness. The polymerized layer is then coated with fresh liquid monomer, and the laser once more polymerizes a cross section of the product, bonding the previous underlying layer to the new one. This process is repeated until the object is complete, at which point it is rinsed to remove excess resin. This approach is mostly used for prototype fabrication and serves as a quick method to create master patterns for injection molding and for biomedical device fabrication.^{55,56} Two-photon polymerization is another 3D printing technique, where polymerization in a pool of resin only occurs when two light beams intersect (Figure 1-6b).^{57,58} The great advantage of this technique is the ability to create complex micron-scale objects with very high-resolution (~100 nm), greater than the diffraction limit of light and is often used to fabricate microprisms and diffractive optical elements. Finally, lattice structures have been produced using collimated light, creating a crosshatch pattern in a pool of monomer (Figure 1-6c).⁵⁹ The resulting polymer acts as a waveguide, focusing the incoming light deeper into the solution to produce structures ~1 cm in length. Dissolution of the unpolymerized materials reveals the lattice structure whose dimensions can be altered simply by adjusting the angle and thickness of the incident light beam. This fabrication method provided entry to the production of metallic lattices that are among the lightest materials ever made and possess shape retention upon deformation. These few examples

demonstrate the versatility and power of the photopolymerization method and how its importance goes beyond polymer science alone.

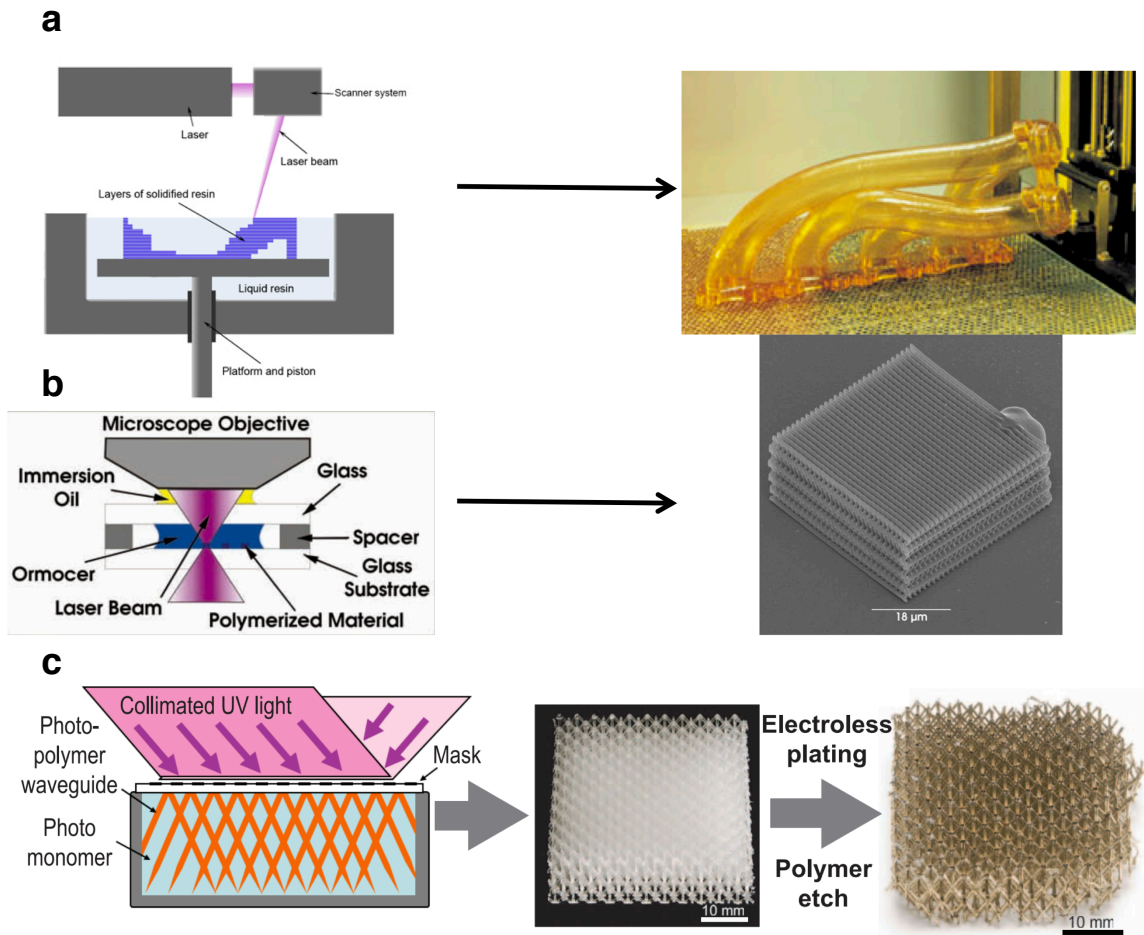


Figure 1-6: Three-dimensional photopolymerization methods, including a) Stereolithography b) Two-photon polymerization and c) Lattice photopolymerization.

1.3.2 Photopolymerization Chemistry

The photopolymerization process begins with initiation of the growing chains, followed by propagation and termination. Most photopolymeric systems contain a mixture of photoinitiator (PI), monomer, and crosslinking agent that react to form a network. The only difference between thermal and photochemical polymerization is in the initiation step, after which the propagation and termination mechanisms are identical.

Unlike homopolymers, which are simply linear chains, networks are formed when those chains are linked together using multi-functional monomers, or through a crosslinking step post polymerization (Figure 1-7).

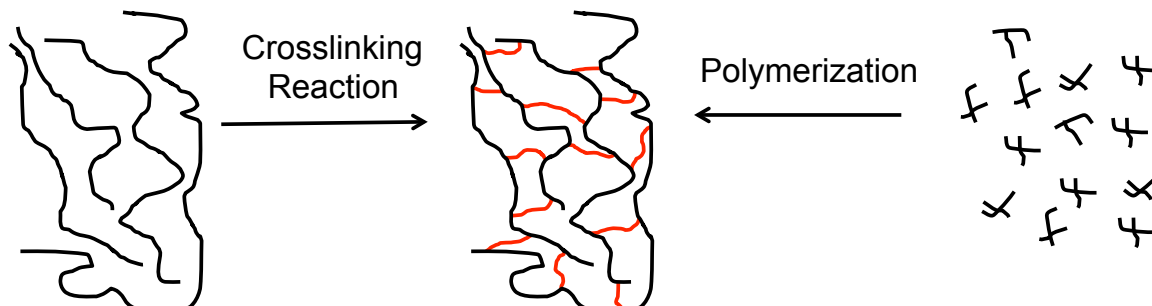


Figure 1-7: Schematic representation of polymer network synthesis by direct polymerization of multifunctional monomers (right) or crosslinking of linear chains (left).

The properties of a polymer network depend not only on chemical functionality, but also the network architecture. Certain factors such as the number and molecular composition of crosslinks between chains, homogeneity, and length, can influence the swellability, moduli, chemistry, and glass transition of the polymer. Loosely crosslinked photopolymers (referred to as gels) are highly swellable in either water (hydrogels) or organic solvents (organogels) and are used in tissue engineering, lenses, and batteries.^{45,54,60} As one would expect, networks composed of hydrophilic monomers swell in polar solvents, while networks comprised hydrophobic monomers swell in non-polar solvents. Photopolymer networks with high crosslink densities are typically much firmer, less swellable, and are used as coatings, dental implants, and photoresists.⁶¹⁻⁶³ The difference in mechanical and chemical properties between networks with differing crosslink densities arises from the ability (or inability) of the polymer chains to move past one another. This diversity in network design allows for the production of many types of materials exhibiting vastly different properties to be exploited.

1.3.3 Photoinitiation

Monomers themselves are not photoactive and thus require the presence of a photosensitive compound that will absorb and transfer the incoming light energy (photoinitiator, Figure 1-8).

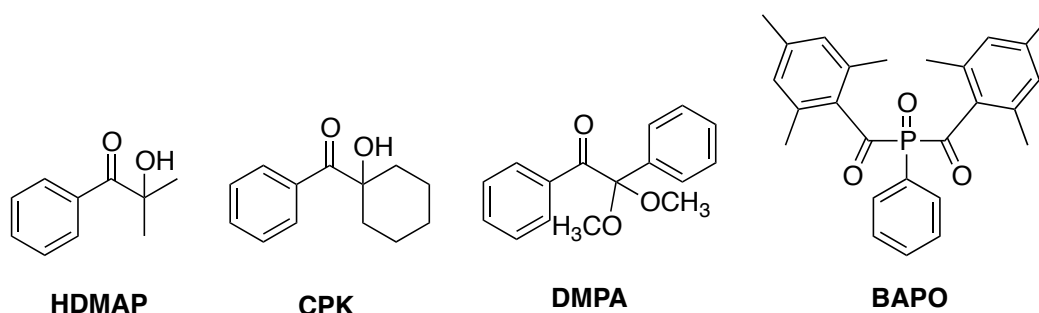


Figure 1-8: Common photoinitiators (PIs) and their trademark abbreviations used for free-radical polymerization.

These molecules decompose upon exposure to light, producing products that begin the polymerization process. Olefin-containing monomers comprise the majority of photopolymer systems and can be polymerized using either cationic or free-radical photoinitiators. Sulfonium or iodonium salts are the most common cationic PIs and result in the formation of a strong acid upon UV exposure. This initiates the addition-polymerization of electron-rich olefins where the propagating species possesses a cationic charge. Free-radical photopolymerization of electron-poor olefins (such as styrene and acrylates) however is much more common and will be of greater focus in this thesis. Initiators based on acetophenone structures are the most common and absorb in the UV spectrum, while bisacylphosphine oxides (BAPO) are also used and absorb well into the visible range. Unlike thermal systems, the limiting factor for photoinitiation is the ability of light to penetrate the monomer solution to generate a sufficient number of radicals, thus making photopolymerization difficult for systems greater than a few millimeters in depth. This phenomenon is best explained by the photoinitiation rate, R_i , given by the expression

$$R_i = 2f\Phi\epsilon[I]I_0$$

where the light intensity $[I]$ and initiator concentration I_0 depend on the location within the liquid film, while the molar absorptivity (ϵ), efficiency (f), and quantum yield (Φ) are PI specific. As the intensity of light or PI concentration drops, so too does the rate of initiation. This process is further complicated for highly coloured systems that absorb or scatter UV light, often encountered in the printing industry. In these cases, very thin

layers are used in conjunction with highly tailored, and often proprietary photoinitiator/sensitizer mixtures that promote “through cure” of the film in addition to “surface cure”. The use of bisacylphosphine oxides (BAPO) PIs represents an improvement in “through cure” as it absorbs light over a wider spectral range, and generates four radicals instead of two observed for acetophenone based systems allowing for its use at lower concentrations.

1.3.4 Propagation, Termination, and Inhibition

Once primary radicals are formed, they react with double bonds to begin the polymerization process. A single radical may promote thousands of bond-forming reactions prior to its termination, occurring faster than most typical step-growth polymerization processes. Multifunctional monomers (monomers capable of forming >2 chemical bonds) within the mixture induce crosslinking between polymer chains to create insoluble networks.

Polymer network growth is a complicated process associated with drastic changes in both material properties and reaction conditions during the course of polymerization.⁵¹ Within a few seconds, a low-viscosity liquid is converted into a hard glassy solid, leading to difficulties in understanding diffusion controlled reactions, temperature, light, and concentration gradients. These factors influence heterogeneities in crosslink density throughout the material and is strongly affected by the experimental conditions under which the material is polymerized.⁵¹ An in depth discussion about the kinetics and diffusion controlled reactions during photopolymerization are beyond the scope of this thesis, however the entire process can be simplified into three different stages (Figure 1-9). First, primary radicals are formed from the PI, which are dispersed throughout the monomer matrix (a). At this stage, polymerization rates are very high because of the abundance of monomer and very low viscosity, leading to the formation of micron-sized polymer network “islands” (or micro gels) surrounded by an ocean of monomer (b). Eventually these domains begin to grow outwards, consuming monomer until each domain meets and bonds with its neighbour, at which point the material begins to gel (c). The gel point is the transition between a liquid and a solid and can be defined as the stage when the molecular mass of the polymer approaches infinity. An inversion begins to

occur as this time, and crosslinked polymer network now surrounds small ponds of unreacted monomer. Left over monomer is common with this polymerization technique as high viscosities and low monomer concentration promotes termination sequences through recombination or chain-transfer. Radicals trapped in highly crosslinked regions may terminate the polymerization process where they remain stable for months to years at a time, unable to react with a nearby olefin.

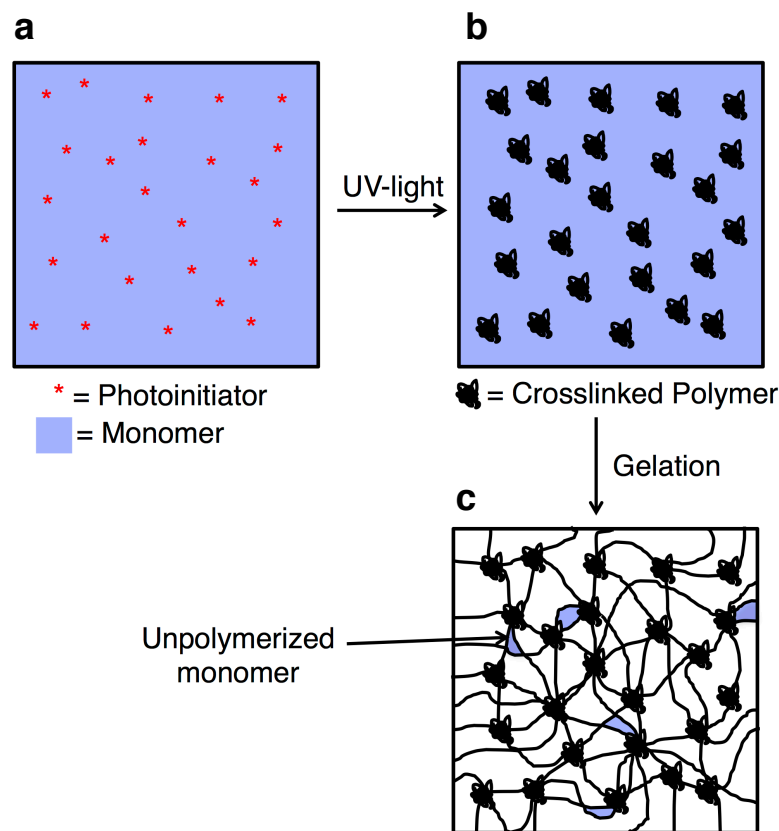


Figure 1-9: a) Photoinitiator is first dissolved in monomer. b) Upon irradiation, photoinitiators cleave to create micron-sized polymer networks. c) Upon gelation, a large polymer network system is formed with some leftover monomer.

The atmosphere in which this chemistry is performed also influences network growth and can affect material properties. Oxygen is the most pervasive inhibitor in free-radical polymerization and is always removed in traditional polymer synthesis, but often

this is not an option in photopolymeric systems for practical reasons. Molecular oxygen reacts with the propagating radical to form a peroxy species that terminates the polymerization process.^{64,65} Upon formation of the primary radicals and during the first stages of polymerization, dissolved oxygen inhibits polymer growth until it has been consumed, after which polymerization proceeds efficiently. At the surface of the liquid monomer film (~10 μm), consumed oxygen is readily replaced by the atmosphere through diffusion, hindering the polymerization process. Further within the liquid film however oxygen is unable to diffuse on a reasonable time scale to compromise the system.

1.4 Scope of the Thesis

This dissertation focuses on applying phosphorus chemistry with photopolymer science to generate new materials and on examining their properties and potential applications. While these two fields are well established on their own, little attention has been given to their synergy and the new materials that could be produced. The goal was to establish new methodologies for the incorporation of phosphorus into photopolymers, while simultaneously highlighting the unique attributes imbued to the material through this approach. Chapter two will focus on the synthesis of highly fluorinated polymerizable phosphonium salts and their surface modifying behaviour in UV-cured films. Structure-activity relationships between the phosphonium monomers and their performance were established, and provided insight into fabricating cationic hydrophobic surfaces. Chapter three describes a high-throughput method to create photopolymerized phosphonium PEs capable of undergoing anion-exchange. This chemistry was exploited to immobilize anion gold nanoclusters in the solid-state, which retain their sensitive chemical and optical properties upon immobilization. Chapter four further explores polyelectrolyte fabrication through the synthesis of a self-crosslinking phosphonium salt. This new class of monomer was capable of increasing charge density and hardness simultaneously in photopolymerized materials, and was then patterned using anion-exchange chemistry. Chapter five expands on the utility of anion-exchange chemistry in photopolymerized phosphonium films as a method to both synthesize and immobilize gold nanoparticles (AuNP). Chapter six describes a new polymerization

method using air-stable phosphines as monomers. Lending perspectives from thiol-ene “click” chemistry, air-stable phosphines were viewed as potential monomers for polymerization with olefins. The resulting materials exhibited a wide variety of chemical and physical properties that were exploited in oxygen scavenging, solid-supported organophosphorus chemistry, and others.

References

- (1) Charles Marie de La Condamine. *A succinct abridgement of a Voyage made within the inland Parts of South America, from the Coasts of the South-Sea, to the Coasts of Brazil and Guiana, down the River of Amazons: as it was read in the Public Assembly of the Academy of Sciences at Paris*; E. Withers, at the Seven Stars.: London, 1747.
- (2) Kauffman, G. B.; Seymour, R. B. *J. Chem. Educ.* **1990**, *67*, 422.
- (3) American Chemical Society National Historic Chemical Landmarks. U.S. Synthetic Rubber Program.
<http://www.acs.org/content/acs/en/education/whatischemistry/landmarks/syntheticrubber.html#early-synthetic-rubber-research> (accessed Sep 16, 2014).
- (4) Smith, J. K. *Technol. Cult.* **1985**, *26*, 34.
- (5) Seymour, R. B.; Carraher, C. E. *Structure-Property Relationships in Polymers*; Plenum Press: New York, 1984.
- (6) Ahmed, F.; Photos, P. J.; Discher, D. E. *Drug Dev. Res.* **2006**, *67*, 4.
- (7) Palmer, R. J. In *Encyclopedia of Polymer Science and Technology*; John Wiley & Sons, Inc., 2002.
- (8) Dobrynin, A. V; Rubinstein, M. *Prog. Polym. Sci.* **2005**, *30*, 1049.
- (9) Hunt, J. N.; Feldman, K. E.; Lynd, N. A.; Deek, J.; Campos, L. M.; Spruell, J. M.; Hernandez, B. M.; Kramer, E. J.; Hawker, C. J. *Adv. Mater.* **2011**, *23*, 2327.
- (10) Mark, J. E.; Allcock, H. R.; Wester, R. *Inorganic Polymers*; Second, Ed.; Oxford University Press, 2005; pp. 3–50.
- (11) Foucher, D. A.; Tang, B. Z.; Manners, I. *J. Am. Chem. Soc.* **1992**, *114*, 6246.
- (12) Arsenault, A. C.; Puzzo, D. P.; Manners, I.; Ozin, G. A. *Nat. Photonics* **2007**, *1*, 468.

- (13) Hilado, C. J.; Schneider, J. E.; Brauer, D. P. *J. Combust. Toxicol.* **1979**, *6*, 109.
- (14) Yousif, E.; Haddad, R. *Springerplus* **2013**, *2*, 398.
- (15) Buch, R.; Hamins, A.; Konishi, K.; Mattingly, D.; Kashiwagi, T. *Combust. Flame* **1997**, *108*, 118.
- (16) Implants, I. of M. (US) C. on the S. of S. B.; Bondurant, S.; Ernster, V.; Herdman, R. *Silicone Toxicology*, 1999.
- (17) Xu, S.; Lehmann, R. G.; Miller, J. R.; Chandra, G. *Environ. Sci. Technol.* **1998**, *32*, 1199.
- (18) Lukevics, E.; Pudova, O.; Sturkovich, R. *Molecular Structure of Organosilicon Compounds.*; Wiley: New York, 1989.
- (19) Lin, W.-C.; Marcellan, A.; Hourdet, D.; Creton, C. *Soft Matter* **2011**, *7*, 6578.
- (20) Gilman, J. *Appl. Clay Sci.* **1999**, *15*, 31.
- (21) Priolo, M. a; Gamboa, D.; Holder, K. M.; Grunlan, J. C. *Nano Lett.* **2010**, 4970.
- (22) Letierrier, Y.; Singh, B.; Bouchet, J.; Månson, J. -a. E.; Rochat, G.; Fayet, P. *Surf. Coatings Technol.* **2009**, *203*, 3398.
- (23) Monge, S.; Canniccioni, B.; Graillot, A.; Robin, J.-J. *Biomacromolecules* **2011**, *12*, 1973.
- (24) Blanzat, M.; Turrin, C.-O.; Perez, E.; Rico-Lattes, I.; Caminade, A.-M.; Majoral, J.-P. *Chem. Commun.* **2002**, 1864.
- (25) Monge, S.; Dacid, G. *Phosphorus-Based Polymers: From Synthesis to Applications*; The Royal Society of Chemistry: Cambridge, 2014.
- (26) Mey-Marom, A.; Behar, D. *J. Appl. Polym. Sci.* **1980**, *25*, 691.
- (27) Granzow, A.; Savides, C. *J. Appl. Polym. Sci.* **1980**, *25*, 2195.
- (28) Ebdon, J. R.; Hunt, B. J.; Joseph, P.; Konkel, C. S.; Price, D.; Pyrah, K.; Hull, T. R.; Milnes, G. J.; Hill, S. B.; Lindsay, C. I.; McCluskey, J.; Robinson, I. *Polym. Degrad. Stab.* **2000**, *70*, 425.
- (29) Price, D.; Bullett, K. J.; Cunliffe, L. K.; Hull, T. R.; Milnes, G. J.; Ebdon, J. R.; Hunt, B. J.; Joseph, P. *Polym. Degrad. Stab.* **2005**, *88*, 74.
- (30) Price, D.; Cunliffe, L. K.; Bullet, K. J.; Hull, T. R.; Milnes, G. J.; Ebdon, J. R.; Hunt, B. J.; Joseph, P. *Polym. Adv. Technol.* **2008**, *19*, 710.

- (31) Kanazawa, A.; Ikeda, T.; Endo, T. *J. Polym. Sci. Part A Polym. Chem.* **1993**, *31*, 335.
- (32) Wu, B.; Wang, Y.-Z.; Wang, X.-L.; Yang, K.-K.; Jin, Y.-D.; Zhao, H. *Polym. Degrad. Stab.* **2002**, *76*, 401.
- (33) Asrar, J.; Berger, P. A.; Hurlbut, J. *J. Polym. Sci. Part A Polym. Chem.* **1999**, *37*, 3119.
- (34) Joseph, P.; Tretsiakova-Mcnally, S. *Polym. Adv. Technol.* **2011**, *22*, 395.
- (35) Wan, I. Y.; McGrath, J. E. *ACS Symp. Ser.* **1995**, *29*.
- (36) Wilkie, C. A.; Morgan, A. B. *Fire Retardancy of Polymeric Materials*; Taylor & Francis Group: Boca Raton, 2010; pp. 107–127.
- (37) Wang, T.-L.; Cho, Y.-L.; Kuo, P.-L. *J. Appl. Polym. Sci.* **2001**, *82*, 343.
- (38) Allcock, H. R.; Kugel, R. L. *J. Am. Chem. Soc.* **1965**, *87*, 4216.
- (39) Tsang, C.-W.; Yam, M.; Gates, D. P. *J. Am. Chem. Soc.* **2003**, *125*, 1480.
- (40) Noonan, K. J. T.; Gates, D. P. *Angew. Chem. Int. Ed. Engl.* **2006**, *45*, 7271.
- (41) Hemp, S. T.; Zhang, M.; Tamami, M.; Long, T. E. *Polym. Chem.* **2013**, *4*, 3582.
- (42) Decker, C. *J. Coating. Technol.* **1987**, *97*.
- (43) Paek, U. C.; Schroeder, C. M. *Appl. Opt.* **1981**, *20*, 1230.
- (44) WICHTERLE, O.; LÍM, D. *Nature* **1960**, *185*, 117.
- (45) Zwiers, R. J.; Dortant, G. C. *Appl. Opt.* **1985**, *24*, 4483.
- (46) Hutchison, J. B.; Haraldsson, K. T.; Good, B. T.; Sebra, R. P.; Luo, N.; Anseth, K. S.; Bowman, C. N. *Lab Chip* **2004**, *4*, 658.
- (47) Beebe, D.; Moore, J.; Bauer, J.; Yu, Q.; Liu, R.; Devadoss, C.; Jo, B. *Nature* **2000**, *404*, 588.
- (48) Kim, H. K.; Ju, H. T.; Hong, J. W. *Eur. Polym. J.* **2003**, *39*, 2235.
- (49) Miao, H.; Cheng, L.; Shi, W. *Prog. Org. Coatings* **2009**, *65*, 71.
- (50) Cramer, N. B.; Couch, C. L.; Schreck, K. M.; Carioscia, J. A.; Boulden, J. E.; Stansbury, J. W.; Bowman, C. N. *Dent. Mater.* **2010**, *26*, 21.
- (51) Bowman, C. N.; Kloxin, C. J. *AIChE J.* **2008**, *54*.
- (52) Decker, C.; Masson, F.; Schwalm, R. *Polym. Degrad. Stab.* **2004**, *83*, 309.
- (53) Malucelli, G.; Di Gianni, A.; Deflorian, F.; Fedel, M.; Bongiovanni, R. *Corros. Sci.* **2009**, *51*, 1762.

- (54) Melchels, F. P. W.; Feijen, J.; Grijpma, D. W. *Biomaterials* **2010**, *31*, 6121.
- (55) D'Urso, P. S.; Earwaker, W. J.; Barker, T. M.; Redmond, M. J.; Thompson, R. G.; Effeney, D. J.; Tomlinson, F. H. *Br. J. Plast. Surg.* **2000**, *53*, 200.
- (56) Cooke, M. N.; Fisher, J. P.; Dean, D.; Rinnac, C.; Mikos, A. G. *J. Biomed. Mater. Res. - Part B Appl. Biomater.* **2003**, *64*, 65.
- (57) Ostendorf, A.; Chichkov, B. N.; Hannover, Z. *Photonics Spectra*. 2006,.
- (58) Kawata, S.; Sun, H. B.; Tanaka, T.; Takada, K. *Nature* **2001**, *412*, 697.
- (59) Schaedler, T. A.; Jacobsen, A. J.; Torrents, A.; Sorensen, A. E.; Lian, J.; Greer, J. R.; Valdevit, L.; Carter, W. B. *Science* **2011**, *334*, 962.
- (60) Song, M.-K.; Cho, J.-Y.; Cho, B. W.; Rhee, H.-W. *J. Power Sources* **2002**, *110*, 209.
- (61) Seo, J.; Jang, E.; Song, J.; Choi, S.; Khan, S. B.; Han, H. **2010**.
- (62) He, J.; Söderling, E.; Lassila, L. V. J.; Vallittu, P. K. *Dent. Mater.* **2012**, *28*, e110.
- (63) Revzin, a; Russell, R. J.; Yadavalli, V. K.; Koh, W. G.; Deister, C.; Hile, D. D.; Mellott, M. B.; Pishko, M. V. *Langmuir* **2001**, *17*, 5440.
- (64) Belon, C.; Allonas, X.; Croutxé-barghorn, C.; Lalevée, J. *J. Polym. Sci. Part A Polym. Chem.* **2010**, *48*, 2462.
- (65) O'Brien, A. K.; Bowman, C. N. *Macromol. Theory Simulations* **2006**, *15*, 176.

Chapter 2

2 Fluorinated polymerizable phosphonium salts from PH_3 : Surface properties of photopolymerized films

2.1 Introduction

The increase in popularity of photopolymerization over the past several decades has given rise to new functional materials in various fields of polymer science, from applications in biomaterials to the construction of 3D microstructures.^{1,2} The breadth of new monomers, oligomers, and additives used in industry and academia is a consequence of this expansion, and the possible applications for photopolymerization are simply limited by the feedstocks available. There exists an expanding niche within this area for more exotic molecules that can only be filled by modern research in synthetic chemistry.

Phosphonium salts are a class of molecules with highly tunable properties that have been used in polymer science.³⁻⁷ By manipulating the molecular architecture around the phosphonium centre, both the physical and chemical properties can be varied. Our research focus in this context includes chemical functionality of the phosphonium cation for hydrophobic performance, and synthetic tunability of the counter anion to alter material hardness.^{8,9} Recently, there has been a growing interest in using phosphonium salts in polymerizable systems. This includes the work of Gin and Long who have demonstrated the use of the phosphonium scaffold for various applications.¹⁰⁻¹³ Much of the work of Long *et al.* in this context is based on thermal polymerization methodologies with the synthesis of various phosphonium homopolymers and copolymers. We are interested in applying similar monomers to polymer networks synthesized using photoinitiated processes.⁹ Despite the rich chemistry of phosphorus and ease with which it can be manipulated, the utility of the polymerizable phosphonium salt has not been widely exploited within photopolymer applications.¹⁰

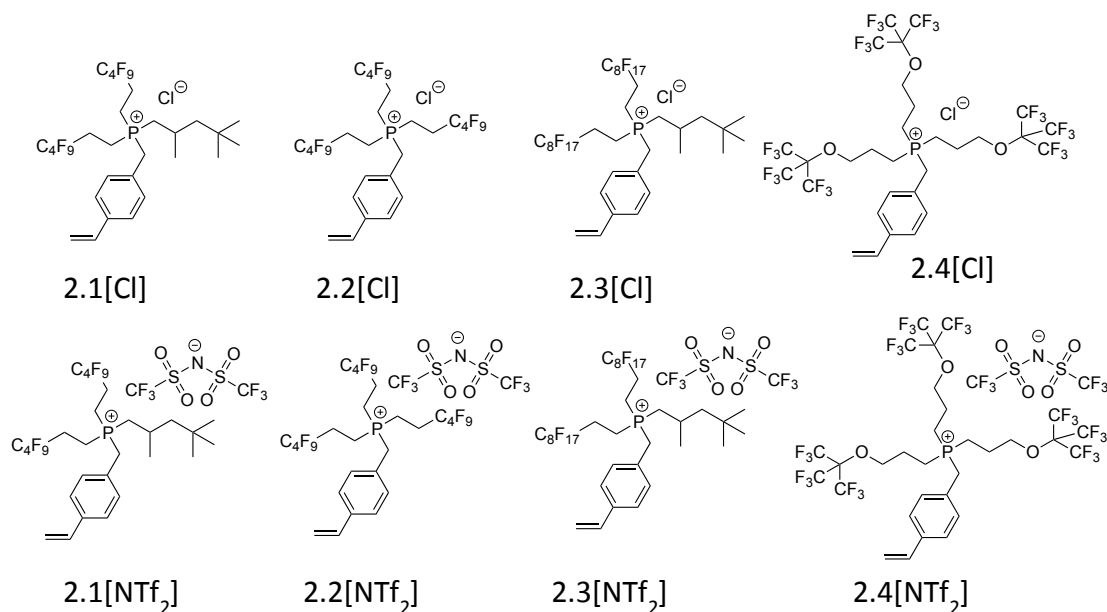


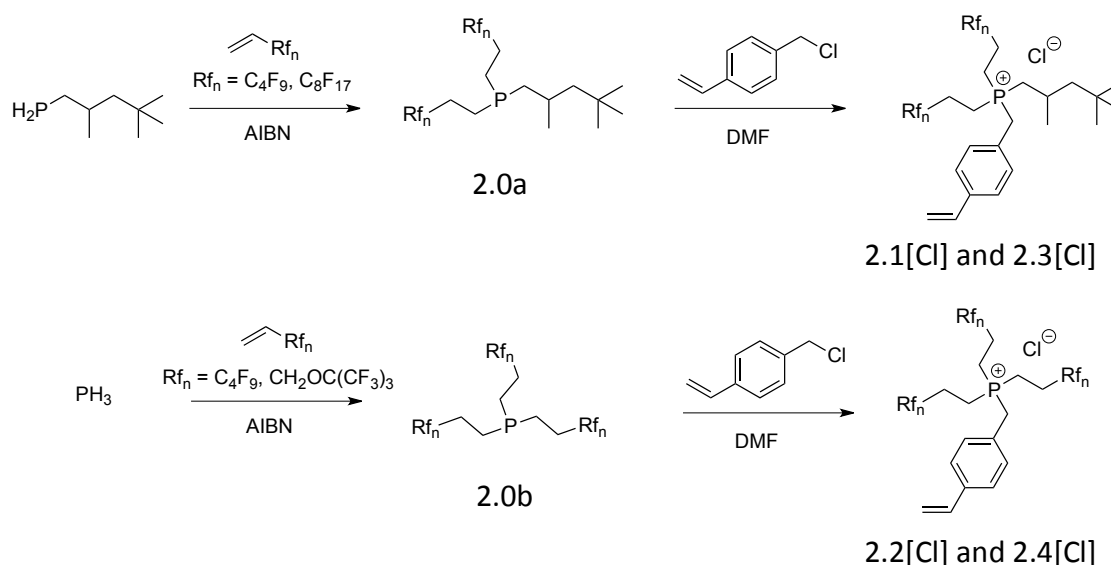
Figure 2-1: All HFPS synthesized in this study for applications in photopolymerizable systems.

Ionic materials in general have been used in UV-cured systems and possess some noteworthy applications. For example, inorganic salts infused into photopolymers have been used for the purpose of fabricating electrically conductive coatings.¹⁴ Organic salts have been shown to assist in the dispersion of charged particles.¹⁵⁻¹⁷ Despite these previous examples, there have been no reports of surface modification using phosphonium salts within the UV-curing field. Previous work from our group demonstrated that a monolayer of thiol-appended, fluorinated phosphonium salts on roughened metal surfaces exhibited excellent water repellency with water contact angles of up to 168°. These proof-of-concept experiments demonstrated that the phosphonium ion scaffold could be used to generate coatings with poor wettability when functionalized with fluorocarbon appendages.¹⁸ On the downside, these films were highly delicate and any physical contact with the surface resulted in a complete loss of performance. One solution to address film resiliency was to incorporate polymerizable groups onto the phosphorus centre in place of a thiol (Figure 2-1). Such functionality would allow for the incorporation of phosphonium salts into photopolymerizable systems to afford durable

films while ideally maintaining hydrophobic character. The tunable nature of phosphonium chemistry also allows for a wide array of different cations, each with uniquely different physical and chemical properties. Such control highlights this class of molecule as a potential candidate for wide applications in photopolymerization technologies where such regulation is critical. As polymerizable fluorocarbons are already being used in photopolymer systems, there may be room for improvement through varying molecular architecture of the active species.¹⁹⁻²¹ In this context, we demonstrate the incredible variety and tailorability of phosphonium salts for the surface modification of photopolymerizable systems. Depending on the substitution around the phosphonium core and anion size/composition, the surface wettability can be drastically altered.

2.1.1 Synthesis

Phosphonium salts **2.1[Cl]** and **2.3[Cl]** were synthesized from the commercially available isooctyl primary phosphine while **2.2[Cl]** and **2.3[Cl]** required a pressurized PH_3 reactor (Scheme 2-1, See Chapter 2 appendix for NMR spectra). Phosphine gas is a pyrophoric substance and was manipulated with a custom built pressure-manifold. Our interest in utilizing PH_3 as a starting material stems from its availability in industrial chemical manufacturing and its unique chemistry. In the presence of an olefin and a radical source (AIBN), both PH_3 and primary phosphines were converted to the corresponding tertiary phosphine in one step.²²



Scheme 2-1: Synthetic route for the synthesis of fluororous phosphonium salts.

A wide variety of tertiary phosphines can be synthesized, and the functional groups can be pre-selected by simply changing the olefin. This work focuses on the synthesis of fluororous phosphines and changing the architecture of the perfluoroalkyl appendage (via the olefin).²³ Reaction progress was monitored by $^{31}\text{P}\{^1\text{H}\}$ NMR spectroscopy and deemed complete upon $\sim 90\%$ conversion to the final product. Formation of the quaternary phosphonium salts proceeded through the $\text{S}_{\text{N}}2$ reaction of a fluororous phosphine ($\text{P}(\text{CH}_2\text{CH}_2\text{Rf}_n)_3$, $\text{Rf}_n = \text{Rf}_4 = \text{C}_4\text{F}_9$ **2.2[Cl]**; $\text{Rf}_n = \text{CH}_2\text{OC}(\text{CF}_3)_3$ **2.4[Cl]**; $\text{R}'\text{P}(\text{CH}_2\text{CH}_2\text{Rf}_n)_2$, $\text{R}' = \text{C}_8\text{H}_{17}$, $\text{Rf}_n = \text{C}_4\text{F}_9$ **2.1[Cl]**; $\text{R}' = \text{C}_8\text{H}_{17}$, $\text{Rf}_n = \text{C}_8\text{F}_{17}$ **2.3[Cl]** ($\delta_{\text{p}} = -40$ to -30 ppm) with a stoichiometric excess of 4-vinylbenzyl chloride at elevated temperature (*ca.* 80°C), providing a broad scope of monomers. Reaction progress was monitored by $^{31}\text{P}\{^1\text{H}\}$ NMR spectroscopy, and deemed complete when a new singlet ($\delta_{\text{p}} = 30$ - 40 ppm) was observed to be at a maximum. Upon work up of the reaction mixture, fluorinated phosphonium salts were isolated in 55-70% yield. Anion-exchange reactions were performed via salt-metathesis of **2.1-2.4[Cl]** with a stoichiometric excess of lithium bis((trifluoromethyl)sulfonyl)imide (LiNTf_2) at room temperature for 24 hours. Ion exchange reaction mixtures were extracted using distilled

water to remove the inorganic salt by-product, then volatiles were removed from the organic fraction to isolate the phosphonium bistriflamide salts in approximately 50% isolated yield.

The number and architecture of perfluoroalkyl groups were varied in order to ascertain a structure-property relationship to reveal the optimum monomer design for achieving a maximized hydrophobicity in the UV cured polymer films. It was additionally important to achieve sufficient water repellency with short perfluoroalkyl groups (i.e. C₄F₉), as it is well established that \geq C₆F₁₃ products have been restricted by the US-EPA due to their environmental persistence.²⁴ The C₈F₁₇ HFPPS monomer was included in our array to provide a benchmark performance indicator, as it is well known that fluoropolymers containing C₈F₁₇ perfluoroalkyl chains exhibit excellent hydrophobicity as a result of the organization of neighbouring C₈F₁₇ chains.²⁵

Given that the constituent surface tension of the CF₃ group (15 mN/m) is lower than the CF₂ group (23 mN/m) we wanted to design a monomer that maximizes the number of CF₃ moieties at the surface.²⁶ The solution would be to change the fluoruous tail architecture from a straight-chain C₄F₉ to a branched C₄F₉, thus increasing the CF₃ groups to 3 per arm. Starting from perfluoro-tert-butanol we successfully synthesized the desired phosphonium salt **2.4**⁺, which contained 9-CF₃ units in the cation compared to 2-CF₃ units for monomer **2.1**⁺/**2.3**⁺ and 3-CF₃ units for monomer **2.2**⁺ (Figure 2-1).

2.1.2 HFPPS Physical and Chemical Properties

In an effort to fully characterize these unconventional monomers, the solubilities of all compounds were evaluated (Figure 2-2).

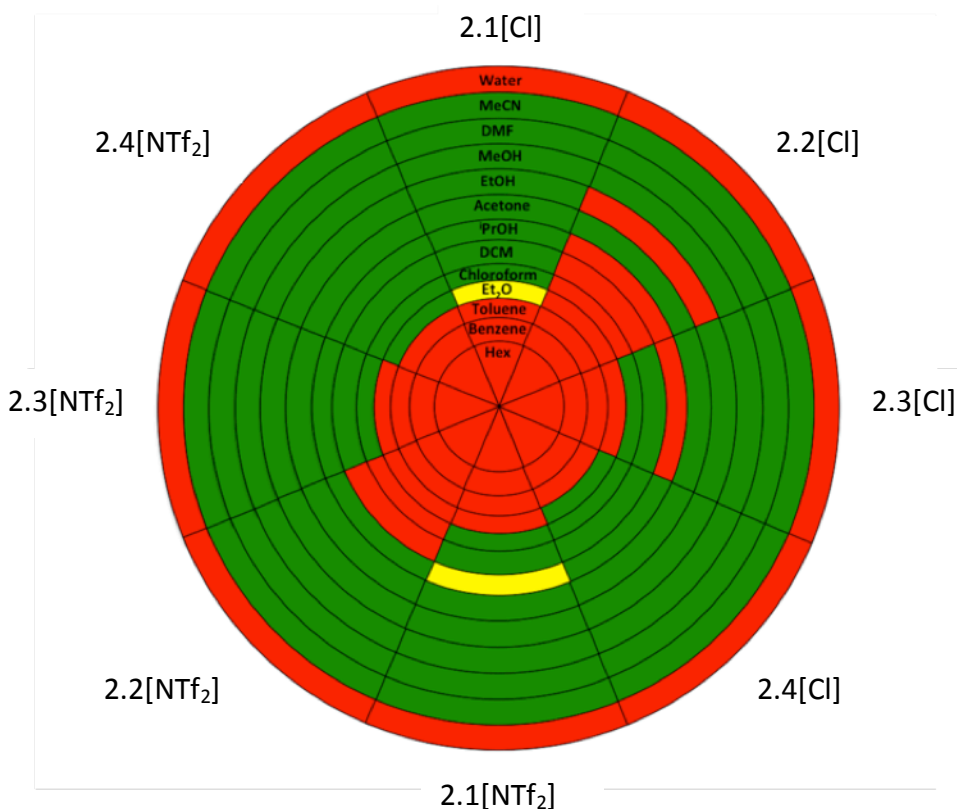


Figure 2-2: Solubilities of all HFPPS in various polar and non-polar solvents. Green = Soluble, Red = Insoluble, Yellow = Emulsion.

While most organic molecules display predictable chemical properties (polar vs non-polar), the solubility of phosphonium salts is highly dependent on the substitution around the phosphorus core and the counter anion. Upon the addition of fluorocarbon chains, the solubility was difficult to predict. Solvents such as H₂O, hexanes, benzene and toluene proved to be poor solvents for the salts of cations **2.1**⁺-**2.4**⁺. The fluorocarbon chains may prevent water from hydrating the cation thus preventing dissociation, while hexanes, benzene, and toluene also proved ineffective at solubilizing these charged species. Polar aprotic solvents such as DMF, acetonitrile, and acetone dissolved all compounds. Methanol was found to be an efficient protic solvent for all compounds tested while

ethanol and isopropanol were successively worse in each case. Compounds **2.1[Cl]**, **2.1[NTf₂]**, **2.3[Cl]**, **2.3[NTf₂]**, **2.4[Cl]**, and **2.4[NTf₂]** were soluble in DCM and chloroform while compounds **2.2[Cl]** and **2.2[NTf₂]** were not. These results inform us of several key points relating solubility to structure. The replacement of an isooctyl chain with a fluorocarbon moiety reduces its solubility in lower polarity such as chloroform and DCM. Despite lengthening two fluorocarbon chains from C₄F₉ to C₈F₁₇, we were still capable of solubilizing the compound. In the case of **2.2⁺**, the presence of three C₄F₉ chains was sufficient to reduce its solubility. Surprisingly, both **2.4[Cl]** and **2.4[NTf₂]**, displayed exceptional solubility in most solvents including diethyl ether. Despite the high fluorine loading, the branched C₄F₉ structure along with the allyl ether linkage may impart greater solubility. The decomposition, glass transition, and melting point of these salts were measured by TGA and DSC experiments (Table 2-1).

Table 2-1: Physical properties of all HFPPS used in this study.

HFPPS	T _{dec} (°C)	T _g (°C)	m.p (°C)
2.1[Cl]	296	-	95-96
2.2[Cl]	291	-	80-81
2.3[Cl]	293	35	73-74
2.4[Cl]	197 ^a	-	140-142
2.1[NTf ₂]	367	-	88-89
2.2[NTf ₂]	371	-	55-56
2.3[NTf ₂]	374	-	64-69
2.4[NTf ₂]	389	2	106-108

The observed decomposition, glass transition, and melting points of all compounds follow a general trend characteristic of phosphonium salt structure, and previous fluoros phosphonium salts.^{8,27} Halide salts typically display higher melting points as compared to their NTf₂⁻ analogues. The reduction in melting point upon greater degrees of fluorination may be attributed to the lower crystal lattice energy of the substances. The perfluoroalkyl groups exhibit very weak intermolecular forces, leading to lower melting points. To our surprise, both **2.4[Cl]** and **2.4[NTf₂]** exhibited much higher melting points suggesting the branched C₄F₉ structure had little effect in reducing the crystal lattice energies. An

exotherm was observed after the glass transition, but before the melting point in the DSC trace for **2.4[NTf₂]** at approximately 50 °C. Decomposition temperatures of compounds **2.1-2.3[Cl]**, were approximately 295 °C, while compounds **2.1-2.3[NTf₂]**, were stable until approximately 370 °C. The decreased basicity of bis(trifluoromethylsulfonyl)imide relative to chloride likely inhibited the E2 decomposition pathway of the β-hydrogen by which phosphonium salts typically undergo when heated. The decomposition point of **2.4[Cl]** was found to be exceptionally low in comparison to its analogues. This led us to believe that an alternative decomposition pathway was present. We postulated that the electronegativity of the perfluoro-tert-butoxy group might allow for its displacement in the presence of a nucleophile (such as Cl⁻) at high temperatures. Deprotonation of a β-hydrogen to form perfluoro-*t*-butanol would result in decomposition (Figure 2-3).

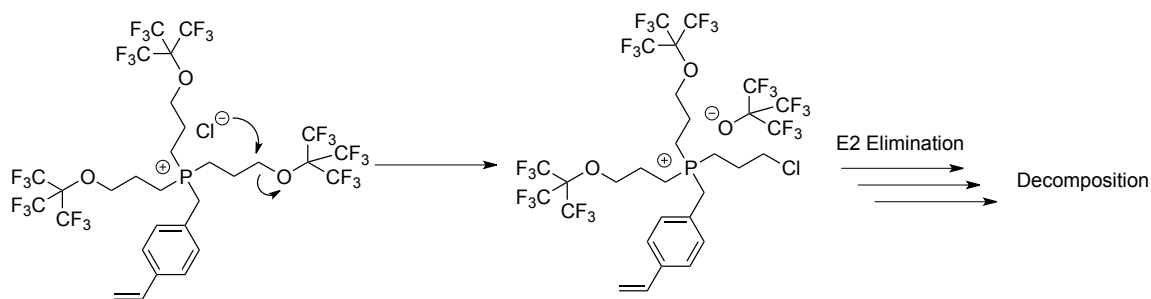


Figure 2-3: Decomposition pathway of **2.4[Cl]** under inert atmosphere.

The plausibility of this mechanism is supported by the relative basicity between chloride and perfluoro-*t*-butoxide, with their conjugate acids having pK_a values of -7 and 5.2, respectively. The increase in thermal stability from 198 to 389 °C upon ion exchange with the bulky, non-nucleophilic NTf₂ anion also supports this mechanism. We decided to further investigate this phenomenon. Compound **2.4[Cl]** was heated slowly within a mass spectrometer and the fragments consistent with perfluoro-*t*-butanol elimination were monitored. After 532 seconds, a positively charged fragment at *m/z* = 197 was observed and attributed to [(CF₃)₃COH - (HF₂)]⁺. Upon further heating, the signal at *m/z* = 197 was observed at a maximum after 889 seconds. The experiment was repeated under identical conditions using **2.4[NTf₂]** and no signal at *m/z* = 197 was observed until 925 seconds, indicating greater thermal stability. Additionally, there was no evidence for the displacement or cleavage of the styrenic moiety from the phosphonium salt. The slight

increase in thermal stability of **2.4[NTf₂]** relative to the other NTf₂ salts may be due to the reduced acidity of the β-hydrogen, as the electron-withdrawing fluorocarbon groups are further in distance. This is supported by the chemical shifts in the ¹H NMR spectra (δ = 2.1 for **2.4[NTf₂]** and ~3.1 for **2.1-2.3[NTf₂]**).

2.1.3 Hydrophobic Surface Modification using HFPPS

Compounds **2.1-2.4[Cl]** were initially screened for their potential use as a fluorinated additive to UV-curable resins (HDDA). Low surface energy materials (such as fluorocarbons) are known to migrate to the liquid-air interface prior to photopolymerization.^{19,20} Initial attempts at solventless polymerization were problematic because of their insolubility in HDDA. Attempts to dissolve the mixture with acetone resulted in the formation of emulsions, translating to hazy films after polymerization. Additional acetone (60-70% by mass) did not remove the emulsion suggesting that changes to the molecular structure of our salts were crucial to increase compatibility. It is well established that the solubility of phosphonium salts is highly dependent on both the anion and cation composition, thus we decided to utilize the hydrophobic bis(trifluoromethylsulfonyl)imide anion in conjunction with our fluorinated phosphonium cation. Compounds **2.1-2.4[NTf₂]** displayed excellent solubility in HDDA with mild heating and stirring. Upon irradiation, the free flowing solution hardened into a transparent, colourless film within seconds. AFM analysis of films containing 0.1 wt% of compounds **2.1-2.4[NTf₂]** in HDDA was conducted to determine surface roughness, as micro/nano features are known to change the hydrophobicity of surfaces. We found that the surfaces were essentially flat with a root-mean square roughness of 0.2-0.3 nm over a 20x20 micron scan window. A line profile of a representative sample can be seen in Figure 2-4.

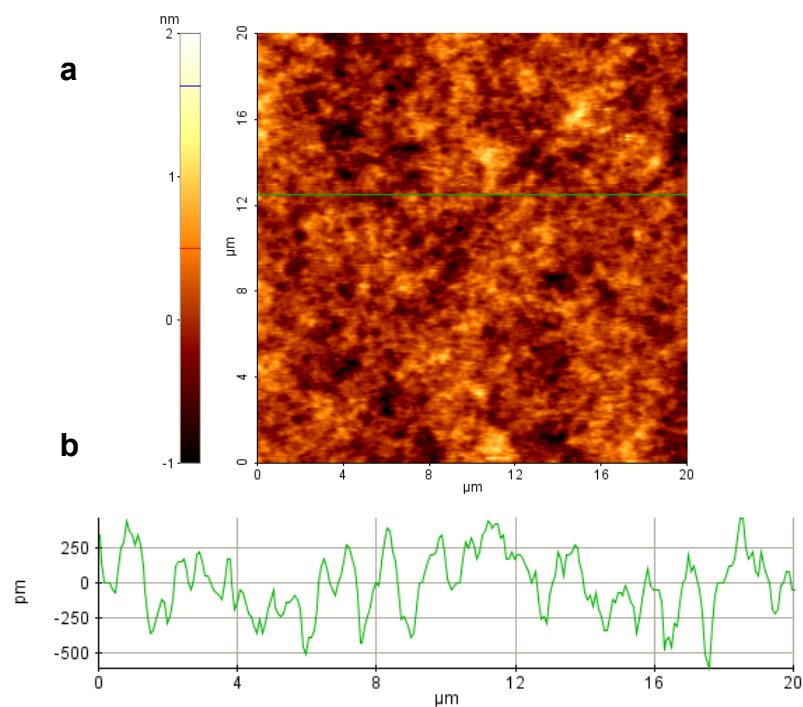


Figure 2-4: a) AFM image of a photopolymerized film containing 0.1 wt% 2.4[NTf₂] in HDDA. b) Roughness profile isolated from the image in (a).

There are no detectable surface features that could contribute to the wetting properties of these polymers. We then evaluated the static water contact angles of films containing various amounts of compounds **2.1-2.4[NTf₂]**. Upon increasing the concentration of compound **2.1[NTf₂]** in HDDA from 0.1 to 1.5 wt %, the WCA increased from 55° on pristine HDDA films to 87° with 1.5 wt % loading (Table 2-2).

Table 2-2: WCA for all HFPPS as a function of wt% in HDDA.

Wt %	2.1[NTf ₂]	2.2[NTf ₂]	2.3[NTf ₂]	2.4[NTf ₂]
0	55 ± 3	55 ± 3	55 ± 3	55 ± 3
0.01	-	-	91 ± 1	73 ± 1
0.05	-	80 ± 1	97 ± 2	90 ± 1
0.1	82 ± 1	89 ± 1	98 ± 1	94 ± 1
0.5	84 ± 1	91 ± 1	101 ± 2	97 ± 2
1	87 ± 1	92 ± 1	-	95 ± 1
1.5	84 ± 1	92 ± 1	-	93 ± 2

A WCA increase of 32° with low fluorinated HFPPS loading is indicative of fluorine migration to the surface. To impart greater degrees of hydrophobicity, we replaced the isooctyl group with an additional perfluorobutyl chain. Upon the addition of **2.2[NTf₂]** to HDDA from 0.05 to 1 wt %, the WCA increased from 55° to 92° (Table 2-2). Despite both **2.1[NTf₂]** and **2.2[NTf₂]** having similar performances at higher loadings, the onset for increasing WCA was shifted significantly with less material required to attain similar contact angles for **2.2[NTf₂]**. These results are significant as they reveal that the replacement of the isooctyl group with a perfluorobutyl chain did not greatly alter the peak hydrophobic effect, but rather shifted the onset where it occurred. By comparing the 1 wt% loading of **2.1[NTf₂]** and the 0.1 wt% loading of **2.2[NTf₂]**, it is clear that they have similar contact angles, yet possess vastly different fluorine economies. Formulations possessing **2.1[NTf₂]** require eight times as many fluorine atoms as **2.2[NTf₂]** to obtain similar hydrophobic effects. Passivation of polymer surfaces with fluorocarbons depends not only on fluorine content, but also molecular architecture imparting fluorocarbon behaviour. Very small amounts of fluorinated salts, despite bearing charges, have the capability to decrease the wettability of photopolymerized surfaces. The capacity to tune the properties of such systems using salts as opposed to standard fluorocarbons may offer new prospects where both charged species and hydrophobicity are desired within a photopolymerizable system.

Despite such findings, the hydrophobic performance of **2.1[NTf₂]** and **2.2[NTf₂]** were noticeably lower than other fluorinated materials on smooth surfaces such as Teflon (WCA = 115°), or compared to other hydrophobic UV-cured systems.¹⁹ This is likely the result of reduced crystallization of the perfluorobutyl groups at the interface. It is well established that longer fluorocarbon chains are capable of undergoing side-chain crystallization at the surface, resulting in much higher degrees of hydrophobicity.²⁵ Reduced ordering of the perfluoroalkyl chains allows water to permeate around the fluorocarbon groups, thus lowering the WCA. For greater performance, we decided to test the efficacy of perfluorinated octyl chains on our phosphonium ion scaffold as a model system. The WCA increased from 55° for pristine HDDA, to 91° with only a 0.01 wt % loading of **2.3[NTf₂]**. Further addition slowly raised the WCA to 101° at 1 wt% (Table 2-2). Attempts to add additional compound unfortunately resulted in poor quality films. In comparison to **2.1[NTf₂]** and **2.2[NTf₂]**, higher degrees of hydrophobicity with a steeper onset was observed when using **2.3[NTf₂]**. These results indicate that phosphonium salts with longer fluorocarbon chains provide enhanced anti-wetting properties of photopolymerized films, consistent with our previous hydrophobic phosphonium studies²⁸. Despite the excellent performance of perfluorooctyl-derived materials within the literature, their bioaccumulation properties renders them a consistent threat to wildlife and humans alike. In light of this reality, we were inspired to investigate the properties of branched perfluoroalkyl groups for hydrophobic applications. We believed that the superb hydrophobicity and steric encumbrance of a phosphonium salt bearing nine -CF₃ groups would passivate the surface and exhibit similar performance to the perfluorooctyl moieties.



Figure 2-5: WCAs of droplets on a) HDDA b) 1.5 wt% of **2.1[NTf₂]** c) 1.5 wt% of **2.2[NTf₂]** d) 1 wt% of **2.3[NTf₂]** and e) 0.5 wt% of **2.4[NTf₂]**.

Upon addition of 0.01-1.5 wt% of **2.4[NTf₂]** to HDDA, we observed a pronounced increase in the WCA, surpassing that of **2.1[NTf₂]** and **2.2[NTf₂]**, and with similar performance to **2.3[NTf₂]** (WCA = 97°). Increased solubility of **2.4[NTf₂]** compared to **2.3[NTf₂]** was also observed allowing for loadings >1 wt%, however with reduced WCA. Using this new molecular structure, we negate the bioaccumulation issues associated with perfluorooctyl groups while simultaneously boosting our fluorine economy, as we provided very similar WCAs using 27 fluorine atoms per cation (**2.4⁺**) as opposed to 34 (**2.3⁺**). Figure 2-5 illustrates the hydrophobic effect as the phosphonium salt is varied.

To determine the mechanism of increased hydrophobicity, the exact nature of the interface was investigated to gain insight into whether or not the fluorinated salt migrates to the surface. To test this hypothesis, TOF-SIMS was employed to examine the composition of the surface material. This technique was chosen because of its surface sensitivity and its capability to identify molecular fragments and to analyze surfaces on the nanometer depth scale.^{29,30}

A photopolymerized film containing 1 wt % of **2.1[NTf₂]** was analyzed using the procedure discussed in the experimental section. A negative ion mass spectrum was obtained and an abundant peak at mass/charge ratio (m/z) 280 was assigned to C₂F₆S₂O₄N⁻, which is the anion [NTf₂]⁻. It is clear from the ion mass spectrum that there are various fragments of the anion, such as CF₃S₂O₃N⁻, CF₃SO₂N⁻, CF₃SO₂⁻, SO₂N⁻ and SON⁻ (Figure 2-6). Other abundant peaks are O⁻, F⁻, hydrocarbons (e.g., C₂H⁻ and C₄H⁻), CN⁻ and C_xH_yO_z⁻. The cation of the photopolymerized film containing 1 wt % of **2.1[NTf₂]** is detected in the positive ion mass spectrum (not shown).

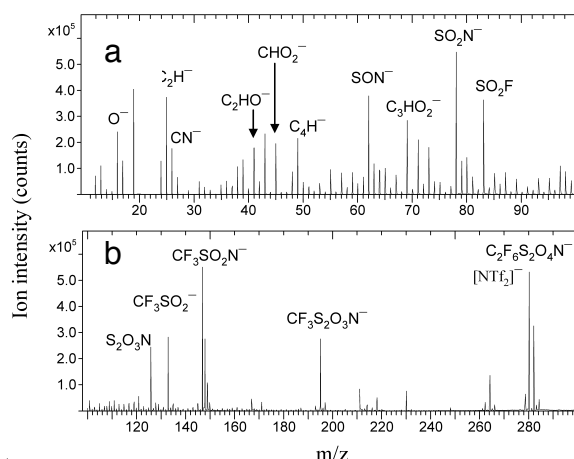


Figure 2-6: Negative ion mass spectrum in m/z ranges of 10-100 (a) and 100-300 (b) obtained on the surface of a photopolymerized film containing 1 wt% of 2.1[NTf₂] in HDDA.

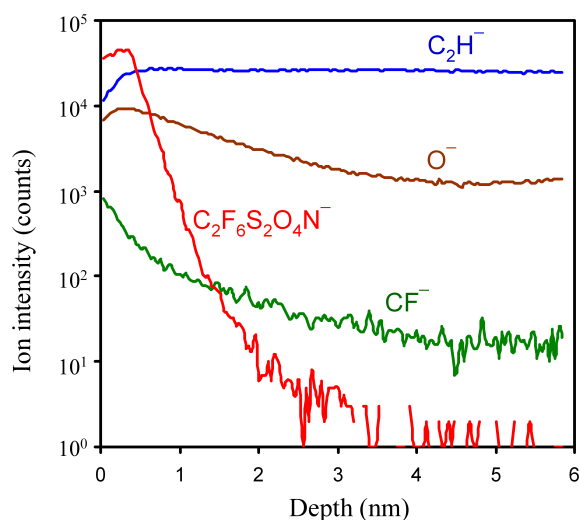


Figure 2-7: Depth profiles of negative ion fragments of O^- , CF^- , C_2H^- , and $C_2F_6S_2O_4N^-$ (which is the anion [NTf₂]⁻) obtained using a 2 keV Cs⁺ beam to sputter the surface and a 25 keV Bi³⁺ ion beam to analyze the surface.

As shown in Figure 2-7, depth profiles of negative ion fragments of interest (O^- , CF^- , C_2H^- and [NTf₂]⁻) were obtained as the surface of the sample containing 1 wt % [1]NTf₂ was ablated with a 3 keV Cs⁺ sputter beam. The depth was obtained with a sputter rate of 0.08 nm/s, which was estimated by sputtering a PET film and measuring the crater depth. Upon continued ablation up to 3 nm, the ion intensity for the anion [NTf₂]⁻ dropped

dramatically. The CF^- ion fragment was also detected at high intensity in the first bombardments, and its intensity dropped off significantly, with a similar time frame for the $[\text{NTf}_2]^-$ anions. These severe reductions in ion detection not only confirm that the $[\text{NTf}_2]^-$ containing HFPPS was more concentrated at the top of the film, but that there was minimal CF^- left beneath the surface. Our TOF-SIMS results thus suggest that the phosphonium salt accumulated at the air-polymer interface of the photopolymerized film. The depth profile of $[\text{NTf}_2]^-$ shown in Figure 2-6 indicates that the ions accumulated mainly within 3 nm of the surface, likely a direct result of the fluorinated phosphonium salt. In contrast, ion fragments associated with both the polyacrylate and HFPPS ablated under the same conditions (i.e., O^- and C_2H^-) remained relatively constant throughout the experiment. The tendency of the anionic sections of the HFPPS to remain unfragmented and charged under experimental conditions is ideal, and has proven to be an excellent handle for TOF-SIMS analysis. We believe that this technique may be applied to other ammonium/phosphonium salts in materials applications.

2.2 Conclusions

An array of HFPPS was synthesized and their physical and chemical properties were characterized. Exchanging the chloride for bis(trifluoromethylsulfonyl)imide resulted in improved solubility in HDDA and increased thermal stability for all phosphonium cations. Through the alteration of the phosphonium salt, either with increased fluorine loading, or through architecture manipulation, a structure-activity relationship was observed. Greater degrees of fluorination increased both the maximum attainable contact angle, along with its onset. **2.4** $[\text{NTf}_2]$ imbued films with water repellent properties with similar efficacy to its perfluorooctyl analogue. TOF-SIMS confirmed the presence of HFPPS at the surface, and demonstrated for the first time that charged species could be selectively directed to a desired location in photopolymerizable systems. The fluorocarbon appendages acted as a shuttle for the charged molecules, forcing the ions to the polymer/air interface. Future work will include the attachment of an additional functionality to the fluorinated phosphorus centre in an attempt to modify the surface with a desired moiety. There are also prospects to access the surface charge through an

ion-exchange process with the photopolymer allowing for surface modification of UV-cured films with very low HFPPS loading.

2.3 Experimental

All compounds were synthesized under a N₂ atmosphere or prepared in a nitrogen-filled MBraun Labmaster 130 glove box unless otherwise noted. Cytop 183 (2,4,4-trimethylpentyl)phosphine, 2,2,4-trimethylpentyl-bis(1H,1H,2H,2H-perfluorohexyl)phosphine, HDMAP (2-hydrox-2-methy-1-phenyl-propanone), and HDDA (hexanediol diacrylate), were donated by Cytec Corporation and used as received. Lithium bis(trifluoromethylsulfonyl)imide was purchased from Alfa Aesar and used as received. Solvents were purchased from Caledon and dried using an MBraun Solvent Purification System. The fluorinated precursors bis(1H,1H,2H,2H-perfluorooctyl)(2,4,4-trimethylpentyl)phosphine (**2.0a**), tris(1H,1H,2H,2H-perfluorohexyl)phosphine (**2.0b**) and sodium nonafluoro-tert-butoxide were prepared using literature procedures, respectively.^{18,23,28} Dried solvents were collected under vacuum in a flame dried Strauss flask and stored over 4Å molecular sieves in the drybox. Deuterated chloroform was purchased from Caledon and stored over 4Å molecular sieves in the drybox. 4-Vinylbenzyl chloride and acetone-*d*₆ were purchased from Sigma Aldrich and used as received. PH₃ (pressurized cylinder) was obtained from Cytec Corporation and was used as received.

Caution! PH₃ is a pyrophoric and toxic gas. It should be handled with extreme caution, including the use of PH₃ monitors, a stainless steel manifold, and deliberate burning of waste streams for eventual conversion into H₃PO₄ (via P₄O₁₀).

Nuclear Magnetic Resonance (NMR) spectroscopy was conducted on a Varian INOVA 400 MHz spectrometer (¹H 400.09 MHz, ³¹P{¹H} 161.82 MHz, ¹⁹F{¹H} 376.15 MHz). All ¹H spectra were referenced relative to incompletely deuterated solvent signals (CDCl₃; ¹H δ_H = 7.26 ppm and CO(CD₃)₂; ¹H δ_H = 2.04). The chemical shifts for ³¹P{¹H} and ¹⁹F{¹H} NMR spectroscopy were referenced using an external standard (85% H₃PO₄ δ_P = 0; trifluorotoluene, PhCF₃ δ_F = -63.9 ppm). Infrared spectra were recorded using a Bruker Tensor 27 spectrometer with an attenuated total reflectance (ATR) attachment using a ZnSe crystal (resolution 4 cm⁻¹). Sonication of the UV curable formulations was

conducted in an E60H Elmasonic sonicator at frequency of 37 kHz using an effective power of 100 W. Deposition of the formulation was performed using a 25-micron Meyer Rod purchased from Gardco on microscope slides purchased from Technologist Choice unless otherwise noted. UV curing was performed using a modified UV curing system purchased from UV Process and Supply Inc. with a mercury bulb. Water contact angles (WCA) were measured with a 5 μ L drop using a Kruss DSA100 Drop Shape Analyzer. Thermal degradation was determined using Thermal Gravimetric Analysis (TGA) on a Q600 SDT TA instrument: a sample of 5-15 mg was placed in an aluminum cup and heated at a rate of 10°C/min from room temperature to 600 °C under nitrogen atmosphere (100 mL/min). Glass transition temperatures were determined using Differential Scanning Calorimetry (DSC) on a DSC Q20 TA instrument: a sample of approximately 10 mg was placed in an aluminum Tzero pan and underwent a heat/cool/heat profile at 10 °C/min under nitrogen atmosphere (50 mL/min). The transitions were determined from the final heat cycle of the heat/cool/heat profile. Melting points of all HFPPS were determined using a Gallenkamp Variable Heater in air. Mass spectrometry was recorded in both positive and negative ion modes using an electrospray ionization (ESI) Micromass LCT spectrometer. Elemental analysis (EA) was performed by the Elemental Analysis Laboratory at the Université de Montréal. Time-of-flight Secondary Ion Mass Spectrometry (TOF-SIMS) measurements were performed using an ION-TOF (Gmbh) TOF-SIMS IV equipped with a Bi cluster liquid metal ion source. A 25 keV Bi³⁺ cluster primary pulsed ion beam (10 kHz, pulse width 20 ns) was used to bombard the surface to generate secondary ions. The positive or negative secondary ions were extracted from the sample surface, mass separated and detected via a reflectron-type time-of-flight analyzer. Depth profiles were obtained by repeating the following cycle: sputtering an area of 500 μ m \times 500 μ m on the sample surface with a 3 keV Cs⁺ ion beam for 0.5 s followed by, with a delay of 2 seconds, collecting mass spectra at 128 \times 128 pixels with the Bi³⁺ ion beam over an area of 245 μ m \times 245 μ m in the centre of the sputtered area. Surface morphology was imaged using dynamic force mode of a Park Systems XE-100 atomic force microscope (AFM). A silicon cantilever having a nominal spring constant of 40 N/m, resonant frequency of 300 kHz and a tip radius of 10nm was used. In the dynamic force mode, the cantilever was vibrated near its resonant frequency and its reduced

oscillation amplitude was used as the feedback parameter to image the surface. Images of 256 x 256 pixels on an area of 20 x 20 μm were collected.

2.3.1 Solubility/Miscibility Tests

Approximately 5 mg of compound was added to a test tube followed by the addition of 1.5 mL of solvent and gentle stirring. If dissolution was not observed, the mixture was further stirred and sonicated for 30 seconds. Material was deemed soluble if the resulting solution was free of particulate and haze, as determined by visual inspection. Material was deemed insoluble if a large majority of the powder did not dissolve. In two cases however, hazy mixtures were formed that we believed to be emulsion.

2.3.2 Film Preparation

A desired amount of photoinitiator (5 wt% HDMAP), crosslinker (HDDA), and phosphonium salt were weighed and combined in screw top vials. The mixture was sonicated at 45 °C for 20 min until the solutions were free of particulate and haze. After cooling to room temperature, the solutions were cast on glass slides using a Meyer rod (25 microns), placed on a conveyor and irradiated with UV light (Irradiance – UVA: 412 mW/cm² UVB: 423 mW/cm² UVC: 79 mW/cm². Energy Density - UVA: 234 mJ/cm² UVB: 238 mJ/cm² UVC: 45 mJ/cm²).

2.3.3 Synthetic Details

Synthesis of 2.1[Cl]

2,2,4-trimethylpentyl-bis(1*H*,1*H*,2*H*,2*H*-perfluorohexane)phosphine (8.04 g, 12.60 mmol) and 4-vinylbenzyl chloride (3.85 g, 25.19 mmol) were dissolved in dimethylformamide (7 mL) and heated to 120 °C under an N₂ atmosphere. The reaction was monitored by ³¹P{¹H} NMR spectroscopy and was complete after 3 hours. The product was precipitated in hexanes as a light brown solid. Reprecipitation (5 mL dichloromethane into 200 mL hexanes, followed by stirring in isopentane) yielded an off-white powder. (4.77 g, 54%); Anal. Calcd for C₂₉H₃₄ClF₁₈P: C 44.04%, H 4.33%. Found: C 44.91%, H 4.08%. T_m: 95.3 - 95.7 °C. IR: $\nu(\text{C-F})$ 1133 cm⁻¹, $\nu(\text{HC}=\text{CH}_2)$ 990 cm⁻¹. ¹H NMR (acetone-*d*₆, δ) 7.60 (d, 2H, ³*J* = 10.8 Hz, Ar-H_{ortho}), 7.38 (d, 2H, ³*J* = 8.0 Hz, Ar-H_{meta}), 6.64 (dd, 1H, ³*J* = 17.4 Hz (trans), ³*J* = 10.8 Hz (cis), CH=CH₂), 5.72 (d, 1H, ³*J* =

17.4 Hz, CH=CH₂-trans), 5.15 (d, 1H, ³J = 11.4 Hz, CH=CH₂-cis), 4.85 (d, 2H, ³J = 16.0 Hz, Ar-CH₂), 3.18-2.91 (m, 4H, PCH₂CH₂), 2.82-2.65 (m, 6H, PCH₂), 2.38-2.26 (m, 1H, PCH₂CH), 1.51-1.28 (m, 2H, CHCH₂C(CH₃)₃), 1.21 (d, 2H, ³J = 6.4 Hz, CHCH₃), 0.89 (s, 9H, C(CH₃)₃). ¹⁹F{¹H} NMR (acetone-*d*₆, δ) -80.9 to -81.2 (m, 6F), -114.75 (bs, 2F), -123.68 (bs, 2F), -125.90 (bs, 2F); ³¹P{¹H} NMR (acetone-*d*₆, δ) 35.7 (s). MS (ESI+, %): 755.1 ([cation]⁺, 100), 1545.3 ([cation]₂ + anion]⁺, 30). MS (ESI-, %): 825.1 ([M + Cl]⁻, 10), 689.1 ([M - C₆H₄CH=CH₂]⁻, 10).

Synthesis of 2.1[NTf₂]

Compound [1]Cl (1.09 g, 1.37 mmol) and lithium bis(trifluoromethylsulfonyl)imide (0.800 g, 2.74 mmol) were dissolved in dichloromethane (12 mL) and stirred under a N₂ atmosphere. Once there was no further visible accumulation of precipitate (40 hours), the reaction mixture was partitioned between dichloromethane (100 mL) and water (100 mL). The organic layer washed with water (2 x 100 mL), dried with MgSO₄, and then the solvent was removed. The resulting pale yellow oil was triturated with diethyl ether/hexanes (10/90, 50 mL) to afford a white powder that was filtered and dried *in vacuo*. (1.24 g, 87%); Anal. Calcd for C₃₁H₃₄F₂₄NO₄PS₂: C 35.95%, H 3.31%, N 1.35%. Found: C 36.19%, H 3.31%, N 1.27%. T_m: 88.1 - 88.8 °C. IR: ν(C-F anion) 1347 cm⁻¹, ν(C-F cation) 1135 cm⁻¹, ν(SO₂) 1057 cm⁻¹, ν(HC=CH₂) 988 cm⁻¹. ¹H NMR (acetone-*d*₆, δ) 7.57 (d, 2H, ³J = 7.6 Hz, Ar-H_{ortho}), 7.48 (d, 2H, ³J = 7.6 Hz, Ar-H_{meta}), 6.76 (dd, 1H, ³J = 17.4 Hz (trans), ³J = 10.8 Hz (cis), CH=CH₂), 5.84 (d, 1H, ³J = 18.0 Hz, CH=CH₂-trans), 5.30 (d, 1H, ³J = 10.8 Hz, CH=CH₂-cis), 4.34 (d, 2H, ³J = 16.0 Hz, Ar-CH₂), 3.08-3.01 (m, 4H, PCH₂CH₂), 2.86-2.74 (m, 6H, PCH₂), 2.43-2.31 (m, 1H, PCH₂CH), 1.51-1.40 (m, 2H, CHCH₂C(CH₃)₃), 1.27 (d, 3H, ³J = 6.4 Hz, CHCH₃), 0.92 (s, 9H, C(CH₃)₃); ¹⁹F{¹H} NMR (acetone-*d*₆, δ) -80.0 (s, 6F), -81.9 to -82.0 (m, 6F), -115.6 to -115.7 (m, 4F), -124.5 (bs, 4F), -126.6 to -126.7 (m, 4F). ³¹P{¹H} NMR (acetone-*d*₆, δ) 34.5 (s). MS (ESI+, %): 755.1 ([cation]⁺, 100), 1790.3 ([cation]₂ + anion]⁺, 10). MS (ESI-, %): 1314.9 ([cation + (anion)₂]⁻, 50), 281.2 ([NTf₂]⁻, 100)

Synthesis of 2.2[Cl]

Tris(*1H,1H,2H,2H*-perfluorohexyl)phosphine (5.15 g, 6.67 mmol) and 4-vinylbenzyl chloride (2.12 g, 13.34 mmol) were dissolved in dimethylformamide (8 mL) and heated to 120 °C while stirring under a N₂ atmosphere. The reaction was monitored by ³¹P{¹H} NMR spectroscopy and was complete after 3 hours. The reaction mixture was precipitated into benzene, filtered, redissolved in acetone and freeze dried *in vacuo*, yielding off-white crystals (3.37 g, 55%); Anal. Calcd for C₂₇H₂₁ClF₂₇P: C 35.06%, H 2.29%. Found: C 35.07%, H 2.28%. T_m: 79.5 - 81.4 °C. IR: ν(C-F) 1133 cm⁻¹, ν(HC=CH₂) 990 cm⁻¹. ¹H NMR (acetone-*d*₆, δ) 7.71 (d, 2H, ³J = 9.6 Hz Ar-H_{ortho}), 7.45 (d, 2H, ³J = 8.4 Hz, Ar-H_{meta}), 6.73 (dd, 1H, ³J = 17.6 Hz (trans), ³J = 10.8 Hz (cis), CH=CH₂), 5.80 (d, 1H, ³J = 17.6 Hz, CH=CH₂-trans), 5.26 (d, 1H, ³J = 11.2 Hz, CH=CH₂-cis), 5.15 (d, 2H, ³J = 16.8 Hz, Ar-CH₂), 3.47-3.35 (m, 6H, PCH₂CH₂), 3.02-2.88 (m, 6H, PCH₂). ¹⁹F{¹H} NMR (acetone-*d*₆, δ) -82.1 (s, 9F), -115.5 to -115.6 (m, 6F), -124.5 (bs, 6F), -126.7 to -126.8 (m, 6F). ³¹P{¹H} NMR (acetone-*d*₆, δ) 38.0 (s). MS (ESI+, %): 889.0 ([cation]⁺, 100). MS (ESI-, %): 959.0 ([M + Cl]⁻, 40), 822.9 ([M - C₆H₄CH=CH₂]⁻, 100).

Synthesis of 2.2[NTf₂]

Compound [2]Cl (1.60 g, 1.73 mmol) and lithium bis(trifluoromethylsulfonyl)imide (1.14 g, 3.97 mmol) were dissolved in chloroform/benzotrifluoride (1:1, 20 mL) and allowed to stir under an N₂ atmosphere (48 hours). The reaction mixture was partitioned between benzotrifluoride (50 mL) and water (50 mL), washed with water (2 x 50 mL), dried (MgSO₄), and the volatiles removed. The oily product was triturated in dichloromethane to afford a white solid that was filtered, rinsed with dichloromethane (2 x 10 mL) and dried *in vacuo*. (1.25 g, 63%); Anal. Calcd for C₂₉H₂₁F₃₃NO₄PS₂: C 29.78%, H 1.81%, N 1.20%. Found: C 29.93%, H 1.52%, N 1.19%. T_m: 55.3 - 56.2 °C. IR: ν(C-F anion) 1344 cm⁻¹, ν(C-F) 1133 cm⁻¹, ν(SO₂) 1061 cm⁻¹, ν(HC=CH₂) 990 cm⁻¹. ¹H NMR (acetone-*d*₆, δ) 7.78 (d, 2H, ³J = 8.4 Hz, Ar-H_{ortho}), 7.50 (d, 2H, ³J = 8.4 Hz, Ar-H_{meta}), 6.77 (dd, 1H, ³J = 18.0 Hz (trans), ³J = 11.2 Hz (cis), CH=CH₂), 5.87 (d, 1H, ³J = 18.0 Hz, CH=CH₂-trans), 5.31 (d, 1H, ³J = 10.8 Hz, CH=CH₂-cis), 4.45 (d, 2H, ³J = 14.8 Hz, Ar-CH₂), 3.28-3.17 (m, 6H, PCH₂CH₂), 2.98-2.81 (m, 6H, PCH₂). ¹⁹F{¹H} NMR

(acetone- d_6 , δ) -80.1 (s, 6F), -82.0 to -82.1 (m, 9F), -115.5 to -115.6 (m, 6F), -124.5 (s, 6F). -126.7 to -126.8 (m, 6F). $^{31}\text{P}\{^1\text{H}\}$ NMR (acetone- d_6 , δ) 37.2 (s). MS (ESI+, %): 888.9 ([cation] $^+$, 100). MS (ESI-, %): 1448.7 ([cation + (anion) $_2$] $^-$, 80), 1169.5 ([M] $^-$, 70), 280.1 ([NTf $_2$] $^-$, 100).

Synthesis of 2.3[Cl]

A 250 mL pressure tube was charged with bis(1*H*,1*H*,2*H*,2*H*-perfluorooctyl)(2,4,4-trimethylpentyl)phosphine (5.0 g, 4.98 mmol) and 2 molar equivalents of 4-vinylbenzyl chloride (1.52 g, 9.96 mmol) in 100 mL of a 2:1 mixture of deoxygenated DMF and trifluorotoluene. The mixture was heated at 125 °C for 6 hours. Volatiles were removed at 60 °C *in vacuo*. The viscous yellow oil was redissolved in a minimal amount of acetone (10 mL) and precipitated in stirring hexanes (100 mL). This process was repeated three additional times. The oil was heated *in vacuo* at 60 °C until a yellow solid was obtained. (4.24 g, 65%); Anal. Calcd for C $_{37}$ H $_{34}$ ClF $_{34}$ P: C 37.31%, H 2.88%. Found C 37.38%, H 3.18%. T $_m$: 72.5 - 73.5 °C; T $_g$: 35 °C. IR: ν (C-F) 1145 cm $^{-1}$, ν (HC=CH $_2$) 952 cm $^{-1}$. ^1H NMR (acetone- d_6 , δ): δ 7.74 (d, 2H, $^3J = 8$ Hz, Ar-H $_{ortho}$), 7.49 (d, 2H, $^3J = 8$ Hz, Ar-H $_{meta}$), 6.75 (dd, 4H, $^3J = 12$ Hz (trans), $^3J = 8$ Hz (cis), CH=CH $_2$), 5.84 (d, 1H, $^3J = 20$ Hz, CH=CH $_2$ -trans), 5.27 (d, 1H, $^3J = 12$ Hz, CH=CH $_2$ -cis), 5.00 (d, 2H, $^3J = 16$ Hz, Ar-CH $_2$), 2.54-3.40 (m, 10H, PCH $_2$ and PCH $_2$ CH $_2$), 2.26-2.4 (m, 1H, PCH $_2$ CH), 1.51 (m, 1H, (CHCHHC(CH $_3$) $_3$)), 1.30-1.45 (m, 1H, (CHCHHC(CH $_3$) $_3$)), 1.25 (d, 3H, $^3J = 8$ Hz, CHCH $_3$), 0.9 (s, 9H, C(CH $_3$) $_3$). ^{19}F NMR (acetone- d_6 , δ) -126.07 (s, 4F), -122.67 (m, 8F), -121.50 (m, 12F), -114.52 (s, 4F), -81.01 (t, $^3J = 8$ Hz, 4F). $^{31}\text{P}\{^1\text{H}\}$ NMR (acetone- d_6 , δ) 34.8 (s). MS (ES+, %) ([cation] $^+$, 100).

Synthesis of 2.3[NTf $_2$]

Dry deoxygenated DCM (15 mL) was added to a 50 mL round bottom flask followed by the addition of [3]Cl (1.04 g, 0.873 mmol). After complete dissolution, 2 molar equivalents of lithium bis((trifluoromethyl)sulfonyl)imide (0.125 g, 0.437 mmol) were added and the mixture was stirred for 12 hours. The slurry was added to a separatory funnel followed by the addition of 30 mL of DCM. The organic layer was washed with distilled water (4 x 10 mL) and then dried with a minimal amount of sodium sulphate.

Volatiles were evaporated *in vacuo* resulting in an orange viscous oil. (0.63 g, 50%); Anal. Calcd for $C_{39}H_{34}F_{40}NO_4PS_2$: C 32.63% H 2.39% N 0.98% S 4.47%. Found: C 32.61% H 2.35% N 0.97% S 4.5%. T_g : $-16\text{ }^\circ\text{C}$. IR: $\nu(\text{C-F anion})$ 1348 cm^{-1} , $\nu(\text{C-F})$ 1134 cm^{-1} , $\nu(\text{SO}_2)$ 1060 cm^{-1} , $\nu(\text{HC}=\text{CH}_2)$ 949 cm^{-1} . $^1\text{H NMR}$ (acetone- d_6 , δ) 7.59 (d, 2H, $^3J = 8\text{ Hz}$, Ar- H_{ortho}), 7.51 (d, 2H, $^3J = 8\text{ Hz}$, Ar- H_{meta}), 6.79 (dd, 4H, $^3J = 12\text{ Hz}$ (trans), $^3J = 8\text{ Hz}$ (cis), $\text{CH}=\text{CH}_2$), 5.85 (d, 1H, $^3J = 18\text{ Hz}$, $\text{CH}=\text{CH}_2$ -trans), 5.30 (d, 1H, $^3J = 20\text{ Hz}$, $\text{CH}=\text{CH}_2$ -cis), 4.35 (d, 2H, $^3J = 16\text{ Hz}$, Ar- CH_2), 2.70-3.20 (m, 10H, PCH_2 and PCH_2CH_2), 2.30-2.50 (m, 1H, PCH_2CH), 1.34-1.51 (m, 2H, $\text{CHCH}_2\text{C}(\text{CH}_3)_3$), 1.30 (d, 3H, $^3J = 8\text{ Hz}$, CHCH_3), 0.95 (s, 9H, $\text{C}(\text{CH}_3)_3$). $^{19}\text{F NMR}$ (acetone- d_6 , δ) -79.44 (s, 6F), -81.19 (m, 6F), -114.80 (s, 4F), -121.77 (m, 12F), -122.86 (m, 8F), -126.2 (s, 4F). $^{31}\text{P}\{\text{H}\}$ NMR (acetone- d_6 , δ) 35.6 (s). MS (ESI+, %): 1155 ([cation] $^+$, 100). MS (ESI-, %): 1715 ([cation + (anion) $_2$] $^-$, 20).

Synthesis of Nonafluoro-tert-butyl allyl ether (2.0c)

A 500 mL pressure round bottom flask was charged with sodium nonafluoro-tert-butoxide (65 g, 0.25 mol), allyl bromide (18.8 g, 0.15 mol) and DMF (150 mL, SPS purified) then heated at $90\text{ }^\circ\text{C}$ for 6 hours. The reaction mixture was poured into a brine solution (200 mL) and the lower organic phase was removed and fractionally distilled under ambient conditions. The first 2 fractions were azeotropes with water ($30\text{-}40\text{ }^\circ\text{C}$ @ 760 mmHg, confirmed by $^1\text{H NMR}$) and the final fraction was the desired olefin, nonafluoro-tert-butyl allyl ether (23.4 g, 85 mmol, 56%, $45\text{-}47\text{ }^\circ\text{C}$ @ 760 mmHg). $^1\text{H NMR}$ (CDCl_3 , δ): δ 5.9 (m, 1H, $\text{CH}=\text{CH}_2$), 5.4 (d, 1H, $^3J_{\text{trans}} = 16\text{ Hz}$, $\text{CH}=\text{CH}_2$), 5.3 (d, 1H, $^3J_{\text{cis}} = 10\text{ Hz}$, $\text{CH}=\text{CH}_2$), 4.6 (d, 2H, $^3J = 5\text{ Hz}$, CH_2). $^{19}\text{F NMR}$ (CDCl_3 , δ): -71.5 (s, 9F); $^{13}\text{C}\{^1\text{H}\}$ NMR (CDCl_3 , δ): δ 131.6 (s, $\text{CH}=\text{CH}_2$), δ 124.9 – 116.2 (q, $^1J_{\text{C-F}} = 292\text{ Hz}$, CF_3), δ 117.1 (s, $\text{CH}=\text{CH}_2$), δ 80.1 (m, $^2J_{\text{C-F}} = 30\text{ Hz}$, $\text{C}(\text{CF}_3)_3$), δ 70.6 (s, OCH_2). MS (ES+, %): 276.1 ($[\text{M}]^+$, 100), 69.1 ($[\text{CF}_3]^+$, 57).

Synthesis of Tris(nonafluoro-tert-butoxypropyl)phosphine (2.0d)

A 50 mL autoclave was charged with nonafluoro-tert-butyl allyl ether (23.4 g, 85 mmol), AIBN (1.5 g, 9.2 mmol) and purged with N_2 . Then PH_3 was added to a pressure of 80 psi (7.9 mmol, calculated) and the sealed autoclave was heated to $70\text{ }^\circ\text{C}$ for 5 hours. After

cooling overnight the autoclave was recharged with PH_3 to 80 psi. The contents were then heated at $70\text{ }^\circ\text{C}$ for a further 3 hours. After cooling the pressure vessel to $10\text{ }^\circ\text{C}$ the remaining PH_3 was removed by careful and continuous purging with N_2 and incineration of the PH_3 residues in a specifically designed burn-box. The yellow reaction mixture was then fractionally distilled under vacuum to isolate the product (6.7 g, 7.8 mmol, 31%, $70\text{--}75^\circ\text{C}$ @ 0.3 mmHg). ^1H NMR (CDCl_3 , δ): δ 4.0 (t, 6H, OCH_2), 1.8 (m, 6H, PCH_2), 1.4 (m, 6H, $\text{CH}_2\text{CH}_2\text{CH}_2$). ^{19}F NMR (CDCl_3 , δ): -70.7 (s, 9F). $^{31}\text{P}\{\text{H}\}$ NMR (CDCl_3 , δ) -32.4 (s). $^{13}\text{C}\{\text{H}\}$ NMR (CDCl_3 , δ): δ 124.7 – 116.0 (q, $^1J_{\text{C-F}} = 292$ Hz, CF_3), δ 79.3 (m, $^2J_{\text{C-F}} = 30$ Hz, $\text{C}(\text{CF}_3)_3$), δ 70.0 (d, $^3J_{\text{C-P}} = 14$ Hz, OCH_2), δ 25.9 (d, $^1J_{\text{C-P}} = 14$ Hz, PCH_2), δ 21.9 (d, $^2J_{\text{C-P}} = 14$ Hz, $\text{CH}_2\text{CH}_2\text{CH}_2$), MS (ES+, %) 877.1 ($[\text{O}=\text{PR}_3 - \text{H}]^+$, 100).

Synthesis of 2.4[Cl]

A 70 mL glass pressure tube was charged with tris(nonafluorobutoxypropyl)phosphine (2.8 g, 3.25 mmol), 4-vinylbenzyl chloride (0.85 g, 6.1 mmol), acetonitrile (5 mL) and trifluorotoluene (5 mL) and heated at $80\text{ }^\circ\text{C}$ for 7 hours. The volatiles were then removed and the remaining yellow oil was washed quickly with Et_2O (2 x 5 mL) and triturated with Et_2O at $-20\text{ }^\circ\text{C}$ to afford a white powder. The solid was filtered in the air on a frit and washed with cold 80/20 Et_2O /hexane (3 x 5 mL), then dried under high vacuum to afford [4]Cl as a microcrystalline solid. It was recrystallised from acetone/benzene at -20°C . (2.3 g, 2.3 mmol, 70%). Anal. Calcd for $\text{C}_{30}\text{H}_{27}\text{ClF}_{27}\text{O}_3\text{P}$: C 35.50%, H 2.68%. Found C 35.50%, H 2.73%. T_m : $120\text{--}122\text{ }^\circ\text{C}$; IR: $\nu(\text{C-F})$ 1154 cm^{-1} , $\nu(\text{HC}=\text{CH}_2)$ 971 cm^{-1} . ^1H NMR (acetone- d_6 , δ): δ 7.6 (d, 2H, $^3J = 8$ Hz, Ar- H_{ortho}), 7.4 (d, 2H, $^3J = 8$ Hz, Ar- H_{meta}), 6.7 (dd, 1H, $^3J = 20$ Hz (trans), $^3J = 12$ Hz (cis), $\text{CH}=\text{CH}_2$), 5.8 (d, 1H, $^3J = 20$ Hz, $\text{CH}=\text{CH}_2$ -trans), 5.2 (d, 1H, $^3J = 12$ Hz, $\text{CH}=\text{CH}_2$ -cis), 4.6 (d, 2H, $^3J = 18$ Hz, Ar- CH_2), 4.2 (pseudo t, 6H, OCH_2), 2.8 (m, 6H, PCH_2), 2.1 (m, 6H, $\text{CH}_2\text{CH}_2\text{CH}_2$). ^{19}F NMR (acetone- d_6 , δ) -71.1 (s, 27F). $^{31}\text{P}\{\text{H}\}$ NMR (acetone- d_6 , δ) 34.1 (s). MS (ES+, %) 978.2 ($[\text{cation}]^+$, 100).

Synthesis of 2.4[NTf₂]

A 20 mL vial was charged with [4]Cl (0.49 g, 0.48 mmol), lithium bis((trifluoromethyl)sulfonyl)imide (0.27 g, 0.93 mmol) and acetone (8 mL). The mixture

was sparged with N₂ for 10 minutes and then stirred for 4 hours. Water (20 mL) was added and the resulting mixture was stirred vigorously for 5 minutes. The upper aqueous phase was then decanted and the remaining oil was dissolved in ethyl acetate (10 mL), dried (Na₂SO₄) and rotary-evaporated to dryness. The colourless oil was then dissolved in a minimum amount of Et₂O (3 mL) and the volatiles removed under high vacuum (performed twice). Further drying for 12 hours *in vacuo* afforded a white crystalline solid (0.50 g, 0.4 mmol, 83%); Anal. Calcd for C₃₂H₂₇F₃₃NO₇PS₂: C 30.51% H 2.16% N 1.11% S 5.09%. Found: C 30.72% H 2.13% N 1.10% S 5.11%. T_g: 1.9 °C. T_m: 106-108°C. IR: ν(C-F anion) 1348 cm⁻¹, ν(C-F) 1154 cm⁻¹, ν(SO₂) 1058 cm⁻¹, ν(HC=CH₂) 971 cm⁻¹. ¹H NMR (acetone-*d*₆, δ) 7.7 (d, 2H, ³J = 8 Hz, Ar-H_{ortho}), 7.4 (d, 2H, ³J = 8 Hz, Ar-H_{meta}), 6.8 (dd, 1H, ³J = 20 Hz (trans), ³J = 12 Hz (cis), CH=CH₂), 5.8 (d, 1H, ³J = 20 Hz, CH=CH₂-trans), 5.3 (d, 1H, ³J = 12 Hz, CH=CH₂-cis), 4.3 (pseudo t, 6H, OCH₂), 4.2 (d, 2H, ³J = 20 Hz, Ar-CH₂), 2.7 (m, 6H, PCH₂), 2.2 (m, 6H, CH₂CH₂CH₂). ¹⁹F NMR (acetone-*d*₆, δ) -71.2 (s, 27F), -80.1 (s, 6F). ³¹P{H} NMR (acetone-*d*₆, δ) 34.8 (s). MS (ESI+, %): 1155 ([cation]⁺, 100). MS (ESI-, %): 1715 ([cation + (anion)₂]⁻, 20).

References

- (1) Hiemstra, C.; Zhou, W.; Zhong, Z. Y.; Wouters, M.; Feijen, J. *J. Am. Chem. Soc.* **2007**, *129*, 9918.
- (2) Schaedler, T. A.; Jacobsen, A. J.; Torrents, A.; Sorensen, A. E.; Lian, J.; Greer, J. R.; Valdevit, L.; Carter, W. B. *Science* **2011**, *334*, 962.
- (3) Gu, S.; Cai, R.; Luo, T.; Jensen, K.; Contreras, C.; Yan, Y. S. *Chemsuschem* **2010**, *3*, 555.
- (4) Kenawy, E. R.; Abdel-Hay, F. I.; Abou El-Magd, A.; Mahmoud, Y. *React. Func. Polym* **2006**, *66*, 419.
- (5) Kenawy, E. R.; Mahmoud, Y. A. G. *Macromol. Biosci.* **2003**, *3*, 107.
- (6) Popa, A.; Davidescu, C. M.; Trif, R.; Ilia, G.; Iliescu, S.; Dehelean, G. *React. Func. Polym.* **2003**, *55*, 151.
- (7) Kenawy, E. R.; Abdel-Hay, F. I.; El-Shanshoury, A.; El-Newehy, M. H. *J. Polym. Sci. A Polym. Chem.* **2002**, *40*, 2384.

- (8) Tindale, J. J.; Na, C.; Jennings, M. C.; Ragogna, P. J. *Can. J. Chem.* **2007**, *85*, 660.
- (9) Berven, B. M.; Oviasuyi, R. O.; Klassen, R. J.; Idacavage, M.; Gillies, E. R.; Ragogna, P. J. *J. Polym. Sci. A Polym. Chem.* **2012**.
- (10) Hatakeyama, E. S.; Ju, H.; Gabriel, C. J.; Lohr, J. L.; Bara, J. E.; Noble, R. D.; Freeman, B. D.; Gin, D. L. *J. Membr. Sci.* **2009**, *330*, 104.
- (11) Cheng, S.; Beyer, F. L.; Mather, B. D.; Moore, R. B.; Long, T. E. *Macromolecules* **2011**, *44*, 6509.
- (12) Cheng, S.; Zhang, M.; Wu, T.; Hemp, S. T.; Mather, B. D.; Moore, R. B.; Long, T. E. *J. Polym. Sci. A Polym. Chem.* **2012**, *50*, 166.
- (13) Hemp, S. T.; Allen, M. H., Jr.; Green, M. D.; Long, T. E. *Biomacromolecules* **2012**, *13*, 231.
- (14) Choi, N. S.; Park, J. K. *Solid State Ionics* **2009**, *180*, 1204.
- (15) Chen, D.; Zang, Y. L.; Su, S. P. *J. Appl. Polym. Sci.* **2010**, *116*, 1278.
- (16) Kim, S. K.; Guymon, C. A. *J. Polym. Sci. A Polym. Chem.* **2011**, *49*, 465.
- (17) Kim, S. K.; Guymon, C. A. *Polymer* **2012**, *53*, 1640.
- (18) Tindale, J. J.; Ragogna, P. J. *Chem. Commun.* **2009**, 1831.
- (19) Miao, H.; Cheng, L. L.; Shi, W. F. *Prog. Org. Coat.* **2009**, *65*, 71.
- (20) Sangermano, M.; Bongiovanni, R.; Longhin, M.; Rizza, G.; Kausch, C. M.; Kim, Y.; Thomas, R. R. *Macromol. Mater. Eng.* **2009**, *294*, 525.
- (21) Hu, Z.; Pitet, L. M.; Hillmyer, M. A.; DeSimone, J. M. *Macromolecules* **2010**, *43*, 10397.
- (22) Alvey, L. J.; Rutherford, D.; Juliette, J. J. J.; Gladysz, J. A. *J. Org. Chem.* **1998**, *63*, 6302.
- (23) Szabo, D.; Mohl, J.; Balint, A. M.; Bodor, A.; Rabai, J. *J. Fluorine Chem.* **2006**, *127*, 1496.
- (24) Stiles, A. R.; Rust, F. F.; Vaughan, W. E. *J. Am. Chem. Soc.* **1952**, *74*, 3282.
- (25) US-EPA 2010/2015 PFOA Stewardship Program - <http://www.epa.gov/oppt/pfoa/pubs/stewardship/index.html> (accessed March 6, 2013)
- (26) Honda, K.; Morita, M.; Otsuka, H.; Takahara, A. *Macromolecules* **2005**, *38*, 5699.

- (27) Hare, E. F.; Shafrin, E. G.; Zisman, W. A. *J. Phys. Chem.* **1954**, *58*, 236.
- (28) Emnet, C.; Weber, K. M.; Vidal, J. A.; Consorti, C. S.; Stuart, A. M.; Gladysz, J. A. *Adv. Synth. Catal.* **2006**, *348*, 1625.
- (29) Benninghoven, A. *Angew. Chem. Int. Ed.* **1994**, *33*, 1023-1043.
- (30) Wagner, M. S. *Anal. Chem.* **2005**, *77*, 911-922.

Chapter 3

3 Anion exchange reactions on a robust phosphonium photopolymer for the controlled deposition of ionic gold nanoclusters

3.1 Introduction

Polyelectrolytes have received significant attention within the past decade. The majority of the current research focuses on layer-by-layer (LbL) assemblies and polymerizable ions or ionic liquids (ILs) to generate new materials for a variety of applications. Examples include membranes,¹ gas barriers,^{2, 3} protective coatings,⁴ and antibacterial surfaces.⁵ Given these, there is a desire for new fabrication techniques to generate charged surfaces that exhibit beneficial properties. Currently, LbL assemblies dominate the polyelectrolyte coatings literature. This is due to their excellent control over thickness and surface functionality.⁶ However, poor mechanical properties, susceptibility to humidity, and morphological changes under acid/basic conditions can be limiting factors in their application.^{2, 7, 8} Through the utilization of polymerizable ions, a new strategy for the generation of mechanically robust, charged surfaces with the capability to perform surface chemistry is presented in this work.

Within the polymerizable IL community, most of the research has focused on nitrogen-based systems. Some of the earliest examples include work by Ohno *et al.* in 2002 and 2004 with the polymerization of vinyl functionalized imidazolium salts.^{9, 10} Phosphonium salts however have received much less attention despite their increased stability and highly tunable chemistry.^{11, 12} Some examples include work by Long *et al.* where free radical polymerization was used to form ABA tri-block copolymers,¹³ and earlier work by McGrath *et al.* with the formation of poly(arylene ether) phosphonium ionomers.¹⁴ Interestingly, there are very few examples of the photopolymerization of ILs, let alone phosphonium salts. Some examples include the work by Veith,¹⁵ Gin,¹⁶ Pojman,¹⁷ and a more recent report outlining the utility of our polymerizable phosphonium-borates in a photopolymeric system.¹⁸ The benefits of photopolymerization are vast and have been discussed in detail elsewhere.¹⁹ Briefly, they include excellent

control over the spatial and temporal polymerization process, reactions that are both solventless and fast, possess tunable chemistry, and have good mechanical properties. However, in all examples previously described, there is no mention of photopolymer coatings using low-melting point phosphonium salts, or their potential applications in materials science. This combination might provide the utility of a charged surface to do chemistry upon, possessing all the benefits of the photopolymerization method, with none of typical issues (mechanical stability, susceptibility to changing pH, solvent, and temperature) that plague LbL assemblies.

Anion-exchange reactions are a convenient and widely used technique to tune the physical and chemical properties of ammonium/phosphonium salts. In our system, we use the same ion-exchange process as a means of surface functionalization of crosslinked phosphonium-acrylate photopolymers using the room-temperature ionic liquid **3.2** (Scheme 3-1). This quick, low energy reaction pathway serves as an excellent method for depositing the desired anion on to a surface. Given the recent interest in “atomically precise” nanoparticles, we have taken advantage of the anionic gold nanocluster (AuNC), [TOA][Au₂₅L₁₈] (TOA = tetraoctylammonium bromide, L = SCH₂CH₂Ph, **3.3**), hereafter referred to simply as [Au₂₅L₁₈]⁻, as an excellent model for demonstrating the utility of our polyelectrolyte. By means of anion-exchange, [Au₂₅L₁₈]⁻ clusters replaced the anions bound to the covalently linked cationic polymer. Our motivation for doing so stems from their known solution phase optical absorptivity,^{20,21} photoluminescent,²²⁻²⁴ magnetic,²⁵ and redox properties, and their applications in organic reactions, catalysis,^{26, 27} optics^{28, 29} and as nano sensors³⁰. Manipulation of these AuNC in the solid state is a crucial step in their application, and thus new methodologies are required for further growth within this field. Their characteristic, yet sensitive physical features also provide an excellent handle to understand the chemistry occurring at the polyelectrolyte surface. To this end, our process yields highly robust and flexible AuNC films on a phosphonium polymer substrate despite repeated solvent rinsing, sonication, and exposure to atmosphere. Most importantly, they retain all physical properties after their controlled deposition to the solid state, a feat not demonstrated thus far. The total processing time from application of the pre-polymer formulation, polymerization, and post modification of the surface with [Au₂₅L₁₈]⁻ occurs in minutes and is amenable to roll-to-roll processing (Scheme 3-1). In

concentrated solutions of [TOA][Br], the deposited AuNC were removed from the surface within a matter of seconds. The stripped clusters retained their properties from the solid state back into solution, demonstrating the benign nature of our controlled deposition/stripping process. The coating showed no signs of degradation when re-functionalized with fresh $[\text{Au}_{25}\text{L}_{18}]^-$ despite repeated cycles. The strong ionic interaction between the cluster and the polymer rendered the AuNC “glued” on to the surface in the absence of any other ions, resulting in excellent adhesion. This illustrates the unique role ion-exchange systems possess as a method for surface functionalization as opposed to covalent systems.

Through the amalgamation of ionic liquids and photopolymerization perspectives, we show how this duo can be used in materials science and the development of new methodologies. Within 90 seconds, robust polyelectrolytes were synthesized and then used for the controlled deposition of $[\text{Au}_{25}\text{L}_{18}]^-$ through anion-exchange. This benign chemistry is highlighted using sensitive $[\text{Au}_{25}\text{L}_{18}]^-$ nanoclusters while its properties are harnessed in the solid state.

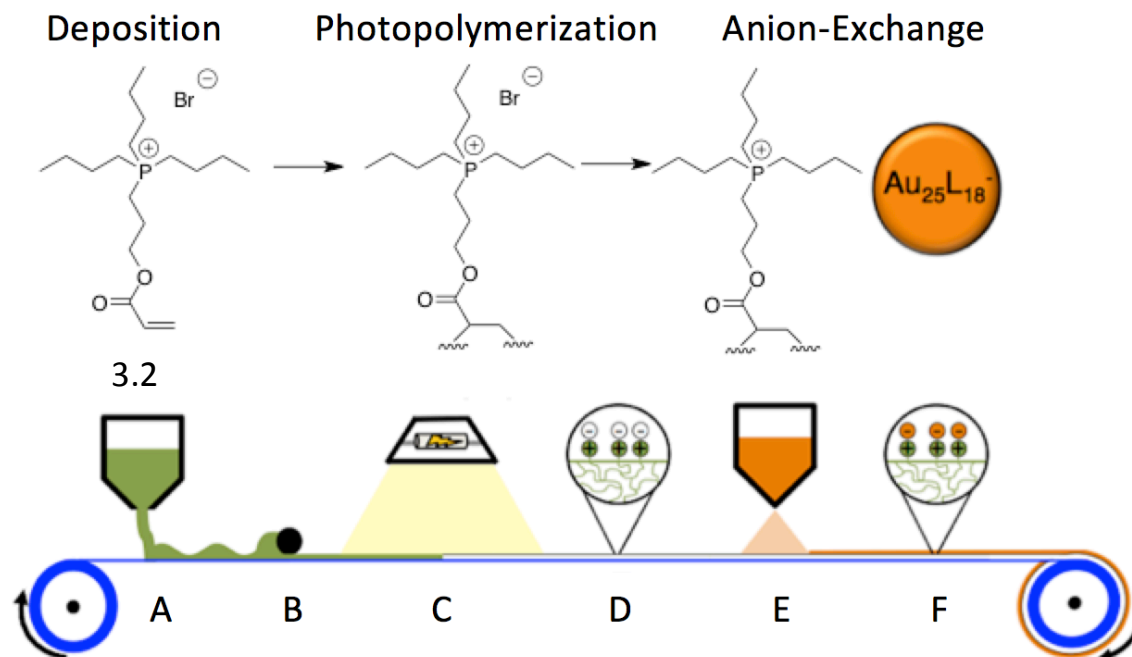


Figure 3-1: Representation of the overall process of applying the pre-polymer formulation containing phosphonium monomer **3.2** (A), drawing an even surface (B), irradiation (C) giving the cured ion exchange coating (D), followed by immersion of the substrate in [TOA][Au₂₅L₁₈] solution (E) to give the final coating (F).

3.2 Results and Discussion

The key phosphonium salt monomer **3.2** was prepared using a simple S_N2 reaction of a slight stoichiometric deficiency of 3-bromo-1-propanol with (*n*-Bu)₃P at elevated temperature. Aliquots of the reaction mixture were sampled at 1 hour intervals and each sample was analyzed by ³¹P{¹H} NMR spectroscopy, where singlet at δ_P = 34 ppm, indicative of the phosphonium bromide product (**3.1**), was observed to be at a maximum. Upon work up of the reaction mixture, the alcohol appended phosphonium salt was isolated in 80% yield. To convert the alcohol to the acrylate, an excess of acryloyl chloride was added drop-wise to a mixture of **3.1** and Et₃N at -35 °C. After stirring at low temperature for 1 hour, and then at rt for a further 24 hours a sample of the reaction mixture was obtained, which revealed a slight upfield shift in the ³¹P{¹H} NMR spectrum (δ_P = 33 ppm). The reaction mixture was worked up via CH₂Cl₂ extraction

followed by a series of aqueous washes. Upon drying of the volatiles *in vacuo*, the product (**3.2**) was isolated in approximately 20% yield (See Chapter 3 appendix for NMR spectra).³¹

To create a crosslinked phosphonium-based polyelectrolyte film (PPF), crosslinking agent Ebecryl 130 (EB130, Tricyclodecanediol diacrylate, see Chapter 3 appendix, Figure 7 for structure) was added to **3.2** in varying amounts and charge density measurements were taken. A well established protocol utilizing fluorescein dye was employed to determine the number of available exchange sites and to relate this quantity back to the percentage of phosphonium monomer.³³ This procedure is commonly used as a characterization technique for films containing surface-bound quaternary salts. To our surprise, no surface charges were detected for films containing between 1 and 25 wt% of **3.2** dissolved EB130. This may be due to surface energy effects, as EB130 is relatively hydrophobic in comparison. At 30 wt% **3.2**, a dramatic increase in the number of quaternary charges was observed (1.5×10^{15} cations/cm²). This sudden increase stems from a decrease of overall crosslink density of the polymer with an increase in hydrophilicity of the polymer allowing water to permeate into the film. Increasing the salt content to 37.5 and 47.5 wt% yielded surfaces with 8.2×10^{15} and 1.4×10^{16} cations/cm², respectively. Any attempt to incorporate more than 47.5 wt% of our electrolyte source resulted in delamination of the film during work up. Coatings with ≤ 47.5 wt% **3.2** displayed excellent adhesion to the substrate as well as maintained a high level of flexibility. These results indicate that a relatively high salt content (> 30 wt%) was necessary to cover the surface with quaternary ions when using EB130 as the crosslinker. Our choice of EB130 as crosslinker stems from its low viscosity, good miscibility with the phosphonium salt, and its low shrinkage properties. Through the exploitation of our low melting phosphonium compound, we maintain a low formulation viscosity despite the high ion content, allowing for ease of handling and deposition. In contrast, incorporating high melting point organic salts in a similar fashion generates formulations with very high viscosities or significant solubility issues, which manifest themselves in poor films. This underscores the importance of the phosphonium-based acrylate monomer **3.2** in the fabrication of the charged surfaces. To demonstrate the utility of

these new materials, films containing 47.5 wt% **3.2** were used in the studies below for the incorporation of $[\text{Au}_{25}\text{L}_{18}]^-$ onto the surface.

The synthesis of $[\text{TOA}][\text{Au}_{25}\text{L}_{18}]$ ($\text{L} = \text{SCH}_2\text{CH}_2\text{Ph}$) was accomplished using methods reported by Murray³⁴ and coworkers and Maran^{35,36} and coworkers with some modification.³⁷ The purity and structure of our Au_{25}NC was established and is described in the SI. While there has been work done on the characterization of these new materials, the charged nature of the $[\text{Au}_{25}\text{L}_{18}]^-$ has yet to be taken advantage of in device fabrication. Given the well-understood chemistry associated with ion exchange processes, it was expected that the bromide anions on the surface of PPF would undergo an anion exchange with $[\text{TOA}][\text{Au}_{25}\text{L}_{18}]$ in solution, to give $[\text{TOA}][\text{Br}]$ as a metathesis by-product, and a $[\text{Au}_{25}\text{L}_{18}]^-$ modified phosphonium-based polyelectrolyte film ($\text{Au}_{25}\text{-PPF}$) (Figure 3-1, **E**). This simple exchange process allows for a fast and highly cost effective route to prepare solid-state films of $[\text{Au}_{25}\text{L}_{18}]^-$, while targeting the retention of their solution phase physical properties (**F**).

Deposition of $[\text{Au}_{25}\text{L}_{18}]^-$ proceeded by a single “dip-and-rinse” approach. Freshly prepared PPF were cut into 0.75 x 2.5 cm strips and then immersed in a concentrated (0.5 wt%, 5.7 mM) solution of $[\text{TOA}][\text{Au}_{25}\text{L}_{18}]$ in acetonitrile. Upon removal of the films from solution, each sample was rinsed and sonicated in toluene to ensure the expulsion of $[\text{TOA}][\text{Br}]$. The resulting product possessed an orange color similar to dilute solutions of $[\text{TOA}][\text{Au}_{25}\text{L}_{18}]$ (Figure 3-2), although the color intensified/weakened with longer/shorter immersion times. Control experiments using the PET substrate with a cured film of only the crosslinker EB130 and photoinitiator did not display any color change after immersion into a solution containing $[\text{Au}_{25}\text{L}_{18}]^-$, nor did the immersion of a blank PET film. This confirms that the deposition requires the phosphonium salt and that the electrostatic forces between the phosphonium cation and the $[\text{Au}_{25}\text{L}_{18}]^-$ cluster are critical for the self-assembly.

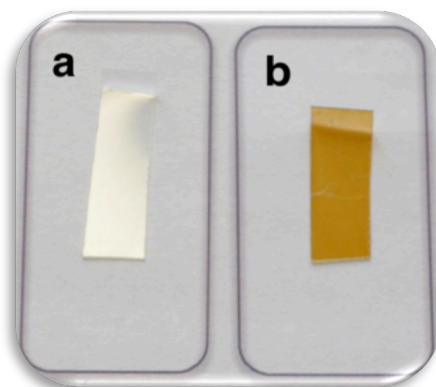


Figure 3-2: Photographs of a polyelectrolyte film containing 47.5 wt% polymerizable phosphonium salt. a) before and b) after immersion in a 0.5 wt% (5.7 mM) solution of [TOA][Au₂₅L₁₈] in acetonitrile.

The distinctive absorbance of [Au₂₅L₁₈]⁻ in the UV-vis spectrum is a diagnostic handle for characterization of these [Au₂₅L₁₈]⁻, and can serve as an excellent indicator for their presence. Figure 3-3 shows the UV-vis spectrum of a 0.025 mM solution of [TOA][Au₂₅L₁₈] dissolved in acetonitrile (spectrum **a**), along with spectra obtained by dipping the polyelectrolyte film in a 1.9 mM solution of [TOA][Au₂₅L₁₈] for varying amounts of time (spectrum **b**). The dilute solution was used to more easily monitor changes in the UV-vis spectrum as a function of immersion time. The increased number of ionically bound [Au₂₅L₁₈]⁻ on the Au₂₅-PPF is evident by the increase in the characteristic absorbance that correlate to the solution UV-vis spectrum of [TOA][Au₂₅L₁₈] ($\lambda_{\text{max}} = 410, 460 \text{ and } 670$)^{35,38}. In Au₂₅-PPF, the peak maxima are slightly shifted to larger wavelength (red shift), consistent with light scattering in the solid state.³⁹ It should be noted that if the [Au₂₅L₁₈]⁻ aggregated significantly or decomposed upon incorporation onto the PPF, then the UV-vis spectral features attributable to [Au₂₅L₁₈]⁻ would be absent.⁴⁰ After 5 minutes of immersion, no further increase in the absorbance maxima were detected (see inset) indicating a saturation of exchangeable sites.

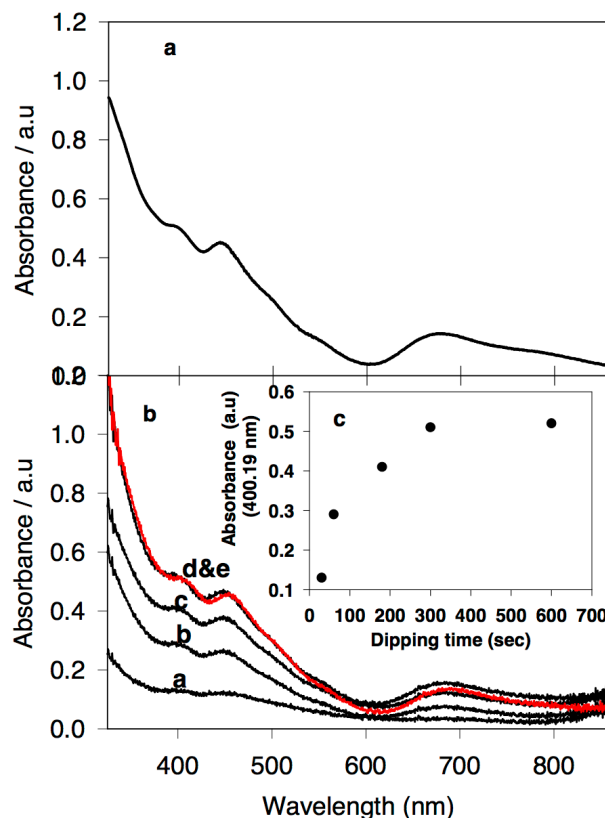


Figure 3-3: UV-vis spectrum of a 0.025 mM solution of $[\text{TOA}][\text{Au}_{25}\text{L}_{18}]$ in acetonitrile (top); UV-vis spectra of the Au_{25} -PPF after 10 sec, 1 min, 3 min, 5 min and 10 min (a-e) dipping in a 1.9 mM solution of $[\text{TOA}][\text{Au}_{25}\text{L}_{18}]$ in acetonitrile (bottom). Figure inset; dipping time vs. absorbance. Plot shows the dipping time after 10 sec, 1 min, 3 min, 5 min and 10 min vs. absorbance of $[\text{Au}_{25}\text{L}_{18}]^-$ at 400 nm.

Successful incorporation of the $[\text{Au}_{25}\text{L}_{18}]^-$ onto the polymer film was also probed using Energy-dispersive X-ray spectroscopy (EDX; Figure 3-4). EDX analysis of samples before and after dipping in the solution of $[\text{Au}_{25}\text{L}_{18}]^-$ revealed intense signals for the presence of Au at 2.1205 keV (M_{α}) and for sulfur at 2.3075 keV (L_{α}), key indicators that the necessary atomic components were present. The persistence of the Br signal before and after immersion is likely a result of the sub-surface bromide anions that were not capable of exchanging, and is consistent with only an outer layer being exposed to solution. Wide-angle PXRD also confirmed the presence of $[\text{Au}_{25}\text{L}_{18}]^-$ at $\sin(2\theta)$ values

of 5.2 and 8.2, consistent with the diagnostic *fcc*-Au configuration already documented in the literature.^{41, 42}

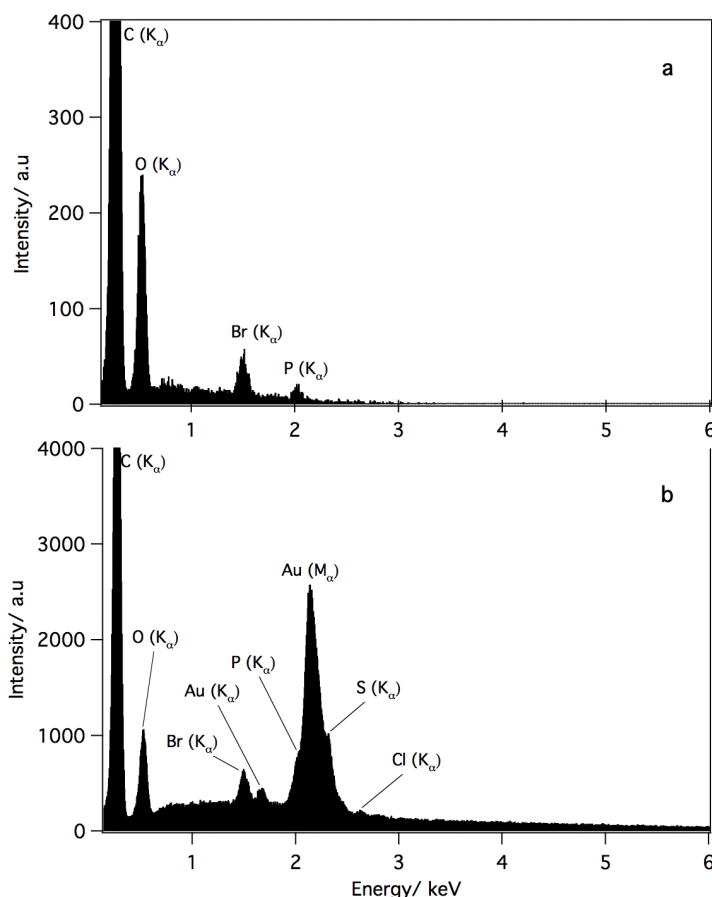


Figure 3-4: Electron Dispersion X-ray (EDX) spectra. Recorded spectrum of PPF before dipping (Top; a); After 10 minutes immersion in a 1.9 mM solution of [TOA][Au₂₅L₁₈] in acetonitrile (Bottom; b); Energy peaks at 2.1205 keV and 2.3075 keV representing Au (M_α) and S (L_α) atoms on the Au₂₅-PPF.

Although the above analytical techniques confirm the incorporation of [Au₂₅L₁₈]⁻ onto the polymer surface, this technique is only valuable if the incorporated clusters maintain their unique physical properties for potential application. The solid-state UV-vis spectra indeed support this expectation, however further experimentation was performed to verify these results. The inherent nature of ionic bonding allows for unique probing methods that are both fast and convenient. Au₂₅-PPF was immersed and shaken in a [TOA][Br] solution for several seconds (THF, 20% w/w) in an attempt to strip the

surface of $[\text{Au}_{25}\text{L}_{18}]^-$, and regenerate native PPF. As soon as the film was immersed, the characteristic color of the $[\text{Au}_{25}\text{L}_{18}]^-$ transferred to solution, which was then analyzed using UV-vis spectroscopy. It was found that the ion-exchange product possessed identical spectral features to $[\text{TOA}][\text{Au}_{25}\text{L}_{18}]$. This not only confirmed that the surface-bound gold was indeed $[\text{Au}_{25}\text{L}_{18}]^-$, but also supported our assertion that $[\text{Au}_{25}\text{L}_{18}]^-$ did not decompose or aggregate irreversibly while residing on the polyelectrolyte surface. The UV-vis spectrum of the remaining film was featureless. Similar to the fluorescein dye experiment, one can utilize the solution UV-vis absorption data of the $[\text{Au}_{25}\text{L}_{18}]^-$ that was exchanged off of the PPF to quantify the number of $[\text{Au}_{25}\text{L}_{18}]^-$ clusters that were originally on the surface of the film. Using the extinction coefficient of $[\text{TOA}][\text{Au}_{25}\text{L}_{18}]$ in THF ($4.3 \times 10^4 \text{ M}^{-1}\text{cm}^{-1}$ at 400 nm), the effective surface density was determined to be $6.4 \times 10^{15} [\text{Au}_{25}\text{L}_{18}]^- \text{ anions/cm}^2$. This value is within a factor of two relative to the fluorescein dye experiment ($1.4 \times 10^{16} \text{ cations/cm}^2$), which we take as excellent agreement and implies that a large majority of the available bromide exchange sites have been occupied. The small difference may be attributed to the slightly larger size of the $[\text{Au}_{25}\text{L}_{18}]^-$ compared to the fluorescein dye. We believe that the mechanism for polymer functionalization occurs through swelling of the polymer in acetonitrile, followed by anion-exchange with $[\text{Au}_{25}\text{L}_{18}]^-$. This process would explain the high charge density observed in our experiments.

Water contact angle (WCA) measurements were conducted to confirm passivation of Au_{25} -PPF, as the $[\text{Au}_{25}\text{L}_{18}]^-$ anion should be significantly more hydrophobic than halogen anions due to the protecting ligands. While pristine PPF samples exhibited near complete wettability, Au_{25} -PPF possessed contact angles slightly below 90° , providing strong evidence for the formation of a highly passivated surface (Figure 3-5).



Figure 3-5: Water contact images of (left) pristine PPF ($WCA = 17^\circ \pm 3$) and (right) Au_{25} -PPF after dipping for 10 minutes in a 1.9 mM solution of $[TOA][Au_{25}L_{18}]$ in acetonitrile ($WCA = 87^\circ \pm 1$).

These experiments gave a quantitative indication of $[Au_{25}L_{18}]^-$ loading on the PPF, however they gave little information on the efficacy of the regeneration of the process and the stability of the polyelectrolyte films themselves. An experiment was designed to determine the ion-exchange efficacy of the polymer film after many exchange processes. Freshly prepared PPF were repeatedly functionalized using $[TOA][Au_{25}L_{18}]$ and stripped using $[TOA][Br]$. After each functionalization and stripping procedure, a UV-vis spectrum of the film was obtained. By comparing the intensity of the $[Au_{25}L_{18}]^-$ absorbance after each functionalization/stripping step, we can monitor any changes in the ion-exchange capability of the film. It was found that even after eight cycles, there was no loss in the exchange capability of the surface, as the absorbance values at both 400 and 683 nm remained essentially identical throughout the experiment (Figure 3-6). These results highlight the efficient chemistry of the ion-exchange process and the reusability of our films.

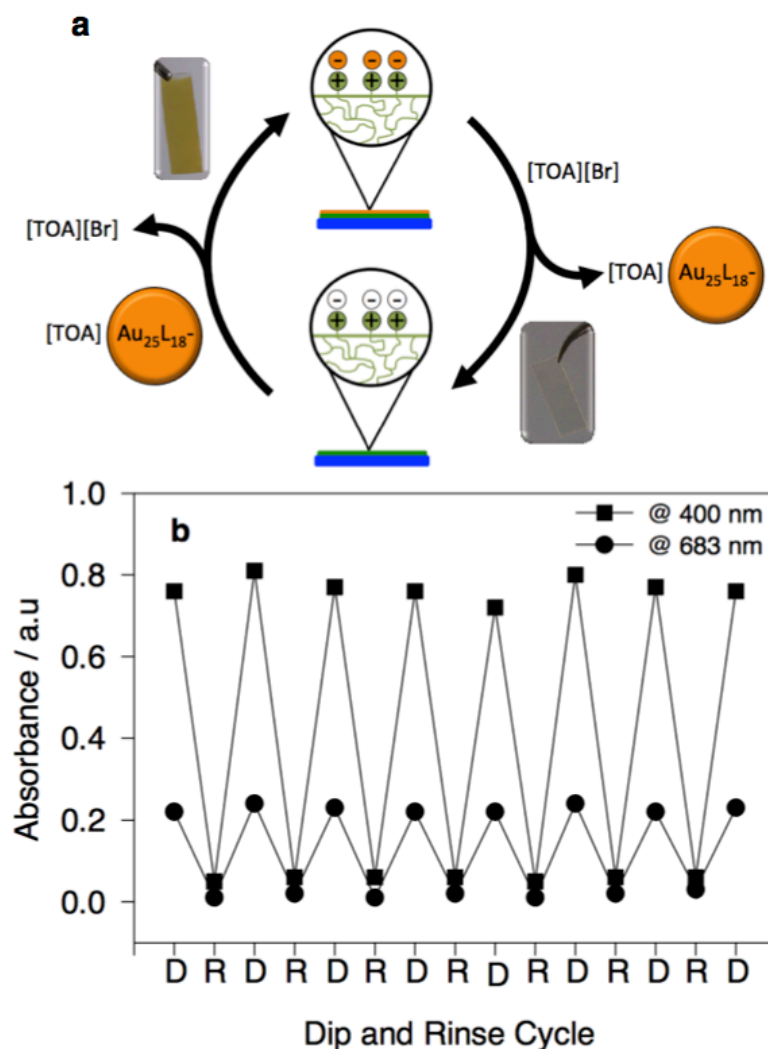


Figure 3-6: a) Representation of the reversible exchange process and b) UV-vis data demonstrating zero loss of polymer activity through eight on/off cycles, monitored at 400 and 683 nm.

While these films are capable of withstanding repeated exposure to organic solvents and ion-exchange reactions, the Au_{25} -PPF film's resilience to the repeated application and removal of Scotch-Tape™ is also remarkable; no evidence for removal of the gold or damage to the polymer itself was observed. This is attributed to the strong ionic interactions between the gold clusters and the polymer substrate. The crosslinked nature of the polyelectrolyte resulted in excellent physical toughness and resistance to sonication in solvents such as water, acetone, THF, toluene, and acetonitrile, a highly desirable feature not often shared by LbL systems. A scratch-test using a diamond-tipped

stylus and nanoindentation were both conducted on pristine PPF to gain further insight into the film's mechanical properties. For the scratch test, a constant load of 0.5 mN was applied to the polymer film and imaged using AFM. A groove of approximately 10 nm in depth and 2 microns in width was formed as a result of the scratch, which is comparable to our previous experiments with photopolymerized polyelectrolytes.¹⁸ A hardness value of 0.11 GPa was obtained from load-displacement nanoindentation analysis, which is also comparable to our previous results.¹⁸

To further demonstrate the retention of the solution photophysical properties on Au₂₅-PPF, the near-IR photoluminescence (Near-IR PL) spectra of the decorated film were recorded (Figure 3-7). A 0.3 mM solution of [TOA][Au₂₅L₁₈] in acetonitrile and Au₂₅-PPF was subjected to excitation at 467 nm, and a peak at 1086 nm was observed for both. The higher occupied molecular orbital (HOMO) and lower unoccupied molecular orbital (LUMO) energy gap are in line with the work published by Murray *et al.*²²⁻²⁴ The corresponding spectrum collected using the Au₂₅-PPF (after 10 minutes dipping in a 1.9 mM solution of the Au₂₅⁻) revealed identical emission peaks indicating [Au₂₅L₁₈]⁻ incorporated onto the surface where it maintains its physical properties.

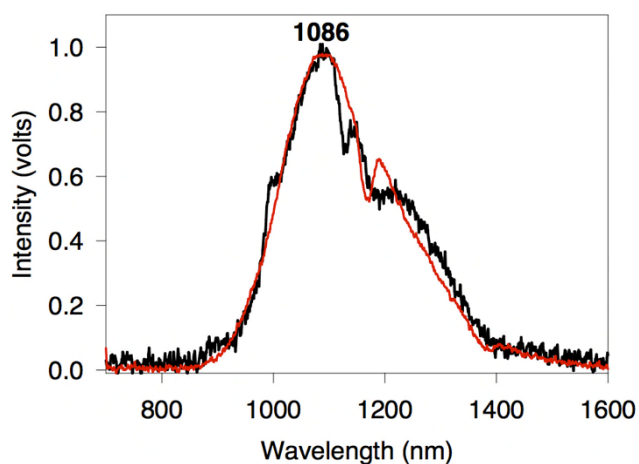


Figure 3-7: Red line, spectrum of [TOA][Au₂₅L₁₈] collected in solution (acetonitrile, C = 0.3 mM). Black line, immobilized Au₂₅-PPF after 10 minutes immersion in the [TOA][Au₂₅L₁₈] stock solution.

3.3 Conclusions

A new class of photopolymerized anion-exchange coatings was fabricated using an acrylate-appended phosphonium salt. The materials for the polymer can be prepared in the bulk scale, while the anion-exchange process is straightforward and takes only a matter of seconds. The number of exchangeable anions on the polymer film was quantified and replaced with $[\text{Au}_{25}\text{L}_{18}]^-$ nanoclusters. The integrity of the solution phase properties of the nanocluster was maintained in the solid-state as a thin film. Both PPF and Au_{25} -PPF were robust, stable in aqueous and organic solvents, and showed good mechanical resiliency. Meanwhile, they can be easily reversed and the functional anion recharged simply in a dip-to-dip process. The ability to maintain the properties of the $[\text{Au}_{25}\text{L}_{18}]^-$ nanocluster, such as the optical and NIR photoluminescence in a well defined film, coupled with a convenient and fast deposition technique, provides many avenues for their exploitation in functional materials. We envision our system to be particularly well suited for preparing solid-supported $[\text{Au}_{25}\text{L}_{18}]^-$ reaction vessels for catalytic reactions, optical devices, and sensors.

The phosphonium-based electrolyte network itself may also serve as a permanently charged, robust substrate on which to perform polyelectrolyte chemistry for other applications. The photopolymerization method to generate ionic surface serves as a complementary approach to LbL assemblies. While LbL systems display excellent control over coating thickness and composition on the nanometer scale, photopolymer constructs provide highly crosslinked networks with tunable properties and rich chemistry. We believe there is great opportunity in combining these approaches—building LbL assemblies on to photopolymerized networks generated from low-melting point polymerizable salts. It is our intention to demonstrate that these non-overlapping disciplines may all benefit from each other to form a system that is greater than simply the sum of its parts.

3.4 Experimental

Synthesis of tributyl(3-hydroxypropyl)phosphonium bromide (3.1)

A 500 mL pressure round bottom flask was filled with 200 mL of deoxygenated acetonitrile in a nitrogen atmosphere. An emulsion formed upon the addition of tributylphosphine (34.80 g, 172 mmol). To the solution, 0.9 molar equivalents of deoxygenated 3-bromo-1-propanol (21.54 g, 155 mmol) was slowly added followed by heating at 100 °C for 7 hours. After cooling to room temperature, the solution was poured into a 1 L round bottom flask followed by the evaporation of volatiles *in vacuo* at 40 °C. The white emulsion was dissolved in a minimal amount of DCM and then precipitated in diethyl ether. After decanting the ether layer, the precipitation process was repeated five times. The emulsion was then heated *in vacuo* to remove volatiles resulting in a clear and colourless oil (42.18 g, 80% yield). T_g : -65.92 °C; $^1\text{H NMR}$ (400 MHz, CDCl_3): δ =3.68 (t, $^3J_{\text{H-H}} = 8$ Hz, 2H; CH_2), 2.43-2.56 (m, 2H; CH_2), 2.23-2.36 (m, 6H; CH_2), 1.78-1.98 (m, 2H; CH_2), 1.40-1.59 (m, 12H; CH_2), 0.92 ppm (t, $^3J_{\text{H-H}} = 8$ Hz, 9H; CH_3). $^{13}\text{C}\{^1\text{H}\}$ NMR (100 MHz, CDCl_3) δ =60.7 (d, $^3J_{\text{P-C}} = 13$ Hz, 1C), 24.7 (d, $^2J_{\text{P-C}} = 4$ Hz, 1C), 23.9 (d, $^3J_{\text{P-C}} = 16$ Hz, 3C), 23.6 (d, $^2J_{\text{P-C}} = 4$ Hz, 3C), 19.1 (d, $^1J_{\text{P-C}} = 47$ Hz, 4C), 16.3 (d, $^1J_{\text{P-C}} = 49$ Hz, 1C), 13.4 ppm (s, 3C). $^{31}\text{P}\{\text{H}\}$ NMR (161.82 MHz, CDCl_3) δ 34.0 (s); FTIR-ATR: ν (cm^{-1}) 3303 (OH), 1063 (C-O). TOF-MS-ES+ observed 260, ($[\text{M-H}]^+$, 100), 261, ($[\text{M}]^+$, 15), 602, ($[\text{2M} + ^{79}\text{Br}]^+$, 60). TOF-MS-ES- observed 421, ($[\text{M} + ^{79}\text{Br} + ^{81}\text{Br}]^-$, 10). Elemental Analysis (found) C, 52.16 (52.79) and H, 10.27 (10.04).

Synthesis of (3-(acryloyloxy)propyl)tributylphosphonium bromide (3.2)

A 1 L round bottom flask was filled with 200 mL of acetonitrile and tributyl(3-hydroxypropyl)phosphonium bromide (25.69 g, 75.5 mmol). The solution was then cooled to -35 °C prior to the addition of 1.1 molar equivalents of triethylamine (8.40 g, 83.0 mmol). After stirring for 5 minutes, 1.1 molar equivalents of acryloyl chloride (7.51 g, 83.0 mmol) was added dropwise (2 drops/second). The solution was stirred for 1 hour and then left to warm to room temperature over 24 hours. Volatiles were evaporated *in vacuo* at 40 °C resulting in a yellow slurry. The slurry was then dissolved in 200 mL of DCM and washed with distilled water (25 mL) 5 times. The organic layer was dried with

a minimal amount of sodium sulphate, filtered and the volatiles evaporated *in vacuo* at 40 °C. The orange oil was then redissolved in a minimal amount of DCM and precipitated in 150 mL of stirring hexanes. The biphasic mixture was left to sit for 10 minutes before decanting the hexanes layer. The orange emulsion was heated *in vacuo* to remove volatiles resulting in clear orange oil (5.95 g, 20% yield). T_g : -56.83 °C; ^1H NMR (400 MHz, CDCl_3): δ =6.41 (d, $^3J_{\text{H-H}} = 16$ Hz, 1H; CH), 6.01 (dd, $^3J_{\text{H-H}} = 12$ Hz (trans), $^3J_{\text{H-H}} = 8$ Hz (cis), 1H; CH), 5.84 (d, $^3J_{\text{H-H}} = 12$ Hz, 1H; CH), 4.27 (t, $^3J_{\text{H-H}} = 4$ Hz, 2H; CH_2), 2.51-1.54 (m, 2H; CH_2), 2.31-2.52 (m, 6H; CH_2), 1.80-2.10 (m, 2H; CH_2), 1.50 (m, 12H; CH_2), 0.94 ppm (t, $^3J_{\text{H-H}} = 8$ Hz, 9H; CH_3). $^{13}\text{C}\{^1\text{H}\}$ NMR (100 MHz, CDCl_3) δ =165.8 (s, 1C), 131.6 (s, 1C), 127.8 (s, 1C), 63.5 (d, $^3J_{\text{P-C}} = 16$ Hz, 1C), 23.8 (d, $^3J_{\text{P-C}} = 15$ Hz, 3C), 23.7 (d, $^2J_{\text{P-C}} = 5$ Hz, 3C), 21.4 (d, $^2J_{\text{P-C}} = 4$ Hz, 1C), 19.0 (d, $^1J_{\text{P-C}} = 47$ Hz, 3C), 16.3 (d, $^1J_{\text{P,C}}=49$ Hz, 1C), 13.4 ppm (s, 3C). $^{31}\text{P}\{\text{H}\}$ NMR (161.82 MHz, CDCl_3) δ =33.2 ppm (s). FTIR-ATR: ν (cm^{-1}) 1718 (C=O), 812 (acrylate C=C-H bend). TOF-MS-ES+ observed 315, ($[\text{M}]^+$, 100), 710, ($[2\text{M} + ^{79}\text{Br}]^+$, 40), 666, ($[2\text{M} + ^{35}\text{Cl}]^+$, 10). TOF-MS-ES- observed 431, ($[\text{M} + ^{79}\text{Br} + ^{35}\text{Cl}]^-$, 20), 475, ($[\text{M} + ^{79}\text{Br} + ^{81}\text{Br}]^-$, 90).*

*Through the formation of $[\text{HNEt}_3][\text{Cl}]$, some of the chloride ions exchanged for the bromide forming $[\text{PR}_4][\text{Cl}]$ and $[\text{HNEt}_3][\text{Br}]$

Film Preparation

To prepare our cross-linked phosphonium-based polyelectrolyte films (PPF), pre-polymer mixtures with desired photoinitiator (HDMAP, 2-hydroxy-2-methyl-1-phenylpropanone, 5 wt% available from Cytec), crosslinker (EB130, tricyclodecanediol diacrylate, available from Cytec), and compound **3.2** were mixed together, deposited on Melinex 725 Teijin PET substrates (Scheme 1, **A**) and metered to a 25 micron thickness using a Meyer rod (**B**). The wet film was then irradiated under UV-light in air (**C**) with an energy density of 1956 mJ/cm^2 and an irradiance of 1383 mW/cm^2 , resulting in a transparent, tack-free polymer coating (**D**) (polymer can also be deposited on glass and peeled off to produce a free standing film). To determine the cure percentage, a comparison of the intensity of the acrylate $\text{CH}_2=\text{CH}$ vibration of the acrylate phosphonium salt (810 cm^{-1}) before and after irradiation relative to an internal standard (C=O stretch, 1750 cm^{-1}) using FTIR-ATR

spectroscopy was performed.⁵⁷ The reduced relative intensity of the peak at 810 cm⁻¹ is indicative of acrylate conversion during polymerization, where the cure percentage was consistently determined to be 80%.

References

- (1) Tagliazucchi, M.; Rabin, Y.; Szleifer, I. *J. Am. Chem. Soc.* **2011**, *133*, 17753.
- (2) Priolo, M. A.; Gamboa, D.; Holder, K. M.; Grunlan, J. C. *Nano Lett.* **2010**, *10*, 4970.
- (3) Yang, Y.-H.; Haile, M.; Park, Y. T.; Malek, F. A.; Grunlan, J. C. *Macromolecules* **2011**, *44*, 1450.
- (4) Andreeva, D. V.; Fix, D.; M^ohwald, H.; Shchukin, D. G. *Adv. Mater.* **2008**, *20*, 2789.
- (5) Karamdoust, S.; Yu, B.; Bonduelle, C. V.; Liu, Y.; Davidson, G.; Stojcevic, G.; Yang, J.; Lau, W. M.; Gillies, E. R. *J. Mat. Chem.* **2012**, *22*, 4881.
- (6) Lehaf, A. M.; Hariri, H. H.; Schlenoff, J. B. *Langmuir* **2012**, *28*, 6348.
- (7) Cho, C.; Zacharia, N. S. *Langmuir* **2011**, *28*, 841.
- (8) Gemici, Z.; Shimomura, H.; Cohen, R. E.; Rubner, M. F. *Langmuir* **2008**, *24*, 2168.
- (9) Yoshizawa, M.; Ogihara, W.; Ohno, H. *Polymer. Adv. Tech.* **2002**, *13*, 589.
- (10) Ohno, H.; Yoshizawa, M.; Ogihara, W. *Electrochim. Acta* **2004**, *50*, 255.
- (11) Tindale, J. J.; Ragogna, P. J. *Chem. Commun.* **2009**, 1831.
- (12) Tindale, J. J.; Moulard, K. L.; Ragogna, P. J. *J. Mol. Liq.* **2010**, *152*, 14.
- (13) Cheng, S.; Beyer, F. L.; Mather, B. D.; Moore, R. B.; Long, T. E. *Macromolecules* **2011**, *44*, 6509.
- (14) Ghassemi, H.; Riley, D. J.; Curtis, M.; Bonaplata, E.; McGrath, J. E. *ChemInform* **1999**, *30*.
- (15) Lin, H.; de Oliveira, P. W.; Veith, M. *Opt. Mater* **2011**, *33*, 759.
- (16) Hatakeyama, E. S.; Ju, H.; Gabriel, C. J.; Lohr, J. L.; Bara, J. E.; Noble, R. D.; Freeman, B. D.; Gin, D. L. *J. Membr. Sci.* **2009**, *330*, 104.

- (17) Jiménez, Z.; Bounds, C.; Hoyle, C. E.; Lowe, A. B.; Zhou, H.; Pojman, J. A. *J. Polym. Sci. A Polym. Chem.* **2007**, *45*, 3009.
- (18) Berven, B. M.; Oviasuyi, R. O.; Klassen, R. J.; Idacavage, M.; Gillies, E. R.; Ragona, P. J. *J. Polym. Sci. A Polym. Chem.* **2012**.
- (19) Bowman, C. N.; Kloxin, C. J. *AIChE Journal* **2008**, *54*, 2775.
- (20) Devadas, M. S.; Bairu, S.; Qian, H.; Sinn, E.; Jin, R.; Ramakrishna, G. *J. Phys. Chem. Lett.* **2011**, 2752.
- (21) Parker, J. F.; Fields-Zinna, C. A.; Murray, R. W. *Acc. Chem. Res.* **2010**, *43*, 1289.
- (22) Wang, G.; Huang, T.; Murray, R. W.; Menard, L.; Nuzzo, R. G. *J. Am. Chem. Soc.* **2004**, *127*, 812.
- (23) Wang, G.; Guo, R.; Kalyuzhny, G.; Choi, J.-P.; Murray, R. W. *J. Phys. Chem. B* **2006**, *110*, 20282.
- (24) Lee, D.; Donkers, R. L.; Wang, G.; Harper, A. S.; Murray, R. W. *J. Am. Chem. Soc.* **2004**, *126*, 6193.
- (25) Zhu, M.; Aikens, C. M.; Hendrich, M. P.; Gupta, R.; Qian, H.; Schatz, G. C.; Jin, R. *J. Am. Chem. Soc.* **2009**, *131*, 2490.
- (26) Zhu, Y.; Qian, H.; Drake, B. A.; Jin, R. *Angew. Chem. Int. Ed.* **2010**, *49*, 1295.
- (27) Zhu, Y.; Wu, Z.; Gayathri, C.; Qian, H.; Gil, R. R.; Jin, R. *J. Catal.* **2010**, *271*, 155.
- (28) Ramakrishna, G.; Varnavski, O.; Kim, J.; Lee, D.; Goodson, T. *J. Am. Chem. Soc.* **2008**, *130*, 5032.
- (29) Muhammed, M. A. H.; Shaw, A. K.; Pal, S. K.; Pradeep, T. *J. Phys. Chem. C* **2008**, *112*, 14324.
- (30) Wu, Z.; Wang, M.; Yang, J.; Zheng, X.; Cai, W.; Meng, G.; Qian, H.; Wang, H.; Jin, R. *Small* **2012**, n/a.
- (31) Substituting 3-bromo-1-propanol with 3-chloro-1-propanol for the quaternization (**3**) resulted in much higher yields after the acrylation reaction. The polymerizable chloride salt (**4**) possessed similar exchange properties to that of the bromide. See SI for synthetic details.
- (32) Lee, B. H.; Choi, J. H.; Kim, H. J. *Jct Research* **2006**, *3*, 221.

- (33) Murata, H.; Koepsel, R. R.; Matyjaszewski, K.; Russell, A. J. *Biomaterials* **2007**, *28*, 4870.
- (34) Parker, J. F.; Weaver, J. E. F.; McCallum, F.; Fields-Zinna, C. A.; Murray, R. W. *Langmuir* **2010**, *26*, 13650.
- (35) Venzo, A.; Antonello, S.; Gascón, J. A.; Guryanov, I.; Leapman, R. D.; Perera, N. V.; Sousa, A.; Zamuner, M.; Zanella, A.; Maran, F. *Anal. Chem.* **2011**, *83*, 6355.
- (36) Antonello, S.; Hesari, M.; Polo, F.; Maran, F. *Nanoscale* **2012**.
- (37) Swanick, K. N.; Hesari, M.; Workentin, M. S.; Ding, Z. *J. Am. Chem. Soc.* **2012**, *134*, 15205.
- (38) Zhu, M.; Aikens, C. M.; Hollander, F. J.; Schatz, G. C.; Jin, R. *J. Am. Chem. Soc.* **2008**, *130*, 5883.
- (39) Amara, J. P.; Swager, T. M. *Macromolecules* **2006**, *39*, 5753.
- (40) Garcia-Raya, D.; Madueno, R.; Blazquez, M.; Pineda, T. *J. Phys. Chem. C* **2009**, *113*, 8756.
- (41) Negishi, Y.; Kamimura, U.; Ide, M.; Hirayama, M. *Nanoscale* **2012**.
- (42) Negishi, Y.; Kurashige, W.; Kamimura, U. *Langmuir* **2011**, *27*, 12289.

Chapter 4

4 Kinetically controlled patterning of highly charged phosphonium photopolymers using simple anion exchange

4.1 Introduction

Polyelectrolytes are a broad class of polymers that are increasingly useful in biomedical devices, solar cells, solid-state electrolytes, gas barriers, and many other applications.¹⁻⁸ The utility of such charged polymers is a testament to their diversity and capabilities to be tailored for a specific application. By far, nitrogen based polymers dominate the cationic polyelectrolyte literature. One contributing reason for this stems from the intense study of nitrogen-based salts within the discipline of polymerizable ionic liquids. Some of the earliest work done by Ohno has shown that polyelectrolytes can be prepared using nitrogen-containing salts bearing a polymerizable group possess the necessary properties to act as membranes for electrochemical applications.^{9, 10, 11} Since then, there has been a wealth of research to further understand and synthesize these new materials, including the lesser studied phosphonium salt variety.¹²⁻¹⁴ Polymerizable cations have made several appearances in photopolymeric systems, and includes noteworthy studies by Ohno,¹⁵ Gin,¹⁶ and Guymon^{17,18}, while the first highly detailed study on the photopolymerization of ionic liquids (ILs) was conducted by Hoyle and Pojman using a simple system comprised of an acid-base reaction between a tertiary amine and acrylic acid.¹⁹ Using ionic compounds bearing two polymerizable groups - one on the cation, and one on the anion, they demonstrated a 5-10 fold increase in polymerization rate, thus demonstrating the importance of a self-crosslinking salt.

Over the last few years, our group has developed an interest in polymerizable phosphonium and borate salts.^{20, 21} We have demonstrated the utility of a phosphonium based photopolymer network for the controlled deposition of anionic gold nanoclusters, where crosslinked polyelectrolytes were fabricated in a facile (seconds), solventless process.²² The key to this approach is a direct result of the low melting temperature of the ionic monomer. The miscibility of the low melting point salt with a crosslinker allows for

full control over the ion content within the network without the need for solvent to aid in processing or solubilizing the components, an almost impossible task using high-melting salts. Such an approach represents the quickest and cleanest possible route for generating ionic networks with very high charge densities. Often within photopolymerizable systems, (meth)acrylate monomers bear at least two polymerizable groups. This approach results in high crosslink densities frequently required for mechanically robust materials (e.g. dental resins,^{23, 24} coatings,²⁵ and photolithographic resists²⁶). These features are not attainable using a phosphonium salt with one acrylate, as high crosslink densities must be achieved using a crosslinker, thus diluting ion content (and its associated properties) within the material. To our knowledge, self-crosslinking phosphonium salts have not been exploited in either thermal and photopolymeric system using free-radical polymerization, and in this context, we have described here a phosphonium ion bearing three methacrylate groups directly attached to the phosphorus centre (**4.2**; Figure 4-1).

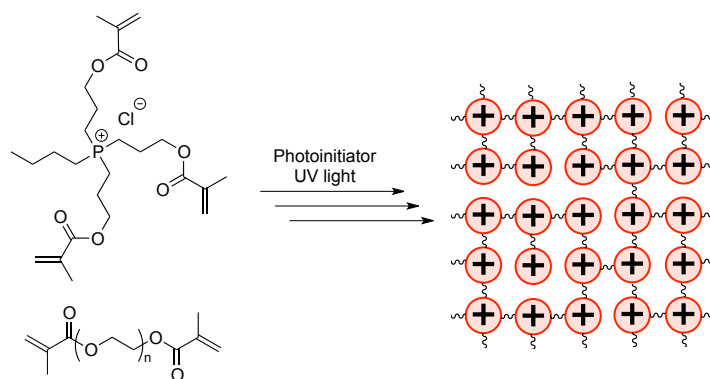


Figure 4-1: Representation of a photochemically synthesized polyelectrolyte from a crosslinking phosphonium salt (**4.2**) and poly(ethylene glycol)dimethacrylate.

The molecule's fluidity at room temperature allows for traditional formulation design, and for solvent-free synthesis of a polyelectrolyte network within seconds. The phosphonium salt acts as both the polymerization medium and as a reagent that is incorporated into the polymer network. This approach is starkly different than other photopolymer/ionic liquid systems where the liquid salt is simply swelled in the network, *not* incorporated.²⁷ This advantageous feature allows for the alteration of glass transition

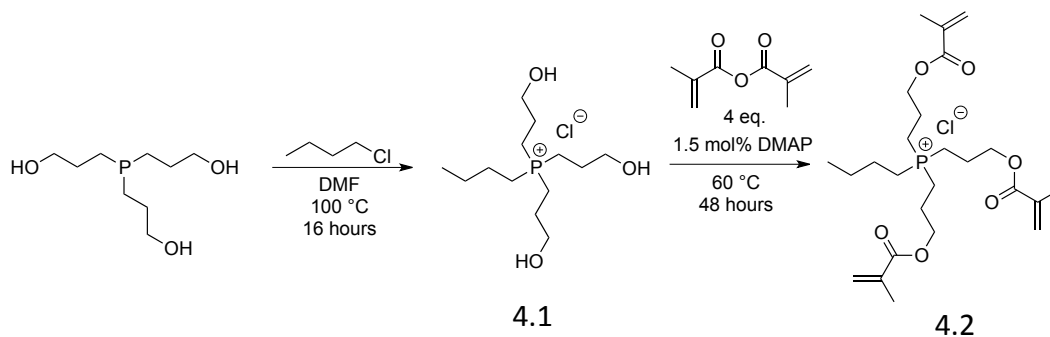
temperature, surface charge density, and wettability as a function of ion content and crosslink density. Depending on the anion within polymer, we can drastically alter the chemical properties of the network, such as swellability, wettability, and anion-exchange rate upon the introduction of a second anionic species. This alteration can be accomplished within seconds by anion exchange with bis(trifluoromethylsulfonyl)imide (NTf₂) or dodecylbenzenesulfonate (DBS). In the case of DBS, surface passivation is obtained disallowing further anion-exchange because of the increase in hydrophobicity of the network. The facile nature of the metathesis reaction allows us to use contact printing techniques to pattern DBS into the polymer, thus creating spatial differences in chemical behaviour. These differences were exploited for selectively patterning an anionic dye in regions that were unexposed to DBS. This general process is amenable to high throughput techniques and may be used to pattern virtually any anionic species.

4.2 Results and Discussion

4.2.1 Polymer Synthesis and Characterization

Synthesis of the self-crosslinking phosphonium salt began with the quaternization of tris(3-hydroxypropyl)phosphine with chlorobutane in DMF for 16 hours (100 °C). The product (**4.1**) was then purified and combined with four stoichiometric equivalents of methacrylic anhydride, 1.5 mol% DMAP, and heated at 60 °C for 48 hours (Scheme 4-1). Within the first 4 hours, approximately 50% of the pendant alcohol groups were functionalized with methacrylate functionalities. Two days was required however to obtain full conversion to the final product. In our previous work, we synthesized a phosphonium salt bearing an acrylate group (**2.2**) using acryloyl chloride and triethylamine.²² While this method proved effective, it was unsuitable for our current goals. Separation of the triethylamine salts from the product was inefficient because of similarities in solubility. Instead, we used methacrylic anhydride, as the only byproduct from the reaction is methacrylic acid. The reaction mixture was then dissolved in DCM and loaded onto silica gel. The polar phosphonium salt **4.2** was retained on the column, while the methacrylic acid and methacrylic anhydride easily eluted in 100% DCM. The presence of methacrylic acid was monitored using a concentrated solution of sodium bicarbonate. When no further acid was detected, the product was eluted using a 10 v/v%

isopropanol in DCM. Elution of the product was deemed complete when no precipitate was observed upon combining fractions with silver nitrate solution. BHT was then added and volatiles were evaporated, leaving a viscous liquid (See Chapter 4 appendix for NMR spectra).



Scheme 4-1: Synthesis of 4.2.

The high number of polymerizable groups relative to its molecular weight suggested that this species should be capable of forming dense crosslinks, which would result in significant volumetric shrinkage. To alleviate this issue, we decided to copolymerize with a high molecular weight/low functionality species such as poly(ethylene glycol)dimethacrylate (PEG-DMA) ($M_n = 750$). The degree of acrylate conversion (or cure percentage) upon irradiation with light was measured by ATR-FTIR spectroscopy. Prepolymer mixtures containing 0-80 wt% phosphonium salt and 5 wt% HDMAP (2-hydroxy-2-methyl-1-phenylpropanone) photoinitiator were prepared and metered on PET substrates to form 25 μm films and irradiated with UV light from a mercury lamp. The cure percentage for formulations containing 20-80 wt% **4.2** increased with increasing phosphonium content and then plateaued at 67% (Chapter 4 appendix Figure 12). The formation of the polyelectrolyte network rendered the polymer insoluble.

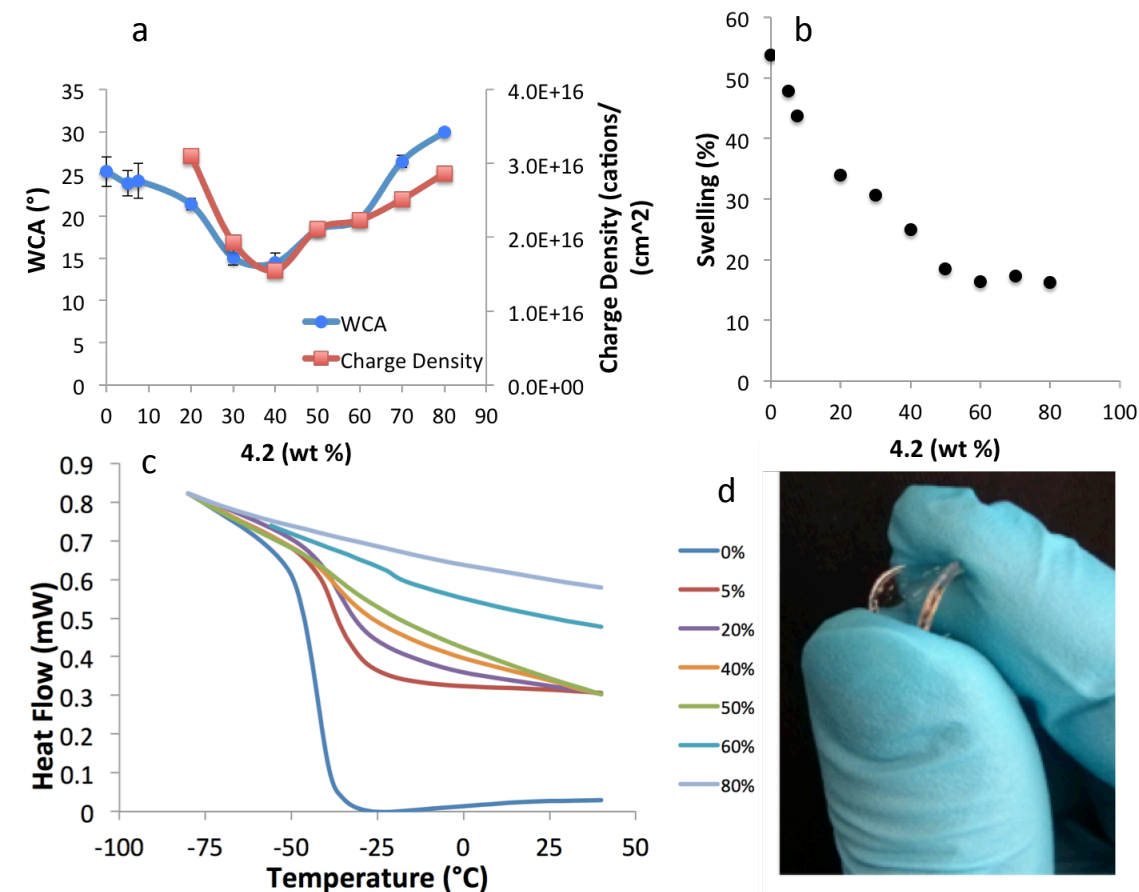


Figure 4-2: WCA and charge density (a) percent swelling in H₂O (b) and DSC data of polymers containing differing amounts of 4.2 (c). WCA and charge density measurements were conducted on 25 microns films while the swelling and DSC data were acquired from bulk polymer samples. (d) A polymer sample with 5 wt% 4.2 in PEG-DMA. This polymer is distinctly firmer, yet still flexible when compared to 100% PEG-DMA.

Both wettability and charge density of a polyelectrolyte are important parameters for applications in materials science. For example, surfaces bearing organic cations have been shown to kill bacteria based on surface charge density and molecular structure.^{14,29,30} Quantification of such surface charges is integral to understanding their potential for application. While the fluorescein dye experiment has previously been used to quantify cation charge density,^{28,31} we demonstrate here that this technique serves as an excellent analytical tool for highly crosslinked polyelectrolytes. Because of the high ion content

within these polymers, we expected low contact angles and high charge density. Figure 4-2a summarizes both the WCA and charge density trends as a function of **4.2** content. The WCA for all formulations were between 15-30°, and the charge density values were high in the range of $1.5\text{-}3.5 \times 10^{16}$ cations/cm². Films containing 0-7.5 wt% **4.2** did not survive the charge density analysis because of the low cure percentage.

Samples made from only PEG-DMA exhibited a glass transition at approximately -45 °C, and were soft and flexible (Figure 4-2c). Upon increasing the content of **4.2**, the T_g value slowly shifted to higher temperatures, indicating that as crosslink density increases, the PEG chains became restricted in the polyelectrolyte matrix forcing its T_g to higher temperatures. From 50-80 wt%, complete disappearance of the T_g was observed. This can be attributed to steric hindrance of PEG chains, which has been previously reported in similar systems.^{33,34}

Utilizing the polymer swelling data and T_g values of the polymer formulations, the observed trends in the charge density and WCA values can be rationalized. It is possible that the wettability and charge density are functions of ion content (number of charges within the network) and surface area (number of charges that are accessible for ion-exchange or hydration). Ion content is a parameter that is dependent on pre-polymer composition, while surface area is highly dependent on the ability for the polymer to swell, which is a function of the chemical composition and crosslinking.

In previous work, we showed that the charge density of a polymer film increased with increasing monoacrylate phosphonium salt (**2.2**, Figure 4-3) content using EB130 as the crosslinker. However, we did not previously analyze the WCA or network swelling. This system, which provides an ideal comparison with the networks formed by **4.2**, has now been analyzed. As shown in Figure 4-3a, the WCA begins at approximately 65° for 0% of **2.2**, but drops to 21° at 47.5 wt%. Thus, the trends in the charge density are reflected in the WCA, as expected. At greater phosphonium concentrations, the polymers exhibit high charge density and excellent wetting behaviour. Since **2.2** only possess one functional group, the swelling and charge densities increased with greater phosphonium content.

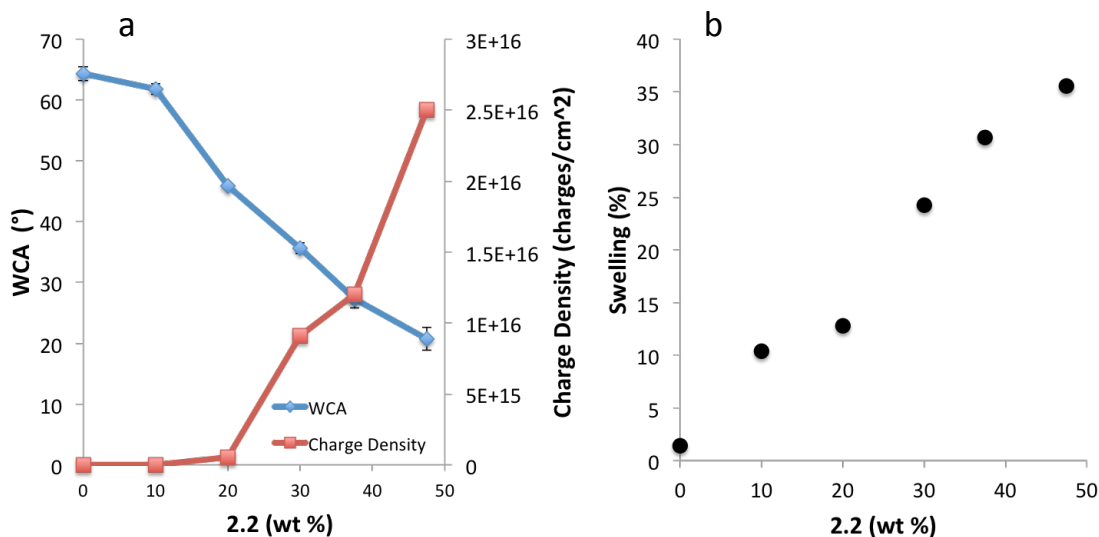


Figure 4-3: WCA, charge density (a) and percent swelling in H₂O (b) of polymer coatings containing differing amounts of phosphonium monomer possessing one acrylate group (2.1) combined with EB130 crosslinker.

The properties of the networks prepared from the 4.2 are significantly different from those prepared from 2.2. This can ultimately be attributed to its self-crosslinking capabilities, where both crosslink density and ion content increase simultaneously. The observed trends in wettability and charge density for this system are a product of competing processes. At low phosphonium content, swelling is high and the crosslink density is low, resulting in contact angles that are expected for PEG-based systems.³⁵ Upon the addition of 20 wt% 4.2, the charge density was very high (3.1×10^{16} cations/cm²), and a slight decrease in the WCA (25° to 21°) was observed. This also corresponds to a significant decrease in swelling (54% to 34%). At 40 wt%, the film possessed the lowest WCA of 15°. It is at this point that the charge density value is also at its lowest (1.6×10^{16} cation/cm²). These results appear contradictory until one considers the swelling. The inability of the polymer to swell results in fewer accessible ion exchange sites, despite greater wettability. This phenomenon is not observed in the monoacrylate systems as crosslink density decreases with increasing phosphonium content.

From 50-80 wt% **4.2**, there is only a modest change in swelling with an increase in both WCA and charge density. The DSC results show the disappearance of the T_g , suggesting a completely glassy polymer. It is at this point that the high crosslinking nature decreases wettability, resulting in a larger WCA value. This behaviour has previously been observed in PEG based systems, where increased crosslink densities promote higher WCAs as a result of reduced swelling.³⁶ The increase in charge density at this stage (50-80 wt%) is simply a result of more ions being present in the network and *not* due to an increase in surface area of the polymer with the solution. This highly dynamic behavior is a feature of a self-crosslinking cation and to our knowledge, there have been little to no studies focusing on the emergent properties of such systems. The tandem increase in both crosslink density and cation content resulting from one molecular species provides a new avenue for polyelectrolyte network design.

4.2.2 Ion-exchange properties and 2D patterning

It is well known within the field of ionic liquids that simply exchanging the anion can alter the properties of a salt. Polymers generated from ionic liquids also exhibit this trend.¹² We were interested in using this phenomenon to alter the properties of the photopolymerized polyelectrolytes, and for 2D surface patterning. The bis(trifluoromethylsulfonyl)imide ion for example is a bulky, hydrophobic, non-coordinating anion often used in ionic liquid chemistry to create hydrophobic materials. The creation of a hydrophobic polyelectrolyte surface should slow the rate of ion-diffusion and anion-exchange through the film relative to hydrophilic surfaces utilizing halogen anions. Surface patterning may be possible by harnessing these differences. There are two approaches possible to generate photopolymerized polyelectrolyte films containing a hydrophobic anion, either the anion-exchange is performed using the monomeric species, or after photopolymerization (post-functionalization). Depending on the application either approach might be suitable, therefore both were investigated.

First, anion exchange was performed on the monomer by dissolving both **4.2** and LiNTf₂ separately in water, followed by mixing of the two solutions. The insolubility of the product (**4.2**[NTf₂]) in water resulted in the formation of a viscous phase, which was isolated. For the purpose of making a direct comparison, the polymer formulation using

this monomer consisted of 2.0 millimoles of phosphonium salt **4.2**[NTf₂] per gram of PEG-DMA, which was the same molar ratio used in a 50 wt% **4.2** described above. As expected, polymer generated using the **4.2**[NTf₂] variety was more hydrophobic, with a WCA of 50° vs. 18° for the chloride salt, and had a swelling value in water of 10% in comparison with 20% for the chloride salt. DSC analysis showed identical glass transitions at -35 °C, suggesting that the PEG portion within the network resides in similar environments.

We also attempted a post functionalization methodology, by conducting an anion exchange with LiNTf₂ directly on the **4.2**-containing polymer. The **4.2**-containing films that were treated with a solution of LiNTf₂ exhibited identical contact angles to those made using the NTf₂ monomer. Given these observations, we further investigated other properties within the polymer network as a function of anion choice through post-modification. During our attempts to obtain charge density values for NTf₂ functionalized films, we noticed a significant delay in colour change upon immersion of the sample in sodium fluorescein solution. This is likely a result of the increased hydrophobicity of the NTf₂ anion, which was less likely to exchange with a fluorescein molecule in solution relative to the chloride anion. Ultimately this manifests itself in different ion-exchange rates between the solution and the polymer. To more closely examine the anion exchange properties of the films, we analyzed the chloride functionalized polymer (60 wt%) by UV-vis spectroscopy after immersion in differing concentrations of sodium fluorescein dye at varying time intervals. The absorbance at 501 nm was determined and plotted against immersion time in solution. The ion exchange occurred rapidly, with signal saturation after 2-10 seconds when immersed in solutions containing 0.05-1 wt% fluorescein in water (Figure 4-4). However this behaviour was not observed when using solutions between 0.01-0.02 wt%, as 5 minutes was required to reach an absorbance of 1.2 for 0.01 wt% solutions fluorescein. At these low concentrations, the rate of mass transfer for fluorescein entering the film becomes slower than the ion-exchange reaction. At higher concentrations, the rate of mass transfer was sufficiently high allowing the ion-exchange to occur quickly.

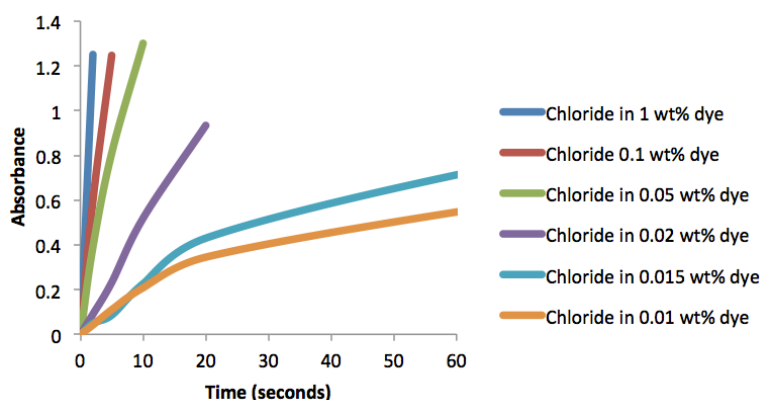


Figure 4-4: Uptake of fluorescein into a 60 wt% **4.2** film as a function of time ($\lambda_{\max} = 501$ nm).

Pristine chloride functionalized films were treated with LiNTf_2 and then analyzed in an identical fashion. Dramatically different ion-exchange behavior was observed. Consistent with the hydrophobicity of the anion, the rate of fluorescein uptake was much slower in comparison to the chloride analogue (Figure 4-5). On timescales between 2-10 seconds however, there was still detectable uptake of fluorescein from solution at all concentrations. We sought to find an anion that would passivate the surface and prevent any detectable ion-exchange, thus demonstrating a drastic change in chemical character upon undergoing a simple metathesis reaction. It is well known that long alkyl chains are capable of passivating surfaces through side chain crystallization. This efficient packing at the interface would greatly slow down the permeation of water, and thus dramatically reduce the rate of ion exchange of the polymer. To test whether this was possible using our system, we treated pristine chloride functionalized films with a concentrated solution (1 wt%) of sodium dodecylbenzenesulfonate (DBS) for 1 min, followed by thorough rinsing with water. The WCA of this film was 84° , significantly higher than either the chloride or NTf_2 functionalized polymer films.

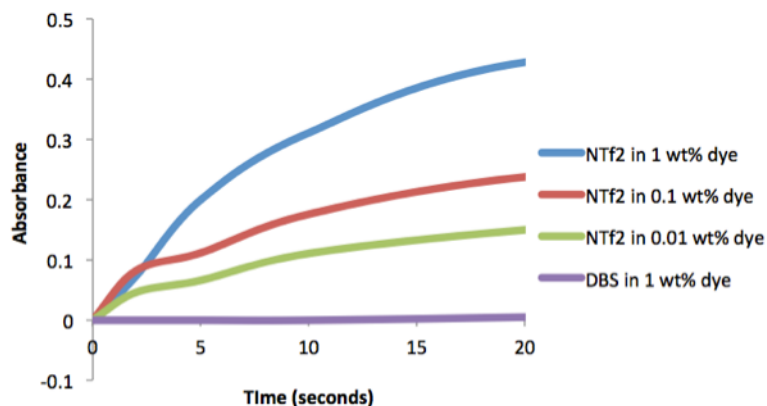


Figure 4-5: Uptake of fluorescein into a 60 wt% **4.2** film functionalized with either NTF₂ or DBS as a function of time ($\lambda_{\text{max}} = 501 \text{ nm}$).

Upon immersion in 1 wt% sodium fluorescein dye solution, a signal at 501 nm was not observed until 20 seconds into the experiment. Only after 5 minutes an absorbance of 0.1 was observed, indicating a high level of passivation. The mechanism by which passivation occurs may be a result of several processes. First, the presence of long alkyl chains at the interface prevents wetting of the surface and permeation of water into the polymer. In addition, within the polymer matrix, the replacement of chloride with a large, hydrophobic anion such as DBS should result in the formation of a more hydrophobic environment in conjunction with a reduction in free volume. To confirm that DBS resides within the network, treated samples were analyzed by ATR-FTIR spectroscopy. New signals at 1035 and 1007 cm^{-1} were observed and are consistent with literature values for DBS vibrations.³⁷ The inability of water and fluorescein to enter the network contributes to a slower kinetic profile for the ion-exchange, despite the high concentration of fluorescein in solution.

We decided to take advantage of the orthogonal behaviour of the chloride versus DBS films to selectively pattern the photopolymer. A PDMS stamp with 1 mm features was coated with sodium DBS and pressed onto a chloride functionalized film. Upon removal of the stamp, the sample was immersed into a 1 wt% sodium fluorescein solution for 3 seconds, followed by rinsing with deionized water. Using short immersion times with high concentration is imperative to take advantage of the kinetic differences.

Regions that were in contact with the stamp underwent anion-exchange to create highly passivated networks. The 1 mm features that were not in contact were free to undergo anion-exchange with fluorescein in solution thus creating the observed pattern (Figure 4-6).

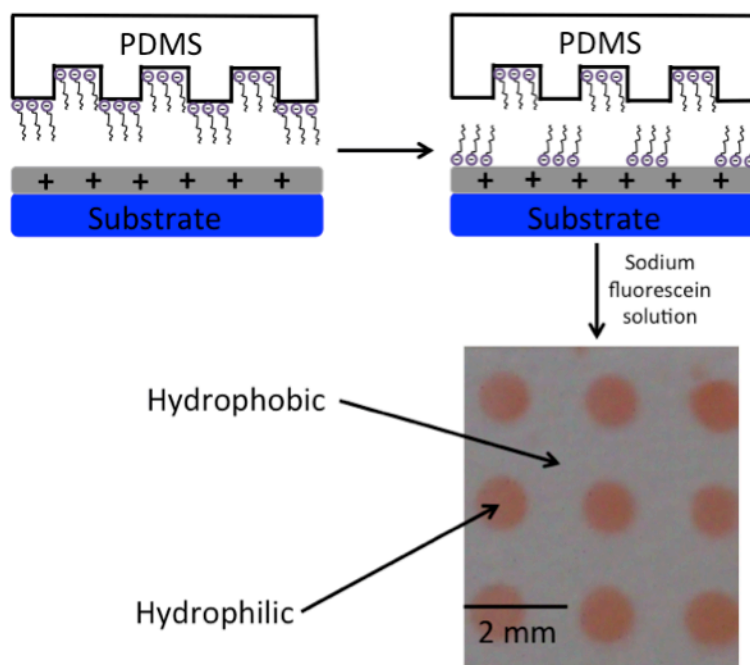


Figure 4-6: A PDMS stamp functionalized with sodium DBS is brought into contact with the phosphonium polymer coating. DBS ion exchanges on to the cationic polymer creating a hydrophobic surface. The untouched regions are then functionalized with a different anion (fluorescein).

The entire assembly may be reverted back to the halogenated form using a cationic surfactant, or by protonation of the organic anions using dilute hydrochloric acid. This feature renders the polymer completely recyclable for multiple deposition processes, a unique trait associated with anion-exchange chemistry. The entire patterning process is kinetically controlled by taking advantage of the different ion-exchange rates between two regions on the polymer. This is in contrast to other successful systems, which rely on selective wetting,³⁸ or covalent bond forming processes. Like any technique, the chemistry one utilizes to facilitate the formation of a pattern is highly dependent on the

molecules of interest, and the final application. While selective wetting provides an incredibly simple and powerful method to pattern a surface with a large variety of molecules, its specificity relies on molecular solubility, a highly unspecific trait. Covalent bond forming processes can be viewed as the opposite approach as this chemistry can be finely tuned for patterning one type of molecule from a mixture. Such specific chemistry sacrifices substrate scope however. We believe the patterning capabilities of ion-exchange chemistry lies in between these two techniques. The specificity relies only in the ability for the species of interest to bare an ionic charge. In the case of anions, there are countless examples including, but not limited to carboxylates, sulfonates, phosphonates, and borates. Differences in pK_a/pK_b of such functional groups could provide an additional level of specificity and control for the patterning process, however this remains to be tested.

4.3 Conclusions

A phosphonium salt bearing three methacrylate groups was synthesized and incorporated into a photopolymeric network. The observed properties of the network were a product of the competing processes resulting from a self-crosslinking nature of the cation. Complete characterization of the networks using WCA, charge density, swellability and DSC analysis allowed us to understand the inner workings of these systems. While one would expect wettability and charge density of the polymer to increase with greater salt content, this was not the case. Instead, a competitive process was observed between the swellability of the network and number ion-exchangeable sites. At lower concentrations of **4.2** (20 wt%), swellability was high providing a greater surface area between the solution and polymer for ion-exchange to occur. As the concentration of **4.2** increased however, the inability of the polymer to swell resulted in a decrease in the number of ion-exchange sites (40-50 wt%). The increase in charge density for **4.2** concentrations between 50-80 wt% cannot be explained by changes in swellability, but rather by the increase in number of ion-exchange sites in the material. The changes in WCA reflect the balance between swellability of the network and ions available for hydration at the solution/polymer interface. Using the monoacrylate analogue **2.2**, the predicted trend was observed where the number of exchangeable anions

increased and wettability decreased with greater **2.2** content. Polymers were evaluated for their performance as substrates for kinetically controlled patterning. DBS was used to passivate regions of the polyelectrolyte by preventing water permeation, and to slow down the rate of anion-exchange with fluorescein in solution. Chloride functionalized regions underwent the metathesis reaction more rapidly than the DBS regions, providing excellent contrast for the reaction. Using a PDMS stamp, 1 mm features were fabricated, demonstrating our ability to take advantage of this orthogonal chemistry. Future work involves expanding the substrate scope of the patterning process, attempting smaller feature design, and higher functional group conversion during polymerization. We believe that this can be obtained by curing under nitrogen, and by evaluating other patterning processes such as inkjet printing, lift-off lithography, or photolithography, using photoactive anions to locally change hydrophobicity upon irradiation.

4.4 Experimental

Chemicals. ADDITOL HDMAP (2-hydrox-2-methy-1-phenyl-propanone), tributylphosphine (94.5%+), and tris(3-hydroxypropyl)phosphine (90%+) were donated by Cytec Corporation and used as received. Poly(ethylene glycol) dimethacrylate (PEG-DMA) ($M_n = 750$), PDMS (Sylgard 184) and sodium dodecylbenzenesulfonate were purchased from Sigma Aldrich and used as received. Melinex 725 Teijin PET films purchased from Tekra and microscope slides were purchased from Technologists Choice. Lithium bis(trifluoromethyl)sulfonate, and 1-chlorobutane were purchased from Alfa Aesar. Fluorescein (sodium salt) was purchased from J.T. Baker Chemical.

The syntheses of oxygen sensitive compounds were conducted in a N_2 atmosphere and prepared in a nitrogen-filled MBraun Labmaster 130 glove box unless otherwise noted. Solvents were purchased from Caledon and dried using an MBraun Solvent Purification System. Dried solvents were collected under vacuum in a flame dried Strauss flask and stored over 4\AA molecular sieves in the drybox. Deuterated chloroform was purchased from Caledon and stored over 4\AA molecular sieves. Nuclear Magnetic Resonance (NMR) spectroscopy was conducted on a Varian INOVA 400 MHz spectrometer (1H 400.09

MHz, $^{13}\text{C}\{^1\text{H}\}$ 158 MHz, $^{31}\text{P}\{^1\text{H}\}$ 161.82 MHz) unless otherwise noted. All ^1H and ^{13}C spectra were referenced relative to tetramethylsilane (CDCl_3 ; ^1H $\delta = 7.26$ and ^{13}C $\delta = 77.2$. CD_2Cl_2 ^1H $\delta = 5.32$). The chemical shifts for $^{31}\text{P}\{^1\text{H}\}$ NMR spectroscopy were referenced using an external standard (85% H_3PO_4 ; $\delta = 0$). Infrared spectra were recorded using a Bruker Tensor 27 spectrometer using attenuated total reflectance mode (ATR) using a ZnSe crystal. Photopolymerization was performed using a modified UV-curing system purchased from UV Process and Supply Inc. with a mercury bulb. Irradiance and energy density were determined by a PP2-H-U Power Puck II purchased from EIT Instrument Markets. Water contact angles (WCA) were measured using a Kruss DSA100 Drop Shape Analyzer and analyzed using Drop Shape Analysis. Droplets (5 μL) were carefully placed on to the surface and allowed to settle until equilibrium or until 1.5 minutes before the measurement was taken. Glass transition temperatures were determined using differential scanning calorimetry (DSC) on a DSC Q20 TA instrument. A sample of approximately 7 mg was placed in an aluminum Tzero pan and underwent a heat/cool/heat profile at 10 $^\circ\text{C}/\text{min}$ under nitrogen atmosphere (50 mL/min). Data was acquired from the final heat cycle of the heat/cool/heat profile. Thermal degradation was determined using thermal gravimetric analysis (TGA) on a Q600 SDT TA instrument: a sample of 10 mg was placed in an alumina cup and heated at a rate of 10 $^\circ\text{C}/\text{min}$ to 600 $^\circ\text{C}$ under a nitrogen atmosphere (100 ml/min). Volume of polymer disks was measured using an IP65 digital caliper. Mass spectrometry for the phosphonium salts was recorded in both positive and negative ion modes using electrospray ionization (ESI) Micromass LCT spectrometer in dichloromethane; reported as m/z . Solid-state UV-visible spectra were recorded using an Ocean Optic fiber optic spectrometer, SD200 detector, with a Mini-D2T light source. The master for PDMS mold fabrication was produced using a Karl Suss MA6 mask aligner, and RIE plasma treatment was conducted using a STS instrument.

Synthesis of butyltris(3-hydroxypropyl)phosphonium chloride (4.1)

Tris(3-hydroxypropyl)phosphine (28 g, 134.5 mmol) and 1.05 stoichiometric equivalents of 1-chlorobutane (13.1 g, 141.2 mmol) were added to 8 mL of DMF and stirred for 16 hours at 100 $^\circ\text{C}$. The solution was then poured into stirring diethyl ether (300 mL) for 15

minutes, resulting in the formation of a viscous oil. The mixture was decanted and rinsed two more times with diethyl ether (2 x 150 mL) and volatiles were evaporated *in vacuo* at 80 °C for 16 hours. A pale yellow viscous oil remained and identified as butyltris(3-hydroxypropyl)phosphonium chloride (37 g, 90%). ^1H NMR (400 MHz, d_6 -DMSO): δ 0.91 (t, 3H, $^3J_{\text{H-H}} = 4$ Hz, CH_3), 1.41 (m, 2H, CH_2), 1.48 (m, 2H, CH_2), 1.64 (m, 6H, CH_2), 2.25 (m, 8H, CH_2), 3.46 (bs, 6H, CH_2OH), 4.90 (s, 3H, OH). $^{31}\text{P}\{^1\text{H}\}$ NMR (161.82 MHz, d_6 -DMSO): δ 35.52 (s), 35.92 (s), 37.96.* $^{13}\text{C}\{^1\text{H}\}$ NMR (100.5 MHz, d_6 -DMSO): δ 13.27 (s, 1C), 14.96 (d, 3C, $^1J_{\text{P-C}} = 49$ Hz), 16.65 (s, 1C, $^1J_{\text{P-C}} = 47$ Hz), 22.63 (s, 1C, $^2J_{\text{P-C}} = 6$ Hz), 23.35 (d, 1C, $^3J_{\text{P-C}} = 16$ Hz), 24.1 (d, 2C, $^2J_{\text{P-C}} = 5$ Hz), 60.35 (d, 3C, $^3J_{\text{P-C}} = 15$ Hz). TOF-MS-ES+: m/z observed 265 (M^+), 565 ($2\text{M} + \text{A}^+$). TOF-MS-ES-: m/z observed 335 ($\text{M} + 2\text{A}^-$), 635 ($2\text{M} + 3\text{A}^-$), 938 ($3\text{M} + 4\text{A}^-$), 1238 ($4\text{M} + 5\text{A}^-$).

Synthesis of butyltris(3-(methacryloyloxy)propyl)phosphonium chloride (4.2)

Butyltris(3-hydroxypropyl)phosphonium chloride (12.7 g, 42.2 mmol) and four stoichiometric equivalents of methacrylic anhydride (25.4 g, 169 mmol) were combined in a roundbottom flask, followed by the addition of 0.015 equivalents of DMAP (0.077g, 0.633 mmol). The mixture was then heated to 60 °C to increase the rate of esterification and to solubilize the phosphonium salt. The reaction was for left stirring 48 hours. The mixture was then cooled to room temperature and poured on to a silica plug (11.5 x 2.5 cm) prepared using DCM to remove excess methacrylic anhydride and methacrylic acid byproduct. Elution of the acid byproduct was monitored using sodium bicarbonate solution. When no acid was detected, the phosphonium salt was eluted using a 10 v/v% isopropanol in DCM. Elution of the product was monitored using AgNO_3 solution. BHT (10 mg) was added and volatiles evaporated *in vacuo* leaving a viscous oil identified as butyltris(3-(methacryloyloxy)propyl)phosphonium chloride (6.74 g, 32%). ^1H NMR (400 MHz, CDCl_3): δ 0.94 (t, 3H, $^3J_{\text{H-H}} = 4$ Hz, CH_3), 1.51 (m, 4H, CH_2), 1.91 (s, 9H, $\text{CH}_2\text{C}(\text{CH}_3)\text{CO}$), 2.01 (m, 6H, CH_2), 2.51 (m, 2H, CH_2), 2.69 (m, 6H, CH_2), 5.86 (t, 6H, $^3J_{\text{H-H}} = 8$ Hz, CH_2OH), 5.59 (s, 3H, $\text{CH}_2\text{C}(\text{CH}_3)\text{CO}$), 6.1 (s, 3H, $\text{CH}_2\text{C}(\text{CH}_3)\text{CO}$). $^{31}\text{P}\{^1\text{H}\}$ NMR (161.82 MHz, CDCl_3): δ 35.09 (s), 35.26 (s), 37.26. $^{13}\text{C}\{^1\text{H}\}$ NMR (100.5 MHz, CDCl_3): 13.61 (s, 1C), 16.30 (d, 3C, $^1J_{\text{P-C}} = 49$ Hz), 18.45 (s, 3C), 19.05 (d, 1C, $^1J_{\text{P-C}} = 47$ Hz), 21.58 (d, 3C, $^2J_{\text{P-C}} = 4$ Hz), 23.84 (d, 1C, $^2J_{\text{P-C}} = 5$ Hz), 24.11 (d, 1C, $^3J_{\text{P-C}} = 16$ Hz),

63.77 (d, 3C, $^3J_{P,C} = 17$ Hz), 126.55 (s, 1C), 135.88 (s, 1C), 167.20 (s, 1C). TOF-MS-ES+: m/z observed 469 (M)⁺, 974 (2M + A)⁺. TOF-MS-ES-: m/z observed 539 (M + 2A)⁻, 1046 (2M + 3A + 2H)⁻.

Synthesis of butyltris(3-(methacryloyloxy)propyl)phosphonium bis(trifluoromethylsulfonyl)imide (4.2[NTf₂])

4.2 (1.62 g, 4.0 mmol) and a slight excess of lithium bis(trifluoromethylsulfonyl)imide (1.21 g, 4.2 mmol) were each dissolved in 10 mL of water. The lithium bis(trifluoromethylsulfonyl)imide solution was added dropwise to 3MA-PCl and the reaction mixture was stirred for one hour. A white viscous oil appeared instantly upon addition. The aqueous layer was decanted and the viscous oil rinsed with water (3 x 10 mL). The product was dried with MgSO₄ in DCM (12 mL) and isolated as a colorless viscous liquid (1.9 g, 63 %). ¹H NMR (400 MHz, CDCl₃): δ 0.95 (t, 3H, $^3J_{H-H} = 8$ Hz, CH₃), 1.51 (m, 4H, CH₂), 1.92 (s, 9H, CH₂C(CH₃)CO), 1.97 (m, 6H, CH₂), 2.23 (m, 2H, CH₂), 2.33 (m, 6H, CH₂), 4.23 (t, 6H, $^3J_{H-H} = 8$ Hz, CH₂OH), 5.60 (s, 3H, CH₂C(CH₃)CO), 6.09 (s, 3H, CH₂C(CH₃)CO). ³¹P{¹H} NMR (161.82 MHz, CDCl₃): δ 35.36 (s), 35.49 (s), 37.63. ¹⁹F NMR (376.15 MHz, CDCl₃): δ 78.91 (s). ¹³C{¹H} NMR (100.5 MHz, CDCl₃): 13.35 (s, 1C), 15.70 (d, 3C, $^1J_{P,C} = 49$ Hz), 18.12 (d, 1C, $^1J_{P,C} = 47$ Hz), 18.37 (s, 3C), 21.14 (d, 3C, $^2J_{P,C} = 4$ Hz), 23.46 (d, 1C, $^2J_{P,C} = 5$ Hz), 23.904 (d, 1C, $^3J_{P,C} = 16$ Hz), 63.49 (d, 3C, $^3J_{P,C} = 17$ Hz), 119.97 (q, 2C, $^1J_{F,C} = 320$ Hz), 126.52 (s, 1C), 135.85 (s, 1C), 167.23 (s, 1C). TOF-MS-ES+: m/z observed 469 (M)⁺, 1219 (2M + A)⁺. TOF-MS-ES- m/z observed 1029.1 (M + 2A)⁻.

Film preparation

Appropriate amounts of phosphonium salt, PEG-DMA, and photoinitiator (HDMAP, 5 wt%) were combined in vials and mixed thoroughly by hand. Solutions were cast on Melinex 725 Teijin PET films using a 25 micron Meyer rod and irradiated five times in air (Irradiance – UVA: 412 mW/cm² UVB: 423 mW/cm² UVC: 79 mW/cm². Energy Density - UVA: 234 mJ/cm² UVB: 238 mJ/cm² UVC: 45 mJ/cm²).

Film Charge Density

The density of accessible phosphonium groups in the polymer films was measured using UV-vis spectroscopy following a previously described procedure.²⁸ Samples were cut into 1 x 1 cm² squares and immersed in 10 mL of a 1 wt% solution of fluorescein (sodium salt) in distilled water for 10 minutes. Each sample was then extensively rinsed with distilled water and then placed in 3 mL of a 0.1 wt% solution of cetyltrimethylammonium chloride. After sonicating for 20 minutes, the dye was desorbed off the film into solution. The absorbance of the resulting solution was measured at 501 nm after adding 10% v/v of 100 mM phosphate buffer (pH 8.0). The concentration of the fluorescein was calculated using an extinction coefficient of 77 mM⁻¹ cm⁻¹. Using the concentration value obtained, the number of fluorescein molecules in solution was calculated. Assuming a 1:1 ratio of fluorescein molecules to phosphonium salts on the surface, an accessible charge density value (cations/cm²) was calculated. Triplicates of each formulation were averaged to obtain the reported values.

Bulk sample preparation

A 100 mg aliquot of the pre-polymer solution was deposited on a microscope slide and sandwiched between a second microscope slide treated with polydimethylsiloxane (PDMS), using two additional slides as spacers (thickness = 1 mm). The assembly was then irradiated under identical conditions relative to the thin films. Upon removing the polymer puck from the mold, it was quickly rinsed with ethanol and dried *in vacuo* for 24 hours.

Functional group conversion

To determine the cure percentage, a comparison of the intensity of the acrylate CH₂=CH vibration of the acrylate phosphonium salt (~810 cm⁻¹) before and after irradiation relative to an internal standard (C=O stretch, ~1750 cm⁻¹) using FTIR-ATR spectroscopy was performed. The reduced relative intensity of the peak at 810 cm⁻¹ is indicative of acrylate conversion during polymerization. Using the equation Percent Cure = (r_u-r_c)/r_u x 100, where r_u = ratio of uncured peaks and r_c = ratio of cured peaks, a conversion value was obtained.

Swelling experiments and gel content

Bulk samples were weighed dry and then immersed in deionized water. Their mass was monitored until it reached a maximum and its swelling ratio was determined using the equation $Q = (m_t - m_o)/m_o$ where m_t = swelled mass, m_o = dry mass, and Q = swelling ratio. Ratios were multiplied by 100 to give percentage values. The volumes of polymer samples were measured by determining thickness and diameter. These measurements were repeated three times and averaged. Using the equation $V = \pi r^2 h$, the volume was determined. Samples were then dried in a vacuum oven at 80 °C over 24 hours and weighed again. By comparing the original weight to the extracted weight, gel content was obtained.

PDMS stamp fabrication and contact printing

The master for the PDMS stamp was custom made in a nanofabrication facility using standard photolithography techniques. The PDMS precursor (Sylgard 184) was degassed *in vacuo* and poured over the master in a Teflon dish. The assembly was then heated in an oven at 110 °C for 30 min to induce crosslinking. A 1 cm² section of the PDMS was carefully cut and removed from the master, followed by an O₂ plasma treatment for 100 seconds. This resulted in the formation of hydroxyl groups at the PDMS-air interface. A few drops of aqueous sodium DBS (1 wt%) was dispensed on to the stamp and left to dry in a 100 °C oven for 8 minutes. The stamp was then placed on to a freshly rinsed and dried polymer coating, applying light pressure evenly to promote contact. After 10 minutes, the stamp was removed and the polymer coating was immersed in a 1 wt% sodium fluorescein solution for 3 seconds. The polymer was then removed, rinsed with deionized water, and dried in air.

References

- (1) Falentin-Daudre, C.; Faure, E.; Svaldo-Lanero, T.; Farina, F.; Jerome, C.; Van de Weerdt, C.; Martial, J.; Duwez, A. S.; Detrembleur, C. *Langmuir* **2012**, *28*, 7233-7241.

- (2) Taranekar, P.; Qiao, Q.; Jiang, H.; Ghiviriga, I.; Schanze, K. S.; Reynolds, J. R. *J. Am. Chem. Soc.* **2007**, *129*, 8958.
- (3) Xi, J. Y.; Wu, Z. H.; Teng, X. G.; Zhao, Y. T.; Chen, L. Q.; Qiu, X. P. *J. Mater. Chem.* **2008**, *18*, 1232-1238.
- (4) Priolo, M. A.; Gamboa, D.; Holder, K. M.; Grunlan, J. C. *Nano Lett.* **2010**, *10*, 4970-4974.
- (5) Gao, R. L.; Ramirez, S. M.; Inglefield, D. L.; Bodnar, R. J.; Long, T. E. *Carbon* **2013**, *54*, 133-142.
- (6) Hemp, S. T.; Allen, M. H., Jr.; Green, M. D.; Long, T. E. *Biomacromolecules* **2012**, *13*, 231-238.
- (7) Pavluchina, S.; Lu, Y.; Patimetha, A.; Libera, M.; Sukhishvili, S. *Polymer Biomacromolecules* **2010**, *11*, 3448-3456.
- (8) Lundberg, P.; Lynd, N. A.; Zhang, Y. N.; Zeng, X. H.; Krogstad, D. V.; Paffen, T.; Malkoch, M.; Nystrom, A. M.; Hawker, C. J. *Soft Matter* **2013**, *9*, 82-89.
- (9) Yoshizawa, M.; Ogihara, W.; Ohno, H. *Polymers. Adv. Tech.* **2002**, *13*, 589-594.
- (10) Ohno, H.; Yoshizawa, M.; Ogihara, W. *Electrochim. Acta.* **2004**, *50*, 255-261.
- (11) Hoshino, K.; Yoshio, M.; Mukai, T.; Kishimoto, K.; Ohno, H.; Kato, T. *J. Polym. Sci A Polym. Chem.* **2003**, *41*, 3486-3492.
- (12) Cheng, S.; Zhang, M.; Wu, T.; Hemp, S. T.; Mather, B. D.; Moore, R. B.; Long, T. E. *J. Polym. Sci A Polym. Chem.* **2012**, *50*, 166-173.
- (13) Cheng, S.; Beyer, F. L.; Mather, B. D.; Moore, R. B.; Long, T. E. *Macromolecules* **2011**, *44*, 6509-6517.
- (14) Kurata, S.; Hamada, N.; Kanazawa, A.; Endo, T. *Dent. Mater. J.* **2011**, *30*, 960-966.
- (15) Yoshio, M.; Kagata, T.; Hoshino, K.; Mukai, T.; Ohno, H.; Kato, T. *J. Am. Chem. Soc.* **2006**, *128*, 5570-5577.
- (16) Carlisle, T. K.; Nicodemus, G. D.; Gin, D. L.; Noble, R. D. *J. Membr. Sci.* **2012**, *397*, 24-37.
- (17) Kim, S. K.; Guymon, C. A. *Polymer* **2012**, *53*, 1640-1650.
- (18) Kim, S. K.; Guymon, C. A. *J. Polym. Sci A Polym. Chem.* **2011**, *49*, 465-475.

- (19) Jiménez, Z.; Bounds, C.; Hoyle, C. E.; Lowe, A. B.; Zhou, H.; Pojman, J. A. *J. Polym. Sci A Polym. Chem.* **2007**, *45*, 3009-3021.
- (20) Guterman, R.; Bradley M., B.; T. Chris, C.; Heng-Yong, N.; Mike, I.; Elizabeth R. G.; Ragogna, P.J. *J. Polym. Sci A Polym. Chem.* **2013**, *51*, 2782-2792.
- (21) Berven, B. M.; Oviasuyi, R. O.; Klassen, R. J.; Idacavage, M.; Gillies, E. R.; Ragogna, P. J. *J. Polym. Sci A Polym. Chem.* **2012**.
- (22) Guterman, R.; Hesari, M.; Ragogna, P. J.; Workentin, M. S. *Langmuir* **2013**, *29*, 6201-6508.
- (23) Cramer, N. B.; Couch, C. L.; Schreck, K. M.; Carioscia, J. A.; Boulden, J. E.; Stansbury, J. W.; Bowman, C. N. *Dent. Mater.* **2010**, *26*, 21-28.
- (24) Buruiana, T.; Melinte, V.; Jitaru, F.; Aldea, H.; Buruiana, E. C. *J. Compos. Mater.* **2012**, *46*, 371-382.
- (25) Sung, S.; Kim, D. S. *J. Appl. Polym. Sci.* **2013**, *129*, 1340-1344.
- (26) Ashley, J. F.; Cramer, N. B.; Davis, R. H.; Bowman, C. N. *Lab on a Chip* **2011**, *11*, 2772-2778.
- (27) Lin, H. C.; de Oliveira, P. W.; Veith, M. *Opt. Mater.* **2011**, *33*, 759-762.
- (28) Murata, H.; Koepsel, R. R.; Matyjaszewski, K.; Russell, A. J. *Biomaterials* **2007**, *28*, 4870-4879.
- (29) Tiller, J. C.; Liao, C. J.; Lewis, K.; Klivanov, A. M. *Proc. Natl. Acad. Sci. U.S.A* **2001**, *98*, 5981-5985.
- (30) Kugler, R.; Bouloussa, O.; Rondelez, F. *Microbiol-SGM* **2005**, *151*, 1341-1348.
- (31) Karamdoust, S.; Yu, B.; Bonduelle, C. V.; Liu, Y.; Davidson, G.; Stojcevic, G.; Yang, J.; Lau, W. M.; Gillies, E. R. *J. Mater. Chem.* **2012**, *22*, 4881.
- (32) Devries, M. E.; Bodde, H. E.; Busscher, H. J.; Junginger, H. E. *J. Biomed. Mater. Res.* **1988**, *22*, 1023-1032.
- (33) Lu, C.-H.; Su, Y.-C.; Wang, C.-F.; Huang, C.-F.; Sheen, Y.-C.; Chang, F.-C. *Polymer* **2008**, *49*, 4852-4860.
- (34) Ozkoc, G.; Kemaloglu, S. *J. Appl. Polym. Sci.* **2009**, *114*, 2481-2487.
- (35) Kim, P.; Kim, D. H.; Kim, B.; Choi, S. K.; Lee, S. H.; Khademhosseini, A.; Langer, R.; Suh, K. Y. *Nanotechnology* **2005**, *16*, 2420-2426.

- (36) Bouteau, M.; Cantin, S.; Fichet, O.; Perrot, F.; Teyssie, D. *Langmuir* **2010**, *26*, 17427-17434.
- (37) Sperline, R. P.; Song, Y.; Freiser, H. *Langmuir* **1994**, *10*, 37-44.
- (38) Watanabe, S.; Akiyoshi, Y.; Matsumoto, M. *Langmuir*, **2013**, *29*, 7743-7748.

Chapter 5

5 The formation of gold nanoparticles in photopolymerized networks

5.1 Introduction

Polymeric matrices are suitable materials for nanoparticle encapsulation by preventing particle aggregation, which can improve polymer properties,^{1,2} thereby providing an avenue for their integration in practical applications. For example, photopatterning of acrylate solutions containing barium titanate nanoparticles results in the formation of 3D piezoelectric materials with improved performance, or the immobilization of Fe/Ni nanoparticles in cellulose membranes for the dechlorination of trichloroethylene, among others.³⁻⁶ One common method used to embed nanoparticles within polymeric materials involves the loading of metal precursor followed by *in situ* nanoparticle formation. For example, Cd, Cu, and Pt, salts have been incorporated into cation-exchange materials such as Nafion (poly(perfluorosulfonic) acid) and sulfonated poly(ether ether ketone) membranes to form nanoparticle composites.^{7,8} Gold nanoparticles (AuNPs) however are of particular interest as they offer diverse applications ranging from catalysis, sensing, and photovoltaics, while their incorporation into polymeric materials can further expand these applications by providing mechanical support, improving recoverability, and performance.⁹⁻¹¹ One convenient *in situ* approach to AuNP synthesis was developed by Huck and Goswami, who explored the use of a cationic polyelectrolyte to support AuCl_4^- , followed by reduction using NaBH_4 to create embedded nanoparticles within a polymer-brush assembly or cellulose membrane.^{12,13} The key advantage to this approach is the capability to create AuNPs within a preformed material, which may possess any given shape or pattern, and the capability to control the distribution of particles within the material itself through diffusion controlled processes.^{14,15} The utility of this method however relies on its broad application with a variety of different polymeric architectures, and the ability to exploit these differences to affect AuNP formation.

Photopolymer networks are an attractive choice to support nanoparticle growth as they can be patterned using photolithography, they possess tunable chemical and mechanical properties, are easily fabricated, and are diverse in their current applications, including polymer electrolytes, coatings and filtration membranes, among others.¹⁶⁻¹⁹ Dispersed AuNPs within photopolymer films have been shown to affect their holographic properties, and also to provide a route for the synthesis of three-dimensional conductive nanomaterials.^{20,21} In this context, our approach is to use the anion-exchange capabilities of phosphonium polymers in combination with photopolymerization to create a patternable polyelectrolyte support with which to perform the AuNP synthesis. A phosphonium polyelectrolyte was used rather than small molecules in order to promote the physical immobilization of the charged species within the photopolymer matrix. This was accomplished by dissolving a phosphonium polymer in liquid monomer then performing photopolymerization. Upon anion-exchange and reduction of AuCl_4^- within the material, AuNPs were formed (Figure 5-1). We demonstrate the utility of this approach by tuning photopolymer stiffness, which affects the concentration of AuNPs within the material, thus providing a means of control for their incorporation. Using a mask, patterns can be produced and used as a substrate for AuNP synthesis, providing a new technique amenable to photolithography.

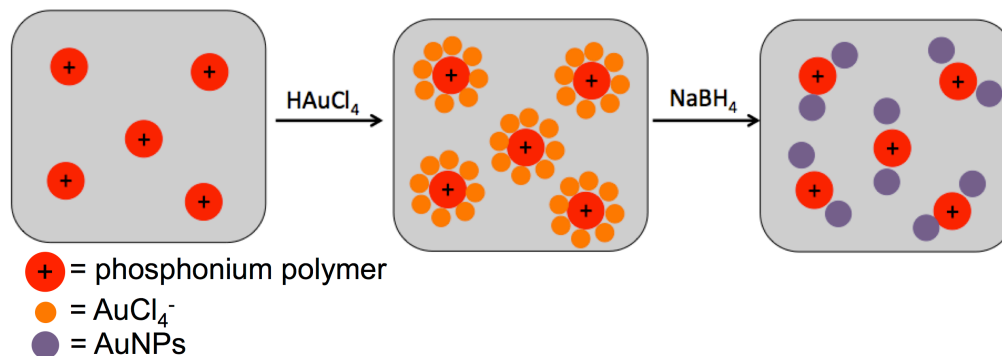
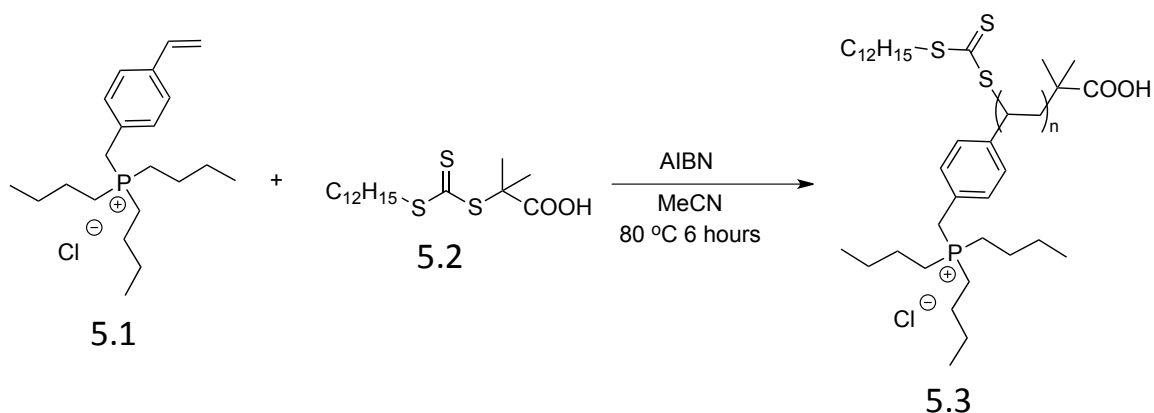


Figure 5-1: Schematic illustration of the *in situ* synthesis of AuNPs within a photopolymer. First, phosphonium polymer is embedded in a photopolymerized film. The film is then treated with HAuCl₄, resulting in functionalization of the immobilized phosphonium polymer with AuCl₄⁻. Finally, the film is treated with NaBH₄ to create AuNPs.

5.2 Results and Discussion

5.2.1 Synthesis and Characterization

A stoichiometric ratio of tributylphosphine and 4-vinylbenzyl chloride were combined in acetonitrile under a nitrogen atmosphere and heated at 100 °C for 6 hours. Volatile compounds were removed *in vacuo*, resulting in the formation of a viscous oil, which was rinsed with diethylether to precipitate the polymerizable phosphonium salt **5.1**. The phosphonium homopolymer was synthesized from this monomer by reversible addition-fragmentation chain transfer (RAFT) polymerization using **5.2** with a target molecular weight of 20 000 g/mol.



Scheme 5-1: Synthesis of a phosphonium polymer by RAFT polymerization. Phosphonium polymer **5.3** was embedded in a photopolymer network by dissolving the polyelectrolyte in 2-hydroxyethyl acrylate (HEA), tetraethyleneglycol diacrylate (TEGDA), and di(trimethylolpropane) tetraacrylate (EB140) (Figure 5-2). Crosslink densities were adjusted by tuning the TEGDA/EB140 ratios, while keeping the concentration of HEA constant (Table 5-1). **5.3** (5 wt%) was added to each mixture in addition to 0.1 wt% dimethoxyphenylacetophenone (DMPA) solution in HEA. Prepolymer solutions (80 mg) were sandwiched between two glass slides with a 200-micron spacer and irradiated with UV-light.

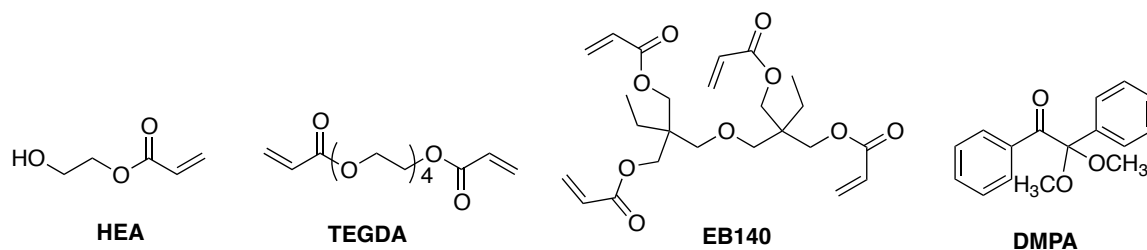


Figure 5-2: Monomers used to create the photopolymer matrix.

Table 5-1: Composition of three formulations possessing different crosslink densities.

Formulation	HEA (wt %)	TEGDA (wt %)	EB140 (wt %)
1	50	50	0
2	50	40	10
3	50	0	50

Initial studies focused on whether the presence of the phosphonium homopolymer affected network formation and whether there were any differences in the physical properties of the resultant networks. Formulations **1-3** with and without the addition of 5 wt% **5.3** were irradiated with UV-light using a mercury lamp. ATR-FTIR spectroscopy was used to monitor acrylate conversion ($\sim 1640\text{ cm}^{-1}$) as a function of energy dosage. Using 0.1 wt% DMPA, the cure % plateaued above $\sim 652\text{ mJ/cm}^2$ for all samples tested (acrylate conversion of $\sim 85\%$). It was determined that the presence of 5 wt% phosphonium homopolymer did not affect acrylate conversion (See chapter 5 appendix Figure 3). While network formation appeared to be unhindered by the presence of the polyelectrolyte, we next investigated whether there was a change in the swellability, gel content, and glass transition (Table 5-2).

Table 5-2: Comparison of the properties of polymer networks with and without 5 wt% **5.3**. The swelling and glass transition data follow predictable trends with small changes observed upon incorporation of the polyelectrolyte.

Formulation #	Mass Swelling Ratio	Gel Content (%)	T _g (°C)
1	0.29 ± 0.01	>98	22
1+ polymer 5.3	0.32 ± 0.01	>98	24
2	0.24 ± 0.01	>98	32
2+polymer 5.3	0.26 ± 0.02	>98	32
3	0.09 ± 0.03	>98	N/A
3+polymer 5.3	0.11 ± 0.03	>98	N/A

All formulations possessed gel contents above 98%, and only one glass transition temperature was observed for all formulations except for **3** and **3+polymer 5.3**, which displayed no discernable glass transition. Formulation **1** possessed the lowest crosslink density, and thus had the lowest glass transition temperature. This is also reflected in the

swellability of the network, with a mass increase of $\sim 30\%$ upon swelling in water. There are however slight differences upon incorporation of the polyelectrolyte with an increase in swelling for each system. The introduction of the polyelectrolyte may promote water uptake resulting in a greater swelling. As the crosslink density increases in formulations **2** and **3**, it becomes difficult to determine whether this slight difference persists. Despite these observations, the polymer networks display similar thermal and swelling properties.

Significant differences between formulations with and without polyelectrolyte were observed upon treatment of the networks with a 0.027 M sodium fluorescein solution in water for 24 hours (Fig. 3). Despite the similarities in swelling behaviour, the presence of only 5 wt% polyelectrolyte provides a large number of anion-exchange sites when compared to the control (no phosphonium polymer). As swellability increases, so too does the anion exchange capacity. Increasing crosslink density hinders this process as seen by the decrease in colour intensity from formulation **1-3**. The uptake of fluorescein is low or undetectable for polymer samples without polyelectrolyte, confirming that the crosslink density affects the anion-exchange capability of the material. This experiment was also conducted with the AuNP precursor HAuCl_4 (0.027 M) in water to determine whether a comparable trend was observed. While a decrease in the intensity of colour was observed for samples containing phosphonium polymer, HAuCl_4 appeared to decompose, creating a reddish-brown colour on the control samples. It is well known that ethylene glycol or poly(ethylene glycol) is capable of reducing gold and silver salts to produce AuNPs, however the role of the phosphonium polymer in preventing this process for our system is unknown. For the purpose of using stable films, all experiments for AuNP preparation contained 5 wt% phosphonium polymer.

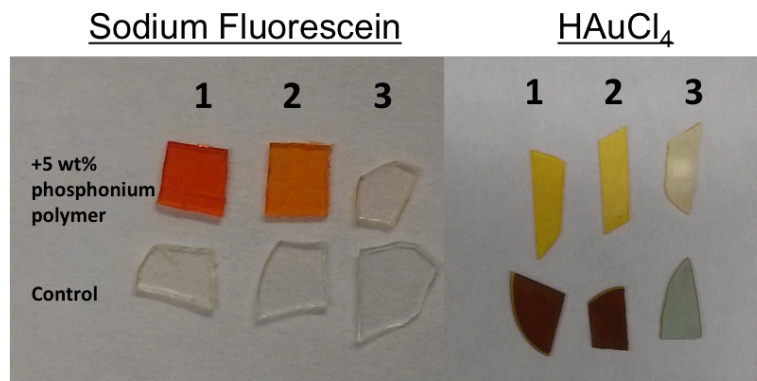


Figure 5-3: Uptake of fluorescein (left) and HAuCl_4 (right) into different bulk polymer samples. Polymer 1 resulted in the greatest uptake of fluorescein due to its ability to swell, while 2 and 3 to lesser degrees. Control samples without dissolved polyelectrolyte displayed very little to no fluorescein uptake. Samples immersed in HAuCl_4 displayed a similar trend, however control samples were found to be unstable resulting in premature AuNP formation.

5.2.2 In-situ Gold Nanoparticle Synthesis and Characterization

The effect of polymer composition on AuNP formation was explored using polymer films (25 μm thick) rather than bulk polymer samples. This approach was employed as spectroscopic analysis became increasingly difficult with thick samples due to high absorbance and long diffusion times. Four formulations were used for this study and were designed for increased scope (Table 5-3). Before AuNP synthesis, we further confirmed that the film properties followed the same trends as described above for the thicker systems. Formulations **A-D** with 5 wt% phosphonium polymer films were produced using a Meyer rod, immersed in fluorescein dye for 10 minutes, rinsed with water, and analyzed by UV-vis spectroscopy to confirm our previous findings. (Figure 5-4a).

Table 5-3: Formulations used for thin films studies and for the formation of AuNPs. All formulations possess 5 wt% phosphonium homopolymer.

Formulation	HEA (wt %)	TEGDA (wt %)	EB140 (wt %)
A	50	50	0
B	50	45	5
C	50	33	17
D	50	25	25

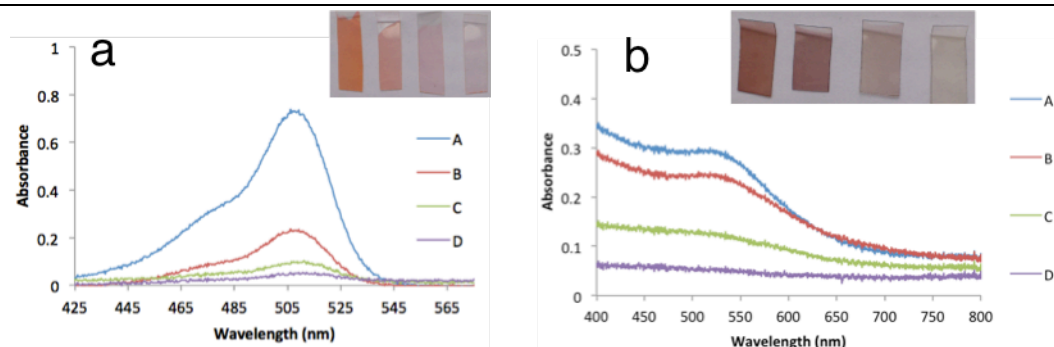


Figure 5-4: a) UV-vis spectra of 25- μ m thick films after immersion in fluorescein dye. The inset shows films from formulation A (left) to formulation D (right). b) UV-vis spectra for formulations A-D after AuNP synthesis. The inset shows formulations A (left) to D (right) after AuNP synthesis.

The spectroscopic data shows that the films possess an identical trend to that of the thicker films, where polymers with lower crosslink densities underwent greater ion-exchange with the fluorescein dye. The effect of the anion exchanged capabilities on AuNP synthesis (Figure 5-1) was then investigated. After polymerization, the network possesses a positive charge from the phosphonium polymer. Upon immersion in an aqueous solution containing HAuCl_4 (0.021 M, 1 min), the AuCl_4^- anion exchanges with Cl^- , thus functionalizing the polymer with AuNP precursor. Upon reduction with NaBH_4 (0.10 M in water, 2 min), AuNPs are formed and embedded within the polymer network. Formulations A-D containing 5 wt% phosphonium salt were subjected to this procedure and analyzed by UV-vis spectroscopy (Figure 5-4b). The ability of the polymer to swell and undergo anion exchange results in greater AuCl_4^- functionalization, and thus a higher concentration of AuNPs within the network, confirmed by the characteristic plasmonic absorbance at ~ 533 nm increasing in intensity. It appears that λ_{max} does not change in

position but rather intensity as a function of crosslink density. In comparison with the results by Goswami, similar λ_{\max} values were obtained despite their use of small-molecule cations in a non-crosslinked polymer system.¹³

The formation of the AuNPs must result in the regeneration of chloride anions within the polymer network to maintain charge balance. We hypothesized that these anions would be capable of undergoing anion exchange with additional AuCl_4^- followed by subsequent reduction to increase the concentration of AuNPs. Upon cycling this process using formulation **C** (Figure 5-5a), the concentration of AuNPs increased in a linear fashion without a discernable shift in λ_{\max} at 533 nm (Figure 5-5b and c, inset). These results indicate that each reduction cycle promotes the formation of new particles rather than increasing the size of the AuNPs formed in the previous cycles. This was confirmed using powder X-ray diffraction comparing samples after the first and eighth cycle. Using the Scherrer equation for the (111) Bragg reflection ($2\theta = 38$), the average AuNP size for both samples was approximately 22 nm (See appendix chapter 5, Figure 4-5).²² In traditional AuNP synthesis, the passivation of the particles with ligands (such as thiols) prevents further AuNP growth. In this system however, these particles are “naked” as there are no stabilizing ligands added to the system. The resulting particle size may be diffusion controlled and physically protected by nearby polymer preventing further growth. Using formulation **A**, patterned photopolymer was created which demonstrates how this technique may be used for spatially oriented AuNP synthesis (Figure 5-5d).

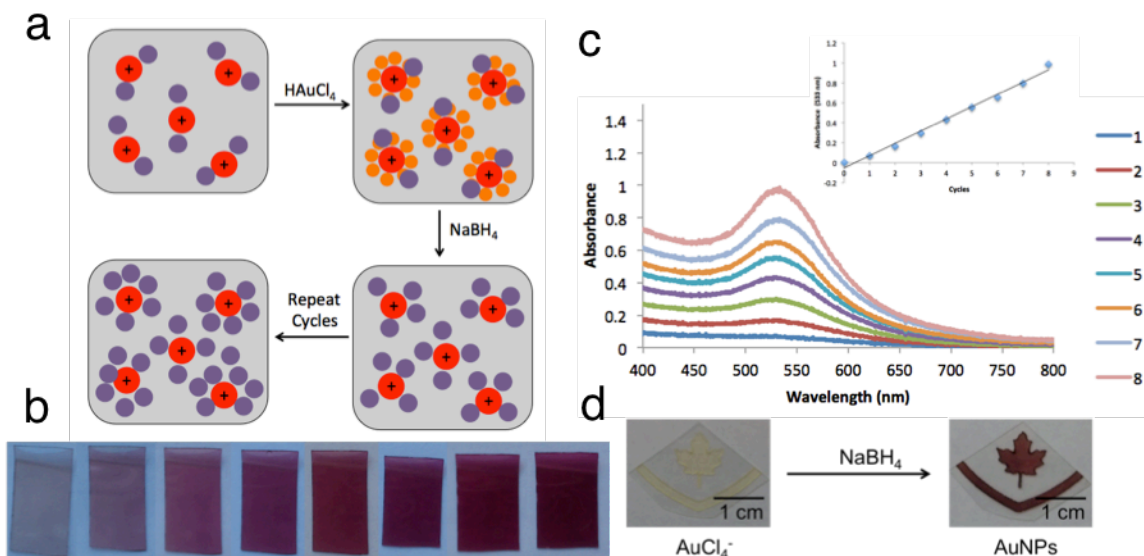


Figure 5-5: a) Schematic representation of the cyclic functionalization of the polymer film C with AuNPs. (b) Polymer film after 8 cycles. (c) Visual spectra of each cycle. The inset shows a plot of the intensity at 533 nm as a function of AuNP deposition cycles. (d) Patterned photopolymers can also be used to spatially orient the AuNPs.

Both SEM and TEM were used to gain further insight into the morphology of the system. A polymer sample (formulation C) functionalized with 8 cycles of AuNPs was coated with Pt and subjected to SEM and EDX analysis (Figure 5-6). The SEM results confirm the presence of Au nanoparticles on the surface of the polymer. Gold aggregates as large as 2 microns and particles as small as 20 nm were observed (Figure 5-6a and b). Upon closer examination, the larger features appear to be composed of smaller aggregates (Figure 5-6c and d). To obtain higher resolution images and finer structure within the polymer film, samples were subjected to TEM analysis (Figure 5-7). The interior of the polymer film possesses a high degree of heterogeneity, containing filaments composed of AuNPs. Particle sizes within these regions appear to range from 10-30 nm, along with some larger aggregates. It is likely that these results provide information on the distribution of phosphonium polymer within the photopolymer matrix, as the anion-exchange reaction is limited to areas where the cationic polymer resides. When the AuNPs are formed, they are restricted to that local area, as diffusion of such particles

through the polymer is not possible. This is in contrast to previous work, where the AuNPs were distributed evenly throughout the matrix.¹³ It is proposed that the difference lies in the choice of cation used within the matrix for the anion exchange process. While Goswami *et al.* used trioctylmethylammonium chloride, our approach utilized phosphonium polyelectrolyte.¹³ Small organic salts can homogeneously dissolve within a given medium, unlike polyelectrolytes that may aggregate because of their highly charged nature, resulting in phase-separation. It is possible these aggregates were frozen in place upon photopolymerization, providing a scaffold to perform AuNP synthesis within the matrix. These findings suggest the possibility of controlling AuNP formation within photopolymeric materials using self-assembly processes on the nanoscale, however this will require further investigation.

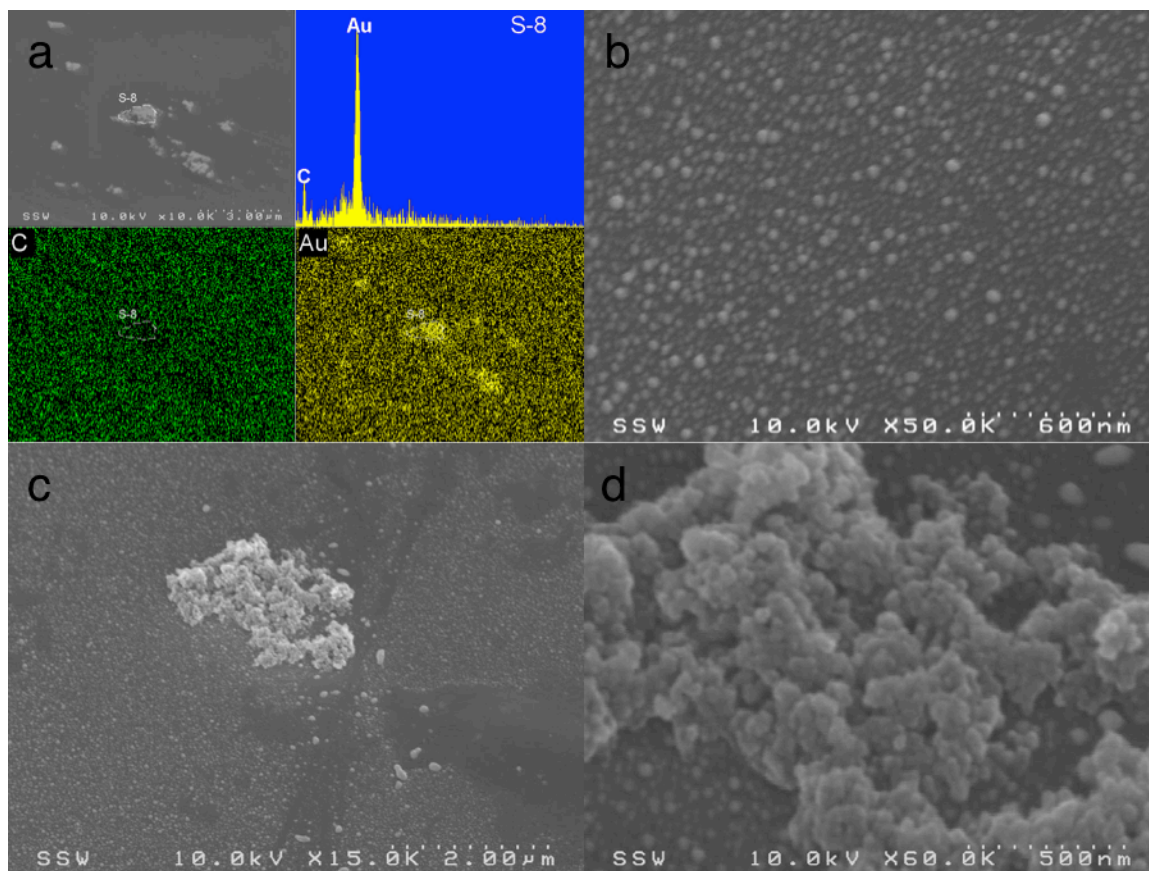


Figure 5-6: (a) SEM and EDX images of a polymer film functionalized 8 times with AuNPs. Gold appears to be present across the entire film with selected regions of

increased density. (b) Magnification shows good coverage of AuNPs on the surface. (c and d) The large structures appear to be aggregates of smaller gold particles.

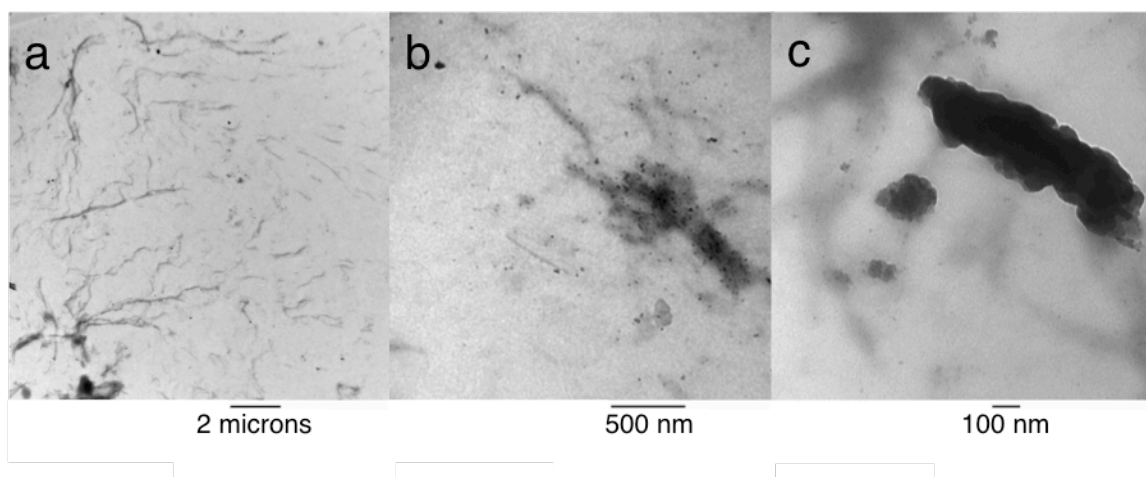


Figure 5-7: TEM images of formulation C after 8 reduction cycles. Darker regions correspond to the presence of gold. Images a show the existence of microstructured gold throughout the polymer matrix. Magnification of the darker regions shows fine nanostructure localized in the larger regions (b and c).

5.3 Conclusions

The synthesis of AuNPs within the polymer network is dictated by its physical properties, with softer networks able to undergo greater anion-exchange using AuCl_4^- . The amount of AuCl_4^- present in the material dictates the concentration of AuNPs formed but not their size. After reduction, the chloride anions are regenerated and may be further exchanged with AuCl_4^- to form new particles. SEM analysis of the surface shows a homogenous distribution of AuNPs with occasional aggregation, while the TEM results show that within the polymer film, there is a high degree of heterogeneity on the microscale. This may be due to phase separation of the polyelectrolyte from the monomer matrix, which is immobilized upon polymerization. The AuNPs are then formed and concentrated within these micro domains and possess a diameter from 10-30 nm. We finally show that both the photopolymer formulations and the *in situ* nanoparticle formation may be patterned, providing entry into their use in photolithographic applications.

5.4 Experimental

General materials and procedures. Tributylphosphine (94.5%+) and di(trimethylolpropane) tetraacrylate (EB 140), were donated by Cytec Corporation and used as received. Tetraethyleneglycol diacrylate, 4-vinylbenzyl chloride, 3-(trimethoxysilyl)propyl methacrylate, and 2,2-dimethoxy-2-phenylacetophenone (DMPA) were purchased from Sigma Aldrich and used as received. Melinex 725 Teijin PET films purchased from Tekra and microscope slides were purchased from Technologists Choice. Hydroxyethyl acrylate was purchased from Alfa Aesar. Fluorescein (sodium salt) was purchased from J.T. Baker Chemical. Deuterated chloroform was purchased from Caledon and stored over 4Å molecular sieves. Nuclear Magnetic Resonance (NMR) spectroscopy was conducted on a Varian INOVA 400 MHz spectrometer (^1H 400.09 MHz, $^{13}\text{C}\{^1\text{H}\}$ 158 MHz, $^{31}\text{P}\{^1\text{H}\}$ 161.82 MHz) unless otherwise noted. All ^1H and ^{13}C spectra were referenced relative to tetramethylsilane (CDCl_3 ; ^1H δ = 7.26 and ^{13}C δ = 77.2. CD_2Cl_2 ^1H δ = 5.32). The chemical shifts for $^{31}\text{P}\{^1\text{H}\}$ NMR spectroscopy were referenced using an external standard (85% H_3PO_4 ; δ_{p} = 0). Infrared spectra were recorded using a Bruker Tensor 27 spectrometer using attenuated total reflectance mode (ATR) using a ZnSe crystal. Photopolymerization was performed using a modified UV-curing system purchased from UV Process and Supply Inc. equipped with a mercury bulb. Irradiance and energy density were determined by a PP2-H-U Power Puck II purchased from EIT Instrument Markets. Glass transition temperatures were determined using differential scanning calorimetry (DSC) on a DSC Q20 TA instrument. A sample of approximately 10 mg was placed in an aluminum Tzero pan and underwent a heat/cool/heat profile at 10 °C/min under nitrogen atmosphere (50 mL/min). Data was acquired from the final heat cycle of the heat/cool/heat profile. Transmission electron microscopy (TEM) was conducted on a Philips CM10 with an AMT digital camera. UV-vis spectra were recorded using an Ocean Optics fiber optic spectrometer equipped with a SD200 detector and a Mini-D2T light source.

Photopolymerization and IR analysis

For bulk polymer disks, prepolymer solutions (80 mg) were sandwiched between two glass slides with a 200-micron spacer and irradiated with UV-light. Thin films (25

micron) were cast using a Meyer rod and irradiated with UV-light under a nitrogen atmosphere. Cure percentage was determined by comparing the intensity ratio of the acrylate $\text{CH}_2=\text{CH}$ vibration ($\sim 1640\text{ cm}^{-1}$) before and after irradiation relative to an internal standard ($\text{C}=\text{O}$ stretch, $\sim 1750\text{ cm}^{-1}$) using FTIR-ATR spectroscopy. Using the equation Percent Cure = $(r_u - r_c)/r_u \times 100$, where r_u = ratio of precured peaks and r_c = ratio of cured peaks, a conversion value was obtained. (Irradiance – UVA: 412 mW/cm^2 UVB: 423 mW/cm^2 UVC: 79 mW/cm^2 .)

Gel content and swelling

Bulk samples were weighed dry and then immersed in deionized water. Their mass was monitored until it reached a maximum (24 hrs) and its swelling ratio was determined using the equation $Q = (m_t - m_o)/m_o$, where m_t = swelled mass, m_o = dry mass, and Q = mass swelling ratio. These measurements were repeated three times and averaged. Samples were then dried in a vacuum oven at $80\text{ }^\circ\text{C}$ over 24 hours and weighed again. By comparing the original weight to the extracted weight, gel content was obtained.

References

- (1) Priolo, M. a; Holder, K. M.; Gamboa, D.; Grunlan, J. C. *Langmuir* **2011**, *27*, 12106.
- (2) Leterrier, Y.; Singh, B.; Bouchet, J.; Månson, J. -a. E.; Rochat, G.; Fayet, P. *Surf. Coatings Technol.* **2009**, *203*, 3398.
- (3) Kim, K.; Zhu, W.; Qu, X.; Aaronson, C.; McCall, W. R.; Chen, S.; Sirbuly, D. J. *ACS Nano* **2014**, *8*, 9799.
- (4) Guterman, R.; Hesari, M.; Ragogna, P. J.; Workentin, M. S. *Langmuir* **2013**, *29*, 6460.
- (5) Meyer, D. E.; Bhattacharyya, D. *J. Phys. Chem. B* **2007**, *111*, 7142.
- (6) Muthuswamy, E.; Ramadevi, S. S.; Vasan, H. N.; Garcia, C.; Noé, L.; Verelst, M. *J. Nanoparticle Res.* **2006**, *9*, 561.
- (7) Smotkin, E. S.; Brown, R. M.; Rabenberg, L. K.; Salomon, K.; Bard, A. J.; Campion, A.; Fox, M. A.; Mallouk, T. E.; Webber, S. E.; White, J. M. *J. Phys. Chem.* **1990**, *94*, 7543.

- (8) Muraviev, D. N.; Macanás, J.; Parrondo, J.; Muñoz, M.; Alonso, A.; Alegret, S.; Ortueta, M.; Mijangos, F. *React. Funct. Polym.* **2007**, *67*, 1612.
- (9) Zhang, J.; Han, D.; Zhang, H.; Chaker, M.; Zhao, Y.; Ma, D. *Chem. Commun.* **2012**, *48*, 11510.
- (10) Loo, S.-L.; Fane, A. G.; Lim, T.-T.; Krantz, W. B.; Liang, Y.-N.; Liu, X.; Hu, X. *Environ. Sci. Technol.* **2013**, *47*, 9363.
- (11) Anka, F. H.; Perera, S. D.; Ratanatawanate, C.; Balkus, K. J. *Mater. Lett.* **2012**, *75*, 12.
- (12) Azzaroni, O.; Brown, A. A.; Cheng, N.; Wei, A.; Jonas, A. M.; Huck, W. T. S. *J. Mater. Chem.* **2007**, *17*, 3433.
- (13) Kumar, R.; Pandey, A. K.; Tyagi, A. K.; Dey, G. K.; Ramagiri, S. V.; Bellare, J. R.; Goswami, A. *J. Colloid Interface Sci.* **2009**, *337*, 523.
- (14) Wang, S.; Liu, P.; Wang, X.; Fu, X. *Langmuir* **2005**, *21*, 11969.
- (15) Sachdeva, A.; Sodaye, S.; Pandey, A. K.; Goswami, A. *Anal. Chem.* **2006**, *78*, 7169.
- (16) Ryou, M.-H.; Lee, Y. M.; Cho, K. Y.; Han, G.-B.; Lee, J.-N.; Lee, D. J.; Choi, J. W.; Park, J.-K. *Electrochim. Acta* **2012**, *60*, 23.
- (17) Bowman, C. N.; Kloxin, C. J. *AIChE J.* **2008**, *54*.
- (18) Tang, Z.; Wei, J.; Yung, L.; Ji, B.; Ma, H.; Qiu, C.; Yoon, K.; Wan, F.; Fang, D.; Hsiao, B. S.; Chu, B. *J. Memb. Sci.* **2009**, *328*, 1.
- (19) Lin, H.; de Oliveira, P. W.; Veith, M. *Opt. Mater.* **2011**, *33*, 759.
- (20) Xue, X.; Hai, F.; Gao, L.; He, F.; Li, C.; Li, Y.; Huang, M. *Opt. - Int. J. Light Electron Opt.* **2013**, *124*, 6987.
- (21) Cai, X.; Anyaogu, K. C.; Neckers, D. C. *J. Am. Chem. Soc.* **2007**, *129*, 11324.
- (22) Klug, H. P.; Alexander, L. E. *X-ray Diffraction Procedures*; Wiley: New York, 1954.

Chapter 6

6 Polymer networks formation using the phosphane-ene reaction: a thiol-ene analogue with diverse post-polymerization chemistry

6.1 Introduction

Polymer networks are crosslinked polymers that have found widespread use in actuators, microelectronics fabrication, synthetic rubbers, coatings, tissue engineering scaffolds, and other areas.¹⁻⁶ The incredible diversity of these materials stems from their highly tunable nature, ranging from soft hydrogels to tough thermosets, with their properties dictated by chemical functionalities in the network as well as their crosslink densities.^{7,8} They can be synthesized thermally, but also photochemically, where the photochemical approach is generally referred to as photopolymerization or UV-curing, and provides the possibility for both spatial and temporal control over the polymerization process.⁹ While the vast majority of polymer networks are synthesized using free-radical polymerization of (meth)acrylates, thiol-ene polymerization has garnered increasing popularity over the past decade as an alternative approach. The network polymerization using thiol-ene chemistry is relatively unique, as it is a radical mediated, air-stable, step-growth process, combining the fast kinetics of radical chemistry with reduced shrinkage, high conversion, and delayed gelation, as described by Hoyle, Bowman, and Hawker.¹⁰⁻¹² The key aspect to this approach is the application of organosulphur chemistry for polymer science. This represents one of relatively few widely used examples of a polymerization reaction utilizing an inorganic element.¹³ It can therefore, serve as a template for the incorporation of other inorganic elements into polymeric materials, thus expanding the scope and application beyond sulphur.¹⁴

One element with the potential to benefit from the fundamental chemical insights of the thiol-ene reaction is phosphorus. In addition to its widespread utility in synthesis and materials science,¹⁵⁻¹⁸ over the past several decades phosphorus has increasingly been employed in polymer chemistry.^{17,19-23} In the 1960s, Pellon reported that thiols and primary phosphines (RPH_2) were similar with regards to their radical mediated hydrothiolation (thiol-ene) and hydrophosphination (phosphane-ene) chemistry.²⁴⁻²⁶ As

shown in Figure 6-1a, upon hydrogen abstraction, phosphinyl and thiyl radicals quickly add to C=C bonds to form a carbon-centred radical, which subsequently abstracts a hydrogen atom from a nearby phosphine/thiol, leading to propagation. While hydrothiolation later became referred to as thiol-ene chemistry in polymer and material science, phosphane-ene chemistry remains entrenched in small molecule synthesis despite several attempts to apply it to the production of macromolecules.²⁷⁻²⁹ This likely stems from the relative limited family of primary phosphines as well as the difficulty in handling them, which unlike thiols, are typically pyrophoric. However, recent developments in fundamental phosphorus chemistry have identified a systematic way to classify specific primary phosphines as air-stable that possess remarkable oxidative resistance not explained simply by substituent steric effects.³⁰ This has initiated what some refer to as “The Primary Phosphine Renaissance”.³¹

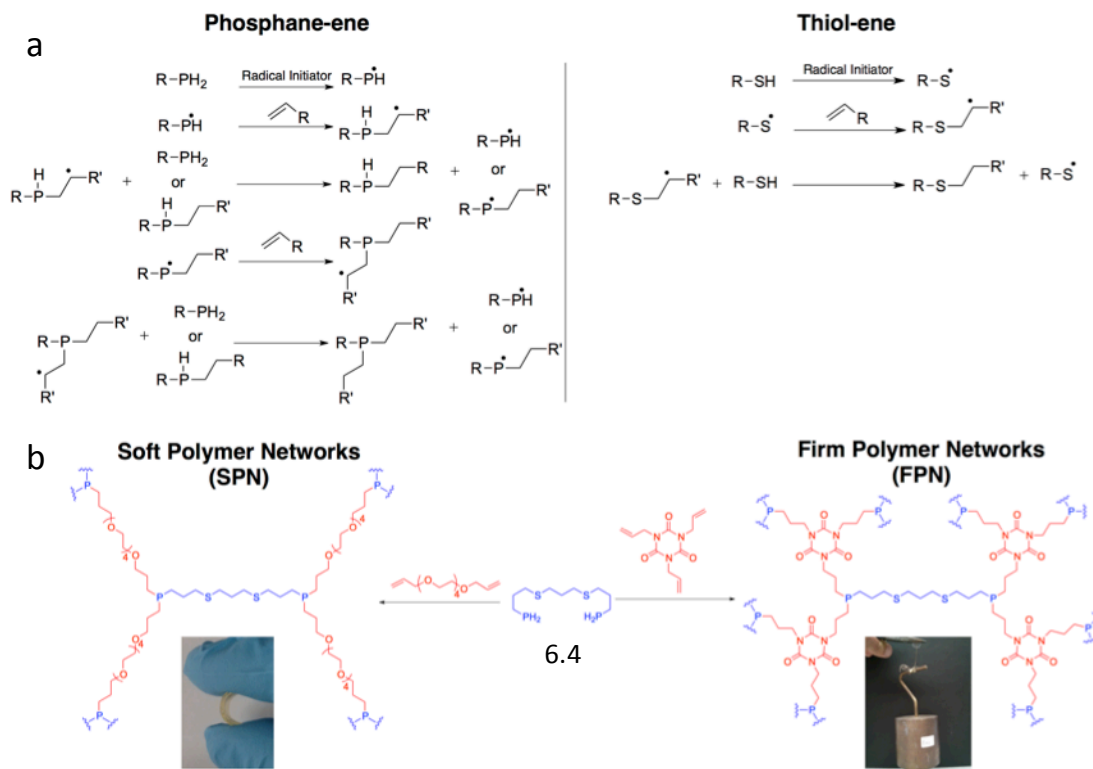


Figure 6-1: a) Mechanism for hydrophosphination/phosphane-ene reaction and for hydrothiolation/thiol-ene reaction. b) Schematic representation of polymer network formation using **6.4** and photoinitiator Irgacure 819, where soft materials are created when using TEGDAE, while firm networks are made using TTT and can hold 1 kg of weight.

Katti *et al.* showed that a variety of air-stable phosphines could be synthesized and incorporated into peptides using standard methods without any oxidation or by-products, a feat not easily accomplished using typical phosphines containing a P-H functionality.³²⁻³⁴ These discoveries allow for the widespread exploration of these interesting, yet simple functional groups beyond constructing small molecules. In this context, we bring new perspective to the long established P-H bond by harnessing its chemistry to develop for the first time the phosphorus analogues of thiol-ene networks (Figure 6-1b). This allows for the generation of polymeric materials with a wide variety of properties and functions including oxygen scavenging, electrochemical activity, polyelectrolytes, and ceramics.

Our approach exploits the concepts established for thiol-ene chemistry, such as appropriate monomer choice, polymerization methodologies, and inhibitor additives, to fabricate these new materials, while at the same time expanding on their utility by exploiting the diverse chemistry of phosphorus in derivatizing the network after polymerization. These materials can be analyzed using ^{31}P solid-state NMR spectroscopy (SS-NMR), providing a unique handle not available in thiol-ene systems to probe these materials and thus investigate the chemistry within the networks.

6.2 Results and Discussion

6.2.1 Phosphane-ene Network Synthesis and Properties

To successfully photopolymerize primary phosphines using phosphane-ene chemistry, the molecule must possess sterically unhindered R-PH_2 functionality, a low molecular weight, transparency to UV-light, and facile olefin addition chemistry. While aryl phosphines have previously been the focus of phosphane-ene reactions of small molecules, the high stability of the arylphosphinyl radical leads to inefficient hydrophosphination. This arises from a reverse-addition reaction as described by Pellon, resulting in sluggish or absent polymerization.^{25,28,35} A more reactive alkylphosphine should be more efficient. Considering also that tetra-alkylthiols are used in thiol-ene networks, we deemed primary phosphine **6.4** as the most suitable candidate for our studies because of its resistance to oxidation, high P-H functionality, alkyl character, and ease of synthesis (Figure 6-1b: See Experimental for synthetic details).³⁶

Thiol-ene networks are typically synthesized by reacting multifunctional thiols with olefins in a step-growth fashion, where the monomer compositions and functional group stoichiometry enables tuning of the chemical, thermal, and mechanical properties of the material.^{3,37} Depending on the bias imposed on the original formulation (i.e. excess olefin or thiol), residual functional groups are supported by the polymer network after polymerization, and then exploited for further chemistry.³⁸ It follows then that trends in both the thermal and chemical properties of phosphane-ene networks should mimic those of the thiol-ene systems upon changing crosslink densities and monomer composition. To evaluate this hypothesis, **6.4** was polymerized in a Teflon mold under an inert atmosphere

with either tetra(ethylene glycol) diallyether (TEGDAE) to create soft polymer networks (**SPN-1** to **SPN-3**) or 1,3,5-triallyl-1,3,5-triazine-2,4,6(1*H*,3*H*,5*H*)-trione (TTT) to create firm networks (**FPN-1** to **FPN-3**) (Figure 6-1b, Table 6-1). Formulations consisting of a PH₂/olefin molar ratio of 0.5:1 should result in complete conversion of both functional groups to form a network, while formulations with excess PH₂ (0.75:1) or olefin (0.38:1) should form polymer networks with supported P-H bonds or olefins, respectively.

Table 6-1: Effect of changing olefin composition and PH₂/olefin ratios on network properties. The %mass increase upon oxidation, Ox was measured and compared to the calculated value, $Ox_{calc} = 100((n_{phos}M_{Oxy}+W_0)/W_0)-1$, where n_{phos} is the moles of phosphorus in the sample, M_{Oxy} is the atomic mass of oxygen, and W_0 is the weight of the sample.

Polymer	PH ₂ :Olefin Ratio	Swelling (%)	Gel Content (%)	T _g (°C)	T _{g-ox} (°C)	Ox _{calc} (%)	Ox _{exp} (%)
SPN-1	0.75:1	92±1	89±1	-61	-39	5.1	5.2
SPN-2	0.5:1	62±1	>98	-52	-37	4.0	4.1
SPN-3	0.38:1	152±26	81±2	-64	-54	3.0	3.4
FPN-1	0.75:1	29±1	>98	56	-	6.6	6.5
FPN-2	0.5:1	5±1	>98	101	-	5.4	1.6
FPN-3	0.38:1	5±1	>98	106	-	4.6	1.6

Free standing pucks were formed after exposure to UV-light on a conveyor assembly and were analyzed by attenuated total reflectance Fourier transform infrared (ATR-FTIR) spectroscopy, which revealed a decrease in both the P-H bond (~2300 cm⁻¹) and olefin (~3050 cm⁻¹) signal intensities (Appendix chapter 6, Figure 1-2). For **SPN-2** and **FPN-2**, complete conversion of all P-H and olefin functional groups was observed, while **SPN-1/FPN-1** and **SPN-3/FPN-3** samples contained unreacted P-H bonds and olefins, respectively after polymerization. The physical and thermal properties of these materials followed an identical trend to that of thiol-ene systems, as all samples possessed a very high gel content, where TEGDAE networks (**SPN-1** to **SPN-3**) were the softest and most swellable, while those comprised of TTT (**FPN-1** to **FPN-3**) were firmer and less swellable because of higher crosslink densities and the rigid olefin structure (Table 6-

1).¹¹³ These data show that highly tunable phosphane-ene networks could be made using a similar approach used in thiol-ene network synthesis with ease, providing a convenient route for the fabrication of network-supported phosphines. The internal composition of the network remained elusive however, as IR spectroscopy alone cannot differentiate between primary (RPH_2) or secondary (R_2PH) phosphine P-H bonds, which has implications for further chemistry of the networks. Unlike ^{33}S , ^{31}P is an ideal nucleus for NMR spectroscopy in solution and in the solid-state, and upon examination of **SPN-1** by ^{31}P SS-NMR spectroscopy, we observed three very well resolved, sharp signals that corresponded to the primary, secondary and tertiary phosphines (Figure 6-2), with spin-spin coupling in the solid-state identical to primary phosphine **6.4** ($^1J_{\text{P,H}} = 192 \text{ Hz}$), even at temperatures well below the polymer T_g ($-100 \text{ }^\circ\text{C}$, Appendix chapter 6, Figure 3). These data suggests that these networks are homogenous in composition with discrete phosphorus environments, and that the polymerization process proceeds with no phosphorus-containing byproducts. The capability to detect each phosphorus signal with such precision should provide the means to monitor chemistry performed at these sites, a unique feature not possible with thiol-ene. To our knowledge, this is the first example of a network-supported primary/secondary phosphine.

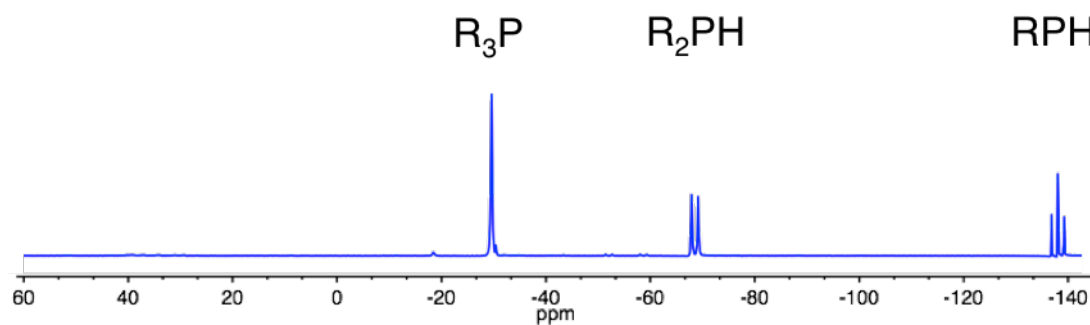


Figure 6-2: ^{31}P SS-NMR spectroscopy of **SPN-1** showing the presence of only three phosphorus functional groups within the polymer network.

6.2.2 Solid-supported Chemistry

A defining feature of thiol-ene networks that has been critical for their successful implementation in materials science is the utilization of either excess thiol or olefin functionality in the network to further modify the material.³⁸ While phosphane-ene networks should be capable of analogous chemistry, the presence of tertiary alkyl phosphines throughout the polymer backbone provides an additional synthetic handle to exploit. These functional groups possess significantly greater reactivity towards electrophiles and oxidants relative to thioethers, and also have potential utility in chemical synthesis and catalysis. In most cases, functional groups become unreactive or less reactive after polymerization, however the nucleophilic and basic character of phosphines increases upon each successive alkylation (polymerization) step, thus creating a reactive polymer network primed to perform further chemistry throughout its backbone. To evaluate this, a series of chemical reactions was performed on **SPN-1** to utilize R_3P , R_2PH and RPH_2 functional groups (Figure 5-3a), and the outcome of these reactions was probed by $^{31}P\{^1H\}$ SS-NMR spectroscopy. This chemistry was also performed in solution on the small molecule **6.3** as a model to compare $^{31}P\{^1H\}$ chemical shifts with those obtained in reactions of **SPN-1** (Figure 6-3b). Compound **6.3** (blue) was reacted with 1-hexene until a spectroscopic profile similar to that of **SPN-1** (red) was obtained. Treatment with ethyl iodide under mild reaction conditions selectively quaternized the highly nucleophilic tertiary phosphines (at $\delta_P = -33$), providing a phosphonium salt/polyelectrolyte network ($\delta_P = 37$; **SPN-1a**). This significantly increased the T_g because of the resulting cation-anion interactions, while leaving all primary and secondary phosphines untouched. The remaining P-H bonds present at this stage were reacted with 1-hexene, forming additional R_3P moieties (**SPN-1b**), which were then quickly oxidized using elemental sulfur ($\delta_P = 50$; **SPN-1c**), increasing the T_g once more (Appendix chapter 6, Figure 4). These results show the diversity of the R_3P functionality and its orthogonal chemistry when compared to both primary/secondary phosphines within the network. Furthermore, these chemical reactions could be monitored using ^{31}P SS-NMR spectroscopy to observe the distribution of phosphorus environments with identical precision to that found in solution, a feature not shared with thiol-ene systems. These two aspects combined illustrate how phosphane-ene networks provide a platform to exploit

organophosphine chemistry in a completely novel manner, allowing for the elucidation of more complex solid-supported phosphine chemistry that would otherwise be impossible to observe.

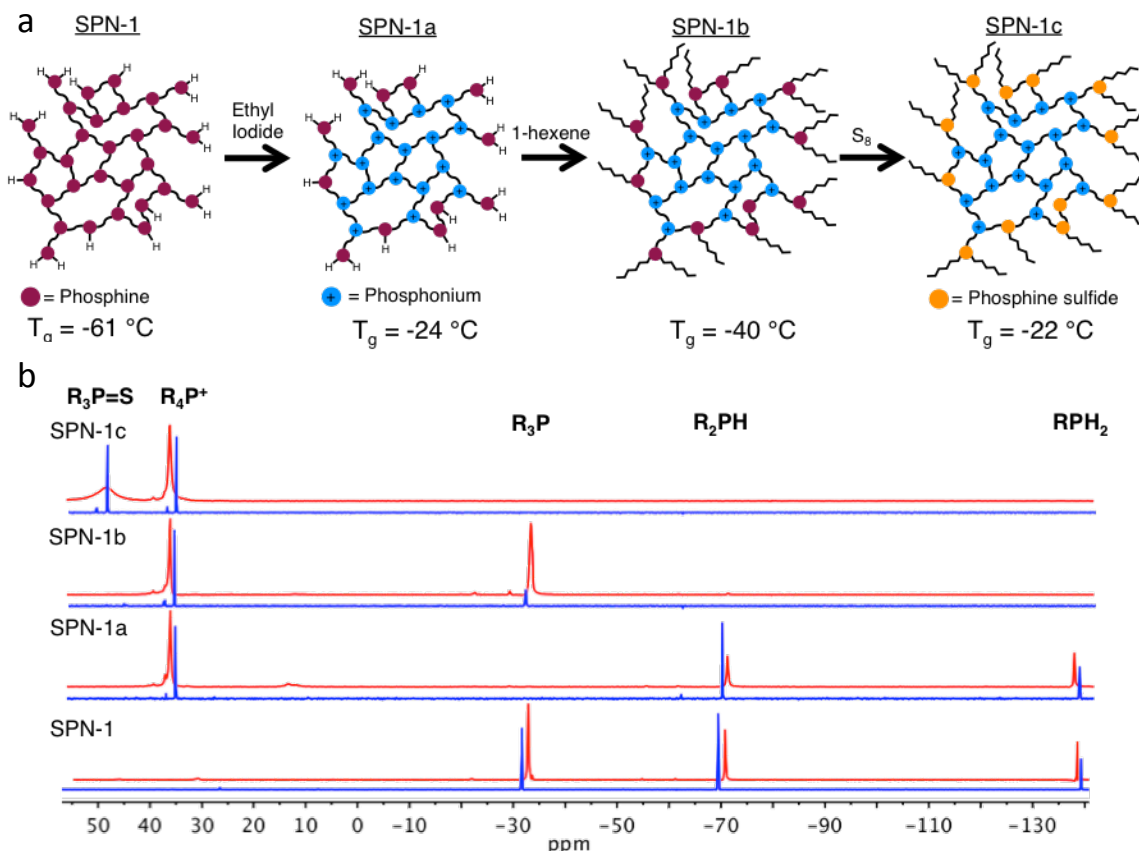


Figure 6-3: a) A schematic representation of the solid-supported reactions illustrates three separate functionalization steps and their effect on glass transition. b) $^{31}\text{P}\{^1\text{H}\}$ NMR spectra comparing identical chemistry (shown in a) performed on the small molecule **6.3** (blue spectra) in solution and **SPN-1** (red spectra) in the solid-state.

6.2.3 Thermoresponsive Oxygen Scavenging

The high phosphine loading and tunable nature of these polymer networks suggests that they may be promising oxygen scavenging materials for packaging of oxygen sensitive substances.³⁹ We examined the oxidation behaviour of these polymers gravimetrically by placing samples (**SPN-1** to **SPN-3**) in a thermogravimetric analysis (TGA) instrument under a flow of air at 25 °C for 30 minutes followed by heating to 100 °C to hasten the

oxidation process (Figure 6-4b, green). Assuming a 1:1 ratio between phosphorus and oxygen, the calculated % mass increase (Ox_{calc}) was compared to the experimentally determined value, Ox_{exp} (Table 6-1). For **SPN-1** to **SPN-3**, these values were in close agreement, demonstrating that the mass increase depends on phosphorus content. Following the oxidation experiments, the $^{31}P\{^1H\}$ SS-NMR spectrum of **SPN-2** was collected and revealed a new resonance at $\delta_p = 51$, consistent with the formation of $R_3P=O$ exclusively, with no evidence for polymer backbone degradation (Figure 5-4B). Glass transition temperatures of the oxidized **SPN-1** to **SPN-3** (T_{g-ox}) were measured and showed a significant increase relative to their nonoxidized states, with this effect being more pronounced with greater phosphine content (Appendix chapter 6, Figure 5). The capability for the polymer to oxidize appeared to depend on T_g , with firmer polymers displaying greater oxidative resistance (**SPN-2**>**SPN-1**>**SPN-3**). As a comparison we analyzed polymers comprised of TTT (**FPN-1** to **FPN-3**), which possess higher T_g values (Figure 6-4b, red). Collectively, these networks were significantly more stable, with **FPN-2** and **FPN-3** ($T_g = 101$ and 106 °C, respectively) exhibiting minimal oxidation over 2 days at 120 °C, while **FPN-1** ($T_g = 56$ °C) displayed excellent stability at 25 °C (0.0016 %/min), but oxidized rapidly upon heating (120 °C), resulting in an increase in its mass to the calculated value. From these results it was concluded that oxidative stability depends on the stiffness of the material, with oxidation occurring rapidly when phosphines are present in a soft environment and to a much lesser extent when in a firm environment. Thus, by simply adjusting the composition and crosslink density of these phosphane-ene polymers, the T_g and therefore the oxidation temperature can be tuned. This system is unique in a sense that the element responsible for the polymerization reaction is also responsible for oxygen scavenging, as opposed to other systems which require fillers, catalysts, and/or UV irradiation, thus providing a simpler means to prepare oxygen scavenging materials.⁴⁰

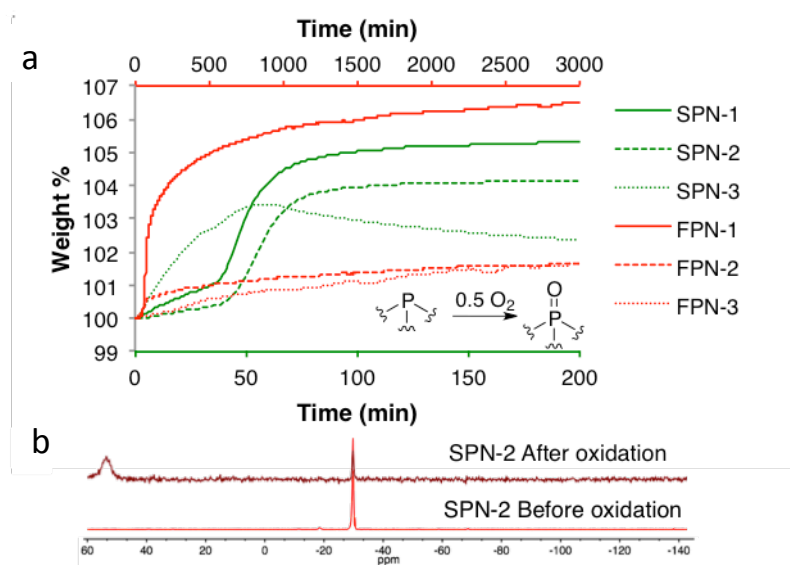


Figure 6-4: a) TGA thermographs for **SPN-1**→**SPN-3** (green lines and axis) and **FPN-1**→**FPN-3** (red lines and axis). All polymers were first held at 25 °C for 30 minutes to ascertain their stability at room temperature, followed by heating to either 100 °C for soft networks or 120 °C for firm networks. b) ³¹P{¹H} NMR spectra of **SPN-2** before and after oxidation in air.

6.2.4 Formulation Stability

Autopolymerization of thiol-ene formulations in the absence of light has been identified as a significant issue hindering potential commercialization of the technology, and is likely a result of impurities, or a charge-transfer complex between the thiol and olefin resulting in S-C bond formation.^{41,42} In this context, we examined the stability of our phosphane-ene systems using ³¹P NMR spectroscopy. While formulation **SPN-2** under a nitrogen atmosphere was stable for over 30 days ($\delta_P = -139$), polymer quickly formed after exposure to air (10 min), suggesting that oxygen may have a role in the autopolymerization. Radical inhibitors were then added as phosphine oxidation is believed to occur via a radical process forming peroxy radicals, which may in turn facilitate phosphane-ene chemistry prematurely, even at very low concentrations.^{43,44} Indeed the addition of either butylated hydroxytoluene (Appendix chapter 6, Figure 6) or diphenylamine (Figure 6-5) significantly increased stability (1 and 5 hours, respectively) after which secondary and tertiary phosphines were detected, while ³¹P NMR

spectroscopy revealed the presence of new signals ($\delta_P = 4$ (t) and 31 (d), $^1J_{P-H} = 452$ Hz), consistent with the formation of primary and secondary phosphine oxides, supporting our postulation that oxidation facilitates polymerization. Photopolymerization of aerated samples containing 0.5 wt% Irgacure 819 and 0.67 wt% diphenylamine was investigated, however greater photoinitiator content (1.15 wt%) was required to obtain complete conversion (Appendix chapter 6, Figure 7). This demonstrates that phosphane-ene systems has the potential to be handled and exploited in air, although phosphines possessing greater resistance to oxidation in addition to inhibitor optimization should increase shelf-life of these formulations.

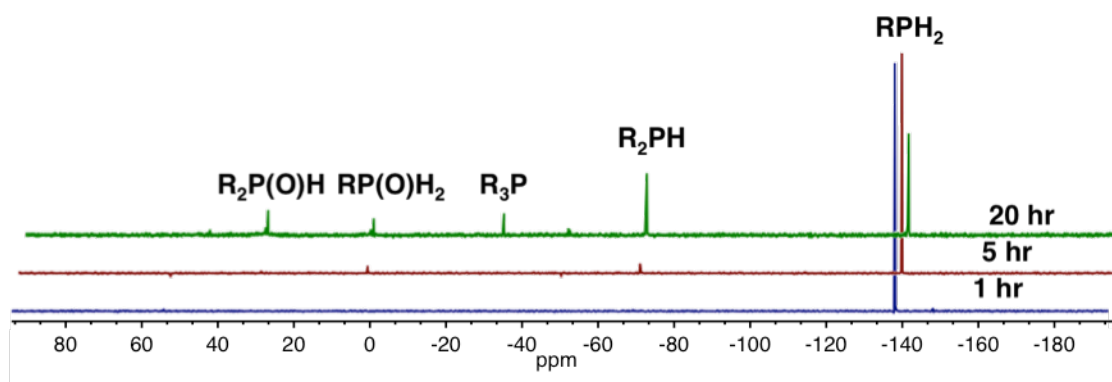


Figure 6-5: $^{31}\text{P}\{^1\text{H}\}$ NMR spectra of formulation **SPN-2** with 2 wt% diphenylamine in air, which imparts increased stability in air.

6.2.5 Metal-containing Phosphane-ene Networks

Given the strong Lewis basic character of the alkylphosphines in the network, it is ideally suited to bind transition metals, and is particularly attractive for metals used in solid-supported catalysis (e.g. Pd; PdCl₂ or Pd(OAc)₂).¹⁵ As a proof of principle, we have achieved palladium loadings of 1.6 mmol/g of **SPN-2**, which corresponds to 65 % of the number of the available alkylphosphines binding to a metal centre. To expand the scope of phosphane-ene polymerization however, compound **6.5**, an air-stable ferrocenyl-containing primary phosphine was incorporated into a polymer network (Figure 6-6a). The redox activity and ceramic forming capabilities of ferrocenyl polymer networks have been of significant interest in recent years, but relatively few fabrication methods exist, prompting us to explore this as a potential synthetic route.⁴⁵ The intense colour of **2**

prevented photopolymerization using previous methods, so instead ferrocene-containing polymer networks (**FcPN**) were prepared by mixing a 1.5:1 molar ratio of **2** and TTT in air followed by dissolution in dimethylformamide (60 wt% solutions) and irradiation in a glass mold (200 μm thick). It is noteworthy that this formulation was observed to be air-stable in ambient light for months without any signs of autopolymerization. This can likely be attributed to the high oxidative stability of **6.5**. **FcPN** films swelled slightly in toluene, possessed high gel content (swelling = 30%, ~93% gel content), and preserved the characteristic orange colour of **6.5**. Upon pyrolysis of the sample (800 $^{\circ}\text{C}$), a black magnetic ceramic was isolated, which retained its original shape, (60 wt% char yield, Figure 6-6b) and contained carbon, oxygen, iron, and phosphorus. The electrochemical properties of a thin film of **FcPN** on a glassy carbon electrode were examined using cyclic-voltammetry, and in each case, a *pseudo-reversible* one-electron oxidation event was observed, confirming that the organometallic networks created using our phosphane-ene chemistry possess redox activity that could be exploited for future applications (Figure 6-6c).

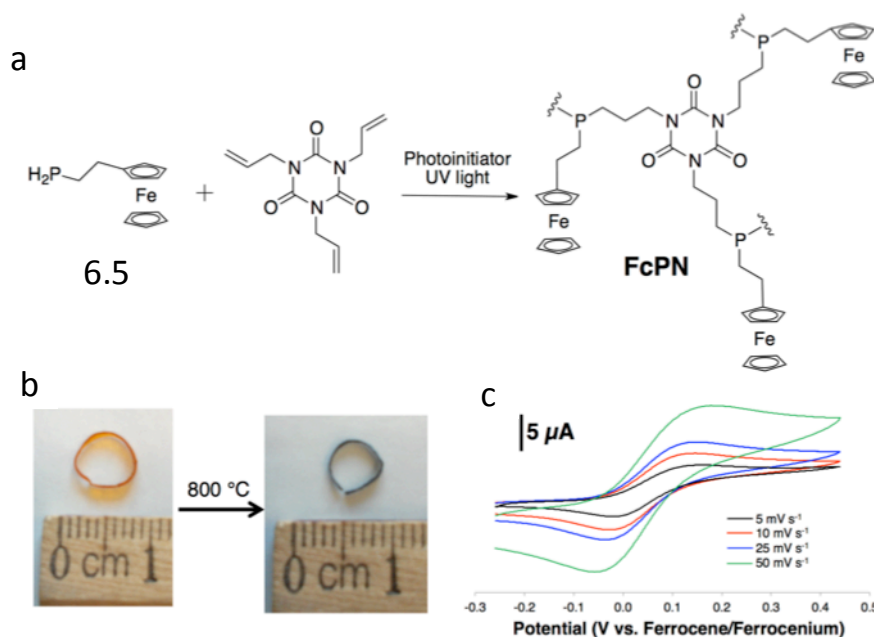


Figure 6-6: a) Synthesis of a ferrocene-containing polymer network (**FcPN**). b) Shaped ceramics can be formed from the pyrolysis of **FcPN**. A thin strip of polymer film was manually formed into a ring, dried in an oven, and retained its shape upon pyrolysis, c)

Cyclic-voltammetry of a thin film of **FcPN** can undergo *pseudo*-reversible one-electron oxidation, demonstrating the redox activity of these materials.

6.3 Conclusions

In summary, we have demonstrated for the first time the feasibility of synthesizing functional polymer networks using phosphane-ene chemistry. The properties of the networks could be readily tuned by the choice of alkene monomer and the pendant groups supported by the resulting network could be selected based on the ratios of the monomers in the formulation. The spectroscopically (NMR) active ^{31}P nucleus allowed for the chemical structures of the networks to be directly probed by ^{31}P SS-NMR spectroscopy, a distinct advantage relative to the ^{32}S nucleus employed in the widely used thiol-ene network formation. In addition, the high level chemical versatility of the resulting phosphines in the networks was exploited to demonstrate the potential utility of these materials (e.g. scavenge oxygen; bind transition metals). The incorporation of a ferrocenyl phosphine afforded a redox-active polymer network that could be pyrolyzed to obtain a magnetic ceramic. Overall, this work demonstrates the immense potential of phosphane-ene chemistry for the formation of functional materials.

6.4 Experimental

Formulations were prepared under a N_2 atmosphere and prepared in a nitrogen-filled MBraun Labmaster 130 glove box unless otherwise noted. Dried solvents were collected under vacuum in a flame dried Strauss flask and stored over 4\AA molecular sieves in the drybox. Photoinitiator (Irgacure 819) was purchased from Ciba Chemicals and 1,3,5-triallyl-1,3,5-triazine-2,4,6(1H,3H,5H)-trione was purchased from Sigma-Aldrich and used as received. Solution phase Nuclear Magnetic Resonance (NMR) spectroscopy was conducted on a Varian INOVA 400 MHz spectrometer (^1H 400 MHz, ^{13}C 158 MHz $^{31}\text{P}\{^1\text{H}\}$ 162 MHz) unless otherwise noted. All ^1H NMR spectra were referenced relative to tetramethylsilane (CDCl_3 ; ^1H $\delta_{\text{H}} = 7.26$ ppm). The chemical shifts for $^{31}\text{P}\{\text{H}\}$ NMR spectroscopy were referenced using an external standard (85% H_3PO_4 ; $\delta_{\text{P}} = 0$). Solid-state NMR spectroscopic experiments were conducted on Varian INOVA

400 MHz at a spin rate of 9300 Hz and referenced using an external standard ((NH₄)₃PO₄; $\delta_P = 0$). High resolution mass spectrometry was performed on a MASPEC II system, and ESI +/- mass spectrometry was performed on a Micromass LCT spectrometer. Infrared spectra were recorded using a Bruker Tensor 27 spectrometer with an attenuated total reflectance (ATR) attachment using a ZnSe crystal. Photopolymerization was performed using a modified UV curing conveyor system purchased from UV Process and Supply Inc. with a mercury bulb (UVA: 154 mW/cm², 189 mJ/cm². UVB: 74 mW/cm², 90 mJ/cm²), except for the synthesis of FcPN which was photopolymerized using a static light source (UVA: 175 mW/cm²). Lamp power was determined by a PP2-H-U Power Puck II purchased from EIT Instrument Markets. All polymer samples were milled by hand and then immersed in toluene for at least 24 hours and dried to remove unpolymerized material prior to thermal analysis. Oxidation experiments were conducted using thermal gravimetric analysis (TGA) on a Q600 SDT TA instrument and analyzed using TA Universal Analysis. For samples **SPN-1**→**SPN-3**, a 5 mg milled sample was placed in an alumina cup and exposed to medical grade air (100 mL/min) for 30 min at 25 °C, following by heating at 2 °C/min until 100 °C and held for 210 minutes. Samples **FPN-1**→**FPN-3** were first heated to 120 °C under a nitrogen atmosphere for 10 minutes to remove residual solvent, and then cooled to 25 °C. At this point, data acquisition began and air (100 mL/min) was introduced for 30 min, after which the sample was heated at 2 °C/min until 120 °C and held for 50 hours, and the rate of oxidation for **FPN-1** was determined from the first 30 minutes of air exposure at 25 °C. The calculated %mass increase (Ox_{calc}) was determined using the equation $Ox_{calc} = 100((n_{phos}M_{Oxy}+W_0)/W_0)-1$, where n_{phos} is the moles of phosphorus in the sample, M_{Oxy} is the atomic mass of oxygen, and W_0 is the weight of the sample, and was compared to the experimentally determined value, Ox_{exp} . Glass transition temperatures were determined using Differential Scanning Calorimetry (DSC) on a DSC Q20 TA instrument and analyzed by TA Universal Analysis. A sample of approximately 5 mg was placed in an aluminum Tzero pan and underwent a heat/cool/heat profile at 10 °C/min under nitrogen atmosphere (50 mL/min). The transitions were determined from the final heat cycle of the heat/cool/heat profile. Cyclic voltammetry experiments were performed with a Bioanalytical Systems Inc. (BASi) Epsilon potentiostat and analyzed using BASi

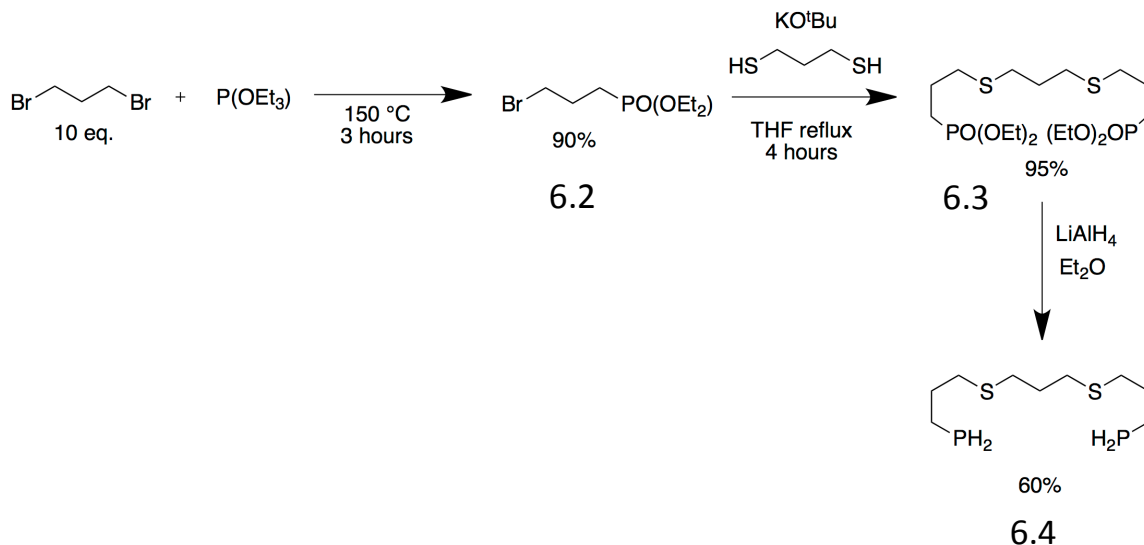
Epsilon software. SEM/EDX analysis was performed on a Hitachi S4500 FESEM equipped with a Quartz XOne EDX system.

Synthesis of tetraethyleneglycol diallylether (TEGDAE, 6.1)

TEGDAE was synthesized according to a modified literature procedure.^{46,47} Briefly, tetraethyleneglycol (5.0 g, 25.7 mmol) and allyl bromide (10 g, 83 mmol) were dissolved in toluene (40 mL) followed by the addition of sodium hydroxide (3.0 g, 75 mmol). The mixture was heated to 45 °C and stirred for 18 hours. The mixture was decanted and volatiles removed *in vacuo*. The product was dissolved in DCM and extracted with water (100 mL x 3), dried with MgSO₄, and decanted. Volatiles were removed *in vacuo* followed by distillation under reduced pressure (0.2 torr). A colourless oil was isolated and identified as tetraethyleneglycol diallylether (5.0 g, 71%).

Synthesis of H₂P(CH₂)₃S(CH₂)₃S(CH₂)₃PH₂ (6.4)

Compound 6.4 was synthesized according to literature procedures (Scheme 6-1).⁴⁸ Briefly, excess 1,3-dibromopropane (261 g, 1290 mmol) and triethylphosphite (15 g, 129 mmol) were combined and heated to reflux for 3 hours. Fractional distillation under reduced pressure (85 °C, 2 torr) yielded compound 6.2 (13.68 g, 90%). 1,3-propanedithiol (2.95 g, 26.45 mmol) and KOBu^t (6.12 g, 52.9 mmol) were added to THF (350 mL) and heated to reflux for 30 min followed by the dropwise addition of 6.2 (13.505 g, 55.5 mmol) and left stirring for 3 hours. Volatiles were removed *in vacuo* at 40 °C and the residual material dissolved in diethylether (300 mL). The mixture was filtered yielding a colourless oil identified as compound 6.3 (10.87 g 95%). Reduction of 6.3 (6.14 g, 14.2 mmol) using LiAlH₄ (1.66 g, 42.55 mmol) followed by an acid extraction (1 M HCl, 200 mL x 3) and fractional distillation (185 °C, 0.1 torr) yielded compound 6.4 (2.18 g, 60%). See chapter 6 appendix, Figures 7-10 for NMR spectra.



Scheme 6-1: Synthesis of **6.4**

Synthesis of $\text{H}_2\text{P}(\text{CH}_2)_2(\text{C}_5\text{H}_4)\text{Fe}(\text{C}_5\text{H}_5)$ (**6.5**)

Vinylferrocene (2.00 g, 9.43 mmol) and azobisisobutylnitrile (AIBN) (0.06 g, 0.4 mmol) were dissolved in dry and degassed toluene (180 mL), added to a Parr reactor, and purged with N_2 gas. The vessel was then charged with PH_3 gas (80 PSI) and heated to $45 \text{ }^\circ\text{C}$ for 16 hours *CAUTION – phosphine gas is toxic and pyrophoric. The excess phosphine gas was burned off under controlled conditions in a fume hood before the Parr reactor was opened inside a glove box. The reaction mixture was transferred to a Schlenk flask before the volatiles were removed *in vacuo* to afford a light orange residue. The residue was dissolved in a minimum amount of dichloromethane and purified by column chromatography (hexanes) using deactivated silica containing 4% deionized water ($R_f \approx 0.2$) as the mobile phase. The solutions were concentrated *in vacuo* and the resulting yellow solid was recrystallized from ethanol, identified as **5** (1.62 g, 70%). Yield = 1.62 g, 70%. M.p. = $51\text{--}53 \text{ }^\circ\text{C}$. ^1H NMR (599.5 MHz, CDCl_3): δ 4.12 (s, 5H, C_5H_5), 4.09 (t, $^3J_{\text{HH}} = 2 \text{ Hz}$, 2H, $\beta\text{-C}_5\text{H}_4\text{R}$), 4.07 (t, $^3J_{\text{H-H}} = 2 \text{ Hz}$, 2H, $\alpha\text{-C}_5\text{H}_4\text{R}$), 2.72 (d of m, $^1J_{\text{H-P}} = 204 \text{ Hz}$, 2H, PH_2 ; this signal overlaps with the signal at δ 2.57), 2.57 (m, 2H, $\text{C}_5\text{H}_4\text{CH}_2$; this signal overlaps with the signal at δ 2.72), 1.72 (m, 2H, CH_2PH_2). ^{31}P NMR (162 MHz, CDCl_3): δ -137 (t, $^1J_{\text{P-H}} = 196 \text{ Hz}$). Mass Spec. (EI, +ve mode): exact mass calculated for $\text{C}_{12}\text{H}_{15}\text{FeP}$: 246.0260; exact mass found: 246.0256; difference: -1.6 ppm .

Photopolymerization

The appropriate molar ratios of phosphine, olefin, and photoinitiator (0.5 wt%) were combined and mixed in vials within a nitrogen filled glovebox. Solutions (~ 75 μL) were pipetted into a circular Teflon mold (1 mm deep, 1 cm in diameter) and placed in a sealed vessel possessing a glass window. The entire assembly was carefully removed from the glovebox and irradiated (UVA: 154 mW/cm^2 , 189 mJ/cm^2 . UVB 74 mW/cm^2 , 90 mJ/cm^2 for each exposure, at a conveyor speed of 0.1 m/s.) The polymer was quickly removed from the mold and stored in the glovebox to minimize oxidation. Polymer **FcPN** was prepared as a 60 wt% solution in DMF with 5 wt% photoinitiator and irradiated (UVA: 175 mW/cm^2 , 6 hours) through a glass mold (200 μm). For stabilized systems, inhibitor (butylated hydroxytoluene or diphenylamine) was added to the formulation within the glovebox and mixed until complete dissolution. Samples were then exposed to an air atmosphere and periodically stirred for 10 minutes prior to casting and photopolymerization through a glass window.

Swelling Experiments and Gel Content

Samples were weighed (~70 mg) and immersed in toluene for 24 hours. Samples were then weighed again and a swelling ratio was determined using the equation $Q = (m_t - m_o)/m_o$ where m_t = swelled mass, m_o = dry mass, and Q = swelling ratio. Q was multiplied by 100 to give percentage values. Samples were then dried in a vacuum oven at 80 °C over 24 hours and weighed again. By comparing the original mass to the polymer mass after toluene extraction, gel content was obtained.

Cyclic Voltammetry

A 1.5:1 molar ratio of **2** and TTT in air were combined followed by dissolution in dimethylformamide (60 wt% solutions), of which a portion (20 μL) was diluted in DCM (400 μL) and drop cast on a 3mm glass carbon electrode. Following the evaporation of DCM the wet film was irradiated (UVA: 175 mW/cm^2) for 6 hours to induce crosslinking. Typical electrochemical cells consisted of a three-electrode setup including a polymer network film-covered glassy carbon working electrode, platinum wire counter

electrode, and silver wire *pseudo*-reference electrode. Experiments were run at variable scan rates in degassed acetonitrile solutions containing 0.1 M tetrabutylammonium hexafluorophosphate ($[\text{Bu}_4\text{N}][\text{PF}_6]$) as supporting electrolyte. Cyclic voltammograms were referenced against an internal standard (~ 1 mM ferrocene) after a small portion of the film had been removed from the glassy carbon electrode surface. Internal cell resistance was corrected using the BASi Epsilon software.

Palladium Loading

Polymer **SPN-2** (150 mg) and a stoichiometric amount of PdCl_2 or $\text{Pd}(\text{OAc})_2$ (0.37 mmol) relative to the number of phosphines in the network were combined in benzene (15 mL) and stirred for 3 days, after which the polymer was centrifuged and rinsed with benzene (3x15 mL), pentane (3x15 mL), and dried *in vacuo*.

Reaction series on SPN-1 and model compound 6.4

$^{31}\text{P}\{^1\text{H}\}$ NMR spectroscopy and DSC was used to monitor reaction progress. Polymer **SPN-1** was milled by hand, immersed in toluene for 24 hours, isolated and dried to remove unpolymerized material. Samples (0.20 g) were swelled in a 1:1 v/v ratio of toluene and acetonitrile (16 mL) followed by the addition of ethyl iodide (0.40 mL). The mixture was stirred for 1 hour and then centrifuged. The polymer was then rinsed with pentane (2 x 15 mL) and dried *in vacuo*. Hydrophosphination of the primary and secondary phosphines proceeded by swelling the quaternized polymer (0.20 g) in a 1:1:1 v/v ratio of toluene, acetonitrile, and 1-hexene (15 mL) followed by the addition of Irgacure 819 (17.5 mg). After 24 hours, IR spectroscopic analysis revealed that most of the available P-H bonds were consumed. An additional 17.5 mg of photoinitiator was then added and irradiated for 5 hours to complete the reaction. Polymer samples were centrifuged, rinsed with toluene (4 x 15 mL), pentane (2 x 15 mL), and then dried *in vacuo*. Sulphurization of these polymer samples proceeded by swelling the polymer in a saturated solution of S_8 (12 mL) and stirring for 24 hours. Polymer was centrifuged, rinsed with toluene (4 x 15 mL), pentane (2 x 15 mL), and dried *in vacuo*.

Compound **6.4** was used as a model to compare the chemistry performed on **SPN-1**. $^{31}\text{P}\{^1\text{H}\}$ NMR spectroscopy was used to monitor the reaction progress. No purification steps were performed aside from removal of volatiles *in vacuo*. A solution of **6.4** containing toluene, 1-hexene, and Irgacure 819 was irradiated until a comparable distribution of primary, secondary, and tertiary phosphines to that of **SPN-1** were obtained (30 seconds). Quaternization of the tertiary phosphines proceeded by dissolving the product in a 1:1 v/v mixture of toluene and acetonitrile (0.8 mL), followed by the addition of 6.5 eq. ethyl iodide (200 μL , 2.5 mmol) and left for 1 hour. Hydrophosphination of the remaining primary and secondary phosphines proceeded by dissolving the quaternized product and photoinitiator (2 mg) in a 1:1 v/v mixture of toluene, acetonitrile, and 1-hexene (1.5 mL). The solution was irradiated for 24 hours to ensure complete P-H bond conversion. Sulphurization of the mixture proceeded in a 1:1 v/v toluene and acetonitrile (1 mL) followed by the addition of S_8 (75 mg). The three possible products from this reaction series were confirmed by ESI \pm mass spectrometry (Supplemental Figure 10).

References

- (1) Zhao, Q.; Dunlop, J. W. C.; Qiu, X.; Huang, F.; Zhang, Z.; Heyda, J.; Dzubiella, J.; Antonietti, M.; Yuan, J. *Nat. Commun.* **2014**, *5*, 4293.
- (2) Kloosterboer, J. G. *Network formation by chain crosslinking photopolymerization and its applications in electronics*; Advances in Polymer Science; Springer-Verlag: Berlin/Heidelberg, 1988; Vol. 84.
- (3) Carlborg, C. F.; Haraldsson, T.; Öberg, K.; Malkoch, M.; van der Wijngaart, W. *Lab Chip* **2011**, *11*, 3136.
- (4) Leterrier, Y.; Singh, B.; Bouchet, J.; Månson, J. E.; Rochat, G.; Fayet, P. *Surf. Coatings Technol.* **2009**, *203*, 3398.
- (5) Zhu, J.; Marchant, R. E. *Expert Rev. Med. Devices* **2011**, *8*, 607.
- (6) Wang, J.; He, R.; Che, Q. *J. Colloid Interface Sci.* **2011**, *361*, 219.
- (7) Xu, J.; Feng, E.; Song, J. *J. Am. Chem. Soc.* **2014**, *136*, 4105.
- (8) De, B.; Karak, N. *J. Appl. Polym. Sci.* **2014**, *131*, n/a.

- (9) Revzin, a; Russell, R. J.; Yadavalli, V. K.; Koh, W. G.; Deister, C.; Hile, D. D.; Mellott, M. B.; Pishko, M. V. *Langmuir* **2001**, *17*, 5440.
- (10) Hoyle, C. E.; Lee, T. Y.; Roper, T. *J. Polym. Sci., Part A: Polym. Chem.* **2004**, *42*, 5301.
- (11) Bowman, C. N.; Kloxin, C. J. *AIChE J.* **2008**, *54*.
- (12) Kade, M. J.; Burke, D. J.; Hawker, C. J. *J. Polym. Sci., Part A: Polym. Chem.* **2010**, *48*, 743.
- (13) Mark, J. E.; Allcock, H. R.; Wester, R. *Inorganic Polymers*; Second, Ed.; Oxford University Press, 2005; pp. 3–50.
- (14) El-Roz, M.; Lalevée, J.; Allonas, X.; Fouassier, J.-P. *Macromol. Rapid Commun.* **2008**, *29*, 804.
- (15) Bai, L.; Zhang, Y.; Wang, J.-X. *QSAR Comb. Sci.* **2004**, *23*, 875.
- (16) Welch, G. C.; San Juan, R. R.; Masuda, J. D.; Stephan, D. W. *Science* **2006**, *314*, 1124.
- (17) Hemp, S. T.; Zhang, M.; Tamami, M.; Long, T. E. *Polym. Chem.* **2013**, *4*, 3582.
- (18) Wu, B.; Wang, Y.-Z.; Wang, X.-L.; Yang, K.-K.; Jin, Y.-D.; Zhao, H. *Polym. Degrad. Stab.* **2002**, *76*, 401.
- (19) Tsang, C.-W.; Yam, M.; Gates, D. P. *J. Am. Chem. Soc.* **2003**, *125*, 1480.
- (20) Bates, J. I.; Dugal-Tessier, J.; Gates, D. P. *Dalton Trans.* **2010**, *39*, 3151.
- (21) Allcock, H. R.; Kugel, R. L. *J. Am. Chem. Soc.* **1965**, *87*, 4216.
- (22) Naka, K.; Umeyama, T.; Nakahashi, A.; Chujo, Y. *Macromolecules* **2007**, *40*, 4854.
- (23) Hodgson, J. L.; Coote, M. L. *Macromolecules* **2005**, *38*, 8902.
- (24) Pellon, J. *J. Polym. Sci.* **1960**, *43*, 537.
- (25) Pellon, J. *J. Am. Chem. Soc.* **1961**, *83*, 1915.
- (26) Stiles, A. R.; Rust, F. F.; Vaughan, W. E. *J. Am. Chem. Soc.* **1952**, *74*, 3282.
- (27) Alvey, L. J.; Rutherford, D.; Juliette, J. J. J.; Gladysz, J. a. *J. Org. Chem.* **1998**, *63*, 6302.
- (28) Obata, T.; Kobayashi, E.; Aoshima, S.; Furukawa, J. *J. Polym. Sci. Part A Polym. Chem.* **1994**, *32*, 475.
- (29) Greenberg, S.; Stephan, D. W. *Inorg. Chem.* **2009**, *48*, 8623.

- (30) Stewart, B.; Harriman, A.; Higham, L. J. *Organometallics* **2011**, *30*, 5338.
- (31) Higham, L. J. *Phosphorus Compounds*; Peruzzini, M.; Gonsalvi, L., Eds.; Catalysis by Metal Complexes; Springer Netherlands: Dordrecht, 2011; Vol. 37, pp. 1–19.
- (32) Gali, H.; Karra, S. R.; Reddy, V. S.; Katti, K. V. *Angew. Chemie Int. Ed.* **1999**, *38*, 2020.
- (33) Prabhu, K. R.; Pillarsetty, N.; Gali, H.; Katti, K. V. *J. Am. Chem. Soc.* **2000**, *122*, 1554.
- (34) Smith, C. J.; Reddy, V. S.; Karra, S. R.; Katti, K. V.; Barbour, L. J. *Inorg. Chem.* **1997**, *36*, 1786.
- (35) Greenberg, S.; Stephan, D. W. *Inorg. Chem.* **2009**, *48*, 8623.
- (36) Cramer, N. B.; Couch, C. L.; Schreck, K. M.; Carioscia, J. A.; Boulden, J. E.; Stansbury, J. W.; Bowman, C. N. *Dent. Mater.* **2010**, *26*, 21.
- (37) Mongkhontreerat, S.; Öberg, K.; Erixon, L.; Löwenhielm, P.; Hult, A.; Malkoch, M. *J. Mater. Chem. A* **2013**, *1*, 13732.
- (38) Gupta, N.; Lin, B. F.; Campos, L. M.; Dimitriou, M. D.; Hikita, S. T.; Treat, N. D.; Tirrell, M. V; Clegg, D. O.; Kramer, E. J.; Hawker, C. J. *Nat. Chem.* **2010**, *2*, 138.
- (39) Ferrari, M. C.; Carranza, S.; Bonnacaze, R. T.; Tung, K. K.; Freeman, B. D.; Paul, D. R. *J. Memb. Sci.* **2009**, *329*, 183.
- (40) Tung, K. K.; Bonnacaze, R. T.; Freeman, B. D.; Paul, D. R. *Polymer (Guildf)*. **2012**, *53*, 4211.
- (41) Cook, W. D.; Chen, F.; Pattison, D. W.; Hopson, P.; Beaujon, M. *Polym. Int.* **2007**, *56*, 1572.
- (42) Kühne, G.; Diesen, J. S.; Klemm, E. *Die Angew. Makromol. Chemie* **1996**, *242*, 139.
- (43) Floyd, M. B.; Boozer, C. E. *J. Am. Chem. Soc.* **1963**, *85*, 984.
- (44) Buckler, S. A. *J. Am. Chem. Soc.* **1962**, *84*, 3093.
- (45) Hempenius, M. A.; Cirmi, C.; Savio, F. Lo; Song, J.; Vancso, G. J. *Macromol. Rapid Commun.* **2010**, *31*, 772.
- (46) Kurian, P.; Zschoche, S.; Kennedy, J. P. *J. Polym. Sci., Part A: Polym. Chem.* **2000**, *38*, 3200.

- (47) Zona, C.; D'Orazio, G.; La Ferla, B. *Synlett* **2013**, 24, 709.
- (48) Smith, C. J.; Katti, K. V.; Volkert, W. A.; Barbour, L. J. *Inorg. Chem.* **1997**, 36, 3928.

Chapter 7

7 Conclusions and Future Work

7.1 Conclusions

Lending perspectives from fundamental phosphorus chemistry and photopolymerization has yielded new materials and approaches. Low melting polymerizable phosphonium salts allow for the generation of highly charged photopolymer coatings without the need for solvent, while the fluorinated varieties serve to alter the surface properties of conventional films. Both phosphonium monomers and polymers may be combined in a photopolymer matrix, which immobilizes the charged species to perform further chemistry. However, using the chemistry of phosphorus itself, primary phosphines may react with olefins using phosphane-ene chemistry to create a new class of phosphorus-containing networks with a multitude of applications. The initial goal to combine photopolymerization and phosphorus chemistry together to create new materials was successful, providing new opportunities for fundamental and applied research.

7.2 Future Research

Future research should focus on two particular topics presented in this thesis. The first is on the fabrication of polyelectrolyte films using low melting point phosphonium salts (chapter 2 and 3) for biomedical applications. While most of this work was dedicated towards fabrication and characterization, the highly charged, cationic nature of these materials serves as an excellent antibacterial coating. The ability to adjust the crosslink density and composition of the matrix provides a highly tunable system, while the ease of deposition makes the entire process commercially feasible. Some issues such as low cure percentage and leaching of small molecules must be resolved before these materials will be suitable for these applications. Nonetheless, this approach is currently being pursued and I believe will result in a useful material.¹

The phosphane-ene networks discussed in chapter 6 already possess a variety of useful properties that could, at least conceivably, lead to a practical material. The most salient feature however is its capability to scavenge oxygen in a tunable manner. Oxygen barriers are incredibly important for packaging food and sensitive electronics and thus serve as a potential niche for phosphane-ene polymers. While it's unlikely that we will package our food in phosphine, electronics however provide a more natural application for these systems. The ability to cast phosphane-ene networks as transparent films provides two levels of protection. The first, serving as a physical barrier to oxygen, which must diffuse through the material to reach the underlying components. The other is by reacting with any dissolved oxygen within the film (Figure 7-1). Given that thiol-ene polymers already demonstrate potential utility as an oxygen barrier,² the similar architecture phosphane-ene systems possess coupled with its scavenging abilities may result in a new generation of barrier materials.

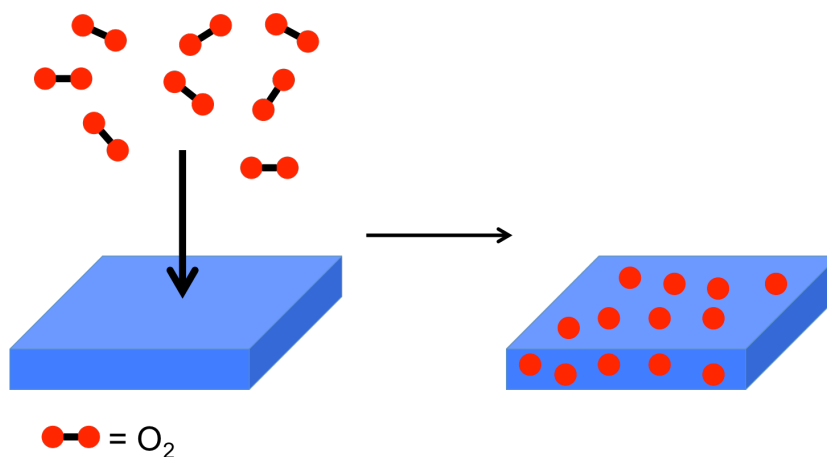
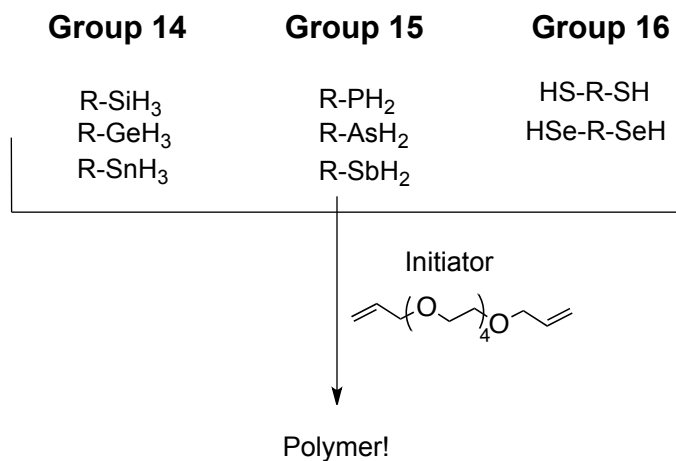


Figure 7-1: Oxygen scavenging film composed of phosphine polymer.

With regards to fundamental chemistry however, there is great opportunity in exploiting other p-block elements for polymer science. Inorganic functional groups like arsines, stibines, selenols, stannanes, germanes, and silanes all possess abstractable hydrogen atoms and may add to double bonds (Scheme 7-1). In fact, such realizations are already in practice in the case of silanes.³ What was considered to be unique only to sulfur for polymer science may in actuality apply to the other p-block elements. A detailed

understanding of the kinetics involved in these radical processes is of great importance for implementing their chemistry for polymerization reactions.



Scheme 7-1: A general approach for making main group element polymers using olefin addition chemistry.

References

- (1) Cuthbert, T.; Guterman, R.; Ragona, P. J.; Gillies, E. R. *J. Mater. Chem. B* **2015**, 3, 1474.
- (2) Kwisnek, L.; Nazarenko, S.; Hoyle, C. E. *Macromolecules* **2009**, 42, 7031.
- (3) El-Roz, M.; Lalevée, J.; Allonas, X.; Fouassier, J.P. *Macromol. Rapid Commun.* **2008**, 29, 804.

Appendix A

Copyrights and Permissions

American Chemical Society's policy on thesis and dissertations

If your university requires you to obtain permission, you must use the RightsLink permission system. See RightsLink instructions at: <http://pubs.acs.org/page/copyright/permissions.html>. This is regarding request for permission to include **your** paper(s) or portions of text from **your** paper(s) in **your** thesis. Permission is now automatically granted; please pay special attention to the **implications** paragraph below. The Copyright Subcommittee of the Joint Board/Council Committees on Publications approved the following:

Copyright permission for published and submitted material from theses and dissertations.

ACS extends blanket permission to students to include in their theses and dissertations their own articles, or portions thereof, that have been published in ACS journals or submitted to ACS journals for publication, provided that the ACS copyright credit line is noted on the appropriate page(s).

Publishing implications of electronic publication of theses and dissertation material

Students and their mentors should be aware that posting of theses and dissertation material on the Web prior to submission of material from that thesis or dissertation to an ACS journal may affect publication in that journal. Whether Web posting is considered prior publication may be evaluated on a case-by-case basis by the journal's editor. If an ACS journal editor considers Web posting to be "prior publication", the paper will not be accepted for publication in that journal. If you intend to submit your unpublished paper to

ACS for publication, check with the appropriate editor prior to posting your manuscript electronically.

Reuse/Republication of the Entire Work in Theses or Collections:

Authors may reuse all or part of the Submitted, Accepted or Published Work in a thesis or dissertation that the author writes and is required to submit to satisfy the criteria of degree-granting institutions. Such reuse is permitted subject to the ACS' "Ethical Guidelines to Publication of Chemical Research" (<http://pubs.acs.org/page/policy/ethics/index.html>); the author should secure written confirmation (via letter or email) from the respective ACS journal editor(s) to avoid potential conflicts with journal prior publication*/embargo policies. Appropriate citation of the Published Work must be made. If the thesis or dissertation to be published is in electronic format, a direct link to the Published Work must also be included using the ACS Articles on

Request author-directed link – see:

<http://pubs.acs.org/page/policy/articlesonrequest/index.html>

* Prior publication policies of ACS journals are posted on the ACS website at:

<http://pubs.acs.org/page/policy/prior/index.html>

Wiley-VCH Rights Retained by Journal Authors

Guterman, R.; Berven, B.B.; Corkery, T.C.; Nie, H.-Y.; Gillies, E.R.; Idacavage, M.J.; and Ragogna, P.J. *J. Polym. Sci. A Polym. Chem.* **2013**, *51*, 2782. Copyright Wiley-VCH Verlag GmbH & Co. KGaA. Reproduced with permission.
<http://onlinelibrary.wiley.com/doi/10.1002/pola.26692/full>

Appendix B

Chapter 2

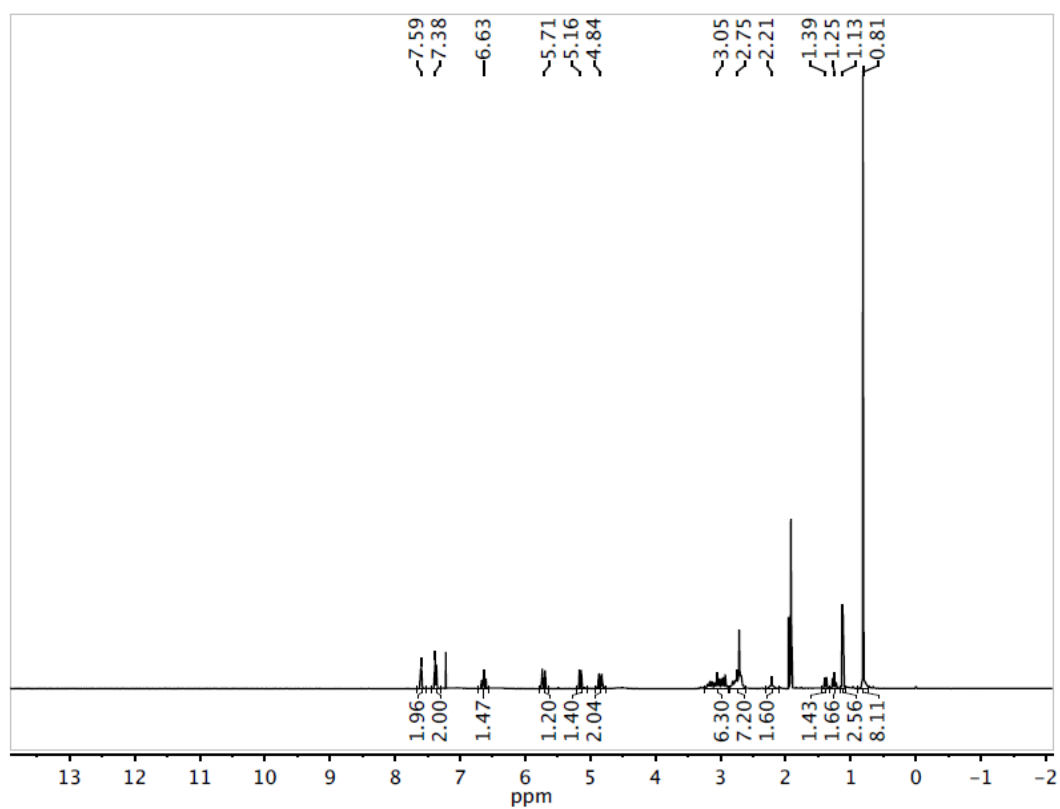


Figure 1: ^1H NMR spectrum of compound 2.1[Cl].

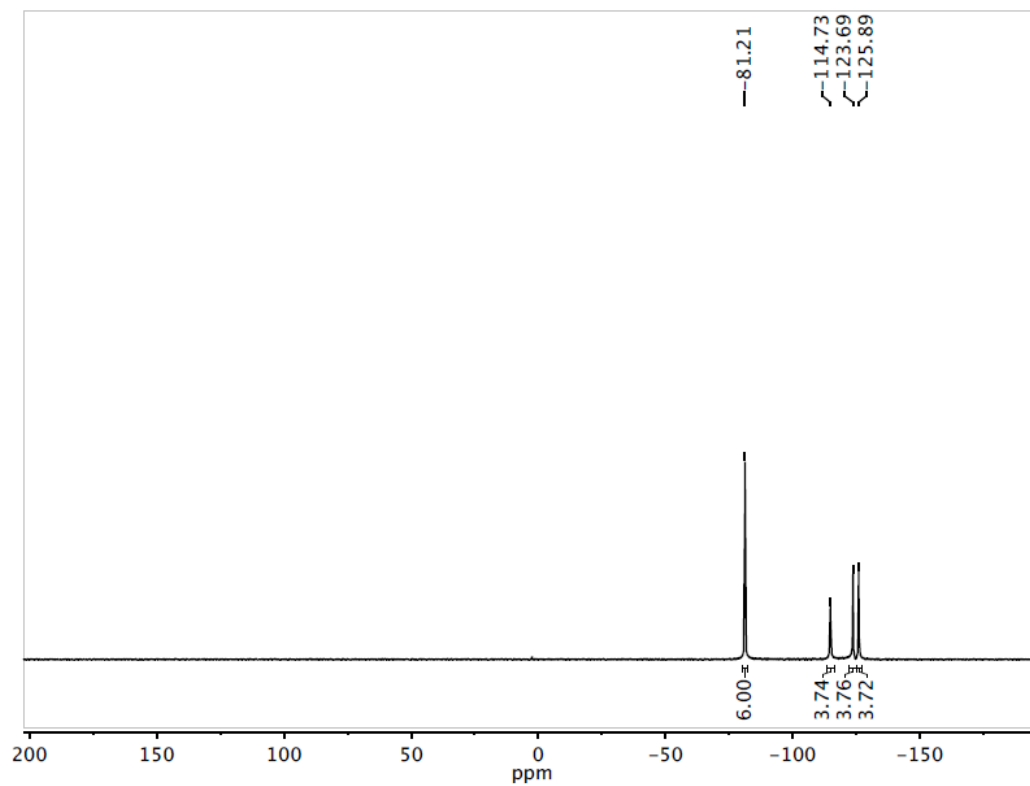


Figure 2: $^{19}\text{F}\{^1\text{H}\}$ NMR spectrum of compound 2.1[Cl].

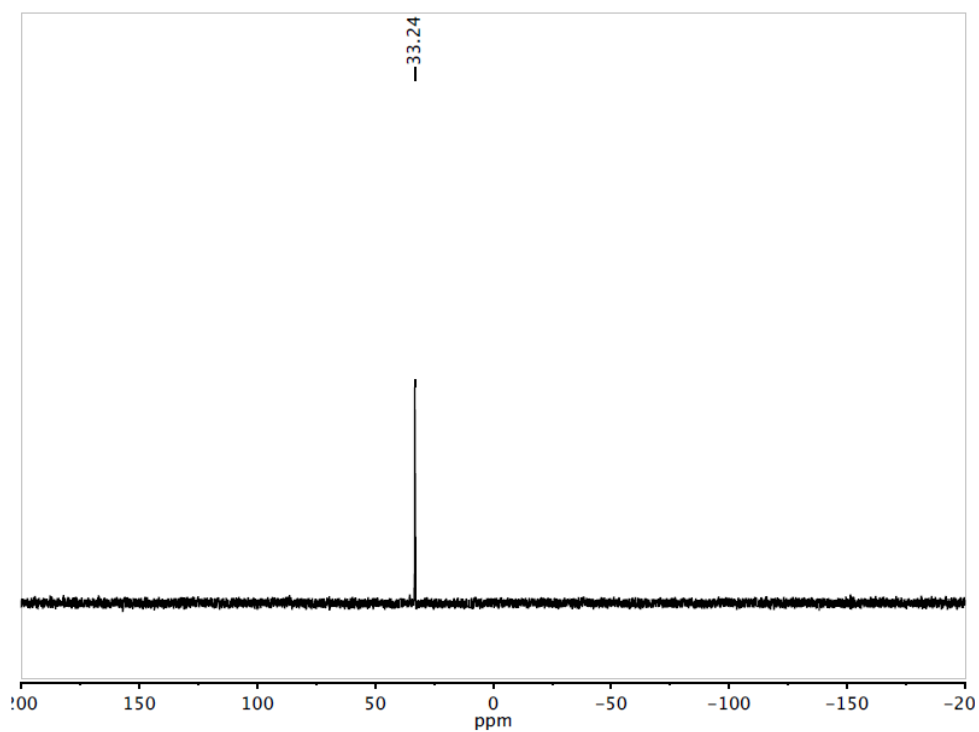


Figure 3: $^{31}\text{P}\{^1\text{H}\}$ NMR spectrum of compound 2.1[Cl].

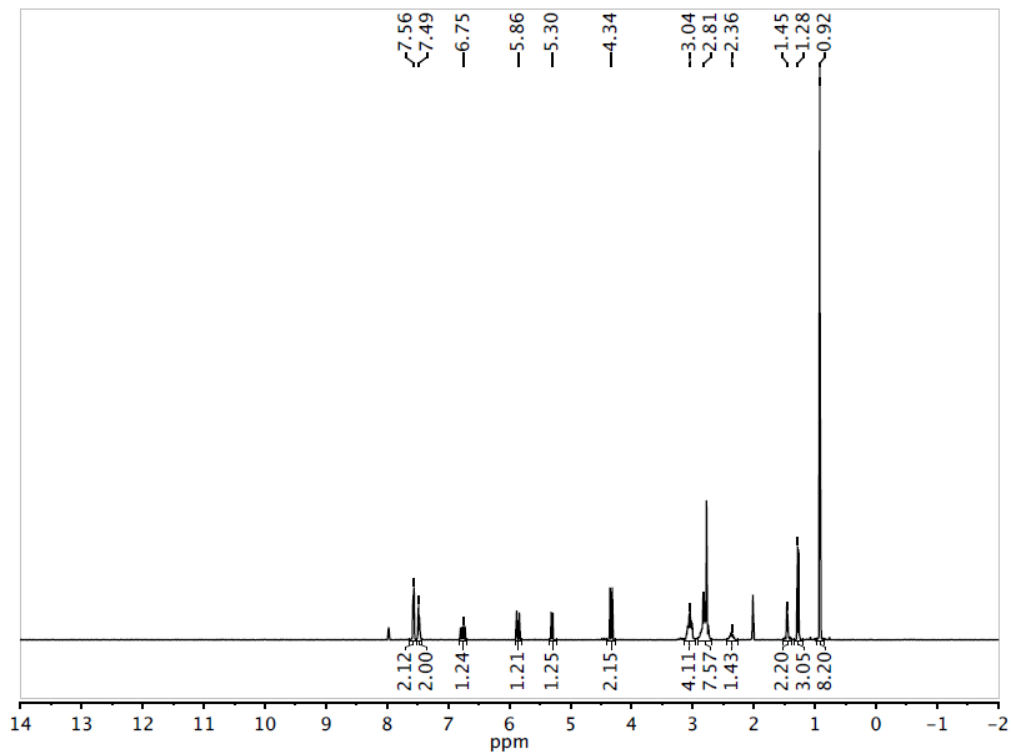


Figure 4: ^1H NMR spectrum of compound **2.1**[NTf₂].

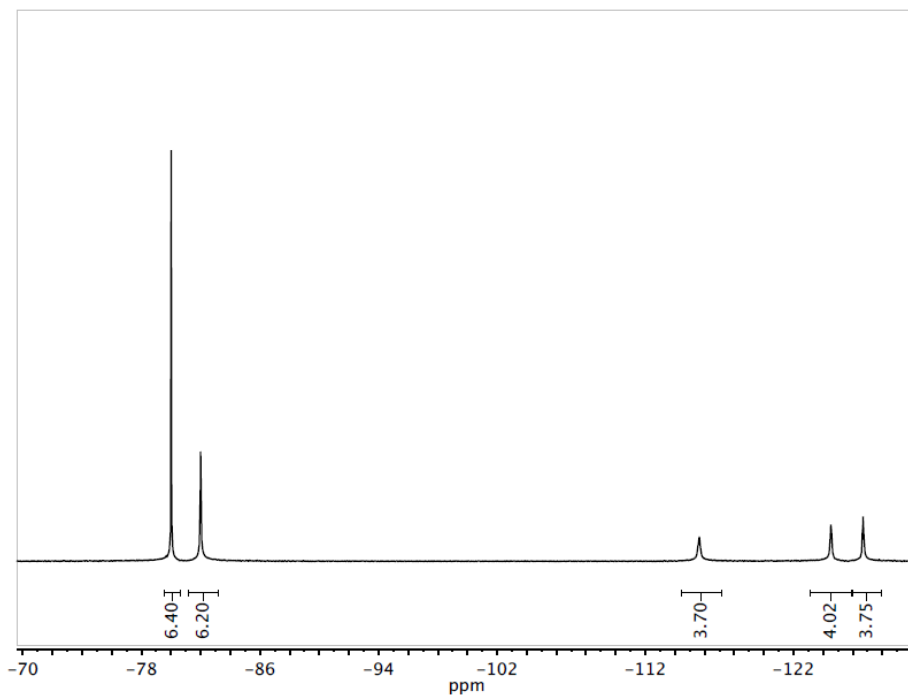


Figure 5: $^{19}\text{F}\{^1\text{H}\}$ NMR spectrum of compound **2.1**[NTf₂].

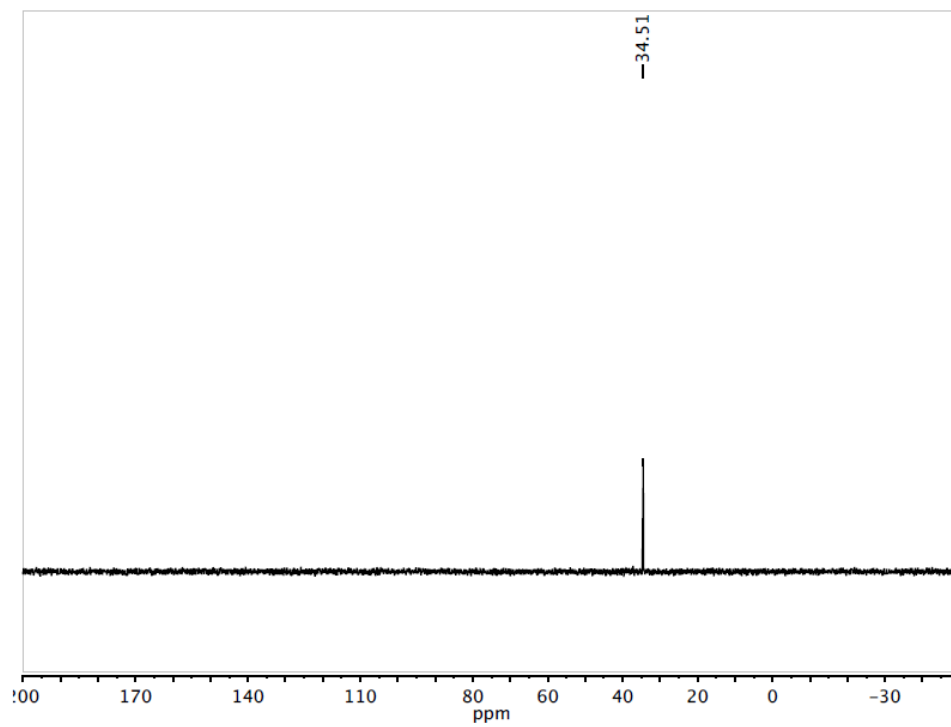


Figure 6: $^{31}\text{P}\{^1\text{H}\}$ NMR spectrum of compound **2.1**[NTf₂].

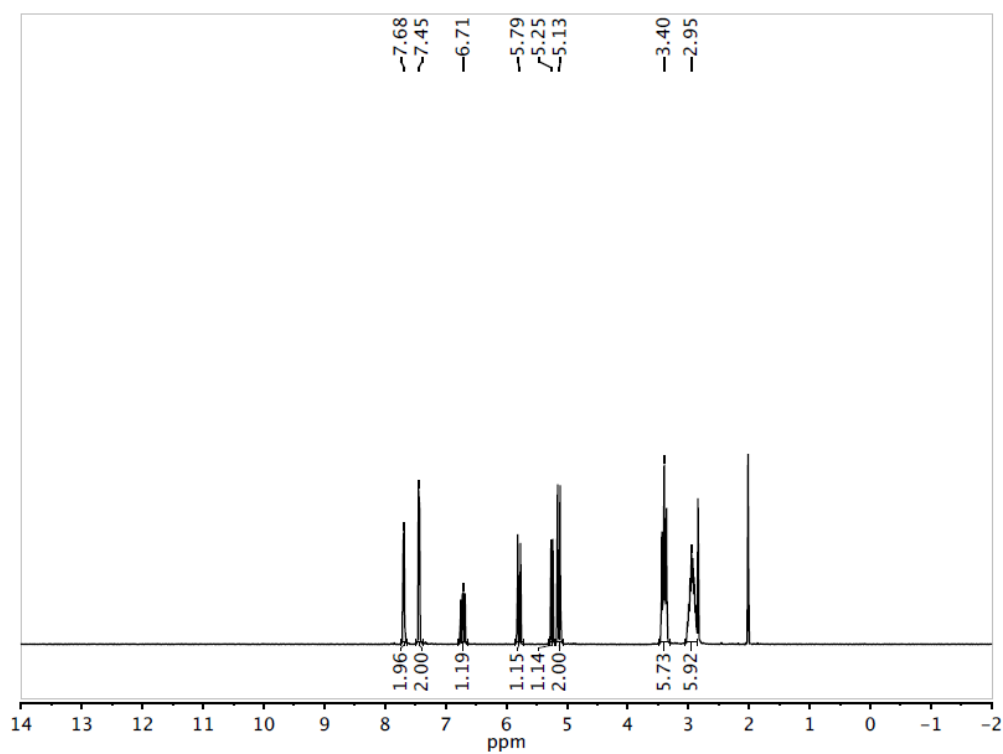


Figure 7: ^1H NMR spectrum of compound **2.2**[Cl].

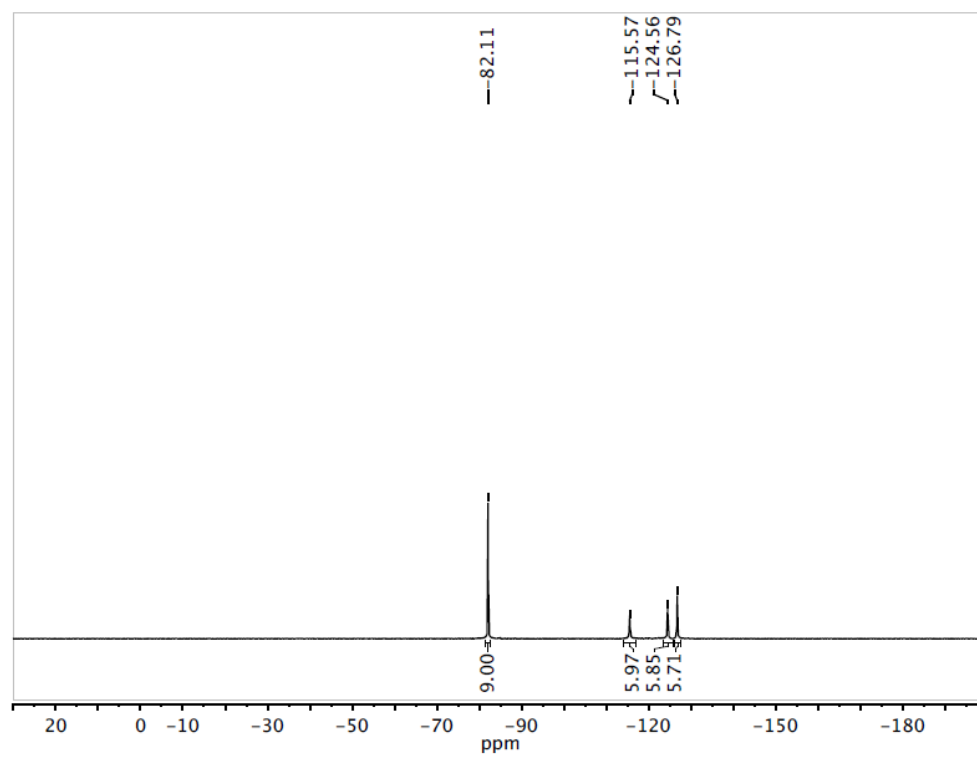


Figure 8: $^{19}\text{F}\{^1\text{H}\}$ NMR spectrum of compound 2.2[Cl].

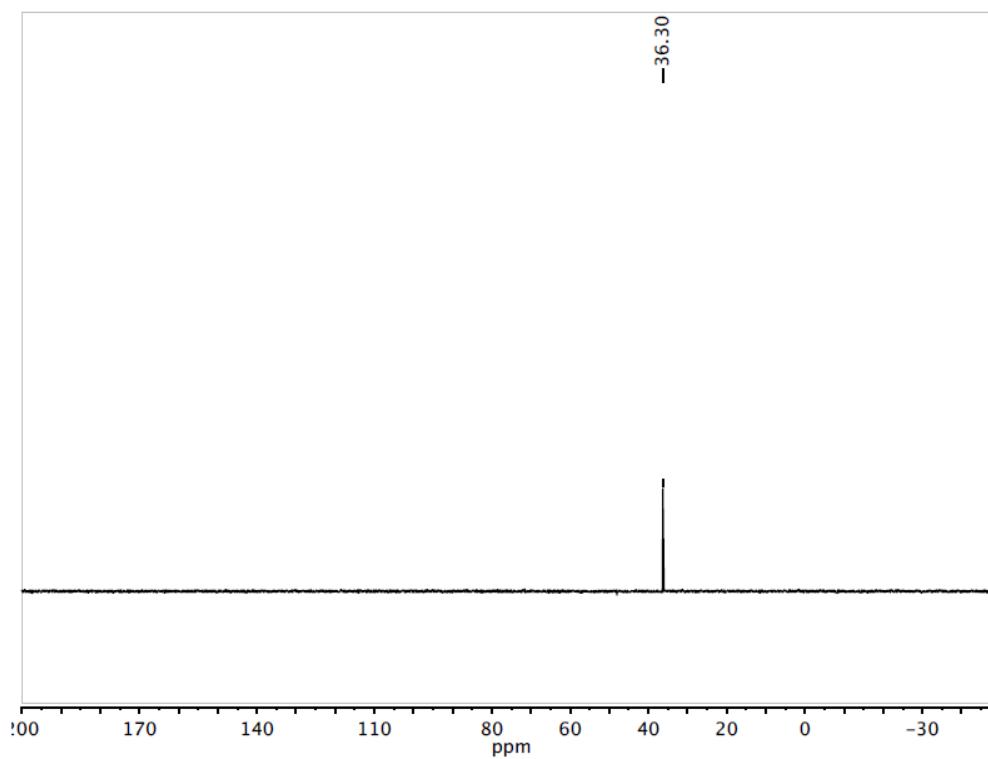


Figure 9: $^{31}\text{P}\{^1\text{H}\}$ NMR spectrum of compound 2.2[Cl].

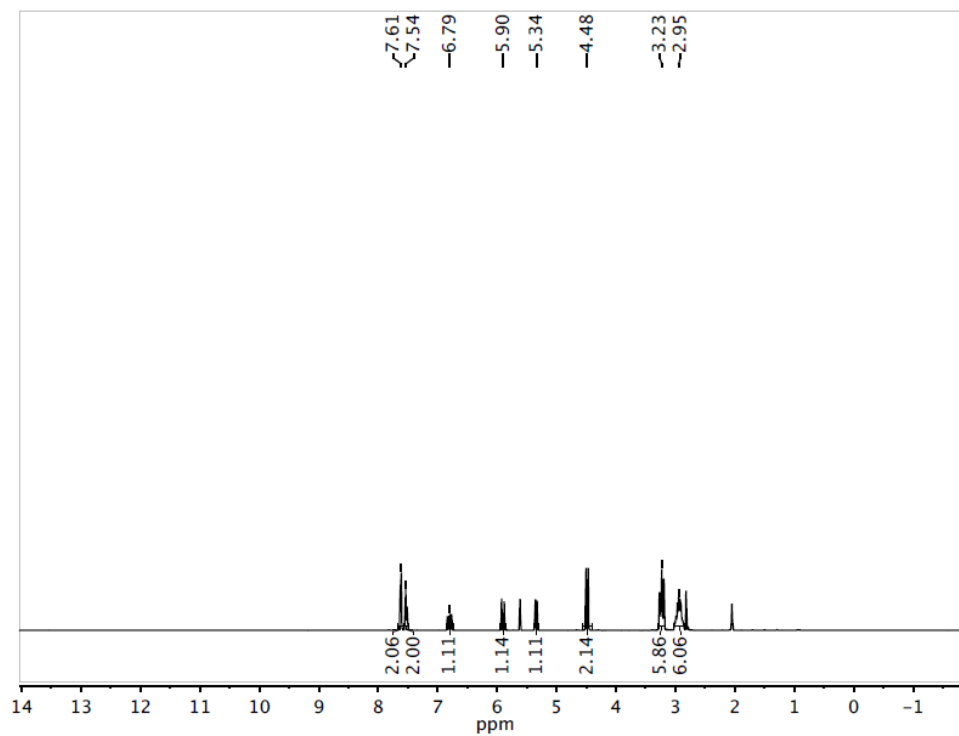


Figure 10: ^1H NMR spectrum of compound **2.2**[NTf₂].

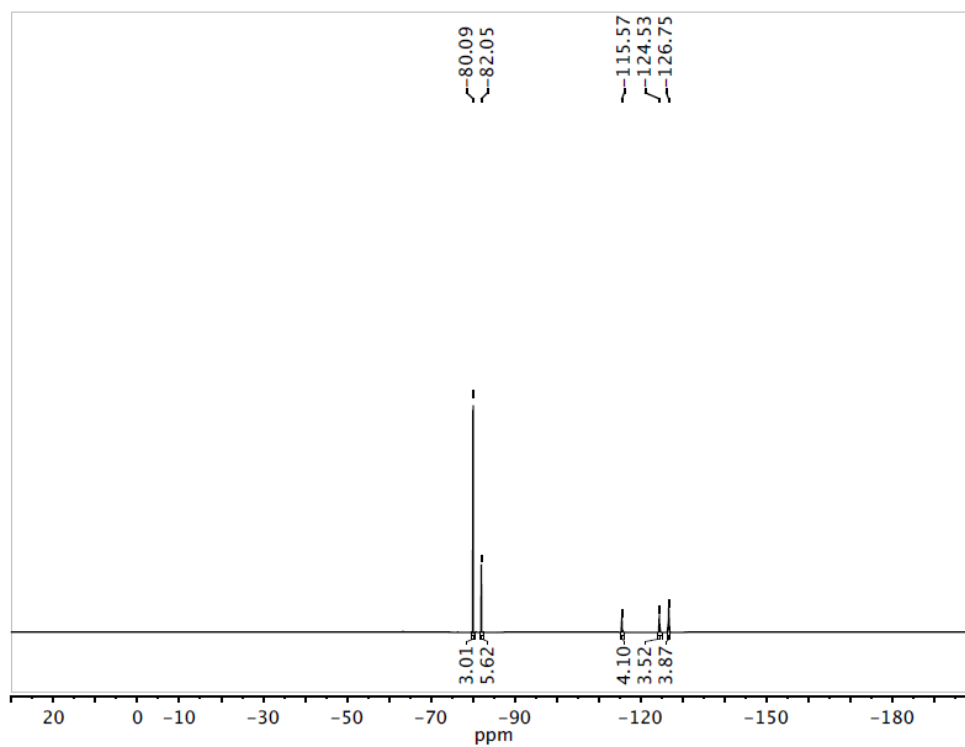


Figure 11: $^{19}\text{F}\{^1\text{H}\}$ NMR spectrum of compound **2.2**[NTf₂].

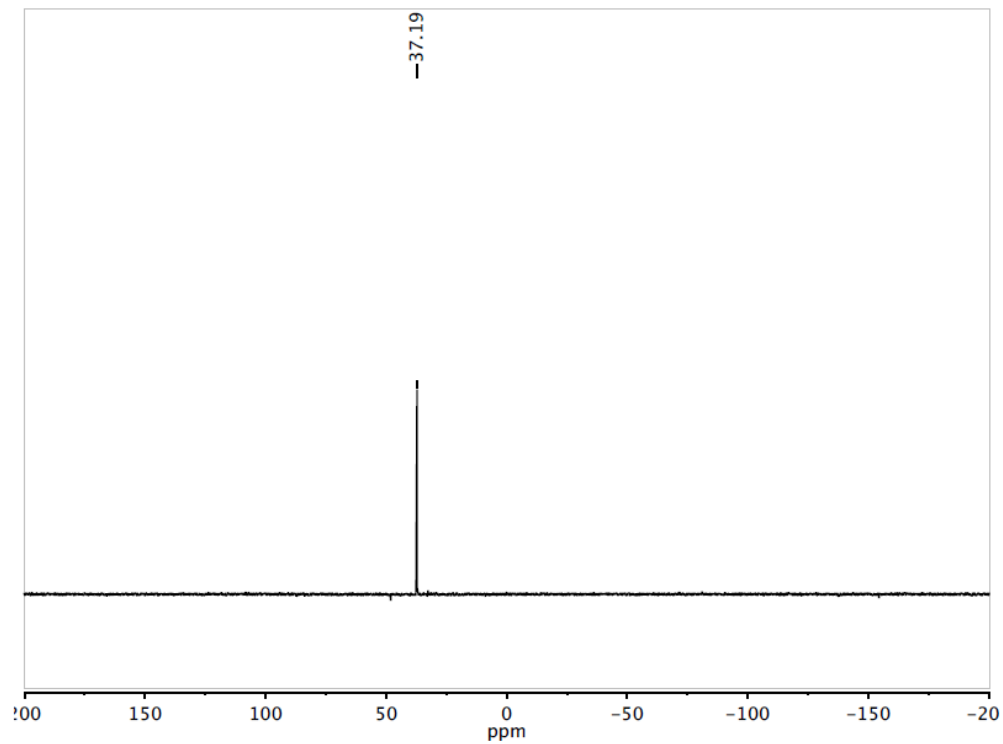


Figure 12: $^{31}\text{P}\{^1\text{H}\}$ NMR spectrum of compound 2.2[NTf₂].

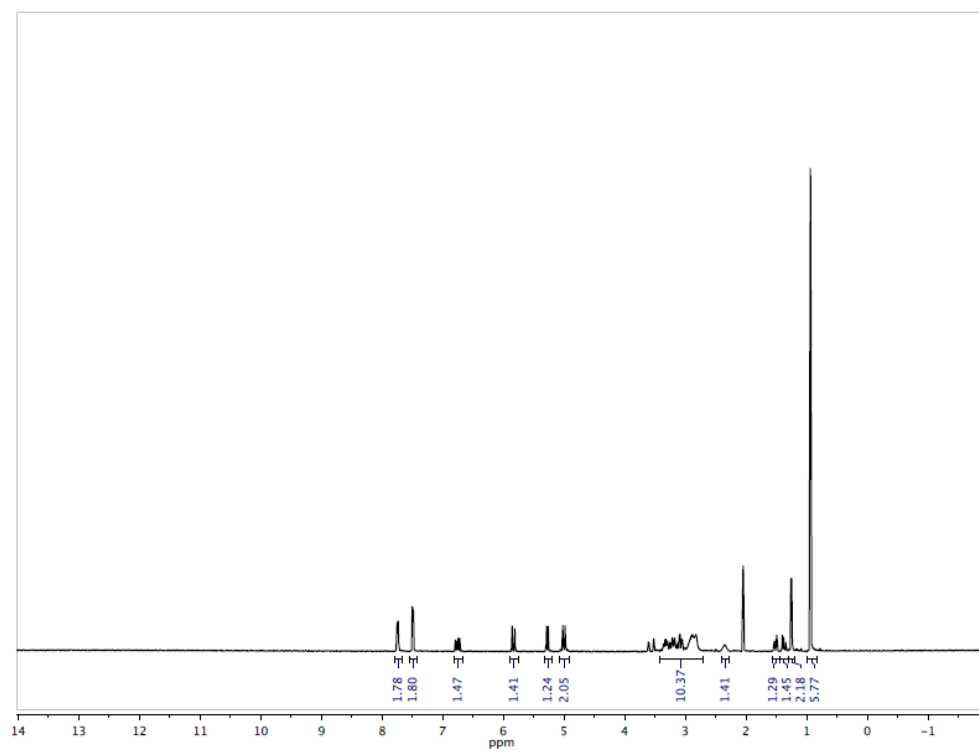


Figure 13: ^1H NMR spectrum of compound 2.3[Cl].

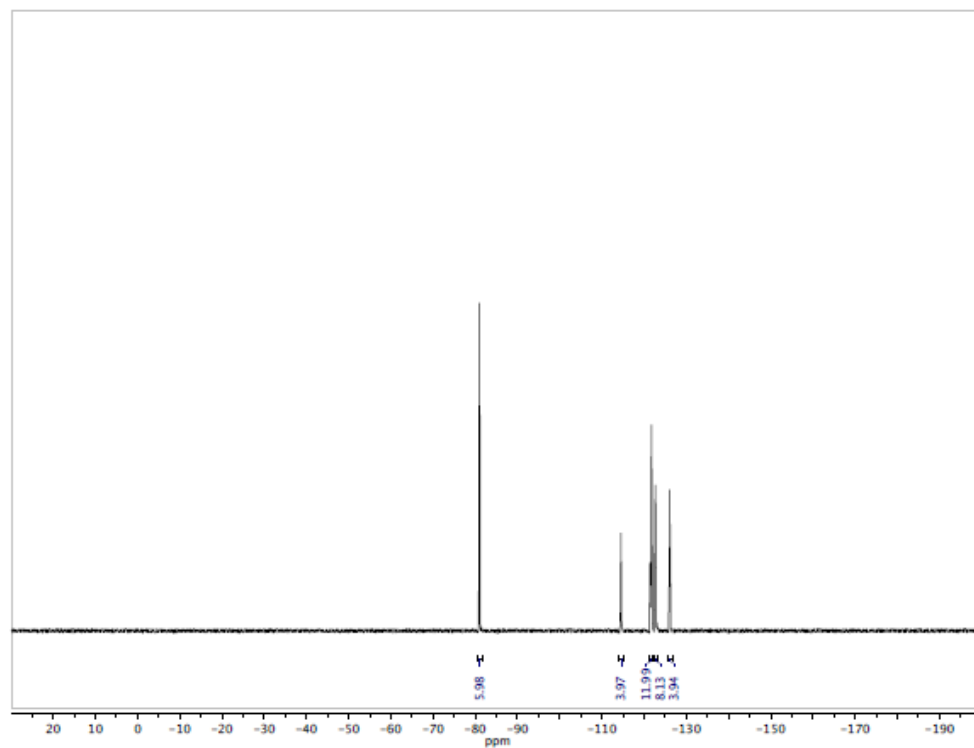


Figure 14: ^{19}F NMR spectrum of compound 2.3[Cl].

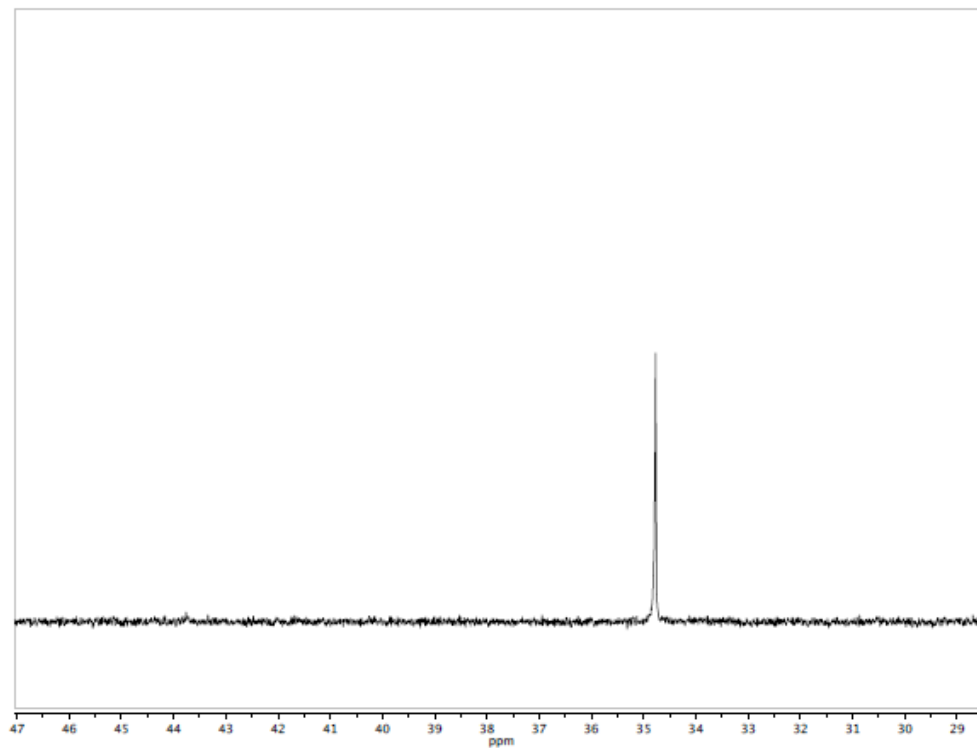


Figure 15: $^{31}\text{P}\{^1\text{H}\}$ NMR spectrum of compound 2.3[Cl].

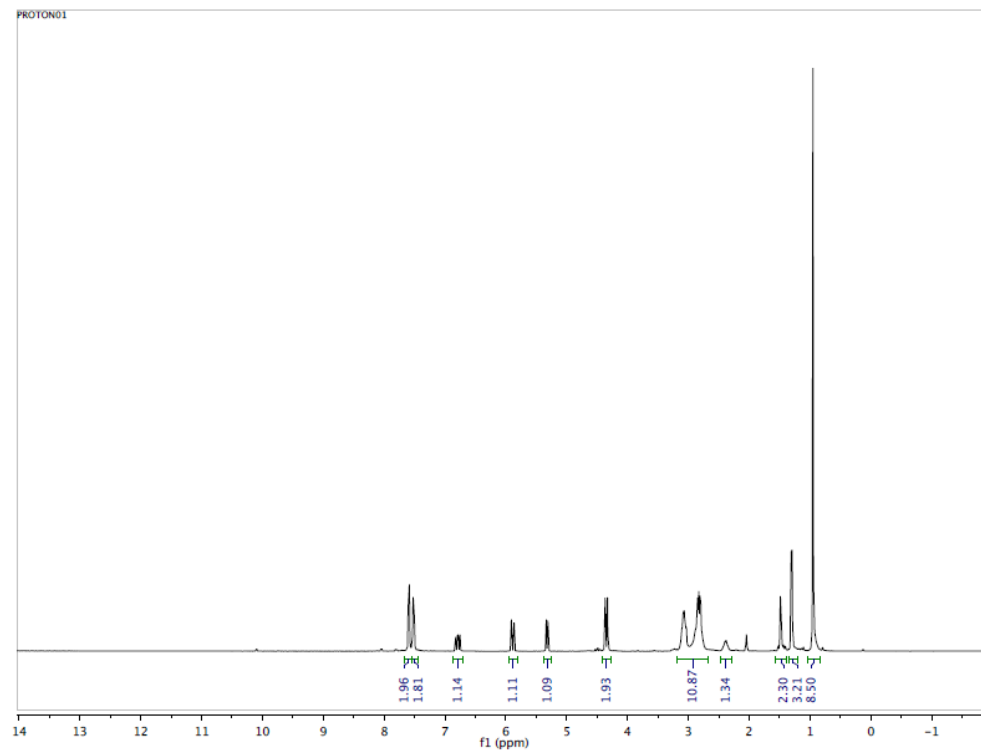


Figure 16: ^1H NMR spectrum of compound **2.3**[NTf₂].

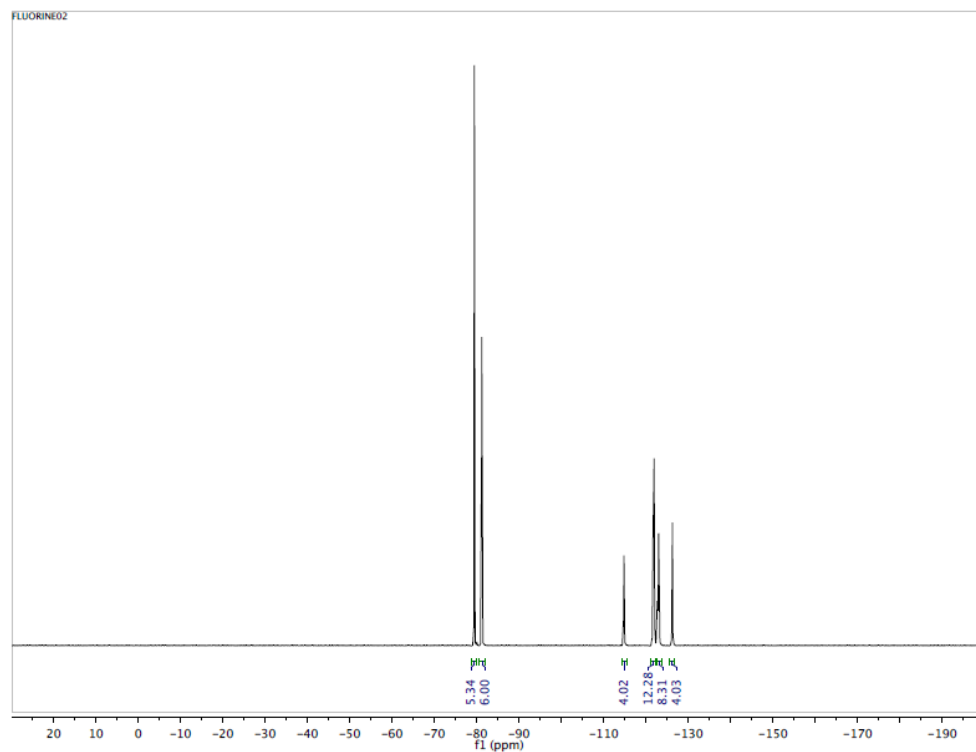


Figure 17: ^{19}F NMR spectrum of compound **2.3**[NTf₂].

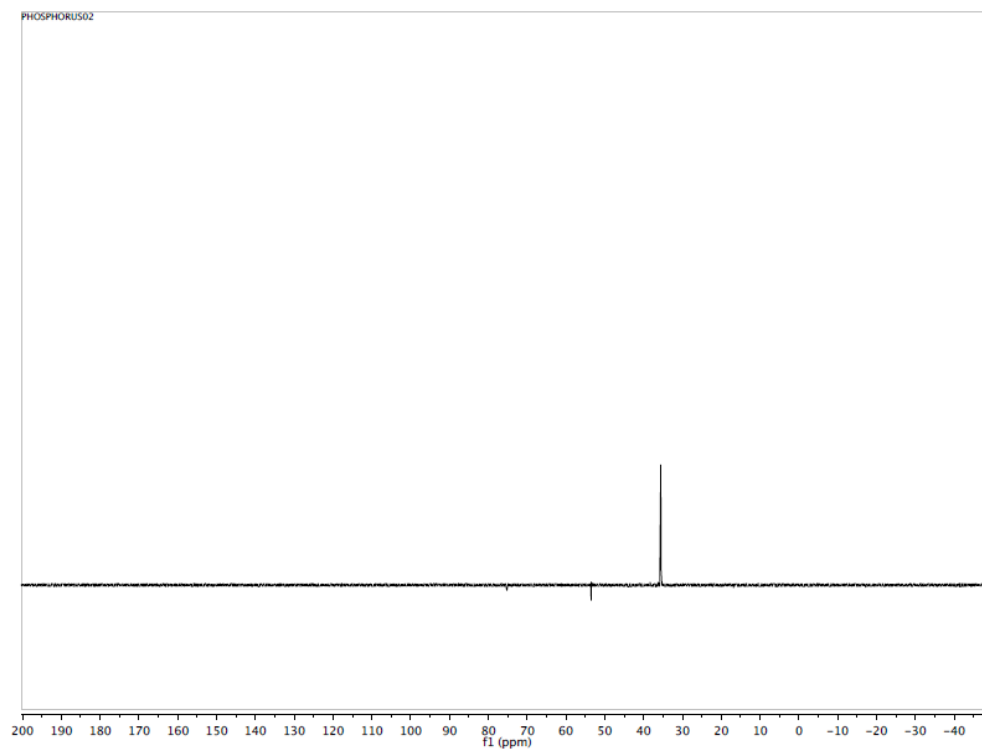


Figure 18: $^{31}\text{P}\{^1\text{H}\}$ NMR spectrum of compound **2.3**[NTf₂].

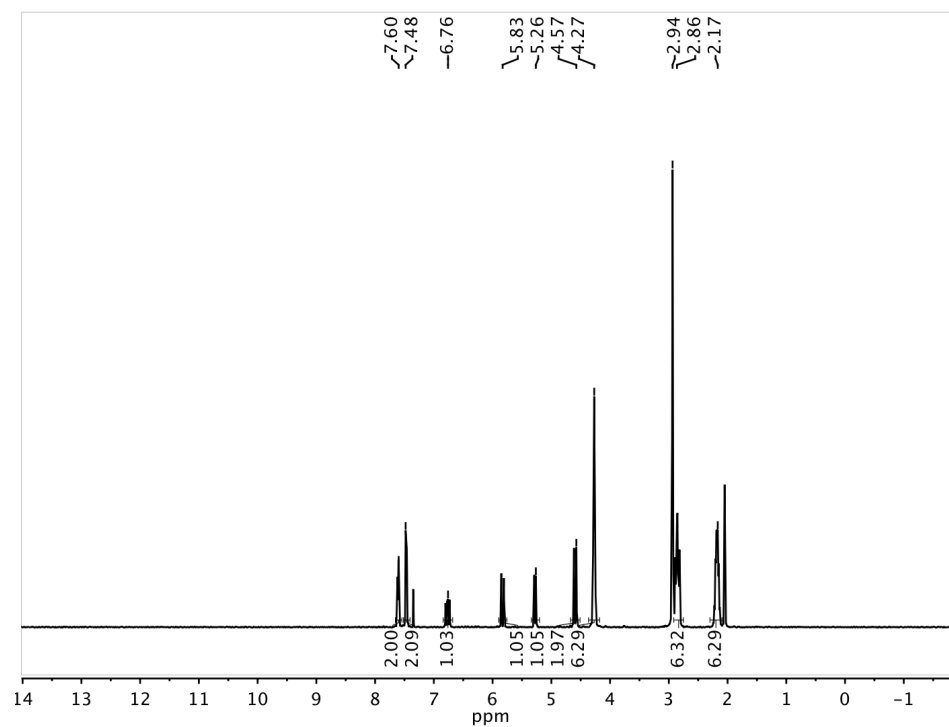


Figure 19: ^1H NMR spectrum of compound **2.4**[Cl].

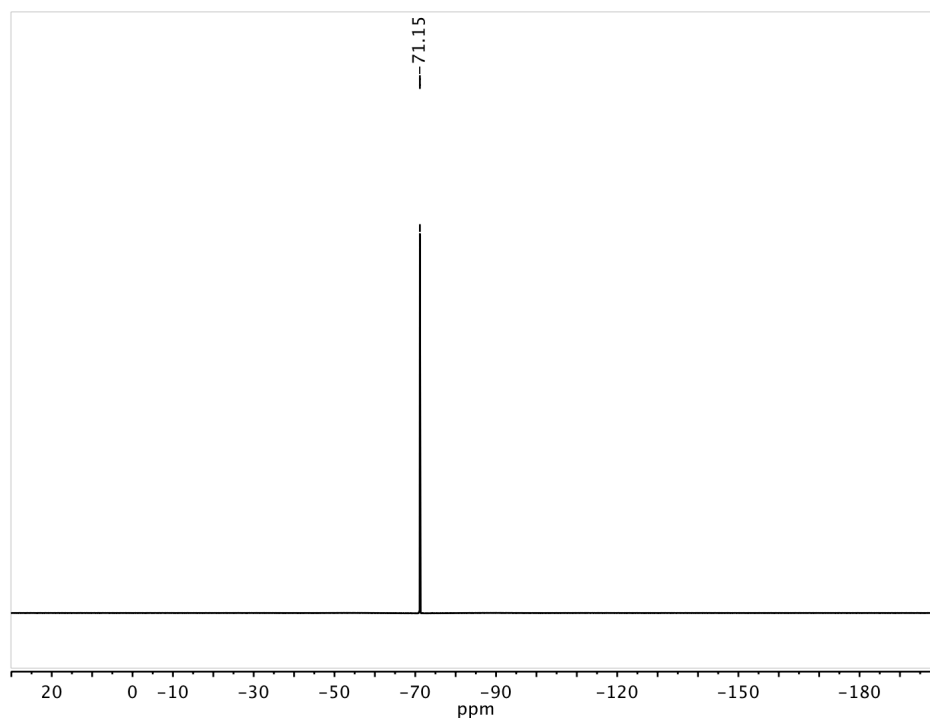


Figure 20: ^{19}F NMR spectrum of compound **2.4[Cl]**.

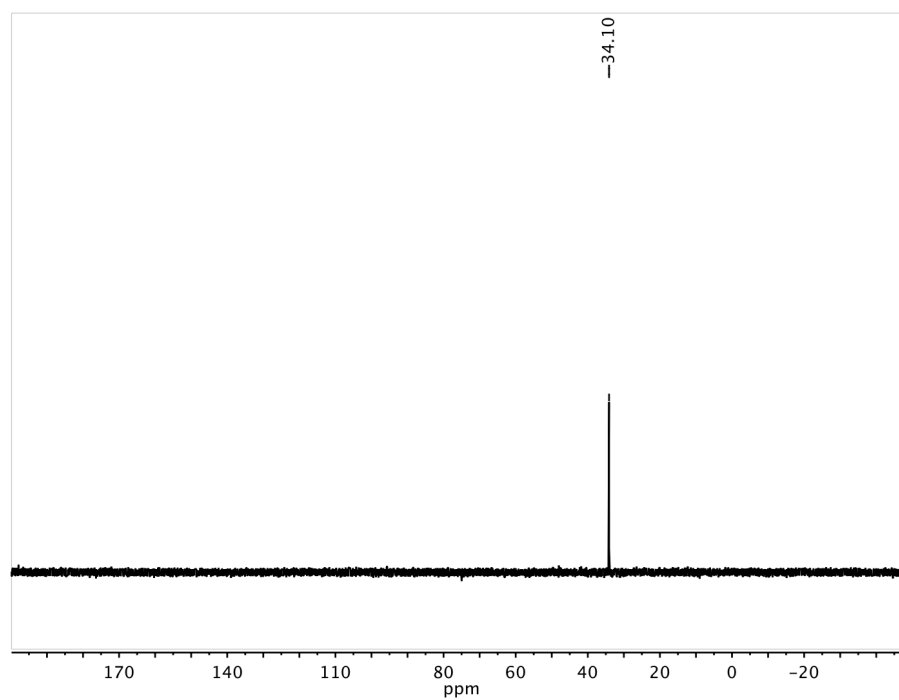


Figure 21: $^{31}\text{P}\{^1\text{H}\}$ NMR spectrum of compound **2.4[Cl]**.

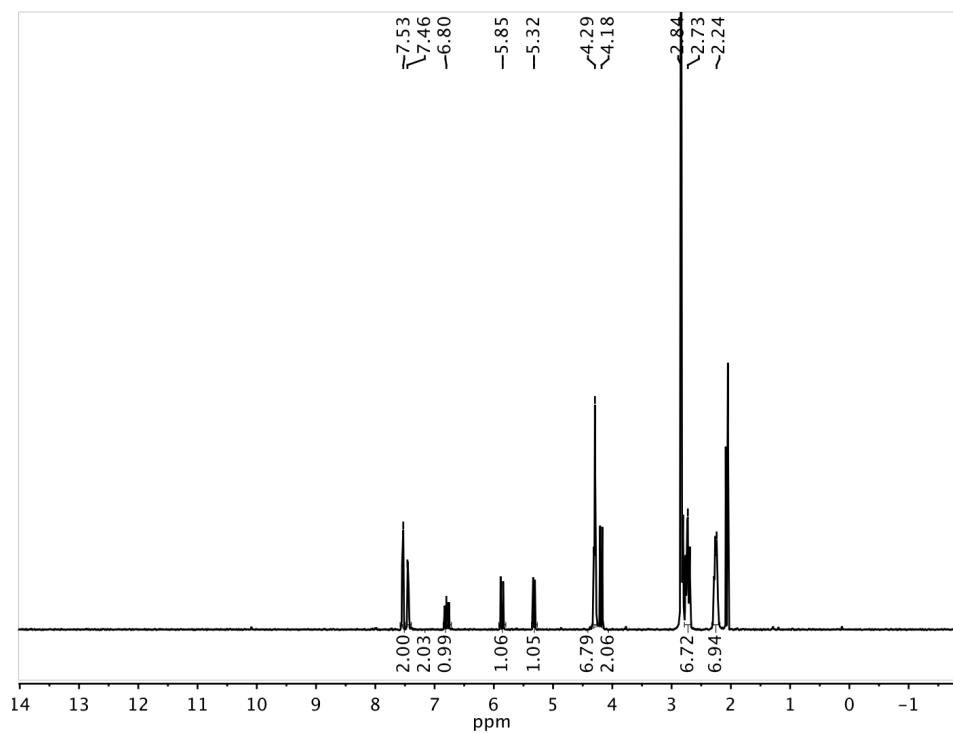


Figure 22: ^1H NMR spectrum of compound 2.4[NTf₂].

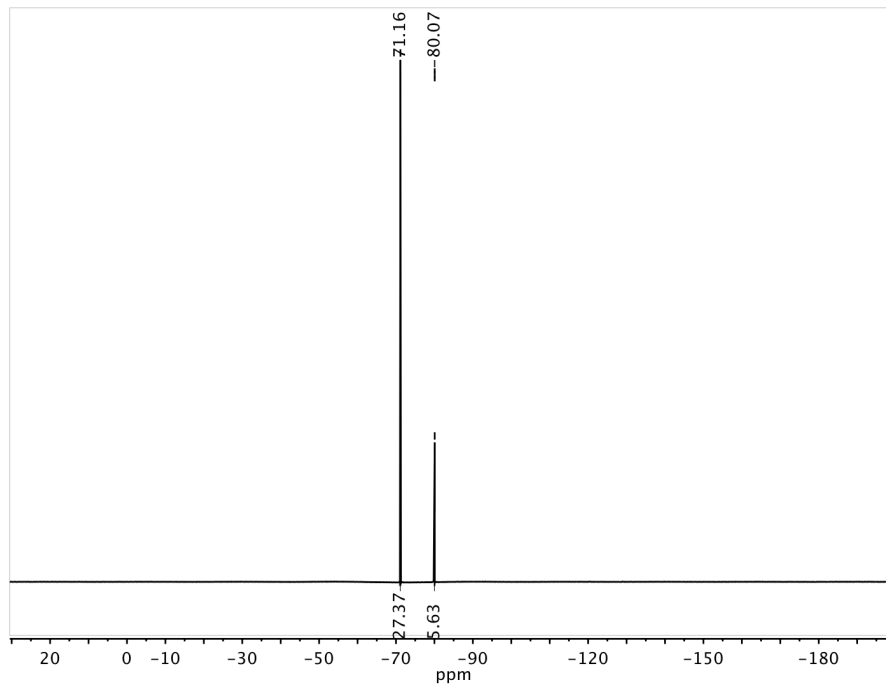


Figure 23: ^{19}F NMR spectrum of compound 2.4[NTf₂].

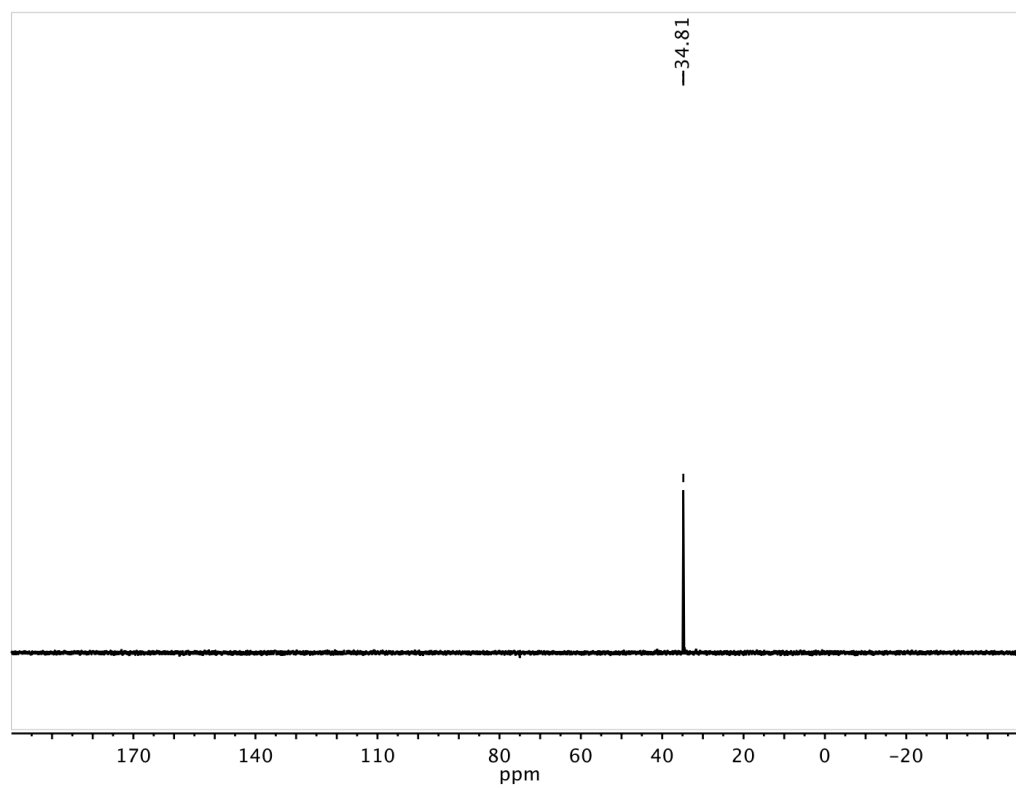


Figure 24: $^{31}\text{P}\{^1\text{H}\}$ NMR spectrum of compound **2.4**[NTf₂].

Chapter 3

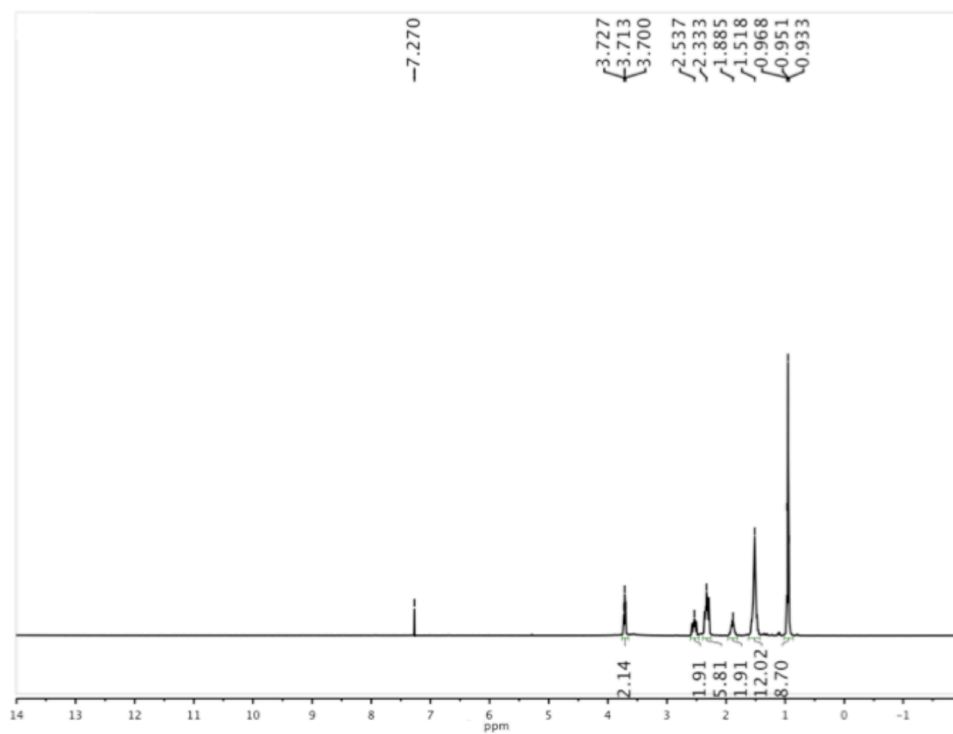


Figure 1: ^1H NMR spectrum of compound 3.1

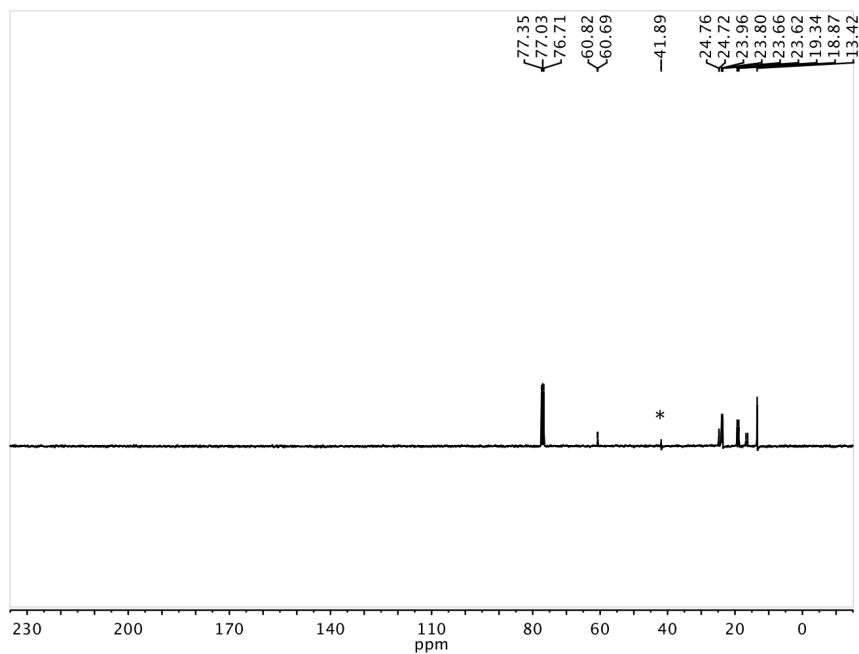


Figure 2: $^{13}\text{C}\{^1\text{H}\}$ NMR spectrum of compound 3.1. *Artifact of the instrument.

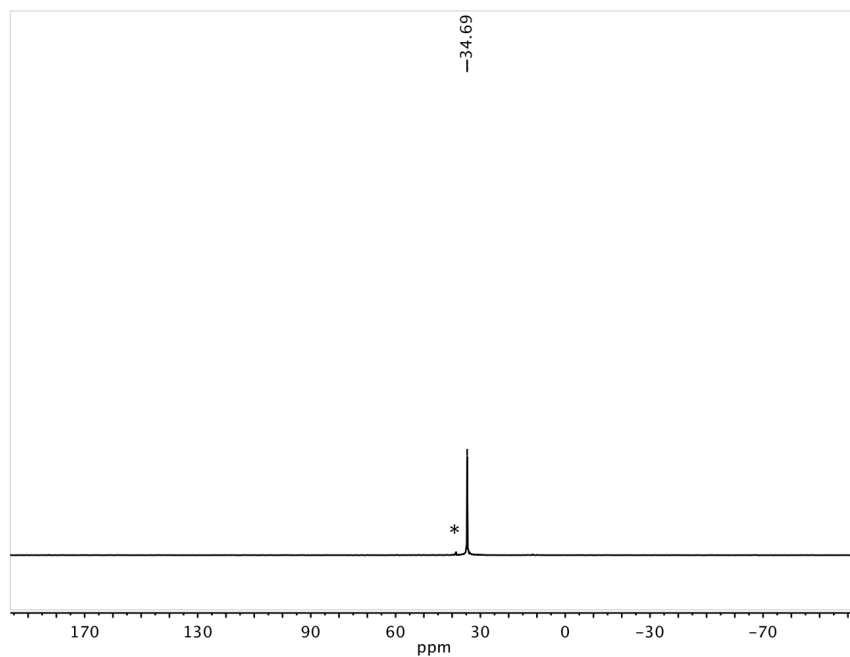


Figure 3: $^{31}\text{P}\{^1\text{H}\}$ NMR spectrum of compound **3.1**. *Isometric impurity from starting material tributylphosphine.

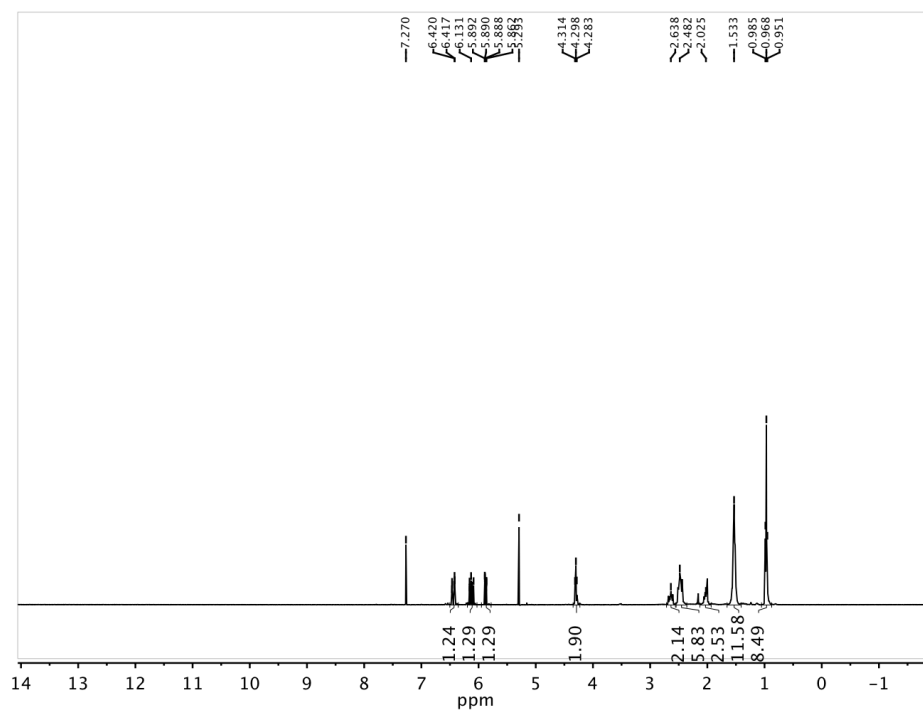


Figure 4: ^1H NMR spectrum of compound **3.2**.

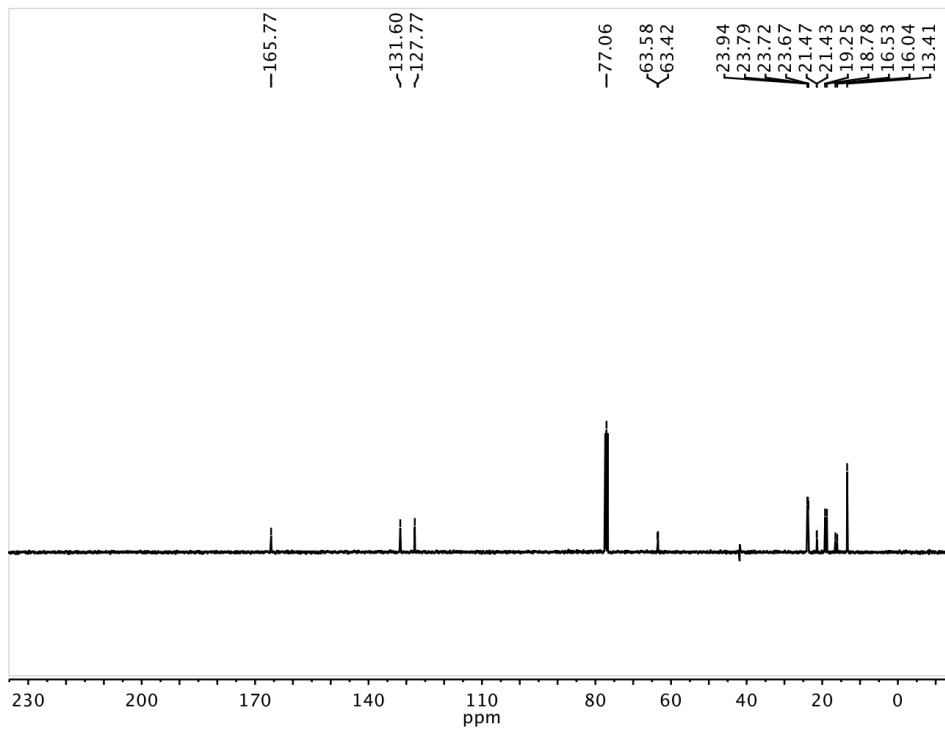


Figure 5: $^{13}\text{C}\{^1\text{H}\}$ NMR spectrum of compound 3.2.

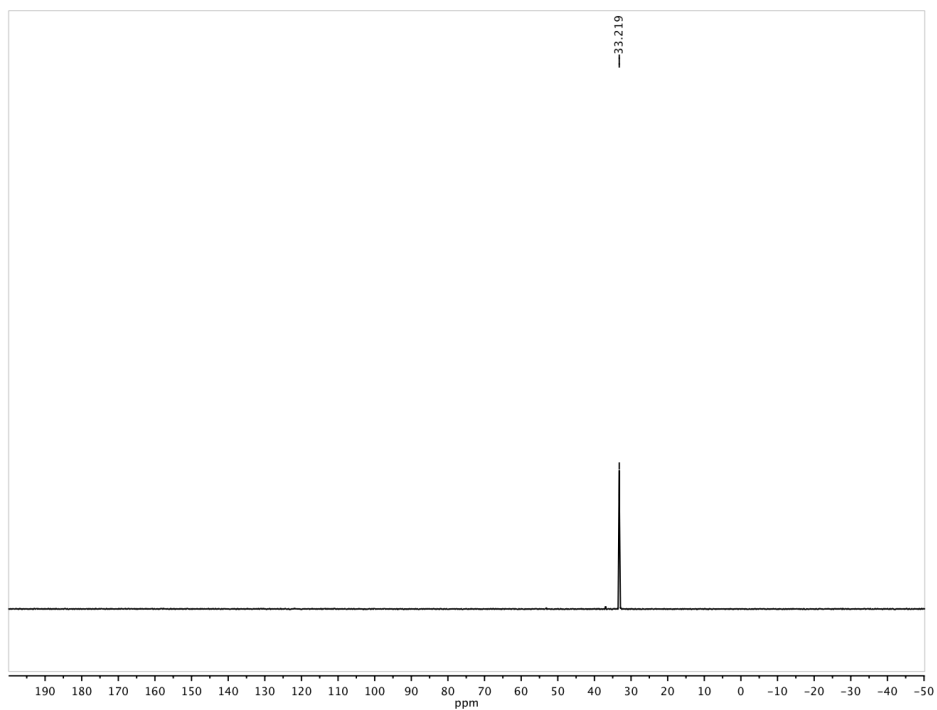


Figure 6: $^{31}\text{P}\{^1\text{H}\}$ NMR spectrum of compound 3.2.



Figure 7: Structure of EB130.

Chapter 4

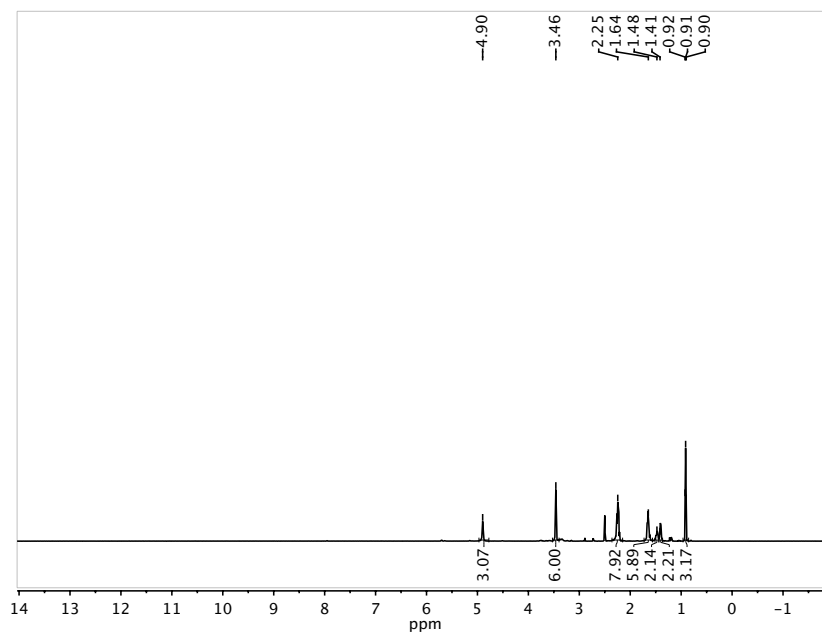


Figure 1: ^1H NMR spectrum of compound 4.1.

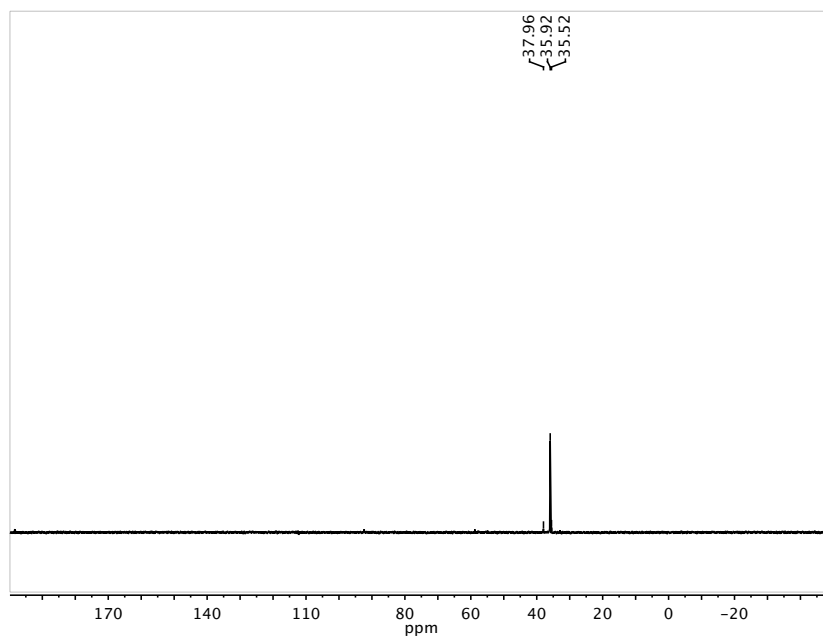
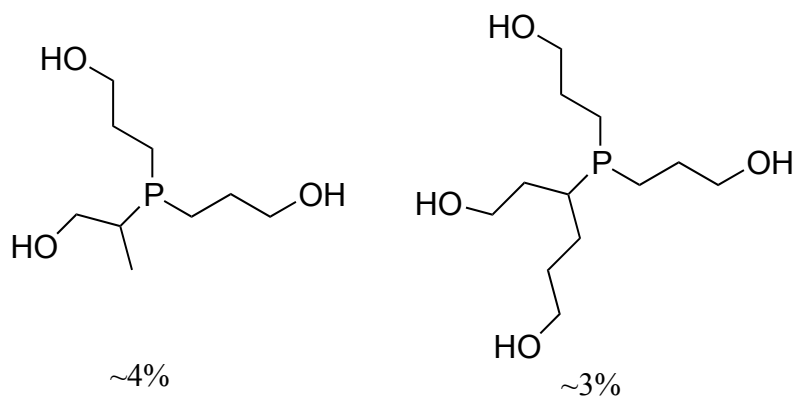


Figure 2: $^{31}\text{P}\{^1\text{H}\}$ NMR spectrum of compound **4.1**. Signals at 37.96 (~4%) and 35.52 (~3%) ppm are isomers present in the starting material. Their structures appear below prior to quaternization.



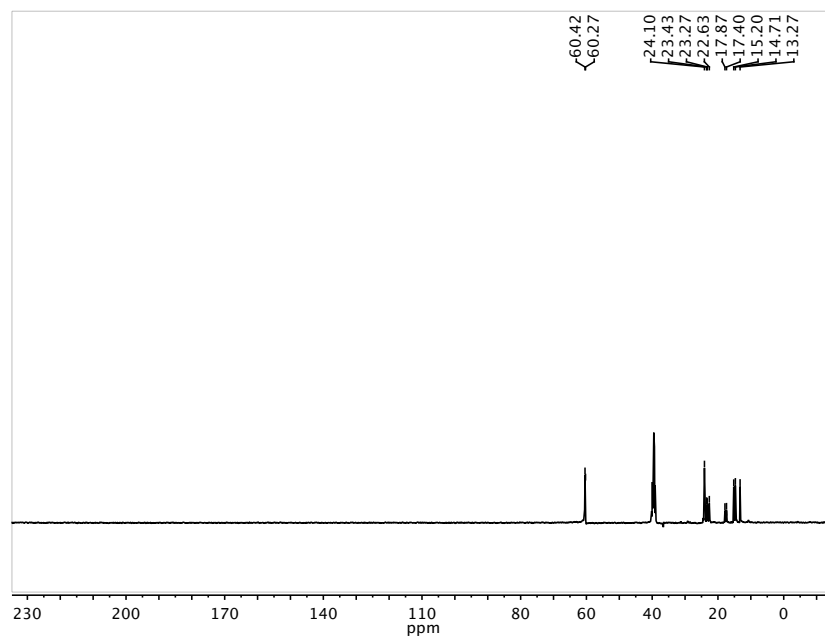


Figure 3: $^{13}\text{C}\{^1\text{H}\}$ NMR spectrum of compound **4.1**.

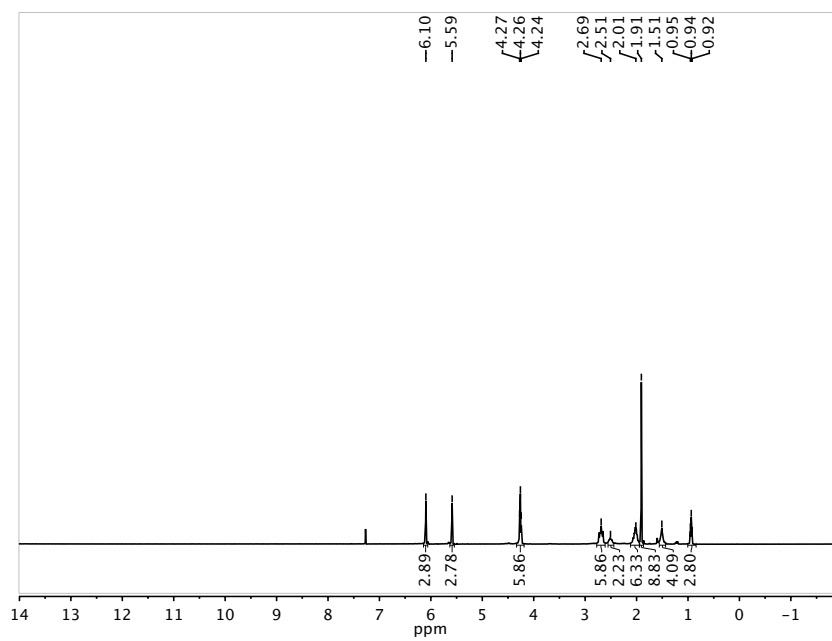


Figure 4: ^1H NMR spectrum of compound **4.2**.

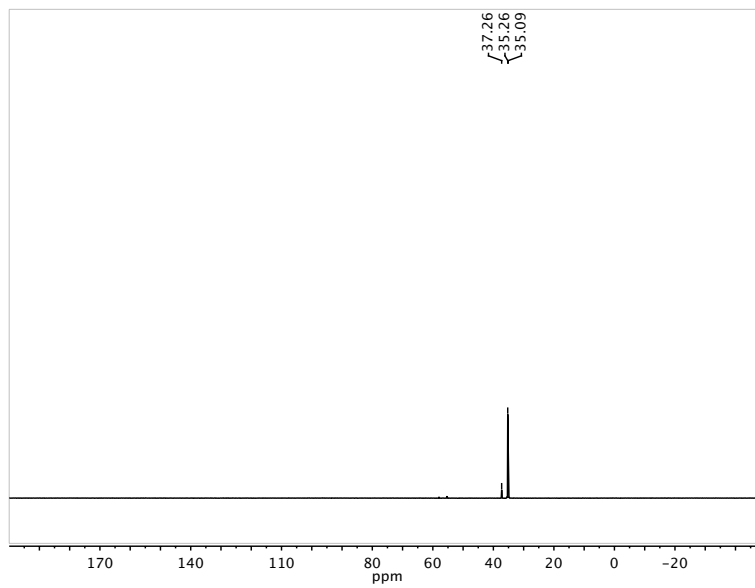


Figure 5: $^{31}\text{P}\{^1\text{H}\}$ NMR spectrum of compound **4.2**.

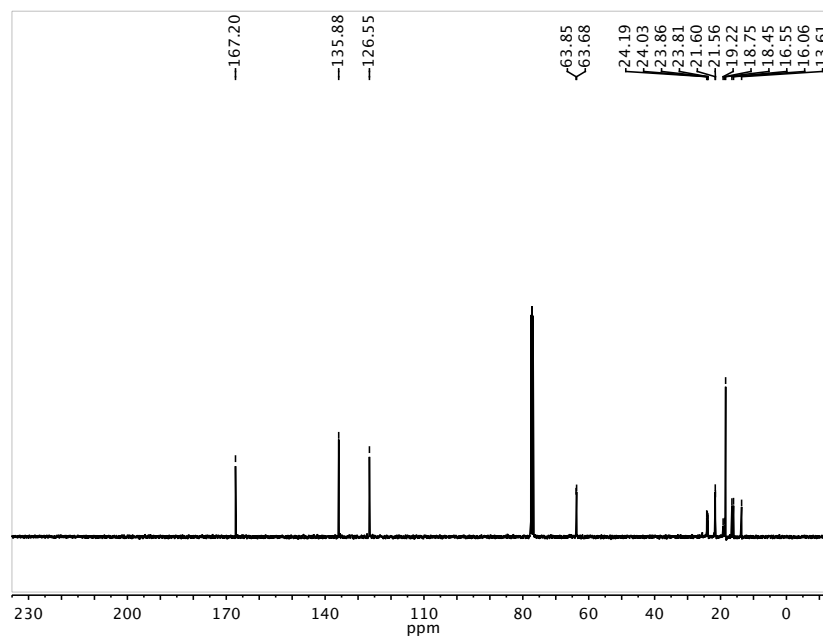


Figure 6 $^{13}\text{C}\{^1\text{H}\}$ NMR spectrum of compound **4.2**.

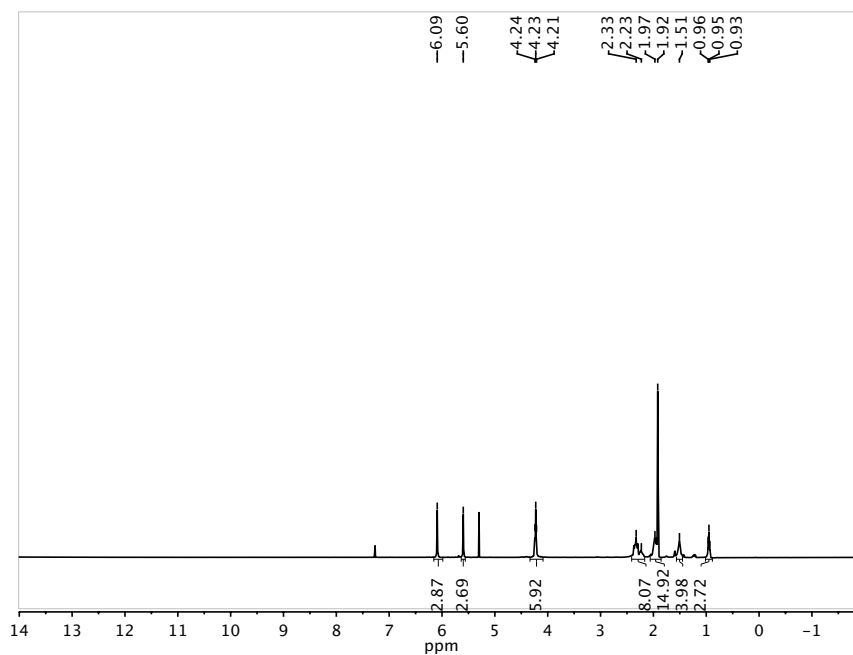


Figure 7: ^1H NMR spectrum of $4.2[\text{NTf}_2]$.

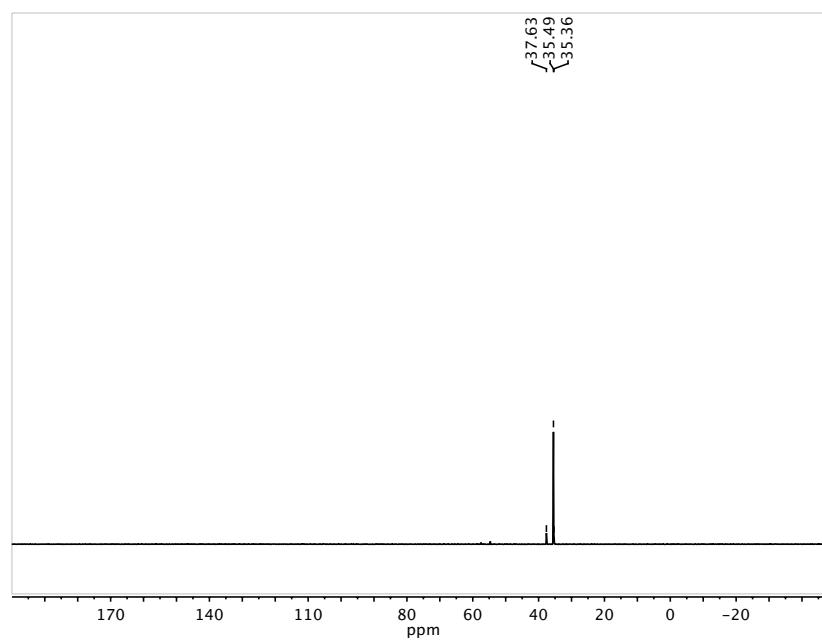


Figure 8: $^{31}\text{P}\{^1\text{H}\}$ NMR spectrum of $4.2[\text{NTf}_2]$.

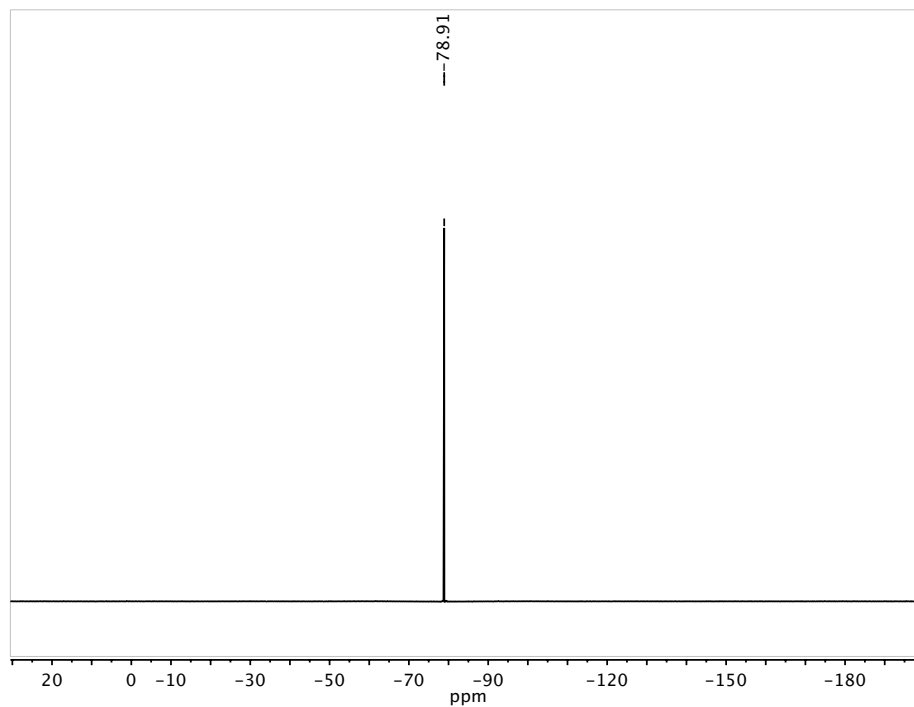


Figure 9: $^{19}\text{F}\{^1\text{H}\}$ NMR spectrum of $4.2[\text{NTf}_2]$.

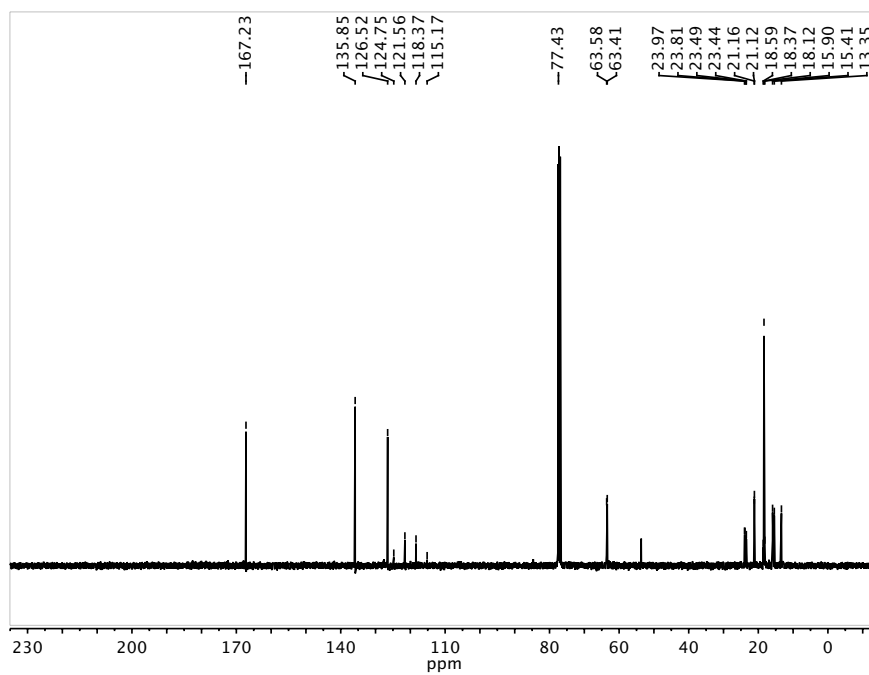


Figure 10: $^{13}\text{C}\{^1\text{H}\}$ NMR spectrum of compound $4.2[\text{NTf}_2]$.

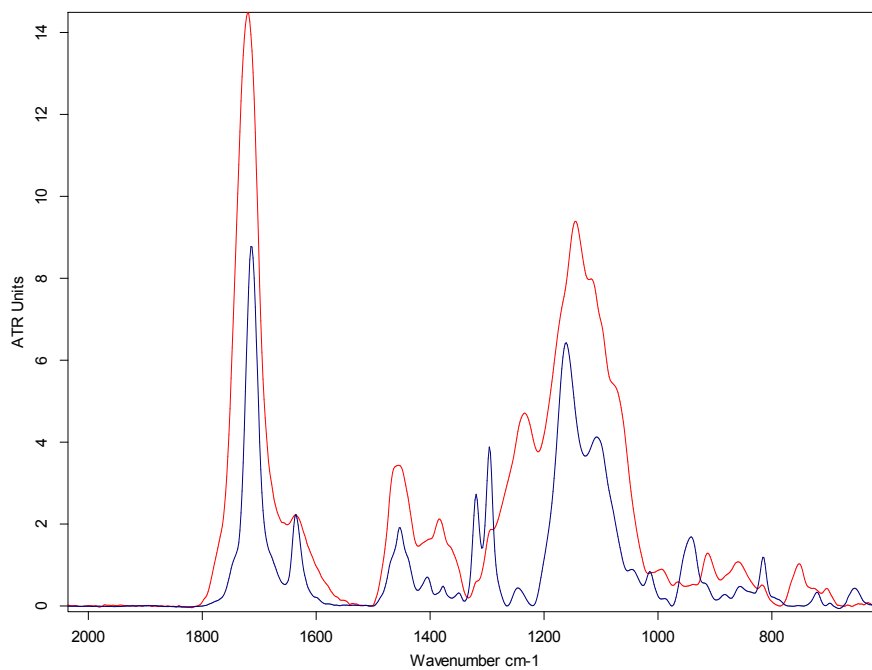


Figure 12: ATR-FTIR spectrum of a 25 micron polymer film before (blue) and after (red) irradiation with UV light.

Chapter 5

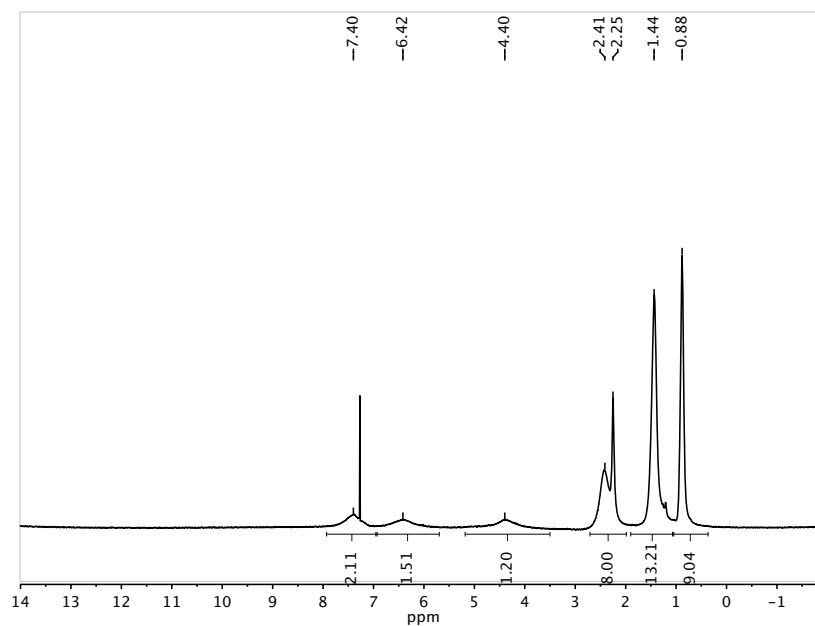


Figure 1: ¹H NMR spectrum of compound 5.3.

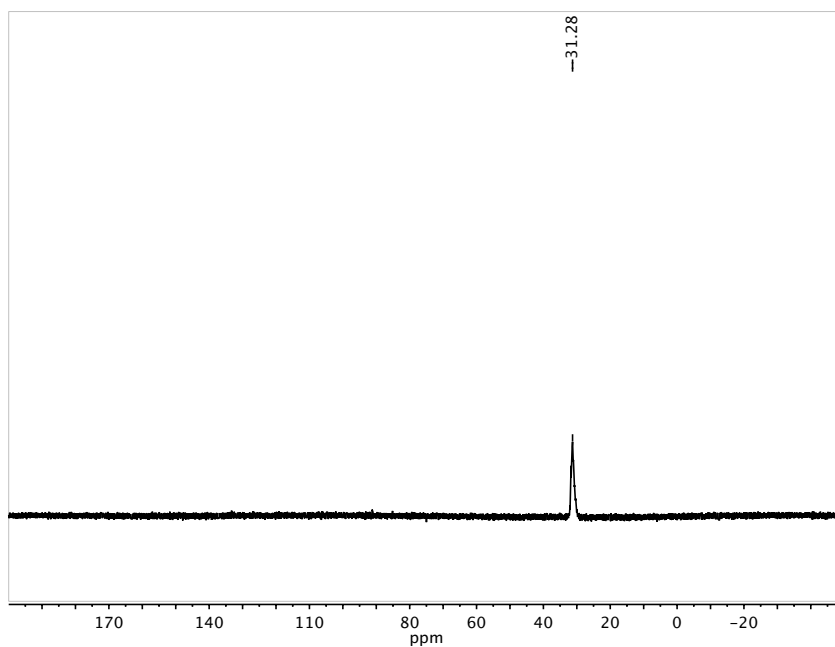


Figure 2: $^{31}\text{P}\{^1\text{H}\}$ NMR spectrum of **5.3**.

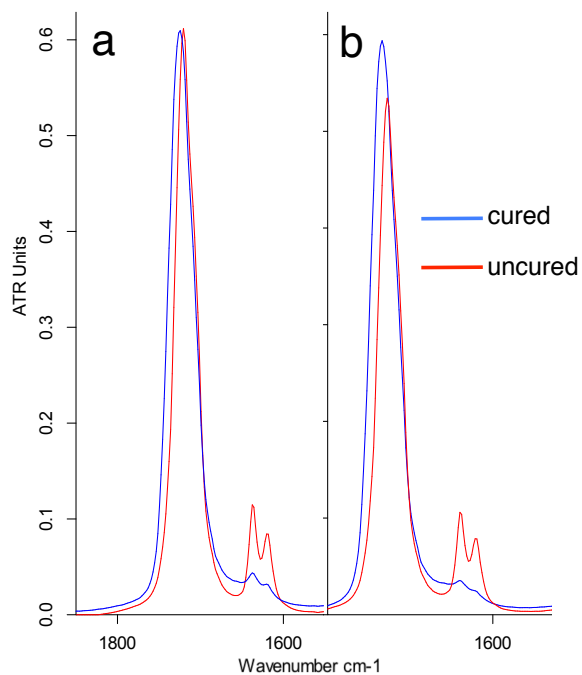


Figure 3: Before and after curing of formulation **1** without (a) and with (b) 5 wt% compound **5.3** added.

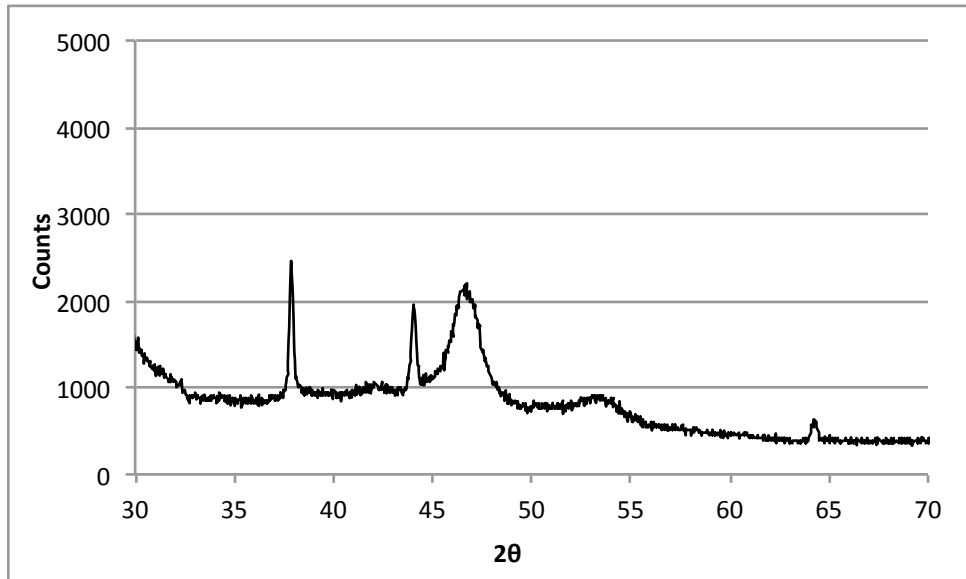


Figure 4: Powder X-ray diffraction spectrum of polymer C after one reduction cycles.

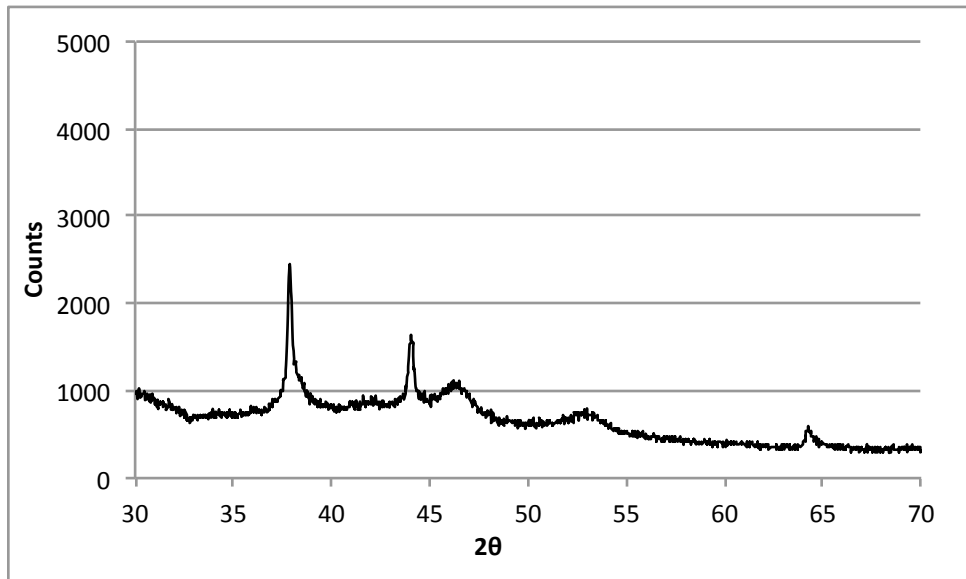


Figure 5: Powder X-ray diffraction spectrum of polymer C after 8 reduction cycles.

Chapter 6

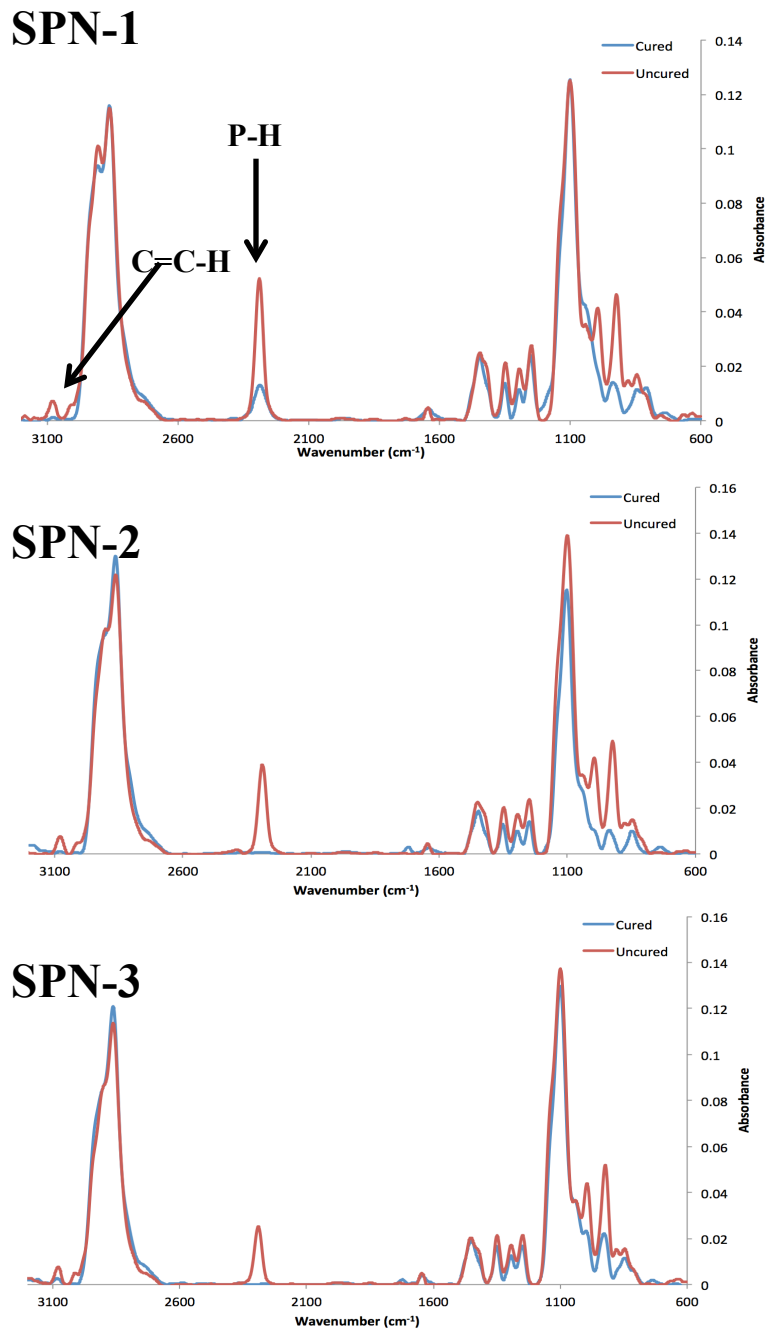


Figure 1: ATR-FTIR spectra of SPN-1→SPN-3 before (red) and after (blue) UV-curing. P-H bonds ($\sim 2300\text{ cm}^{-1}$) and olefin ($\sim 3050\text{ cm}^{-1}$) vibration.

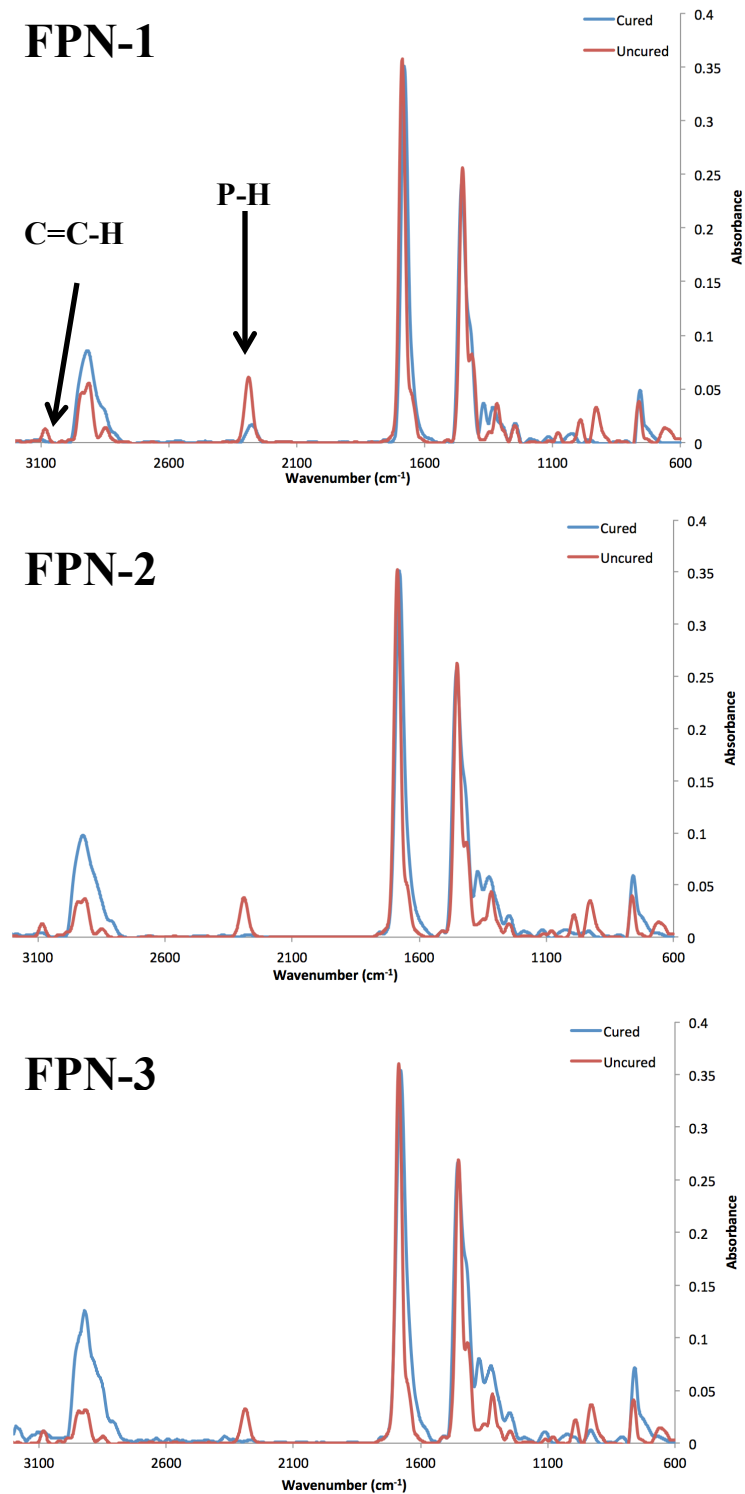


Figure 2: ATR-FTIR spectra of FPN-1→FPN-3 before (red) and after (blue) UV-curing. P-H bonds ($\sim 2300\text{ cm}^{-1}$) and olefin ($\sim 3050\text{ cm}^{-1}$) vibration intensities decrease upon UV exposure.

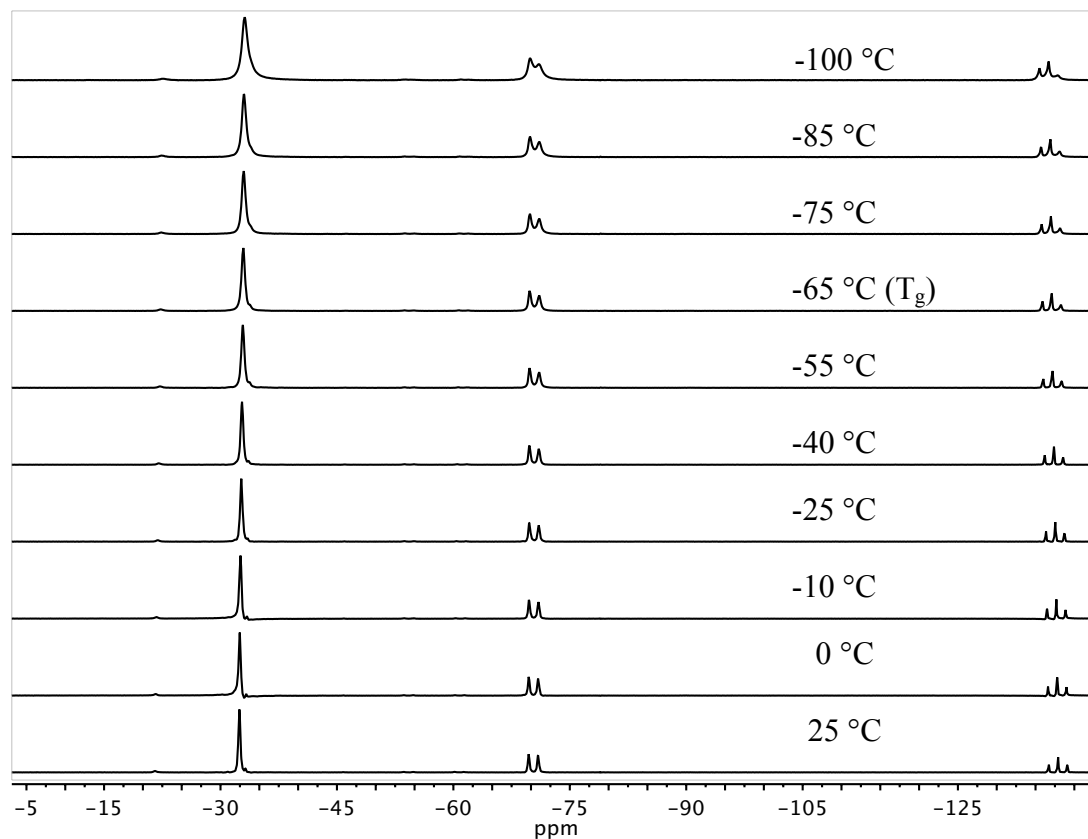


Figure 3: Variable temperature, solid-state ^{31}P hydrogen coupled NMR spectra of SPN-1, displaying phosphorus-hydrogen coupling ($^1J_{\text{P-H}} = 192 \text{ Hz}$).

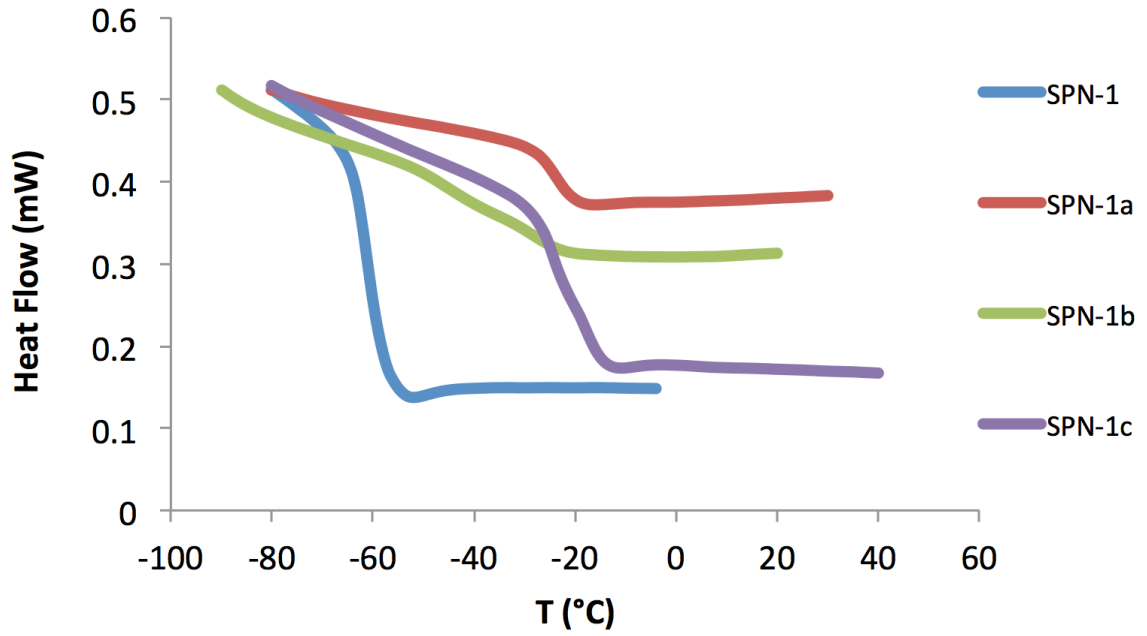


Figure 4: DSC curves for the reaction series conducted on **SPN-1** showing how the T_g changed upon each manipulation step.

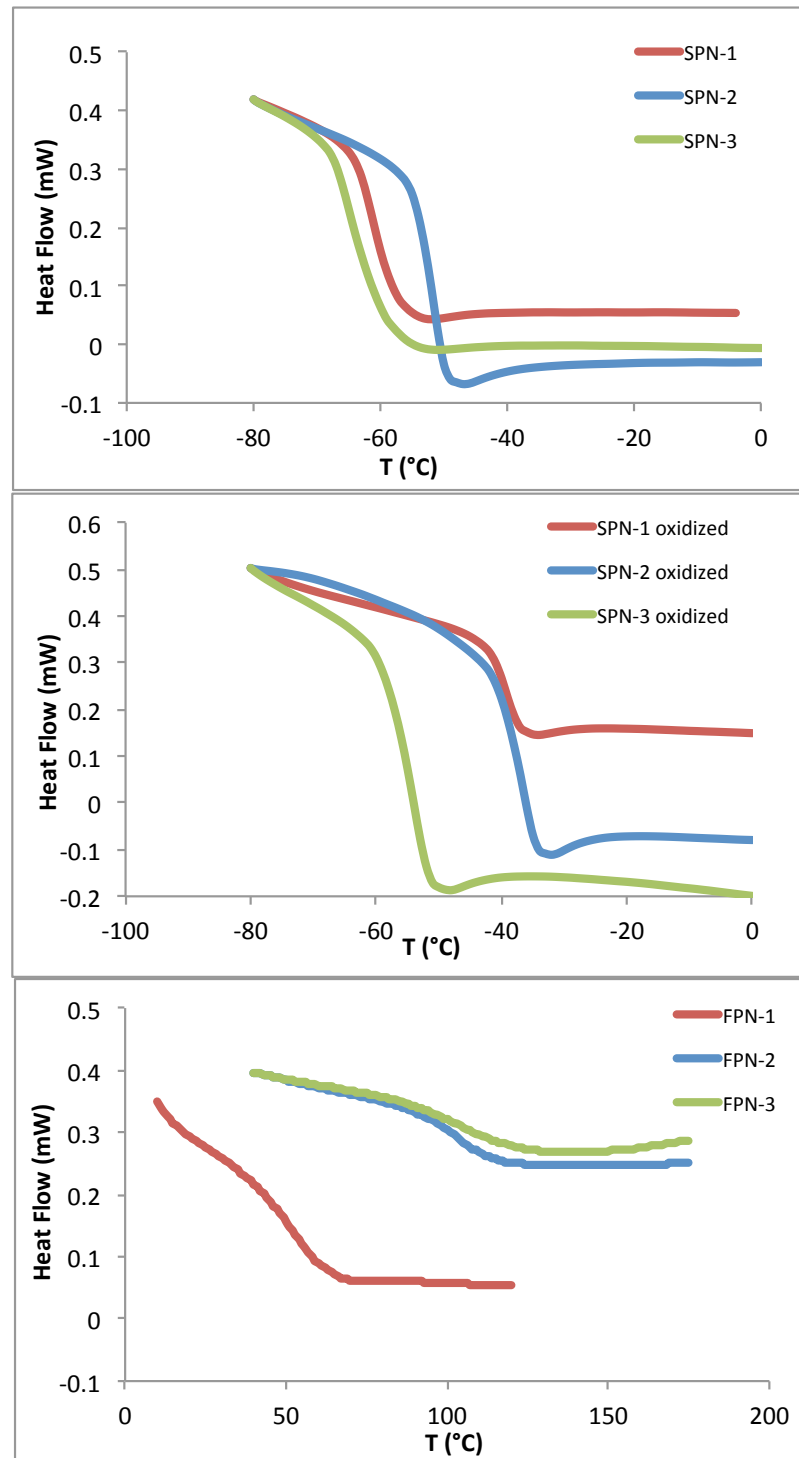


Figure 5: DSC curves for **SPN-1**→**SPN-3**, oxidized **SPN-1**→**SPN-3**, and **FPN-1**→**FPN-3** showing the glass transitions.

20 hours, hydrogen-coupled spectrum

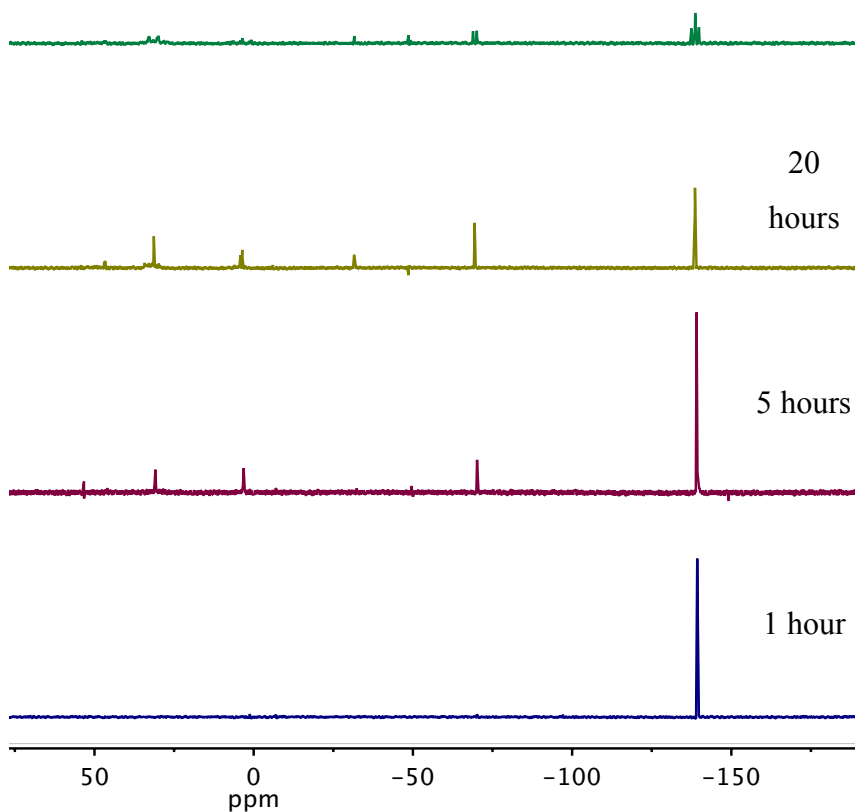


Figure 6: $^{31}\text{P}\{^1\text{H}\}$ NMR spectra of formulation **SPN-2** with 2 wt% butylated hydroxytoluene exposed to air and a ^{31}P NMR spectrum after 20 hours in air indicating the presence of primary/secondary phosphine oxides ($\delta_{\text{P}} = 4$ (t) and 31 (d), $^1J_{\text{P-H}} = 452$ Hz).

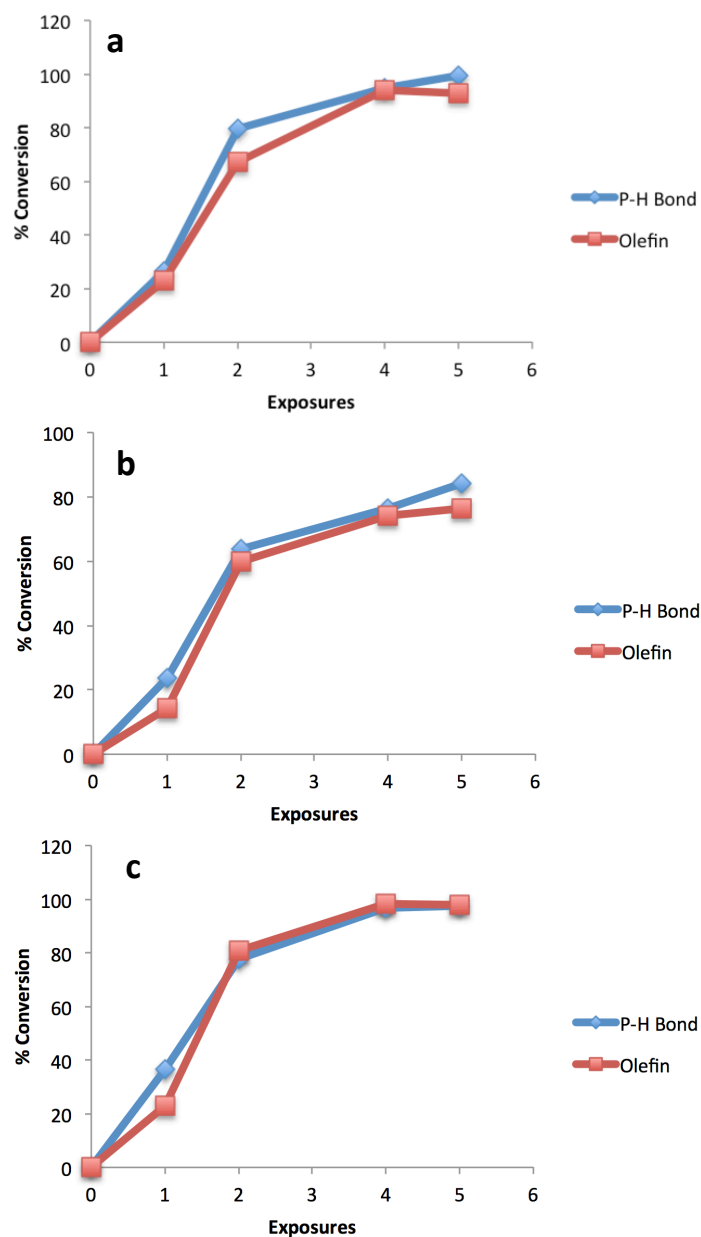


Figure 7: Functional group conversion of **SPN-2** determined by FTIR-ATR spectroscopy after exposure to UV light. **a)** 0.5 wt% Irgacure 819 under a nitrogen atmosphere. **b)** 0.5 wt% Irgacure 819 and 0.67 wt% diphenylamine cured in air. **c)** 1.15 wt% Irgacure 819 and 0.67 wt% diphenylamine cured in air. Conversion was determined by comparing signal integration before and after irradiation. Air-cured samples were hand mixed in air for 5 minutes prior to irradiation.

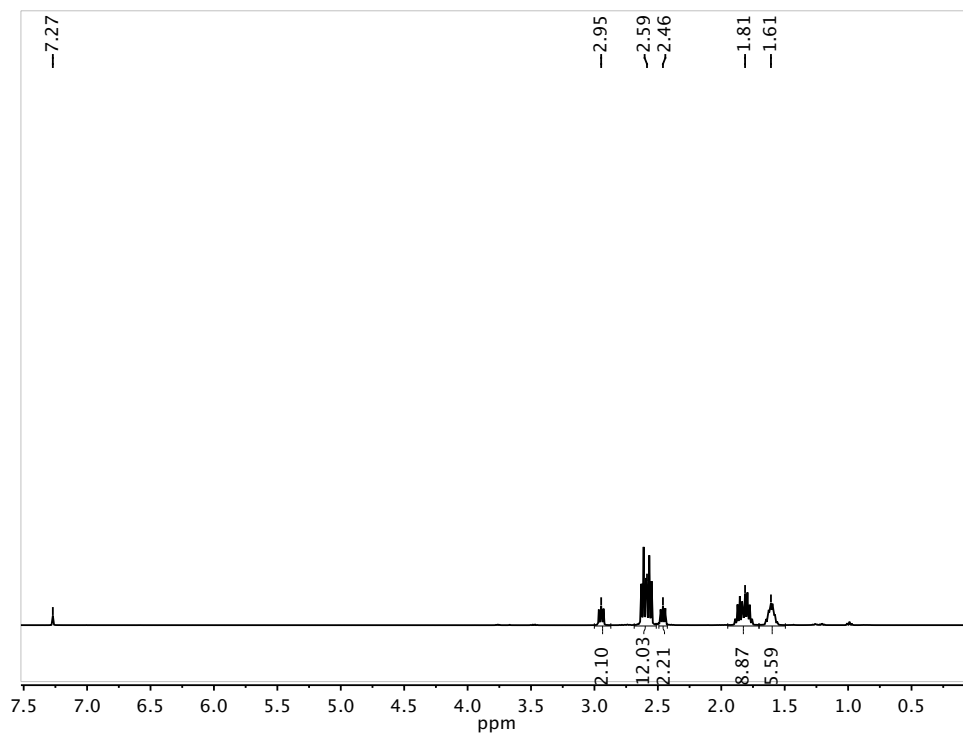


Figure 8: ^1H NMR spectrum of 6.4.

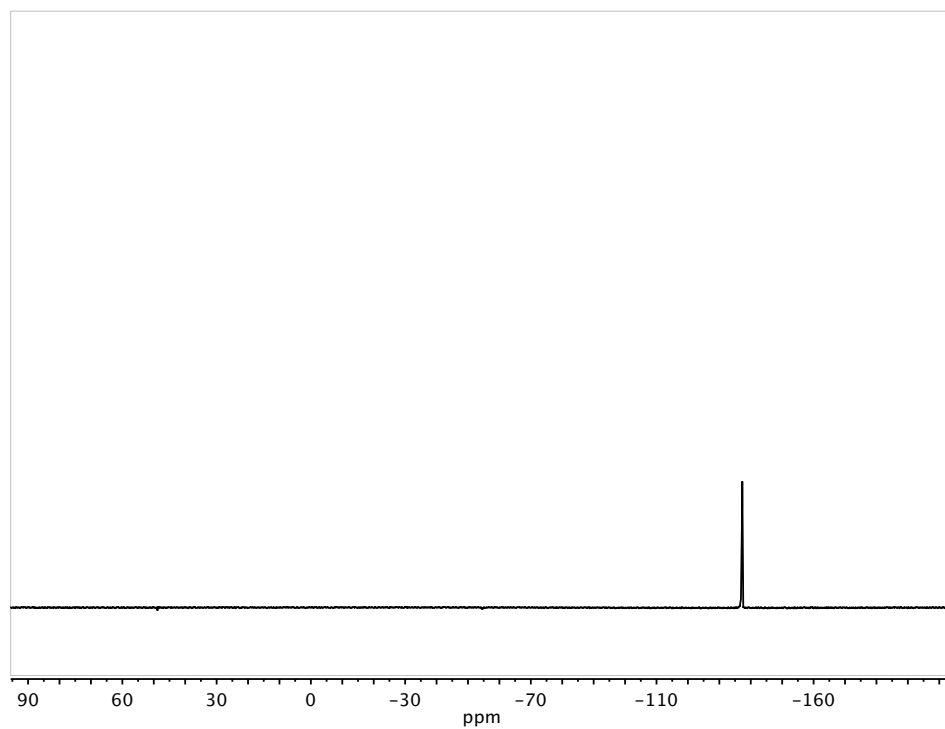


Figure 9: $^{31}\text{P}\{^1\text{H}\}$ NMR spectrum of 6.4.

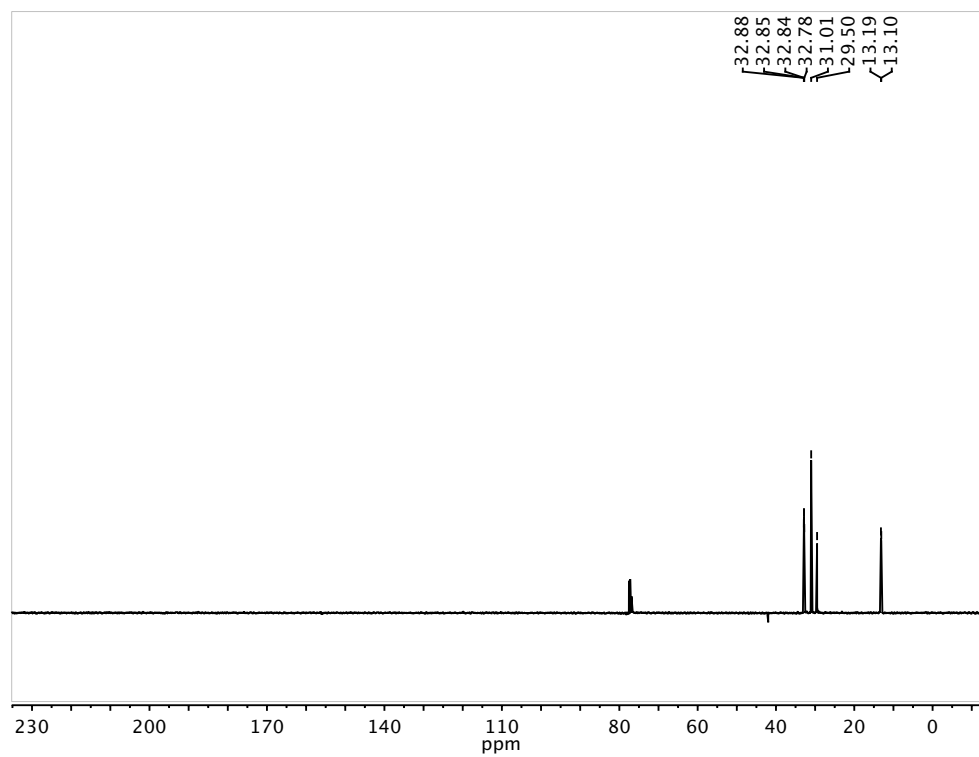


Figure 10: $^{13}\text{C}\{^1\text{H}\}$ NMR spectrum of **6.4**.

Curriculum Vitae

Name:	Ryan Guterman
Post-secondary Education and Degrees:	University of Western Ontario, Ontario, Canada 2006-2010, B.Sc
	The University of Western Ontario London, Ontario, Canada 2010-2015, Ph.D.
Honours and Awards:	Province of Ontario Graduate Scholarship 2013-2014, 2014-2015, \$15 000/yr
	Peter Hobson Prize for Best Oral Presentation 2013, \$750.00
	Three Minute Thesis (3MT) 3 rd place 2013, \$500.00
	Nanofabrication Faculty Scholarship 2012, \$500.00
	Three Minute Thesis (3MT) Competition Finalist 2012, \$500.00
Related Work Experience	Teaching Assistant The University of Western Ontario 2010-2014 (2213a, lab coordinator for 2273a, 2223b, 3300g)

CONTRIBUTIONS TO RESEARCH

Publications

- 1) **Guterman, R.;** Gillies, E.R.; Ragogna, P.J. The Formation of Gold Nanoparticles in Photopolymerized Networks (accepted **2015**)
- 2) **Guterman, R.;** Gillies, E.R.; Ragogna, P.J. Kinetically Controlled Patterning of Highly Crosslinked Phosphonium Photopolymers using simple Anion Exchange. *Langmuir* **2015**, *18*, 5181-5189.

- 3) **Guterman, R.**; Kenaree, A.R.; Gilroy, J.B.; Gillies, E.R.; Ragogna, P.J. Polymer network formation using the phosphane-ene reaction: a thiol-ene analogue with diverse post-polymerization chemistry *Chem. Mater.* **2015**, *27*, 1412.
- 4) Cutherbert, J.T.; **Guterman, R.**; Ragogna, P.J.; Gillies, E.R. Contact active antibacterial phosphonium coatings cured with UV light *J. Mater. Chem. B* **2015**, *3*, 1474.
- 5) **Guterman, R.**; Hesari, M.; Workentin M.S.; Ragogna, P.J.* Anion-Exchange Reactions on a Robust Phosphonium Photopolymer for the Controlled Deposition of Ionic Gold Nanoclusters *Langmuir* **2013**, *29*, 6460. (Front Cover).
- 6) **Guterman, R.**; Berven, B.B.; Corkery, T.C.; Nie, H.-Y.; Gillies, E.R.; Idacavage, M.J.; and Ragogna, P.J.* Fluorinated Polymerizable Phosphonium Salts from PH_3 : Surface Properties of Photopolymerized Films *J. Polym. Sci. A Polym. Chem.* **2013**, *51*, 2782 (Inside cover).

Patents

Ragogna, P.J.; **Guterman, R.**; Corkery, T.C.; Berven, B.; Gillies, E. (The University of Western Ontario, Canada) Anion Exchange Surfaces Utilizing Phosphonium Salts (provisional patent submitted March 2012, HS Ref: 349-225-P.)

Conference Oral Presentations

- 1) **Guterman, R.***; Gillies, E.R.; Ragogna, P.J. (2014) Phosphane-ene Photopolymerization. Oral presentation held at the Inorganic Discussion Weekend (IDW) conference at the University of Montreal.
- 2) **Guterman, R.***; Gillies, E.R.; Ragogna, P.J. (2013) Kinetically Controlled Patterning of Highly Crosslinked Phosphonium Homopolymers Using Simple Anion Exchange. Oral presentation held at The Centre of Materials and Biomaterials Research (CAMBR) conference at Western University.

3) **Guterman, R.***; Gillies, E.R.; Ragogna, P.J. (2013) The Synthesis and Application of Phosphonium Salts for Photopolymeric Systems. Oral presentation held at the EUPOC 2013 Polymers and Ionic liquids conference in Gargnano, Italy.

4) **Guterman, R.***; Gillies, E.R.; Ragogna, P.J. (2013) Formation and Utilization of Polyelectrolyte Networks from Polymerized Phosphonium Salts. Oral presentation held at the Surface and Interfacial Science: Energy, Materials, and Environment conference at Western University.

5) **Guterman, R.***; Gillies, E.R.; Ragogna, P.J. (2012) UV-Curable Phosphonium Salts as Surface Modifying Agents: Accessing the Surface Charges. Oral presentation held at the 24th Canadian Materials Science Conference at Western University.

6) **Guterman, R.***; Gillies, E.R.; Ragogna, P.J. (2012) Incorporating Phosphonium Salts into UV-curable Formulations: Accessing the Surface Charges. Oral Presentation held at the 95th Canadian Chemistry Conference and Exhibition in Calgary, Alberta.

7) Hesari, M.*; Akbari, R.; Swanick, K.; **Guterman R.**; Ragogna P.J; Fanchini, G.; Ding, Z.; Workentin, M.S. (2012) Evolution and Applications of the Properties of Au₂₅L₁₈ (+1, 0, -1) Nanoclusters. Oral Presentation held at the 95th Canadian Chemistry Conference and Exhibition in Calgary, Alberta.

8) **Guterman, R.***; Corkery, T.C.; Berven, B.; Idacavage, M.; Gillies, E.; Ragogna, P.J. (2011) Fluorinated Phosphonium Ion Monomers for the Fabrication of Hydrophobic Films. Oral presentation held at the Photopolymerization Fundamentals 2011 International Conference in Breckenridge Colorado.

Conference Poster Presentations

1) Cuthbert, T.J.; **Guterman, R.***; Gillies, E.R.; Ragogna, P.J. (2013) UV-cured Antimicrobial Phosphonium Films: A New Approach. Poster presentation held at the EUPOC 2013 Polymers and Ionic Liquids conference in Gargnano, Italy.

2) **Guterman, R.***; Hesari, M.; Workentin, M.S.; Ragogna, P.J. (2012) Ion-Exchange Chemistry of a Novel UV-Cured Phosphonium Support – Harnessing the Solution Phase

Properties of Au₂₅ Nanoclusters. Poster presentation held at the Polymer Networks Group 2012 meeting in Jackson Wyoming.

3) **Guterman, R.***; Berven, B.; Corkery, T.C.; Ragona, P.J. (2012) High Throughput Surface Modification via New UV-Curing Technologies. Poster presentation held at the Research Industry Showcase at Western University

4) **Guterman, R.***; Greer, A.; Gillies, E.; Ragona, P.J. (2011) The Thermal and Hydrophobic Behaviour of Various Crosslinked UV Cured Fluorinated Phosphonium Polymers: A Comparative Study. Poster presentation held at the 2011 Inorganic Discussion Weekend in Niagara Falls.

5) **Guterman, R.***; Gillies, E.; Ragona, P.J. (2011) Fluorinated Phosphonium Ion Monomers for the Fabrication of Hydrophobic Films. Poster presentation held at The Centre for Advanced Materials and Biomaterials Research conference at Western University.

6) Ingratta, M.*; **Guterman, R.**; Ragona, P.J. Highly Fluorinated Phosphonium Ionic Liquid Polymers as Hydrophobic Coatings – a UV Approach. Poster Presentation held at The Ontario Regional Advanced Manufacturing and Materials (AMM) Showcase at Western University.